



US009925559B2

(12) **United States Patent**  
Lee et al.

(10) **Patent No.:** US 9,925,559 B2  
(45) **Date of Patent:** Mar. 27, 2018

(54) **GRAPHENE-CONTAINING COATING FILM, AND METHOD FOR PREPARING THE SAME**

(71) Applicants: **Hyundai Motor Company**, Seoul (KR); **Korea Institute of Ceramic Engineering and Technology**

(72) Inventors: **Kyu Geol Lee**, Gyeonggi-do (KR); **Kwang Il Chang**, Gyeonggi-do (KR); **Seung Hun Hur**, Seoul (KR)

(73) Assignees: **Hyundai Motor Company**, Seoul (KR); **Korea Institute of Ceramic Engineering and Technology**, Jinju, Gyeongsangnam-do (KR)

(\*) Notice: Subject to any disclaimer, the term of this patent is extended or adjusted under 35 U.S.C. 154(b) by 191 days.

(21) Appl. No.: **14/945,081**

(22) Filed: **Nov. 18, 2015**

(65) **Prior Publication Data**

US 2017/0059117 A1 Mar. 2, 2017

(30) **Foreign Application Priority Data**

Aug. 25, 2015 (KR) ..... 10-2015-0119555

(51) **Int. Cl.**

**B32B 3/10** (2006.01)  
**B05D 3/00** (2006.01)

(Continued)

(52) **U.S. Cl.**

CPC ..... **B05D 3/007** (2013.01); **C08K 3/00** (2013.01); **C09C 1/00** (2013.01); **C09D 7/1266** (2013.01); **C01B 32/194** (2017.08); **C01B**

2204/04 (2013.01); **C01B 2204/22** (2013.01); **C01B 2204/32** (2013.01); **C08K 3/04** (2013.01); **C08K 2201/003** (2013.01); **C08K 2201/011** (2013.01); **F21S 48/1233** (2013.01); **F21S 48/30** (2013.01)

(58) **Field of Classification Search**

None

See application file for complete search history.

(56) **References Cited**

U.S. PATENT DOCUMENTS

8,257,867 B2 9/2012 Liu et al.  
2010/0009094 A1\* 1/2010 Lochtman ..... H05K 3/027  
427/555

(Continued)

FOREIGN PATENT DOCUMENTS

KR 2012-0035659 A 4/2012  
KR 2012-0039799 A 4/2012

(Continued)

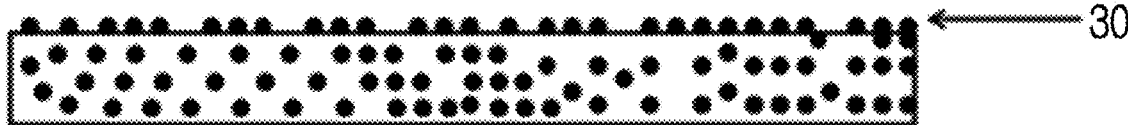
*Primary Examiner* — Christopher Polley

(74) *Attorney, Agent, or Firm* — Mintz Levin Cohn Ferris Glovsky and Popeo, P.C.; Peter F. Corless

(57) **ABSTRACT**

A graphene-containing coating film includes at least one hydrate represented by Chemical Formula 1 as described herein, a graphene positioned in a shape on the surface of the hydrate represented by Chemical Formula 1, and a silica particle positioned on the surface of the hydrate of Chemical Formula 1 and positioned on the surface of the graphene in a shape of discontinuous island. Particularly, the silica particle includes agglomeration of a plurality of silica nanoparticles. A method of preparing the graphene-containing coating film and a vehicle part such as a head lamp including the same are also provided.

25 Claims, 12 Drawing Sheets



(51)	<b>Int. Cl.</b>	
	<i>C08K 3/00</i>	(2018.01)
	<i>C09C 1/00</i>	(2006.01)
	<i>C09D 7/12</i>	(2006.01)
	<i>F21S 8/10</i>	(2006.01)
	<i>C08K 3/04</i>	(2006.01)
	<i>C01B 32/194</i>	(2017.01)

(56) **References Cited**

## U.S. PATENT DOCUMENTS

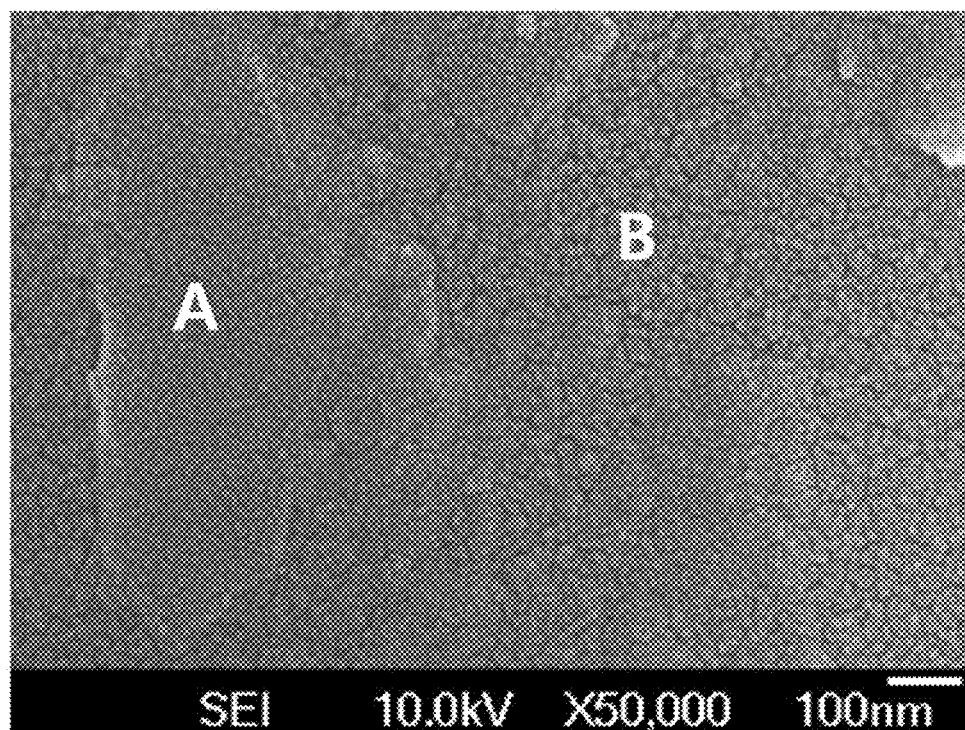
2010/0021657 A1 \* 1/2010 Lochtman ..... H05K 3/046  
427/597  
2012/0149554 A1 6/2012 Lin et al.  
2015/0099214 A1 \* 4/2015 Khe ..... H01B 1/24  
429/523  
2015/0159039 A1 6/2015 Croutxe-Barghorn et al.

## FOREIGN PATENT DOCUMENTS

KR	2012-0053399	A	5/2012
KR	2012-0092431	A	8/2012
KR	2013-0014327	A	2/2013
KR	2013-0067337	A	6/2013
KR	10-1317756	B1	10/2013
KR	2014-0076650	A	6/2014
KR	2014-0120450	A	10/2014
KR	10-1510805	B1	4/2015
KR	10-1510806	B1	4/2015
KR	10-2015-0075503	A	7/2015

\* cited by examiner

FIG. 1



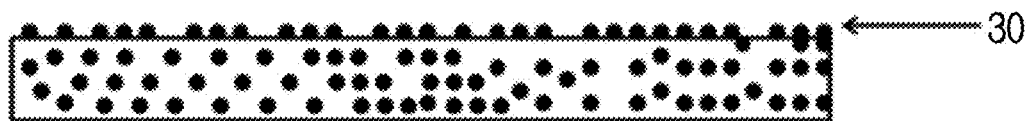
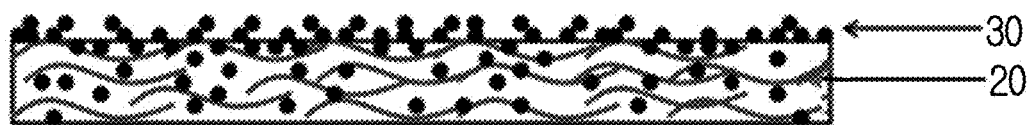
**FIG. 2A****FIG. 2B****FIG. 2C**

FIG. 3

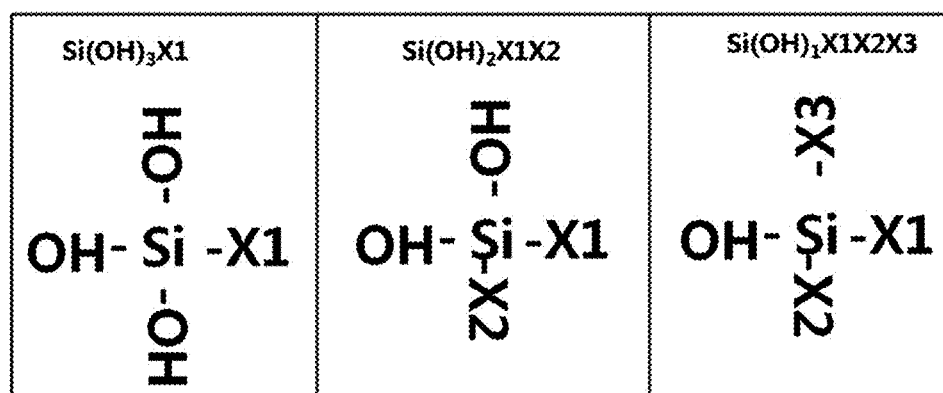


FIG. 4

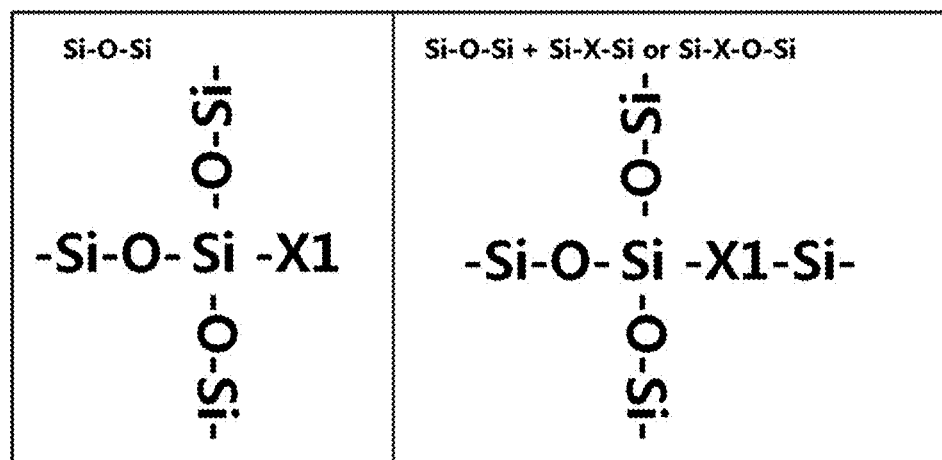
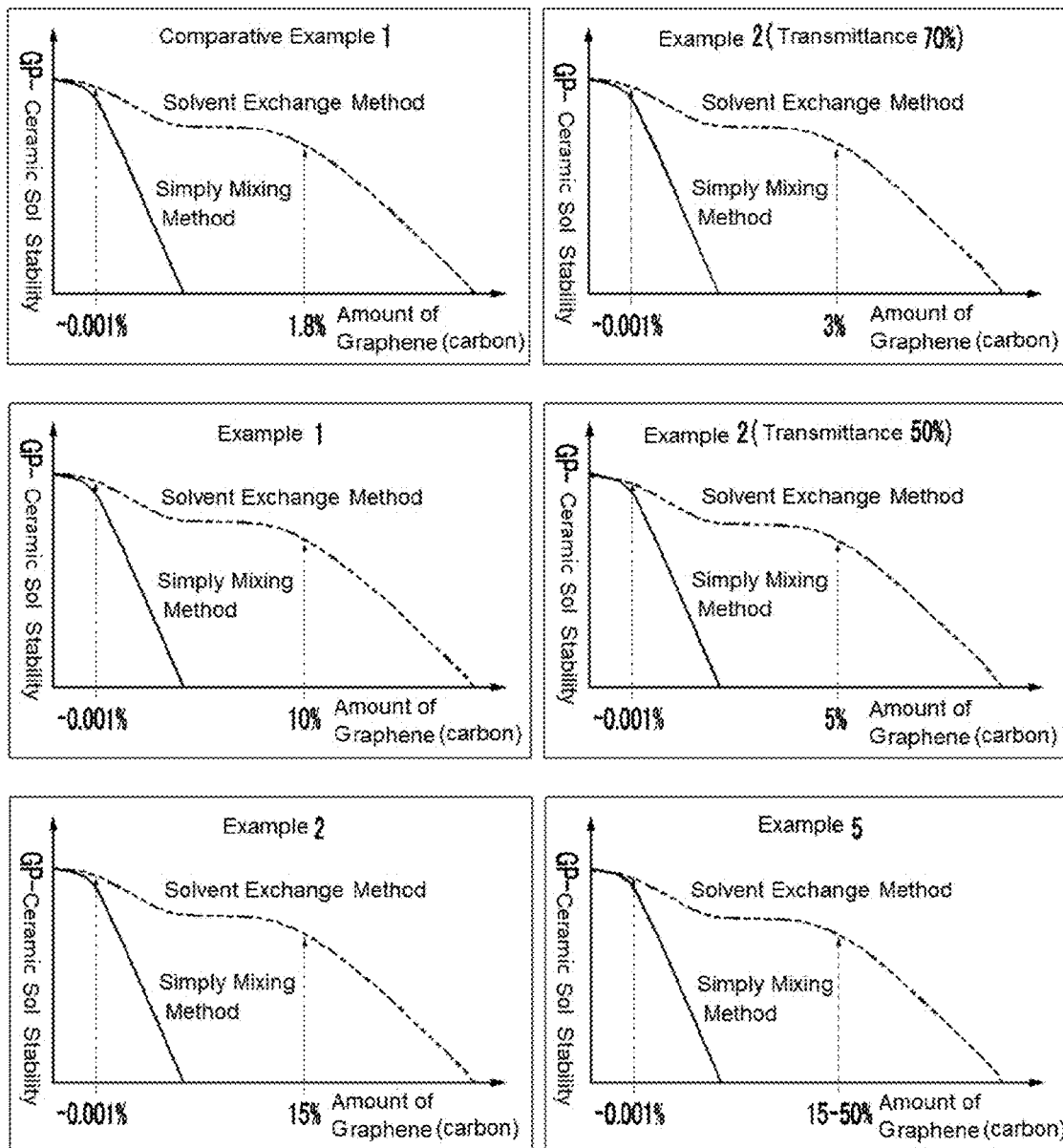
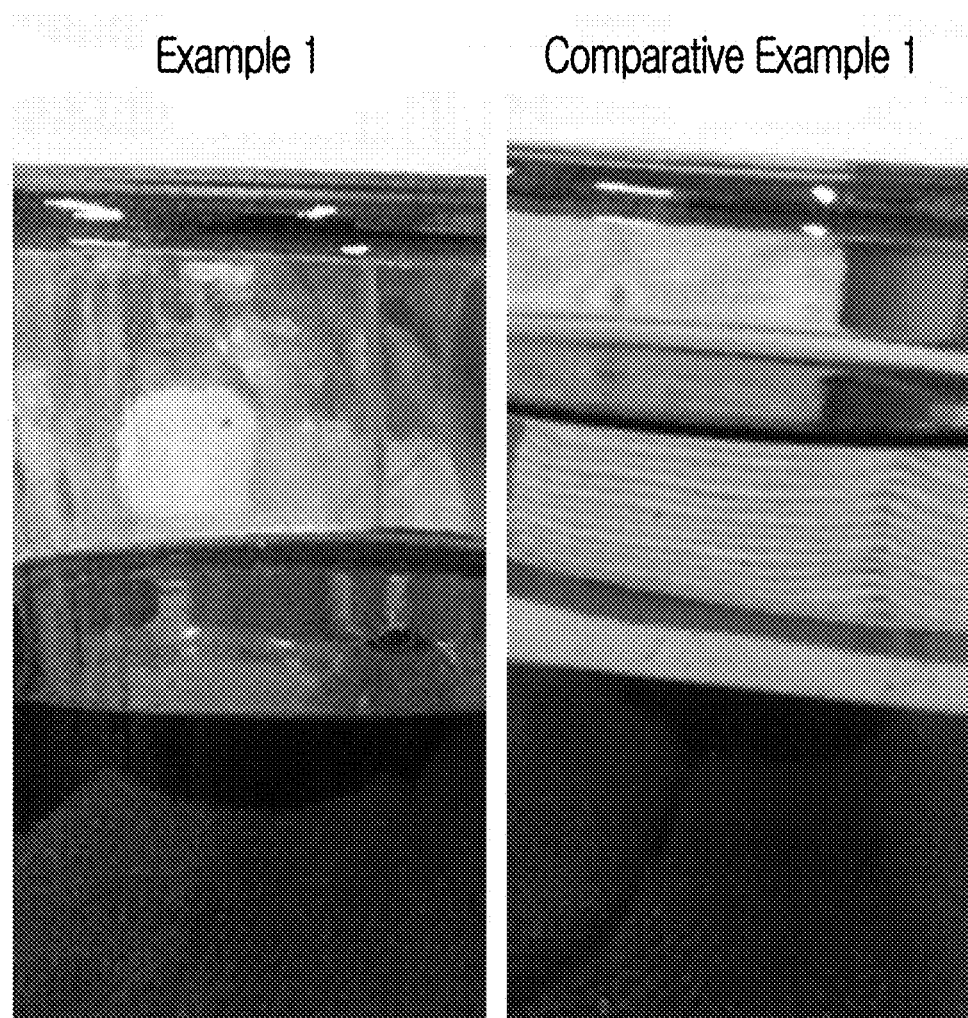


FIG. 5



**FIG. 6**



**FIG. 7**

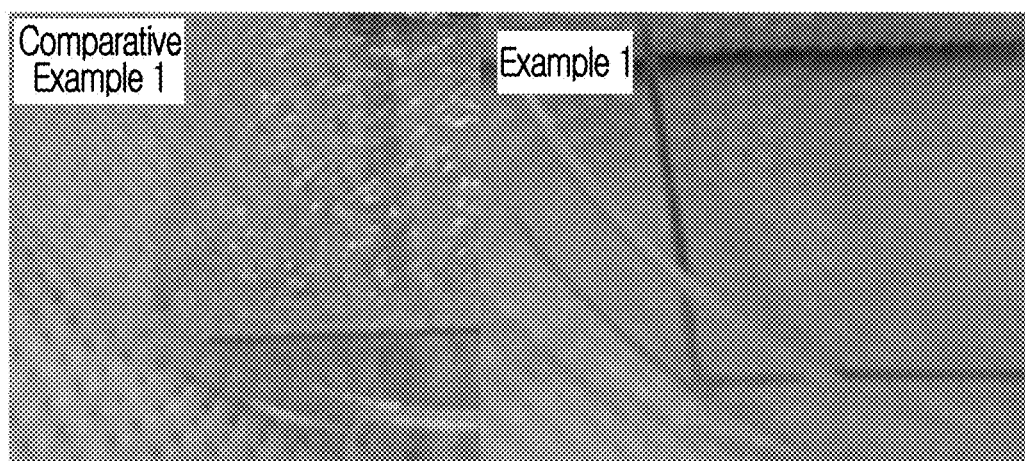


FIG. 8

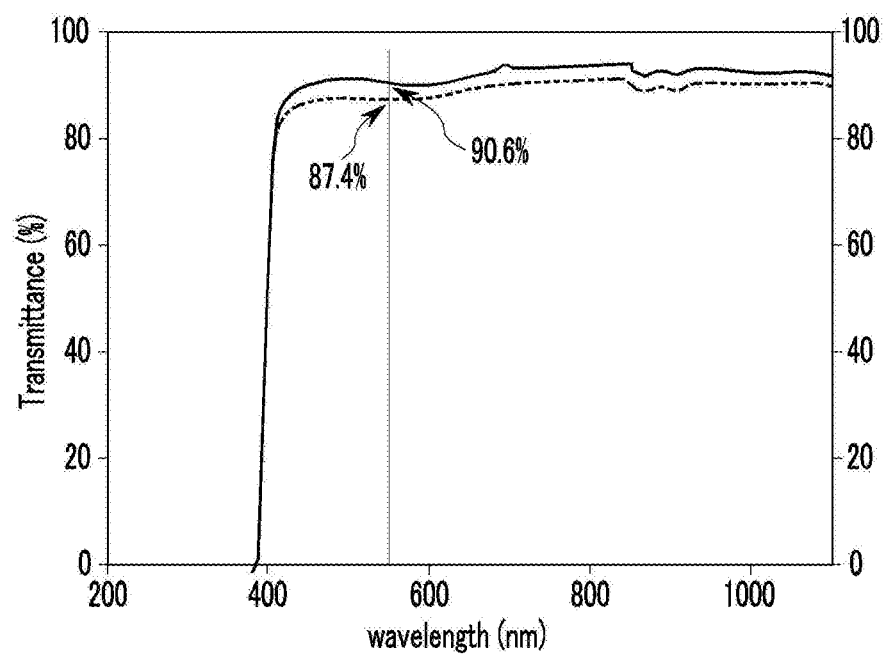


FIG. 9

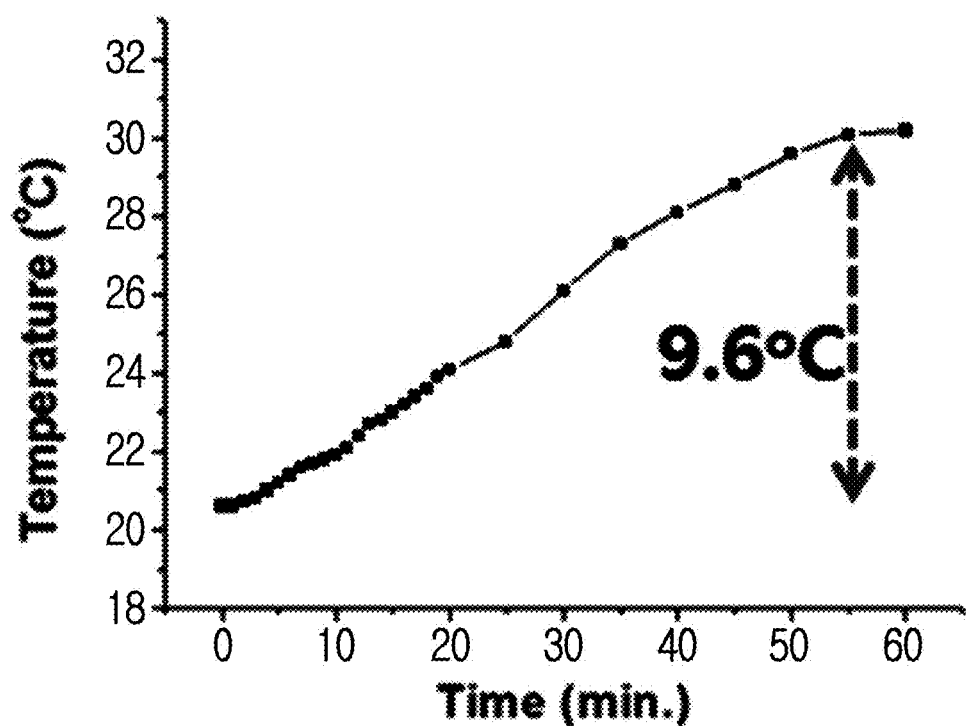
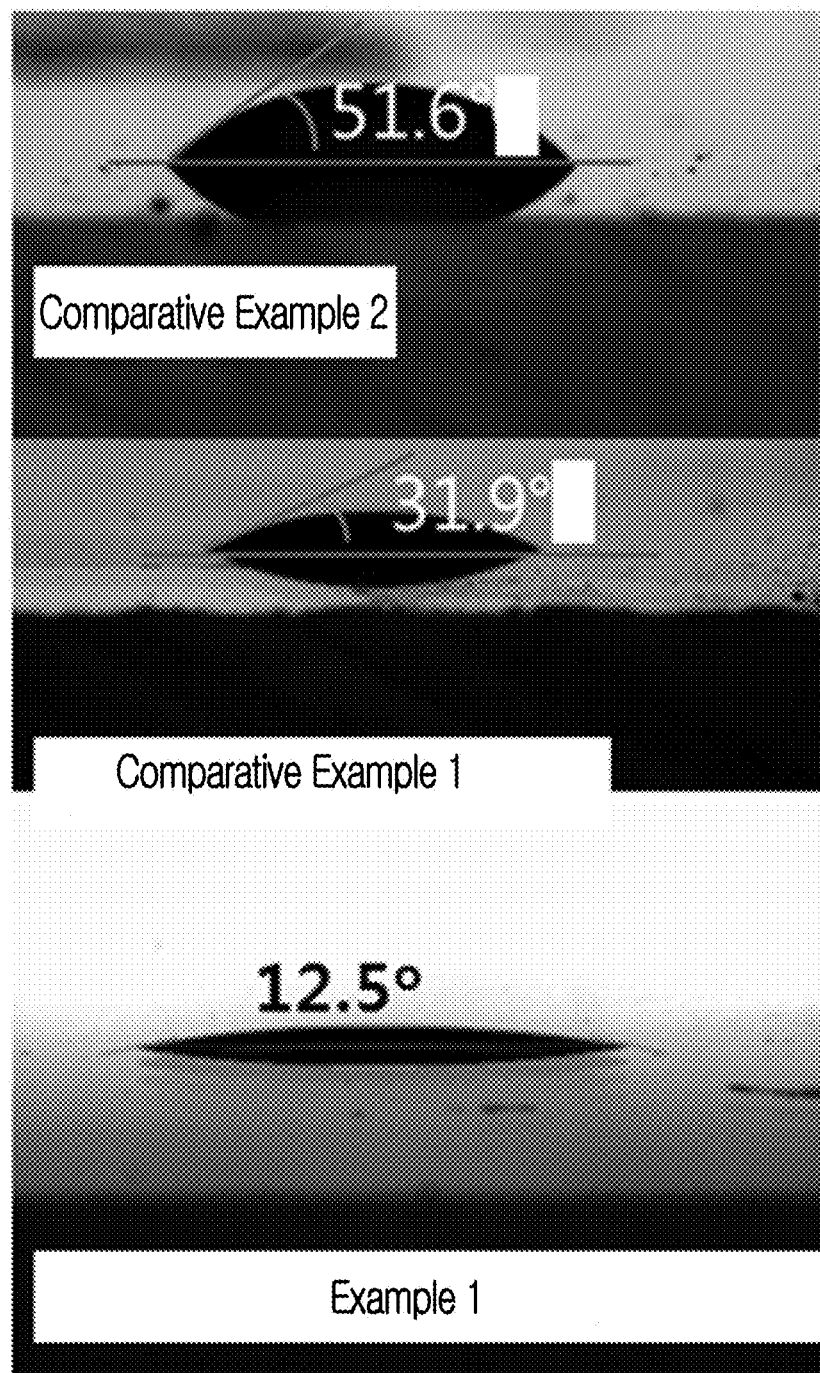
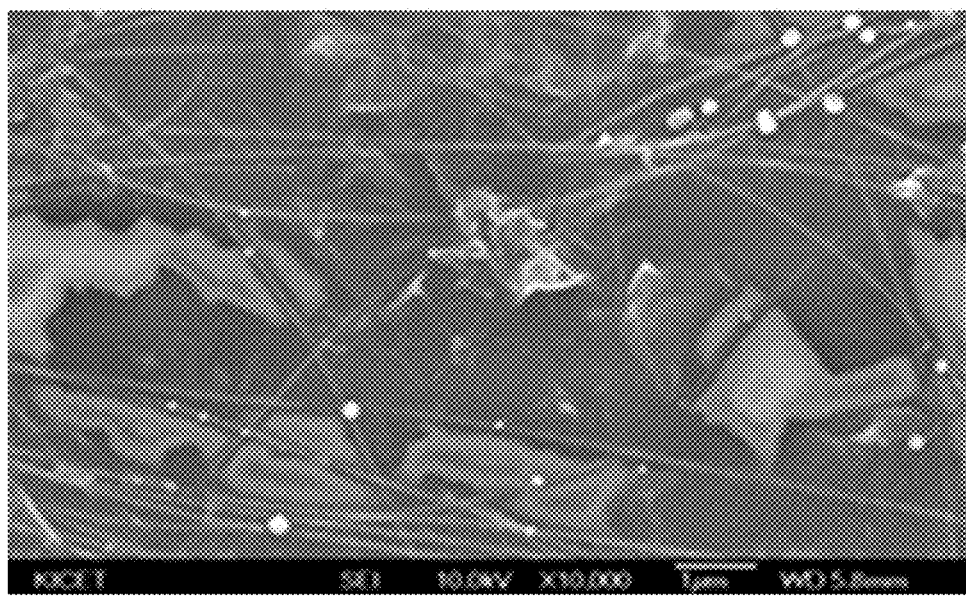


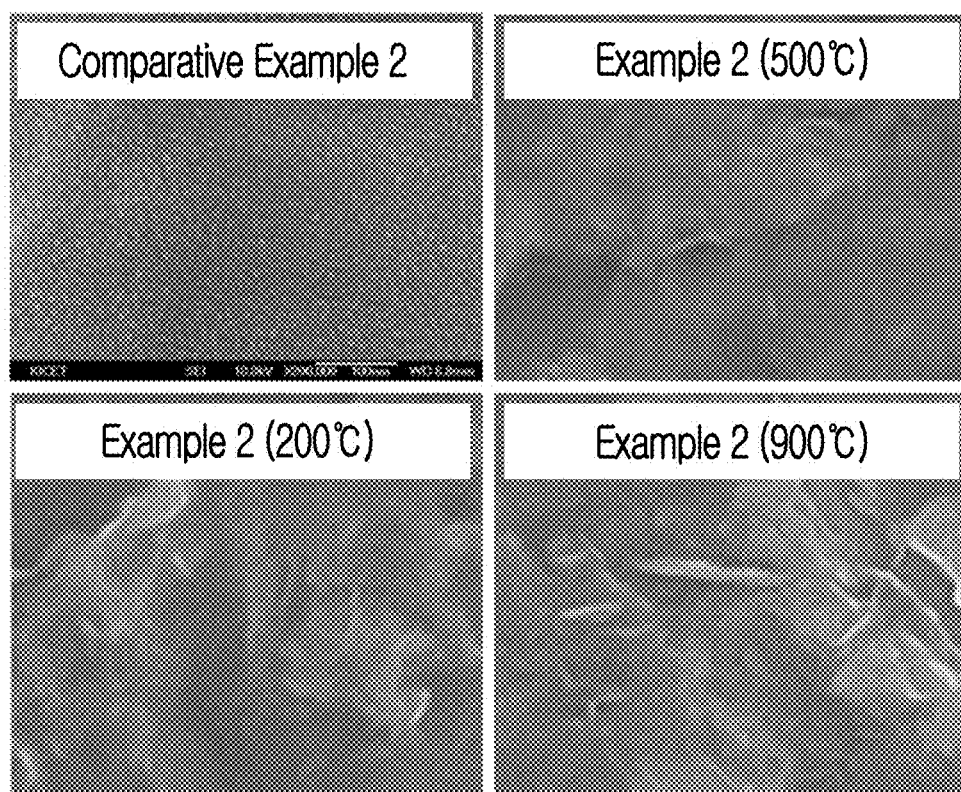
FIG. 10



**FIG. 11**



**FIG. 12**



## 1

**GRAPHENE-CONTAINING COATING FILM,  
AND METHOD FOR PREPARING THE  
SAME**

**CROSS-REFERENCE TO RELATED  
APPLICATION**

This application claims priority to and the benefit of Korean Patent Application No. 10-2015-0119555 filed in the Korean Intellectual Property Office on Aug. 25, 2015, the entire contents of which are incorporated herein by reference.

**TECHNICAL FIELD**

The present invention relates to a graphene-containing coating film and a method of preparing the same.

**BACKGROUND OF THE INVENTION**

Graphene oxide (or graphite oxide, hereinafter GO) is a sheet-shaped carbon material prepared by acid treating graphite, and has a large amount of a hydrophilic functional group such as a carboxyl group (—COOH), a hydroxyl group (—OH), and the like on the surface. The surface oxidizing groups produced through an acid treatment process spontaneously produce hydrogen-bonds with H<sub>2</sub>O molecules, and thus the GO can be prepared in a form of a hydration or in a water-containing slurry state. In general, a solid concentration of the slurry is of about 2 to 8 wt % unless otherwise specifically treated.

When the GO is appropriately included in a film or a structure, strength thereof may be improved and suitable thermal conductivity may be provided, but treatment of the contained moisture may hinder properties.

In general, GO may be prepared in a form of graphene through a chemical reduction method (a hydrazine treatment and the like) and a thermal reduction method. Herein, reduced graphene is particularly referred to as reduced graphene oxide (RGO).

It is evidenced that a part of the oxidizing groups on the RGO surface is not sufficiently removed. Generally, oxygen content of the surface oxidizing groups is less than or equal to about 5 wt % relative to a carbon backbone, and thus graphene (RGO) of the present invention has an oxygen content of less than or equal to about 5 wt % because of the surface oxidizing groups relative to a carbon backbone.

A heterogeneous mixture of GO, and RGO and a conventional material has recently evoked active interest, and this may improve synergic effects between materials exceeding a limit of the conventional material. The heterogeneous mixture may be used in a high strength composite material and a fuel cell. In certain examples, a graphene-nanowire (semiconductor) hybrid structure where light energy is absorbed in a graphene conductive part and electron-hole pairs are generated (KR 10-2012-0092431 A), a hybrid composite manufacturing method including graphene sheet/carbon nanotube/a polymer nanoparticle (KR 10-2012-0053399 A), a method of manufacturing a positive electrode graphene material for a lithium rechargeable battery that is a hybrid material formed by adding an Fe precursor and a PO<sub>4</sub> precursor (KR 10-2012-0035659 A), a method of manufacturing a graphene composite calcinated body having an excellent charge and discharge ratio by sintering graphene and a metal oxide particle in air (U.S. Pat. No. 8,257,867), a method of manufacturing a graphene-TiO<sub>2</sub> hybrid material by mixing a TiO<sub>2</sub> nanopowder with graphene at a high

## 2

temperature and high pressure and reacting them (US 2012-0149554 A), a method of manufacturing a graphene ceramic composite (KR 2012-0039799A, and KR 2013-0014327A), and the like have been explored.

In addition, Publication Laid-open KR 10-2012-0039799 discloses a technology of improving coating properties of graphene itself by directly chemically bonding a ceramic precursor with a carboxyl group (—COOH) on the edge of GO to improve dispersion. For example, the graphene itself is coated on the edge of the GO through a chemical bond and may induce high electrical conductivity. However, the coating may be weak, since there is no binder between the GO and the coated graphene layer. Publication Laid-open KR 10-2013-0014327 also discloses a method of making a graphene composite by mixing a salt type (e.g., chloride) ceramic precursor with graphene or a graphene oxide and then, calcinating the mixture at a high temperature. However, when the ceramic and the graphene have a directly chemical bond, the sheet-shaped structure of the graphene itself is broken, and the graphene may lose inherent properties.

This problem becomes severe, particularly when the ceramic is oxide, since a carbon component in the graphene is bonded with an oxygen component in the ceramic and released as gas such as CO and CO<sub>2</sub>, leaving a carbon residue as a particle. When an oxide ceramic precursor or oxide ceramic sol is calcinated with graphene, there is a similar problem to the above.

In addition, when graphene is reacted at a low temperature that the graphene has no reaction with oxygen without calcination in order to reduce the problem, there is a stripping problem due to severe deterioration of an interface bond between oxide ceramic and graphene. In other words, hydrophobicity of the graphene may resist against hydrophilicity of the ceramic.

In general, when a ceramic film is formed by coating ceramic sol and gelating it, the film may be destroyed due to evaporation of a solvent and an osmotic pressure during the drying. Meanwhile, when graphene is used to form a hybrid film, the hybrid film including the graphene in an appropriate concentration is actually difficult to form due to diffusion of the graphene into a solvent and prevention of drying (non-uniform drying since a graphene layer is positioned on the surface and prevents movement and diffusion of the solvent).

The hybrid film has difficulty in terms of commercial availability, since the graphene is hardly dispersed layer by layer in a solid-phase matrix to realize properties of a graphene-containing composite. In addition, a specific process example has not been provided yet.

Accordingly, in order to solve the problems, a method of reducing a metal precursor at room temperature to powder it and plating and sputtering graphene to manufacture composite powder or a composite layer has been suggested, and another method of using a polymer resin in an entire amount to avoid the fundamental problem of a ceramic composite is mostly used.

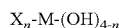
However, the above graphene composite materials are not sufficiently dispersed, and the polymer resin also has a drawback of sharply deteriorating thermal conductivity of the graphene and durability of the film.

**SUMMARY OF THE INVENTION**

In preferred aspects, the present invention provides a graphene-containing coating film having improved thermal

conductivity and surface functionality (hydrophilicity) and a method of preparing the same.

In one aspect, provided is a graphene-containing coating film. The coating film may comprise: at least one hydrate represented by Chemical Formula 1, graphene positioned on the surface, particularly in a shape of discontinuous island, of the hydrate represented by Chemical Formula 1, and a silica particle positioned on the surface of the hydrate of Chemical Formula 1 and positioned on the surface of the graphene in a shape of discontinuous island. In particular, the silica particle may include agglomeration of a plurality of silica nanoparticles.



[Chemical Formula 1]

In Chemical Formula 1,  
M is selected from the group consisting of Si, Ti, Ag, Sn, In, and Zn, or a combination thereof,

X is: a) a C1 to C30 alkyl group substituted or unsubstituted with at least one functional group selected from the group consisting of an epoxy group, a glycidoxyl group, a vinyl group, an acryl group, a methacryl group, a carboxyl group, an amino group, a thiol group, a phosphoric acid group, a fluoro group, a chloro group, a bromo group, an iodine group, a hydroxy group, a substituted or unsubstituted C1 to C10 alkoxy group, a substituted or unsubstituted C1 to C10 ketone group, a substituted or unsubstituted C1 to C10 amine group, a substituted or unsubstituted C1 to C10 sulfur group, a substituted or unsubstituted C1 to C10 ester group, and a substituted or unsubstituted C1 to C10 silyl group; b) a C1 to C30 alkenyl group substituted or unsubstituted with at least one functional group selected from the group consisting of an epoxy group, a glycidoxyl group, a vinyl group, an acryl group, a methacryl group, a carboxyl group, an amino group, a thiol group, a phosphoric acid group, a fluoro group, a chloro group, a bromo group, an iodine group, a hydroxy group, a substituted or unsubstituted C1 to C10 alkoxy group, a substituted or unsubstituted C1 to C10 ketone group, a substituted or unsubstituted C1 to C10 amine group, a substituted or unsubstituted C1 to C10 sulfur group, a substituted or unsubstituted C1 to C10 ester group, and a substituted or unsubstituted C1 to C10 silyl group; or

c) a C1 to C30 alkynyl group substituted or unsubstituted with at least one functional group selected from the group consisting of an epoxy group, a glycidoxyl group, a vinyl group, an acryl group, a methacryl group, a carboxyl group, an amino group, a thiol group, a phosphoric acid group, a fluoro group, a chloro group, a bromo group, an iodine group, a hydroxy group, a substituted or unsubstituted C1 to C10 alkoxy group, a substituted or unsubstituted C1 to C10 ketone group, a substituted or unsubstituted C1 to C10 amine group, a substituted or unsubstituted C1 to C10 sulfur group, a substituted or unsubstituted C1 to C10 ester group, and a substituted or unsubstituted C1 to C10 silyl group, and n is an integer of 1 to 3.

The “silica nanoparticles” as used herein refer to particles made of silica or substantially homogeneous silica and the particles may have average size less than about 990 nm, less than about 900 nm, less than about 800 nm, less than about 700 nm, less than about 600 nm, less than about 500 nm, or less than about 400 nm. The graphene-containing coating film may include: 1) a first region including the hydrate represented by Chemical Formula 1 and the silica particle bound with each other; and 2) a second region including the hydrate represented by Chemical Formula 1, the graphene and the silica particle bound with one another.

An average diameter of the silica particle of the first region may be from about 5 nm to about 50 nm, and an average diameter of the silica particle of the second region may be from about 5 nm to about 25 nm.

5 An average diameter of the silica nanoparticle may be from about 5 nm to about 30 nm. A thickness of the graphene may be from about 0.4 nm to about 5 nm. A major axis length of the graphene may be from about 100 nm to about 10,000 nm, and a minor axis length of the graphene may be from about 100 nm to about 900 nm.

10 An amount of the graphene may be from about 0.001 wt % to about 50 wt % based on the total weight of the hydrate represented by Chemical Formula 1, the graphene, and the silica nanoparticle.

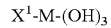
15 When transmittance is greater than or equal to about 70%, the amount of the graphene may be from about 0.001 wt % to about 3 wt % based on the total weight of the hydrate represented by Chemical Formula 1, the graphene, and the silica nanoparticle.

20 The “transmittance” as used herein refers to a fraction (%) of the light transmitted through the graphene-containing coating film from the initially radiated light. The wavelength of the light transmitted through the film is not particularly limited, but the transmittance may be measured with the light having the wavelength within infrared, visible light or ultraviolet (UV) light regions. For instance, the transmittance of the film may be measured at visible light regions at the wavelength of about 400 nm to 700 nm.

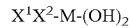
25 The graphene-containing coating film may have a thickness of about 100 nm to 2  $\mu\text{m}$ .

30 When transmittance is greater than or equal to about 70%, the graphene-containing coating film may have a thickness of about 200 nm to 500 nm.

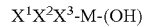
35 The Chemical Formula 1 may be represented by one of Chemical Formulae 1-1 to 1-3.



[Chemical Formula 1-1]



[Chemical Formula 1-2]



[Chemical Formula 1-3]

In Chemical Formulae 1-1 to 1-3,

M is selected from the group consisting of Si, Ti, Ag, Sn, In, and Zn, or a combination thereof,

45  $X^1$ ,  $X^2$ , and  $X^3$  are each independently a) a C1 to C30 alkyl group substituted or unsubstituted with at least one functional group selected from an epoxy group, a glycidoxyl group, a vinyl group, an acryl group, a methacryl group, a carboxyl group, an amino group, a thiol group, a phosphoric acid group, a fluoro group, a chloro group, a bromo group, an iodine group, a hydroxy group, a substituted or unsubstituted C1 to C10 alkoxy group, a substituted or unsubstituted C1 to C10 ketone group, a substituted or unsubstituted C1 to C10 amine group, a substituted or unsubstituted C1 to C10 sulfur group, a substituted or unsubstituted C1 to C10 ester group, and a substituted or unsubstituted C1 to C10 silyl group;

50 b) a C1 to C30 alkenyl group substituted or unsubstituted with at least one functional group selected from an epoxy group, a glycidoxyl group, a vinyl group, an acryl group, a methacryl group, a carboxyl group, an amino group, a thiol group, a phosphoric acid group, a fluoro group, a chloro group, a bromo group, an iodine group, a hydroxy group, a substituted or unsubstituted C1 to C10 alkoxy group, a substituted or unsubstituted C1 to C10 ketone group, a substituted or unsubstituted C1 to C10 amine group, a substituted or unsubstituted C1 to C10 sulfur group, a substituted or unsubstituted C1 to C10 ester group, and a substituted or unsubstituted C1 to C10 silyl group;

55 c) a C1 to C30 alkynyl group substituted or unsubstituted with at least one functional group selected from an epoxy group, a glycidoxyl group, a vinyl group, an acryl group, a methacryl group, a carboxyl group, an amino group, a thiol group, a phosphoric acid group, a fluoro group, a chloro group, a bromo group, an iodine group, a hydroxy group, a substituted or unsubstituted C1 to C10 alkoxy group, a substituted or unsubstituted C1 to C10 ketone group, a substituted or unsubstituted C1 to C10 amine group, a substituted or unsubstituted C1 to C10 sulfur group, a substituted or unsubstituted C1 to C10 ester group, and a substituted or unsubstituted C1 to C10 silyl group;

60 d) a C1 to C30 alkyl group substituted or unsubstituted with at least one functional group selected from an epoxy group, a glycidoxyl group, a vinyl group, an acryl group, a methacryl group, a carboxyl group, an amino group, a thiol group, a phosphoric acid group, a fluoro group, a chloro group, a bromo group, an iodine group, a hydroxy group, a substituted or unsubstituted C1 to C10 alkoxy group, a substituted or unsubstituted C1 to C10 ketone group, a substituted or unsubstituted C1 to C10 amine group, a substituted or unsubstituted C1 to C10 sulfur group, a substituted or unsubstituted C1 to C10 ester group, and a substituted or unsubstituted C1 to C10 silyl group;

65 e) a C1 to C30 alkenyl group substituted or unsubstituted with at least one functional group selected from an epoxy group, a glycidoxyl group, a vinyl group, an acryl group, a methacryl group, a carboxyl group, an amino group, a thiol group, a phosphoric acid group, a fluoro group, a chloro group, a bromo group, an iodine group, a hydroxy group, a substituted or unsubstituted C1 to C10 alkoxy group, a substituted or unsubstituted C1 to C10 ketone group, a substituted or unsubstituted C1 to C10 amine group, a substituted or unsubstituted C1 to C10 sulfur group, a substituted or unsubstituted C1 to C10 ester group, and a substituted or unsubstituted C1 to C10 silyl group;

f) a C1 to C30 alkynyl group substituted or unsubstituted with at least one functional group selected from an epoxy group, a glycidoxyl group, a vinyl group, an acryl group, a methacryl group, a carboxyl group, an amino group, a thiol group, a phosphoric acid group, a fluoro group, a chloro group, a bromo group, an iodine group, a hydroxy group, a substituted or unsubstituted C1 to C10 alkoxy group, a substituted or unsubstituted C1 to C10 ketone group, a substituted or unsubstituted C1 to C10 amine group, a substituted or unsubstituted C1 to C10 sulfur group, a substituted or unsubstituted C1 to C10 ester group, and a substituted or unsubstituted C1 to C10 silyl group;

## 5

substituted or unsubstituted C1 to C10 ester group, and a substituted or unsubstituted C1 to C10 silyl group; or c) a C1 to C30 alkynyl group substituted or unsubstituted with at least one functional group selected from an epoxy group, a glycidoxyl group, a vinyl group, an acryl group, a methacryl group, a carboxyl group, an amino group, a thiol group, a phosphoric acid group, a fluoro group, a chloro group, a bromo group, an iodine group, a hydroxy group, a substituted or unsubstituted C1 to C10 alkoxy group, a substituted or unsubstituted C1 to C10 ketone group, a substituted or unsubstituted C1 to C10 amine group, a substituted or unsubstituted C1 to C10 sulfur group, a substituted or unsubstituted C1 to C10 ester group, and a substituted or unsubstituted C1 to C10 silyl group.

Preferably, M may be Si or Ti.

The graphene-containing coating film may further include an additive selected from the group consisting of an inorganic powder, an organic additive, and a combination thereof.

The inorganic powder may have an average diameter of about 5 nm to 50 nm.

In another aspect, provided is a method of preparing a graphene-containing coating film. The method may comprise: dispersing a graphene; mixing and dispersing a silica nanoparticle and the precursor of the hydrate represented by Chemical Formula 1 in a hydrophilic solvent and mixing the same with the dispersed graphene; performing hydrolysis and condensation reactions of the mixed dispersed solution to prepare a graphene-containing sol solution; coating the graphene-containing sol solution on a substrate and drying the same at a temperature of about 25° C. to 400° C.; and heat-treating the dried film at a temperature of about 50° C. to 900° C.

The silica nanoparticle may be present in an amount of about 5 to 20 wt % based on the total amount of the mixed dispersed solution; the precursor of the hydrate represented by Chemical Formula 1 may be present in an amount of about 10 to 40 wt % based on the total amount of the mixed dispersed solution; the dispersed graphene may be present in an amount of about 0.001 to 15 wt % based on the total amount of the mixed dispersed solution; and the hydrophilic solvent may be present in a balance amount.

The graphene may be dispersed by mechanical disperse treatment, or a solvent exchange method.

Preferably, the solvent exchange method may include: preparing dispersion by mixing a graphene powder, a first dispersing agent and a first non-aqueous based solvent; preparing a mixture by adding a second non-aqueous based solvent and a precursor of the hydrate to the dispersion; preparing a graphene-containing sol solution by mixing the mixture with a second dispersing agent and water.

In the process of the mixing and dispersing of a silica nanoparticle and the precursor of the hydrate represented by Chemical Formula 1 in a hydrophilic solvent and mixing the same with the dispersed graphene, an additive selected from the group consisting of an inorganic powder, an organic additive, and a combination thereof may be further included.

The inorganic powder may be mixed in an amount of about 5 parts by weight to 30 parts by weight based on 100 parts by weight of the mixed dispersed solution.

The organic additive may be mixed in an amount of about 0.01 parts by weight to 10 parts by weight based on 100 parts by weight of the mixed dispersed solution.

Preferred precursors of the hydrate represented by Chemical Formula 1 may be, for example, selected from the group consisting of trimethoxysilane, triethoxysilane, methyltrimethoxysilane, methyltriethoxysilane, ethyltrimethoxysilane, ethyltriethoxysilane, propyltrimethoxysilane, propyltriethoxysilane, isobutyltriethoxysilane, glycidoxypropyltrimethoxysilane, glycidoxypropyltriethoxysilane, cyclohexyltrimethoxysilane, phenyltrimethoxysilane, phenyltriethoxysilane, vinyltrimethoxysilane, vinyltriethoxysilane, allyltrimethoxysilane, allyltriethoxysilane, dimethyltrimethoxysilane, dimethyldiethoxysilane, diphenyltrimethoxysilane, diphenyldiethoxysilane, (N,N-dimethylaminopropyl)trimethoxysilane, (N,N-dimethylaminopropyl)triethoxysilane, and N,N-{(2-aminoethyl)(3-aminopropyl)}trimethoxysilane, or a combination thereof.

Further provided are vehicle parts that comprising the graphene-containing coating film as described above. Such vehicle parts may include a head lamp of a vehicle.

The present invention also includes vehicles that comprise a vehicle part such as a head lamp that comprises the graphene-containing coating film as described herein.

The present invention may provide a graphene-containing sol solution having improved stability and dispersability. In particular, the graphene-containing coating film may have improved dispersion of graphene, an interface bond, graphene stability, and surface functionality. Further provided are vehicle parts such as a head lamp of a vehicle comprising the graphene-containing coating film as described herein.

Also provided are vehicles that comprise the vehicle parts such as a head lamp that comprises the graphene-containing coating film as described herein.

## 30 BRIEF DESCRIPTION OF THE DRAWINGS

FIG. 1 shows a FE-SEM photograph of an exemplary graphene-containing coating film according to an exemplary embodiment of the present invention.

FIGS. 2A-2B show exemplary graphene-containing coating films according to Example 1 (FIG. 2C), and Comparative Examples 1 (FIG. 2A) and 2 (FIG. 2B).

FIG. 3 shows various forms of hydrate included in an exemplary coating composition for forming an exemplary graphene-containing sol according to an exemplary embodiment of the present invention.

FIG. 4 shows the condensed form of an exemplary hydrate precursor in an exemplary graphene-containing coating film according to an exemplary embodiment of the present invention.

FIG. 5 is a graph showing the content of graphene in graphene-containing coating films maintaining sol stability in various exemplary embodiments of the present invention.

FIG. 6 shows a photographic view of dispersion stability and storage-stability of an exemplary coating composition for forming an exemplary graphene-containing sol according to an exemplary embodiment of the present invention.

FIG. 7 shows a photographic view of uniformity and transparency of an exemplary graphene-containing coating film according to an exemplary embodiment of the present invention.

FIG. 8 is a graph showing transmittance of an exemplary graphene-containing coating film according to an exemplary embodiment of the present invention.

FIG. 9 is a graph showing thermal conductivity of an exemplary graphene-containing coating film according to an exemplary embodiment of the present invention.

FIG. 10 shows waterdrop contact angle of exemplary graphene-containing coating films according to various exemplary embodiments of the present invention.

FIG. 11 shows a field emission-scanning electron microscope (FE-SEM) photograph of an exemplary graphene-

containing coating film according to an exemplary embodiment of the present invention.

FIG. 12 shows FE-SEM photographs of exemplary heat-treated graphene-containing coating films according to various exemplary embodiments of Comparative Example and the present invention.

#### DESCRIPTION OF SYMBOLS

10: ceramic sol

20: graphene

30: silica nanoparticle

#### DETAILED DESCRIPTION

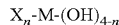
The terminology used herein is for the purpose of describing particular exemplary embodiments only and is not intended to be limiting of the invention. As used herein, the singular forms “a”, “an” and “the” are intended to include the plural forms as well, unless the context clearly indicates otherwise. It will be further understood that the terms “comprises” and/or “comprising,” when used in this specification, specify the presence of stated features, integers, steps, operations, elements, and/or components, but do not preclude the presence or addition of one or more other features, integers, steps, operations, elements, components, and/or groups thereof. As used herein, the term “and/or” includes any and all combinations of one or more of the associated listed items.

Unless specifically stated or obvious from context, as used herein, the term “about” is understood as within a range of normal tolerance in the art, for example within 2 standard deviations of the mean. “About” can be understood as within 10%, 9%, 8%, 7%, 6%, 5%, 4%, 3%, 2%, 1%, 0.5%, 0.1%, 0.05%, or 0.01% of the stated value. Unless otherwise clear from the context, all numerical values provided herein are modified by the term “about.”

Further, it is understood that the term “vehicle” or “vehicular” or other similar term as used herein is inclusive of motor vehicles in general such as passenger automobiles including sports utility vehicles (SUV), buses, trucks, various commercial vehicles, watercraft including a variety of boats and ships, aircraft, and the like, and includes hybrid vehicles, electric vehicles, plug-in hybrid electric vehicles, hydrogen-powered vehicles and other alternative fuel vehicles (e.g. fuels derived from resources other than petroleum). As referred to herein, a hybrid vehicle is a vehicle that has two or more sources of power, for example both gasoline-powered and electric-powered vehicles.

Hereinafter, embodiments of the present invention are described in detail. However, these embodiments are exemplary, and this disclosure is not limited thereto.

An graphene-containing coating film according to an exemplary embodiment may comprise: at least one hydrate represented by Chemical Formula 1, a graphene positioned in a shape of discontinuous island on the surface of the hydrate represented by Chemical Formula 1 and a silica particle positioned on the surface of the hydrate of Chemical Formula 1 and positioned on the surface of the graphene in a shape of discontinuous island. In particular, the silica particle may include agglomeration of a plurality of silica nanoparticles.



[Chemical Formula 1]

In Chemical Formula 1,

M is selected from the group consisting of Si, Ti, Ag, Sn, In, and Zn, and a combination thereof,

X is: a) a C1 to C30 alkyl group substituted or unsubstituted with at least one functional group selected from the group consisting of an epoxy group, a glycidoxyl group, a vinyl group, an acryl group, a methacryl group, a carboxyl group, an amino group, a thiol group, a phosphoric acid group, a fluoro group, a chloro group, a bromo group, an iodine group, a hydroxy group, a substituted or unsubstituted C1 to C10 alkoxy group, a substituted or unsubstituted C1 to C10 ketone group, a substituted or unsubstituted C1 to C10 amine group, a substituted or unsubstituted C1 to C10 sulfur group, a substituted or unsubstituted C1 to C10 ester group, and a substituted or unsubstituted C1 to C10 silyl group; b) a C1 to C30 alkenyl group substituted or unsubstituted with at least one functional group selected from the group consisting of an epoxy group, a glycidoxyl group, a vinyl group, an acryl group, a methacryl group, a carboxyl group, an amino group, a thiol group, a phosphoric acid group, a fluoro group, a chloro group, a bromo group, an iodine group, a hydroxy group, a substituted or unsubstituted C1 to C10 alkoxy group, a substituted or unsubstituted C1 to C10 ketone group, a substituted or unsubstituted C1 to C10 amine group, a substituted or unsubstituted C1 to C10 sulfur group, a substituted or unsubstituted C1 to C10 ester group, and a substituted or unsubstituted C1 to C10 silyl group; or c) a C1 to C30 alkynyl group substituted or unsubstituted with at least one functional group selected from the group consisting of an epoxy group, a glycidoxyl group, a vinyl group, an acryl group, a methacryl group, a carboxyl group, an amino group, a thiol group, a phosphoric acid group, a fluoro group, a chloro group, a bromo group, an iodine group, a hydroxy group, a substituted or unsubstituted C1 to C10 alkoxy group, a substituted or unsubstituted C1 to C10 ketone group, a substituted or unsubstituted C1 to C10 amine group, a substituted or unsubstituted C1 to C10 sulfur group, a substituted or unsubstituted C1 to C10 ester group, and a substituted or unsubstituted C1 to C10 silyl group.

n is an integer of 1 to 3.

The hydrate represented by Chemical Formula 1 may be stably bound to the interface of the silica nanoparticle and the graphene in a hydrophilic sol solution because an organic functional group of the hydrate is fused with a hydrophilic group of the hydrophilic sol solution due to at least one organic functional group represented by “X”. These may be stable during drying and heat-treating processes, and have buffering effect even an excess amount of an organic additive and an organic additive, forming a stable film.

The functional group of the hydrate may have hydrophilic characteristics, for example an epoxy group, a ketone group, a carboxyl group, a hydroxy group, an amino group, an amine group (e.g., primary, secondary, or tertiary amine), a thiol group, a phosphoric acid group, a halide group (e.g., F, Cl, Br, or I), an ester group, or an alkyl group, an alkenyl group, or an alkynyl group including O, S, P, N, Si, and the like in the backbone, or a salt of an organic or inorganic material.

X is not particularly limited to a size of a molecular weight. However, when being an oligomer, a macromolecule or a polymer, X may bind neighboring molecules by a hydrated functional group therein being capable of inducing a second, a third sol-gel reaction, that is —Si—OH, —Si(OH)<sub>2</sub>, or —Si(OH)<sub>3</sub> and may spread a sol-gel reaction.

Examples of the organic functional group of X may be a substituted or unsubstituted C1 to C30 alkyl group; C1 to C30 alkenyl group; or C1 to C30 alkynyl group substituted with at least one functional group selected from the group consisting of an epoxy group, a glycidoxyl group, a vinyl

group, an acryl group, a methacryl group, a carboxyl group, an amino group, a thiol group, a phosphoric acid group, a fluoro group, a chloro group, a bromo group, an iodine group, a hydroxy group, a substituted or unsubstituted C1 to C10 alkoxy group, a substituted or unsubstituted C1 to C10 ketone group, a substituted or unsubstituted C1 to C10 amine group, a substituted or unsubstituted C1 to C10 sulfur group, a substituted or unsubstituted C1 to C10 ester group and a substituted or unsubstituted C1 to C10 silyl group.

By stating herein that a particular group may be "substituted or unsubstituted" means that the group may be optionally substituted at one or more available positions by groups such as, for example, an epoxy group, a glycidoxyl group, a vinyl group, an acryl group, a methacryl group, a carboxyl group, an amino group, a thiol group, a phosphoric acid group, a fluoro group, a chloro group, a bromo group, an iodine group, a hydroxy group, a substituted or unsubstituted C1 to C10 alkoxy group, a substituted or unsubstituted C1 to C10 ketone group, a substituted or unsubstituted C1 to C10 amine group, a substituted or unsubstituted C1 to C10 sulfur group, a substituted or unsubstituted C1 to C10 ester group and a substituted or unsubstituted C1 to C10 silyl group.

The Chemical Formula 1 may be represented by one of Chemical Formulae 1-1 to 1-3.



In Chemical Formulae 1-1 to 1-3,  $X^1$ ,  $X^2$  and  $X^3$  may be the same as X, or may be different.

M may be selected from the group consisting of Si, Ti, Ag, Sn, In, and Zn, and a combination thereof. Preferably, M may be Si or Ti.

In an exemplary embodiment, when the M is Si, exemplary precursors of silicon-based compounds may be selected from the group consisting of trimethoxysilane, triethoxysilane, methyltrimethoxysilane, methyltriethoxysilane, ethyltrimethoxysilane, ethyltriethoxysilane, propyltrimethoxysilane, propyltriethoxysilane, isobutyltriethoxysilane, glycidoxypropyltriethoxysilane, cyclohexyltrimethoxysilane, phenyltrimethoxysilane, phenyltriethoxysilane, vinyltrimethoxysilane, vinyltriethoxysilane, allyltrimethoxysilane, allyltriethoxysilane, dimethyl-dimethoxysilane, dimethyltriethoxysilane, diphenyldimethoxysilane and diphenyldiethoxysilane, (N,N-dimethylaminopropyl)trimethoxysilane, (N,N-dimethylaminopropyl)triethoxysilane, and N,(2-aminoethyl)(3-aminopropyl)trimethoxysilane, or combinations thereof, but are not limited thereto.

In addition, the silicon-based compounds may be precursors that have a M-OR bond (alkoxy bond) with other metal, M, or a M-OOR bond (ester bond).

Preferably, the hydrate represented by Chemical Formula 1 may be a hydrolyzed ceramic precursor, for example  $X^1\text{-Si-(OH)}_3$ ,  $X^1X^2\text{-Si-(OH)}_2$ ,  $X^1X^2X^3\text{-Si-(OH)}$  and the like as shown in FIG. 3. Herein, when an organic material component, a precursor reagent including  $X^1$ ,  $X^2$ , and  $X^3$  is hydrolyzed, modified groups (chemical modification, or formation of a complex, or a salt) of  $X^1$ ,  $X^2$  and  $X^3$ , interface properties with graphene may be improved and organic materials may first react with carbon of the graphene, protecting graphene.

The  $X^1$ ,  $X^2$ , and  $X^3$  may be the same or different.

During formation of the graphene-containing coating film,  $X^1$ ,  $X^2$ , and  $X^3$  may be polymerized (forming a network) as shown in FIG. 4. It may have a condensed form where a —Si—O—Si-bond is formed, and substituent moieties of  $X^1$ ,  $X^2$ , and  $X^3$  may provide a —Si- and —O—Si-bond. Particularly, when a X moiety includes an organic functional group such as an epoxy group, a hardener may be used to cure the X moiety.

The hardener may cure a curable resin, and the curing may be performed by a reaction using a catalyst, or cross-linking by a hardener.

The hardener is not particularly limited, and may be any commercial compound for a hardener of a general epoxy resin. For example, the hardener may be selected from the group consisting of an amine-based compound, an amide-based compound, an acid anhydride-based compound, a phenol-based compound and the like. Specifically, the amine-based compound may be diaminodiphenylmethane, ethylenediamine, diethylenetriamine, triethylenetetramine, diaminodiphenylsulfone, isophoronediamine, imidazole, BF<sub>3</sub>-amine a complex, guanidine derivative, and the like, the amide-based compound may be dicyandiamide, a polyamide resin synthesized from a linolenic acid dimer ethylenediamine, an acid anhydride-based compound, phthalic anhydride, trimellitic anhydride, pyromellitic anhydride, maleic anhydride, tetrahydrophthalic anhydride, methyltetrahydrophthalic anhydride, methyl nadic anhydride, hexahydrophthalic anhydride, methylhexahydrophthalic anhydride, and the like, the phenol-based compound may be a polyvalent phenol compound such as a phenol novolac resin, a cresol novolac resin, an aromatic hydrocarbon formaldehyde resin a modified phenol resin, a dicyclopentadienephenol addition-type resin, a phenol aralkyl resin (xylok resin), a polyvalent phenol novolac resin synthesized from a polyvalent hydroxy compound and formaldehyde such as resorcin novolac resin, a naphthol aralkyl resin, a trimethylolmethane resin, a tetraphenylolethane resin, a naphthol novolac resin, a naphthol-phenol cocondensed novolac resin, a naphthol-cresol cocondensed novolac resin, a biphenyl modified phenol resin (a polyvalent phenol compound including a bis-methylene group linked to a phenolic nucleus), a biphenyl modified naphthol resin (a polyvalent naphthol compound including a bis-methylene group linked to a naphtholic nucleus), a aminotriazine modified phenol resin (a polyvalent phenol compound including melamine, benzoguanamine, and the like linked to phenolic nucleus by a methylene bond) or an alkoxy group-containing aromatic ring modified novolac resin (a polyvalent phenol compound including a phenolic nucleus and alkoxy group-containing aromatic ring linked to formaldehyde) and mixtures thereof.

In an epoxy resin composition of the present invention, amounts of an epoxy resin and a hardener are not particularly limited, but active groups of the hardener may be preferably used in about 0.7 to 1.5 equivalents based on 1 equivalent of the sum of epoxy groups of an epoxy resin.

For example, in the case of glycidoxypropyltriethoxysilane, a hardener such as ethylene diamine may be used for an epoxy group that is an organic functional group of X moieties.

The graphene may be positioned in a shape of discontinuous island on the surface of the hydrate represented by Chemical Formula 1, and a silica particle including a plurality of silica nanoparticle may be agglomerated and positioned on the surface of the graphene.

The "shape of discontinuous island" means that a plurality of island shapes are discontinuously arranged, and the island

## 11

shape refers to a spherical, semispherical, non-spherical, or amorphous shape having a volume, but it is not limited to these specific shapes.

The graphene may improve thermal conductivity, and may be positioned in a shape of discontinuous island, that is a thin and wide sheet-shape on the surface of the hydrate represented by Chemical Formula 1, and thus stability may increase at the interface between the hydrate represented by Chemical Formula 1 and graphene and at the interface between the graphene and the silica nanoparticle.

Particularly, since the silica particles on the surface of the graphene has relatively dense agglomeration relative to silica particle on the surface of the hydrate represented by Chemical Formula 1, a small amount of grain boundaries between the particles may be distributed, and thus it may have a favorable structure for providing characteristics near to hyperhydrophilicity and improved thermal conductivity characteristics.

A thickness of the graphene may be from about 0.4 nm to 5 nm, from about 0.4 nm to about 4 nm, or particularly from about 0.4 nm to about 2.8 nm.

The graphene may have a thickness of about 4 nm, when it has about 10 layers at maximum and a thickness of about 2.8 nm, when it has about 7 layers at maximum.

A major axis length of the graphene may be from about 100 nm to about 10,000 nm, and a minor axis length of the graphene may be from about 100 nm to about 900 nm.

Particularly, the major axis length may be from about 100 nm to about 2,000 nm, and the minor axis length may be from about 100 nm to about 500 nm.

When the graphene has the above thickness and size, hydrophilicity and thermal conductivity of the graphene-containing coating film may be improved, and further hyperhydrophilicity may be provided.

Prefereably, the graphene of the present invention may be a sheet-shaped material having a BASAL plane with a thickness of an atom/molecule to a nano unit, for example, graphene oxide (graphite oxide) consisting of sheet-shaped BASAL planes comprising carbon, rGO (reduced graphene oxide), and a graphene nanoplate (stripped expanded graphite) and further, modified graphene oxide (modification of a substituent, a derivative, a combination with a third material, and like) or doped graphene oxide.

The graphene of the present invention may be manufactured by preparing graphene oxide (commonly called to be GO), radiating energy into the graphene oxide (using a microwave, a photon, IR, a laser, and the like) or reducing the GO in a liquid phase, a gas phase, and a solid-phase. Herein, the reduction includes thermal reduction and chemical reduction.

In addition, the graphene may be stripped layer by layer after being dipped in a solvent having excellent affinity with with graphite and then, treated by an ultrasonic wave and the like. The solvent having excellent affinity with graphite may representatively include GBL, NMP, and the like. The graphene obtained in this method can have good quality but difficulty in a mass production.

In addition, the graphene may be obtained from a chemical synthesis method, a bottom production method, a method of chemically splitting carbon nanotube and folding it, and the like. Further, the graphene may be obtained from a solvent-stripping method of graphite, a mechanically-grinding method of graphite (ultrasonic wave, milling, a gas-phase high speed blading method, an electrical stripping method, a synthesis method, and the like).

On the other hand, oxidizing groups on the surface of the graphene may be completely removed by any currently-

## 12

known method, and an oxygen content by the oxidizing groups on the surface of the graphene except for GO may be less than or equal to about 5 wt % based on the amount of a carbon backbone. In the present invention, unless otherwise indicated, ‘graphene’ is defined when the oxygen content by oxidizing groups on the surface is even less than or equal to about 5 wt % based on the amount of a carbon backbone.

In the present invention, all the above forms are uniformly called as graphene.

In the present invention, highly dispersed graphene is used, and a method of dispersing graphene is described in connection with a manufacturing method later.

The graphene-containing coating film may include 1) a first region including the hydrate represented by Chemical Formula 1 and the silica particle bound with each other; and 2) a second region including the hydrate represented by Chemical Formula 1, the graphene and the silica particle bound with one another.

A structure of the graphene-containing coating film according to an exemplary embodiment of the present invention can be described referring to FIG. 1.

FIG. 1 shows a FE-SEM photograph of an exemplary graphene-containing coating film according to an exemplary embodiment of the present invention.

Referring to FIG. 1, an A region corresponds to the second region, and a B region corresponds to the first region.

The first and second regions may be distinguished by a silica particle shape on the mostouter surface.

The silica particle may comprise silica nanoparticles mostly having an average diameter ranging from about 5 nm to about 30 nm, the silica nanoparticles may be aggregated and variously shape the silica particle. The shape of the particle may be determined depending on a region where these silica nanoparticles are present, that is, a region where these silica nanoparticles are present on the surface of hydrate or where these silica nanoparticles are present on the surface of graphene. The silica nanoparticle may have an average particle diameter ranging from about 5 nm to about 30 nm, or particularly, from about 7 nm to about 25 nm, and accordingly, the present invention may use a silica nanoparticle having, for example, an average particle diameter of about 7 nm, about 15 nm, or about 25 nm.

When the silica nanoparticle has an average particle diameter of greater than about 30 nm, the silica nanoparticle may not be sufficiently attached to a coating film formed from a hybrid sol solution but make the surface of the coating film rough and increase a waterdrop contact angle and thus cause an adverse effect of reducing hydrophilic characteristics.

The first region, in particular, is a region where graphene may not be protruded on the surface and where the silica particle may be directly bonded on the surface of the hydrate represented by Chemical Formula 1.

The silica particle of the first region may have an average diameter of about 5 nm to 50 nm, or particularly of about 10 nm to 50 nm, for example, of about 10 nm to 30 nm.

The silica particle of the first region includes a plurality of grain boundary that may be relatively widely distributed between silica particles while maintaining large and round shape.

On the other hand, the second region may be a region where graphene is protruded on the surface and where graphene is bonded on the surface of the hydrate represented by Chemical Formula 1 and the silica particle is bonded on the surface of the graphene.

The silica particle of the second region may have an average diameter of about 5 nm to 25 nm, or particularly of about 5 nm to 20 nm, for example, of about 5 nm to 15 nm.

The silica particles present in the second region may be densely agglomerated and distributed with a relatively small grain boundary among themselves.

Since the second region where the silica particles formed of densely agglomerated silica nanoparticles is present in the graphene-containing coating film, a waterdrop contact angle may be formed advantageously for hydrophilicity, and thermal conductivity may be improved by graphene included in the second region.

In addition, the graphene included in the second region has a wide and thin sheet-shape and thus may improve bonding stability on the interface and stability of the graphene-containing coating film.

An amount of the graphene in the graphene-containing coating film may be from about 0.001 wt % to about 50 wt %, from about 0.001 wt % to about 30 wt %, or particularly from about 0.001 wt % to about 15 wt % based on the total weight of the hydrate represented by Chemical Formula 1, the graphene, and the silica nanoparticle.

Highly uniformly dispersed graphene may be used. For example, the amount of the graphene may be increasingly included up to about 30 wt % at most in the hybrid coating film by an interaction of the graphene with hydrophilic groups present in an organic functional group of the hydrate represented by Chemical Formula 1 and the silica nanoparticle. Alternatively, the amount of the graphene may be increasingly included up to about 50 wt % at most by adding an additive such as a dispersing agent and the like.

The graphene included in the graphene-containing coating film may improve strength and thermal conductivity of a coating film. However, when the graphene is included in a predetermined level, moisture contained in the graphene may cause non-uniformity of a graphene-ceramic mixture and thus a bonding problem on the interface, failing in obtaining a coating film with a smooth and uniform surface.

Accordingly, the present invention is to improve strength and thermal conductivity of a coating film without a bond on the interface despite addition of graphene beyond a predetermined level.

The additive may be selected from the group consisting of an inorganic powder, an organic additive, and a combination thereof.

The inorganic powder may be further included to apply film functionalities such as stability (a composite effect) and hyperhydrophilicity to the coating film.

Most preferable example of the inorganic powder may be a ceramic particle, and examples of the ceramic particle may be  $\text{SiO}_2$ ,  $\text{Al}_2\text{O}_3$ ,  $\text{Li}_4\text{Ti}_5\text{O}_{12}$ ,  $\text{TiO}_2$ ,  $\text{SnO}_2$ ,  $\text{CeO}_2$ ,  $\text{ZrO}_2$ ,  $\text{V}_2\text{O}_5$ ,  $\text{B}_2\text{O}_3$ ,  $\text{BaTiO}_3$ ,  $\text{Y}_2\text{O}_3$ ,  $\text{WO}_3$ ,  $\text{MgO}$ ,  $\text{CuO}$ ,  $\text{ZnO}$ ,  $\text{AlPO}_4$ ,  $\text{AlF}_3$ ,  $\text{Si}_3\text{N}_4$ ,  $\text{AlN}$ ,  $\text{TiN}$ ,  $\text{WC}$ ,  $\text{SiC}$ ,  $\text{TiC}$ ,  $\text{MoSi}_2$ ,  $\text{Fe}_2\text{O}_3$ ,  $\text{GeO}_2$ ,  $\text{Li}_2\text{O}$ ,  $\text{MnO}$ ,  $\text{NiO}$ , zeolite, hollow ceramics, and the like, but are not limited thereto.

The ceramic particle may be applied to graphene to obtain a graphene-ceramic composite powder in a method of graphene-metal precursor reduction, graphene-ceramic precursor heat treatment, plating, substitution, sputtering, and the like.

The inorganic powder may have a diameter of about 5 nm to 50 nm, of about 5 nm to 30 nm, or particularly of about 7 nm to 25 nm, for example about 10 nm to 20 nm.

When the diameter is out of the range, film properties may be deteriorated.

The organic additive may be further included to improve dispersion, coating properties, stability, adherence, leveling, viscosity, coating film property, drying property, and the like.

5 The organic additive may be hardeners, resin binders, monomers, a dispersing agents, dispersion stabilizers, surfactants, polyimide precursors, organic solvents, amphiphilic solvents, hydrophilic solvents, oils, acids, bases, salts, ions, leveling agents, adhesives, silane coupling agents, 10 thermoplastic resins, conductive polymers, or combinations thereof, but is not limited thereto.

For example, the resin binders may be thermosetting resins such as urethane resins, epoxy resins, melamine resins, polyimide, and a mixture thereof. In addition, the 15 resin binders may be photocurable resins such as epoxy resins, polyethylene oxide, urethane resins, and mixtures thereof. Further, the resin binders may be polymers of which reactive oligomers are epoxy acrylate, polyester acrylate, urethane acrylate, polyether acrylate, thiolate, organic silicon polymers, organic silicon copolymers and mixtures thereof; polymers of which reactive monomers are mono-functional monomers of 2-ethylhexylacrylate, octyldecylacrylate, isodecylacrylate, tridecylmethacrylate, 2-phenoxyethylacrylate, nonylphenolethoxyatemonoacrylate, 20 tetrahydrofurfurylate, ethoxyethylacrylate, hydroxyethylacrylate, hydroxyethylmetaacrylate, hydroxypropylacrylate, hydroxypropylmetaacrylate, hydroxybutylacrylate, hydroxybutylmetaacrylate, and the like;

25 polymers of which reactive monomers are bi-functional monomers of 1,3-butanedioldiacrylate, 1,4-butanedioldiacrylate, 1,6-hexanedioldiacrylate, diethylene glycoldiacrylate, triethylene glycoldi methacrylate, neopentylglycoldiacrylate, ethylene glycoldimethacrylate, tetraethylene glycolmethacrylate, polyethylene glycoldimethacrylate, 30 tripropylene glycoldiacrylate, 1,6-hexanedioldiacrylate and mixtures thereof; polymers of which reactive monomers are tri-functional monomers of trimethylolpropanetriacrylate, trimethylolpropanetrimethacrylate, pentaerythritoltriacrylate, glycidylpentatriacrylate, glycidylpentatriacrylate, and a mixture thereof; or polymers of which photoinitiators are benzophenone-based, benzylidemethylketal-based, acetophenone-based, or anthraquinone-based photoinitiators and mixtures thereof,

35 Further, examples of monomers may be thermosetting monomers, UV curable monomers, chemically curable monomers, and the like.

The dispersing agent and the dispersion stabilizer may include, but not be particularly limited to, Triton X-100, polyethyleneoxide, polyethyleneoxide-polypropyleneoxide 50 copolymer, polyvinylpyrrole, polyvinyl alcohol, Ganax, starch, monosaccharides, polysaccharides, sodium dodecylbenzene sulfate, sodium dodecyl benzene sulfonate ( $\text{NaD-DBS}$ ), sodium dodecylsulfonate (SDS), cetyltrimethylammonium 4-vinylbenzoate, pyrene-based derivative(pyrene derivatives), gum arabic (GA), Nafion, and mixture thereof, and other surfactants may be LDS (Lithium Dodecyl Sulfate), CTAC (Cetyltrimethyl Ammonium Chloride), DTAB (Dodecyl-trimethyl Ammonium Bromide), nonionic C12E5 (Pentaethoxylatedecyl ether), polysaccharide (Dextrin), 55 PEO (Poly Ethylene Oxide), Gum Arabic (GA), EC (ethylene cellulose), commercial BYK, block copolymer, BTK-Chemie, Germany), leveling agents, and the like,

60 The silane coupling agents may be compounds being capable of forming  $\text{Si}(\text{OH})_4$  through hydrolysis and then, condensation reactions, and may be selected from: a) tetraalkoxysilanes such as tetramethoxysilane, tetraethoxysilane, tetra-n-propoxysilane, tetra-i-propoxysilane, tetraiso-

propoxysilane, tetra-n-butoxysilane, tetra-sec-butoxysilane, tetra-tert-butoxysilane and mixtures thereof; trialkoxysilanes such as methyltrimethoxysilane, methyltriethoxysilane, ethyltrimethoxysilane, ethyltriethoxysilane, n-propyltrimethoxysilane, n-propyltriethoxysilane, i-propyltrimethoxysilane, i-propyltriethoxysilane, n-butytrimethoxysilane, n-butytriethoxysilane, n-hexyltrimethoxysilane, n-heptyltrimethoxysilane, n-octyltrimethoxysilane, vinyltrimethoxysilane, vinyltriethoxysilane, cyclohexyltrimethoxysilane, cyclohexyltriethoxysilane, phenyltrimethoxysilane, phenyltriethoxysilane, 3-chloropropyltrimethoxysilane, 3,3,3-trifluoropropyltrimethoxysilane, 3,3,3-trifluoropropyltriethoxysilane, 3-aminopropyltrimethoxysilane, 3-aminopropyltriethoxysilane, 2-hydroxyethyltrimethoxysilane, 2-hydroxyethyltriethoxysilane, 2-hydroxypropyltrimethoxysilane, 2-hydroxypropyltriethoxysilane, 3-hydroxypropyltriethoxysilane, 3-mercaptopropyltrimethoxysilane, 3-mercaptopropyltriethoxysilane, 3-isocyanatepropyltrimethoxysilane, 3-isocyanatepropyltriethoxysilane, 3-glycidoxypropyltrimethoxysilane, 3-glycidoxypropyltriethoxysilane, 2-(3,4-epoxycyclohexyl)ethyltrimethoxysilane, 2-(3,4-epoxycyclohexyl)ethyltriethoxysilane, 3-(meth)acryloxypropyltrimethoxysilane, 3-(meth)acryloxypropyltriethoxysilane, 3-ureidopropyltrimethoxysilane, 3-ureidopropyltriethoxysilane, and mixtures thereof; b) dialkoxy silanes such as dimethyldimethoxysilane, dimethyldiethoxysilane, diethyldimethoxysilane, diethyldiethoxysilane, di-n-propyldimethoxysilane, di-n-propyldiethoxysilane, di-i-propyldimethoxysilane, di-i-propyldiethoxysilane, di-n-butyldimethoxysilane, di-n-butyldiethoxysilane, di-n-pentyldimethoxysilane, di-n-pentyldiethoxysilane, di-n-hexyldimethoxysilane, di-n-hexyldiethoxysilane, di-n-heptyldimethoxysilane, di-n-heptyldiethoxysilane, di-n-octyldimethoxysilane, di-n-octyldiethoxysilane, di-n-cyclohexyldimethoxysilane, di-n-cyclohexyldiethoxysilane, diphenyldimethoxysilane, diphenyldiethoxysilane and mixtures thereof; and c) mixtures thereof. These may act as dispersion stabilizers.

Thermoplastic resins may be selected from the group consisting of polystyrene and a derivative thereof, polystyrene butadiene copolymer, polycarbonate, polychloridevinyl, polysulfone, polyethersulfone, polyetherimide, polyacrylate, polyester, polyimide, polyamic acid, cellulose acetate, polyamide, polyolefin, polymethylmethacrylate, polyetherketone, polyoxyethylene, and mixtures thereof. Further, the conductive polymers may be selected from the group consisting of polythiophene-based homopolymer, polythiophene-based copolymer, polyacetylene, polyaniline, polypyrrole, poly(3,4-ethylenedioxothiophene), pentacene-based compounds, and mixtures thereof.

In addition to the inorganic powder and the organic additive, in order to improve film functionality, other additives such as an antioxidant, carbon nanotube, metal nanowire (e.g., silver nanowire), metal flake, nanoparticle, metalnanoparticle, fullerene, a semiconductor nanoparticle, a semiconductor nano wire, a semiconductor nanoplate, and quantum dot may be added as needed.

When transmittance increases up to greater than or equal to about 50% in order to improve transparency of the graphene-containing coating film, an amount of the graphene may be about 0.001 wt % to 5 wt % based on the total weight of the hydrate represented by Chemical Formula 1, the graphene, and the silica nanoparticle.

When transmittance increases up to greater than or equal to about 70%, an amount of the graphene may be of about

0.001 wt % to 3 wt % based on the total weight of the hydrate represented by Chemical Formula 1, the graphene, and the silica nanoparticle.

In order to increase transparency, graphene should be less used but may be used in an amount of about 3 wt % to 5 wt % uniformly dispersed in a coating film, while transparency is maintained in a predetermined level or high. Accordingly, a graphene-containing coating film according to the present invention may have excellent transparency as well as excellent thermal conductivity.

FIGS. 2A-2B show exemplary graphene-containing coating compositions according to an exemplary embodiment of the present invention.

FIG. 2A relates to a coating composition obtained by adding graphene 20 to an organic ceramic sol 10 according to Comparative Example 1,

FIG. 2B relates to a coating composition obtained by adding only a silica nanoparticle 30 without graphene to an organic ceramic sol 10 according to Comparative Example 2,

FIG. 2C relates to a coating composition obtained by further adding the silica nanoparticle 30 as an additive to the ceramic sol 10 of the (a) according to Example 1 in an exemplary embodiment of the present invention.

FIG. 2A and FIG. 2C show improvement of thermal conductivity due to graphene included in a ceramic component having very low thermal conductivity.

Particularly, the FIG. 2C shows that the coating composition including only nanoparticle without graphene forms a film having a rough surface as compared with the coating composition of the FIG. 2B. The rough surface may be caused when the nanoparticle is laid on the curved or wrinkled graphene and thus activates its surface function. This surface form may improve hydrophilicity or water repellency, bring about an effect of increasing a haze and enlarging the surface area of the surface area, and the like.

The graphene-containing organic-inorganic ceramic hybrid coating film may have a thickness of about 100 nm to 2 μm, or particularly of about 200 nm to 900 nm.

When the coating film has a thickness within the range, uniformity and stability of a film surface may be ensured.

When transmittance increases up to greater than or equal to about 70% in order to improve transparency transmittance, a thickness of the graphene-containing coating film may be from about 200 nm to about 500 nm.

A substrate for supporting the coating film may be a substrate made of an inorganic material of glass or quartz, a silicon substrate and the like; or a resin substrate of polyethylene terephthalate (PET), polyethylene naphthalate (PEN), polycarbonate (PC), cycloolefin polymer (COP), polymethyl methacrylate (PMMA), polystyrene (PS), polyimide (PI), polyarylate, and the like.

In the present invention, the substrate may be used as a large area substrate, a curved substrate, and the like regardless of a kind or shape thereof.

A method of preparing a graphene-containing coating film according to an exemplary embodiment may include: dispersing a dispersed graphene; mixing and dispersing a silica nanoparticle and the precursors of the hydrate represented by Chemical Formula 1 in a hydrophilic solvent and mixing the same with the dispersed graphene; performing hydrolysis and condensation reactions of the mixed dispersed solution to prepare a graphene-containing sol solution; coating the graphene-containing sol solution on a substrate and drying the same at a temperature of about 25° C. to 400° C.; and heat-treating the dried film at a temperature of about 50° C. to 900° C.

The silicananoparticle may be present in an amount of about 5 to 20 wt % based on the total amount of the mixed dispersed solution; the precursors of the hydrate represented by Chemical Formula 1 may be present in an amount of about 10 to 40 wt % based on the total amount of the mixed dispersed solution; the dispersed graphene may be present in an amount of about 0.001 to 15 wt % based on the total amount of the mixed dispersed solution; and the hydrophilic solvent may be present in a balance amount.

A uniform coating composition may be prepared by respectively dispersing graphene, a silica nanoparticle, and a precursor mixed solution of hydrate represented by Chemical Formula 1 and mixing them. Accordingly, the silica nanoparticles or ceramic precursor molecule species corresponding to the hydrate may be dispersed at most into the graphene of a sheet-shaped nano structure and adsorbed therein.

The dispersed graphene may be prepared by a mechanical dispersion treatment or a solvent exchange method,

Herein, commercially available aqueously-dispersed graphene may be used as the dispersed graphene without a separate process.

The mechanical dispersion treatment may be performed about dry graphene powder, and the dry graphene powder may be obtained by heat-treating graphene oxide (GO) or chemically reducing the graphene oxide an then, drying the obtained graphene or heat-treating it again. This graphene powder may be very highly agglomerated and may be dispersed in physical, chemical, and mechanical methods. Representatively, the dispersion may be performed by ultrasonication with an ultrasonic wave, stiffness, application of shear stress and shearing force, using a homogenizer and a bead ball, or a combination thereof.

The solvent exchange method may also be applied to wet graphene, and graphene obtained in a hydrazine reduction method and the like may be wet in water, and moisture that is firmly adsorbed in the graphene may be removed through a strong heat treatment. However, since the strong heat treatment may cause a severe problem of agglomerating the graphene, the graphene needs to be dispersed again into a solvent having similar properties to a solvent included in a coating liquid after removing the moisture at room temperature.

The solvent exchange method may be, for example performed according to the steps (1) to (9), as follows:

- (1) Addition of non-aqueous based solvent of reaction A
- (2) Addition of additive I of reaction A (dispersing agent)
- (3) Dispersion of graphene (ultrasonic wave, shearing force)
- (4) Preparation of graphene dispersion
- (5) Reaction A: non-aqueous based solvent+ceramic precursor
- (6) Reaction B: Resultant of reaction A +H<sub>2</sub>O+additive II
- (7) GP-ceramic hybrid sol (Coating liquid)
- (8) Coating process
- (9) Transparent thermally conductive coating film

The solvent exchange method may include: (1) preparing a dispersion by mixing a graphene powder, a first dispersing agent and a first non-aqueous based solvent; (2) preparing a mixture by adding a second non-aqueous based solvent and a precursor of the hydrate to the dispersion; and (3) preparing a graphene-containing sol solution mixing the mixture with a second dispersing agent and water.

The graphene powder, the first dispersing agent, and the first non-aqueous based solvent may be further mechanical dispersion-treated after the mixing and may be further

washed with a non-aqueous based solvent before the mechanical dispersion treatment.

The washing with the non-aqueous based solvent may maximize suitability in the second half. In particular, the washing may use the same solvent as or a similar solvent to the first non-aqueous based solvent.

The process of washing the non-aqueous based solvent may be performed to thoroughly remove moisture (H<sub>2</sub>O) adsorbed on the surface of the graphene. It may be a simple 10 washing process, or may be performed through an ultrasonication dispersion treatment or after an ultrasonication dispersion treatment. This process may be performed as many times as needed. Through the process of washing with the non-aqueous based solvent, a removal degree of moisture at 15 the surface of the graphene may have an effect on long-time stability of the sol solution. Therefore, a method of performing washing and/or a washing degree may control moisture and thus resultant properties. In particular, when moisture is removed, a sol stability effect may be maximized. In the first 20 process of the method for preparing a coating layer of a graphene-ceramic hybrid according to an exemplary embodiment of the present invention, sol stability may be reduced by added moisture even if a small amount of moisture is added. Although an amount of moisture adsorbed on the graphene is small, stability of the entire 25 graphene-ceramic hybrid mixed sol may be dramatically reduced because there is serious interface instability at an interface with the sol.

The first dispersing agent and second dispersing agent 30 used in the solvent exchange method may be each independently selected from the group consisting of polyethylene glycol (PEG), glycerol, hydrochloric acid (HCl), acetic acid, formic acid, citric acid, binder, and a combination thereof.

The first non-aqueous based solvent and second non-aqueous based solvent may be each independently an amphilic solvent, a water-soluble solvent except water, a non-water-soluble solvent, a polar solvent, a nonpolar solvent, or a combination thereof.

In particular, the first non-aqueous based solvent and 40 second non-aqueous based solvent may be each independently selected from the group consisting of isopropyl alcohol(iso-propyl alcohol), ethanol, acetone, methylketone, methylalcohol, ethylalcohol, isopropylalcohol, 45 acetylacetone, butylalcohol, ethylene glycol, polyethylene glycol, tetrahydrofuran, dimethyl formamide, dimethyl acetamide, N-methyl-2-pyrrolidone, hexane, cyclohexanone, toluene, chloroform, dichlorobenzene, dimethylbenzene, trimethylbenzene, pyridine, methylnaphthalene, nitromethane, acrylonitrile, octadecylamine, aniline, dimethylsulfoxide, and a combination thereof.

The graphene may have a uniform size by dispersing 50 graphene, centrifuging the dispersion to remove a supernatant, and centrifuging a precipitate therefrom to obtain a precipitate again and then, at least twice repeating these all processes.

In an exemplary embodiment of the present invention, in the process of the mixing and dispersing of a silica nanoparticle and the precursors of the hydrate represented by 60 Chemical Formula 1 in a hydrophilic solvent and mixing the same with the dispersed graphene, an additive selected from an inorganic powder, an organic additive, and a combination thereof may be further included.

For example, the inorganic powder may be mixed in an 65 amount of about 5 parts by weight to 30 parts by weight based on 100 parts by weight of the mixed dispersed solution.

19

In particular, the inorganic powder may be included in an amount of about 5 parts by weight to 25 parts by weight, of about 7 parts by weight to 20 parts by weight, or particularly of about 7 parts by weight to 10 parts by weight.

When the amount of the inorganic powder is out of the range, coating properties may be deteriorated.

For example, the organic additive may be mixed in an amount of about 0.01 parts by weight to 10 parts by weight based on 100 parts by weight of the mixed dispersed solution.

Particularly, it may be included in an amount of about 0.01 parts by weight to 5 parts by weight, of about 0.1 parts by weight to 3 parts by weight, or particularly of about 0.01 parts by weight to 2 parts by weight.

When the amount of the organic additive is out of the range, coating properties may be deteriorated.

The silica nanoparticle and the hydrate represented by Chemical Formula 1 may be mixed and dispersed in a hydrophilic solvent.

The hydrophilic solvent may be a medium playing the most important role for stability and reactivity. Herein, a precondition under which graphene is dispersed into the hydrophilic solvent may be made to easily mix the graphene with a hydrophilic sol solution.

The hydrophilic solvent comprising a single component or more than two components may be required, since the hydrophilic solvent provides water necessarily required in a sol-gel reaction as a main reaction of the present invention. Accordingly, the hydrophilic solvent may be easily mixed with H<sub>2</sub>O molecule as a resulting material from the reaction, and well mixed with an alcohol group of silanol (—Si—OH) produced as a reaction intermediate of a precursor of the hydrate represented by Chemical Formula 1.

When the precondition that graphene is dispersed into the hydrophilic solvent is not made, hydrophilic sol may not be uniformly mixed with the graphene.

Herein, “the precondition that the graphene is dispersed into the hydrophilic solvent” may include, for example, the following three cases.

First, an aqueous graphene dispersion dispersed into water may be used.

The aqueous graphene dispersion may be prepared by applying electric current to graphite in a liquid, and graphene produced therefrom may be aqueously dispersed, since organic functional groups at the edge of the graphene are substituted with aqueous substituents (—OH, —COOH). This aqueous graphene dispersion may be simply mixed with an aqueous ceramic sol, preparing a uniform graphene-ceramic hybrid sol solution. In other words, the aqueous graphene dispersion as a commercial product may be used in a mixing process without a dispersing agent or an additional process.

Second, graphene including a plurality of hydrophilic group on the surface may be used in a small amount.

According to an exemplary embodiment of the present invention, since graphene in a small amount of about 0.01 wt % to 0.1 wt % is mixed with a ceramic sol solution, a uniform hybrid sol solution may not be obtained by dispersing graphene having a large amount of a hydrophilic group on the surface into the hydrophilic solvent such as water or alcohol and adding it to a ceramic sol solution.

Further, a binder, an inorganic powder, an organic additive, or the like added therewith may play an assistant role of preventing agglomeration of the graphene.

Third, graphene may be highly dispersed by dispersing it into a non-aqueous based solvent and then, substituting the non-aqueous based solvent with an aqueous solvent. In the

20

present invention, the method is referred to a solvent exchange method, and the solvent exchange method is the same as described above.

Particular examples of the hydrophilic solvent may be water; alcohols such as methanol, ethanol, propanol, butanol, or isopropylalcohol (IPA), glycol; or a combination thereof, but is not limited thereto. For example, a mixed solvent of water and alcohol may be used.

A mixing amount of the hydrophilic solvent may be as follows: an amount of about 10 to 500 parts by weight of ethanol (or alcohols including one or more components) based on a 100 parts by weight of water, and in particular, a mixing weight ratio of water:alcohols may be about 100:50, about 100:100, about 100:150, about 100:200, about 100:300, about 100:400 or about 100:500. Exemplary mixing weight ratio may be of about 100:100, or about 100:200.

The precursors of the hydrate represented by Chemical Formula 1 may be a silicon-based compound, titanium isopropoxide (TTIP), tetramethyl orthosilicate (TMOS), and the like.

The silicon-based compound may be selected from the group consisting of betrimethoxysilane, triethoxysilane, methyltrimethoxysilane, methyltriethoxysilane, ethyltrimethoxysilane, ethyltriethoxysilane, propyltrimethoxysilane, propyltriethoxysilane, isobutyltriethoxysilane, glycidoxypropyltrimethoxysilane, glycidoxypropyltriethoxysilane, cyclohexyltrimethoxysilane, phenyltrimethoxysilane, phenyltriethoxysilane, vinyltrimethoxysilane, vinyltriethoxysilane, allyltrimethoxysilane, allyltriethoxysilane, dimethylidemethoxysilane, dimethylidethoxysilane, diphenyldimethoxysilane, diphenyldiethoxysilane, (N,N-dimethylaminopropyl)trimethoxysilane, (N,N-dimethylaminopropyl)triethoxysilane, and N,N-{(2-aminoethyl) (3-aminopropyl)}trimethoxysilane, or a combination thereof.

The Chemical Formula 1 may be represented by one of Chemical Formulae 1-1 to 1-3.



In Chemical Formulae 1-1 to 1-3, M and X<sup>1</sup>, X<sup>2</sup>, and X<sup>3</sup> are the same as described above.

Preferably, the M may be Si.

For example, the precursors of the hydrate may be glycidoxypropyltrimethoxysilane, and may be mixed with a silane coupling agent selected from the group consisting of tetramethoxysilane, tetraethoxysilane, diphenylethoxysilane and a combination thereof.

The coating process may be performed by a general coating method, such as dip coating, spin coating, spray coating, paint coating, bar coating, flow coating, roll coating, or a combination thereof. Preferably, dip coating, spin coating, or spray coating may be used, however the process may not be limited thereto.

The coating process according to an exemplary embodiment may be performed using spray coating, regardless of kinds or shapes of substrates such as a large area, a curved substrate, and the like, but is not limited thereto.

Yet another embodiment of the present invention provides a vehicle part, such as head lamp. The vehicle part may comprise the graphene-containing coating film as described herein.

21

Particularly, a function to suppress fogging due to thermal conductivity by lamp heat may be expected due to effects of the present invention, for example excellent thermal conductivity as described above.

As a specific industrial application, it may be applied to a lens (PC curved substrate) of a vehicle head lamp to reduce fogging problems.

### EXAMPLE

Hereinafter, specific exemplary embodiments of the present invention are described. However, the specific exemplary embodiments are merely used to exemplarily illustrate the present invention in more detail, and are not to be seen as limiting the present invention.

Furthermore, what is not described in this disclosure may be sufficiently understood by those skilled in the art who have knowledge in this field.

#### Preparation Example 1

##### Preparation of Graphene Oxide

10 g of natural graphite and 7.5 g of sodium nitrate were put in a reactor and 621 g of 96% sulfuric acid was slowly added while stirring. After the three materials were sufficiently mixed, 45 g of manganese peroxide was added. Because the manganese peroxide has an explosion possibility and generates heat and gases when reacting with strong sulfuric acid, it was added over 1 hour little by little. After adding the manganese peroxide, the resultant was stirred at room temperature and reacted for 4 to 6 days. Then, 1 L of 5% sulfuric acid was added. Because a large amount of heat and gases may be generated, the reactor was suitably cooled and it was added slowly over 1 hour, and then the resultant was placed at room temperature for one day while being stirred. After one day, 30 g of 30% hydrogen peroxide was slowly added and reacted for 2 hours. In order to remove a large amount of sulfuric acid and hydrogen peroxide in the resulting product, washing and centrifugation were performed many times. The process was performed as follows: centrifugation was performed to remove a supernatant, a mixed solution including 3% sulfuric acid and 0.5% hydrogen peroxide at 1:1 was put in the remaining precipitate, and the resultant was sufficiently agitated and centrifuged and a supernatant was removed. Then, the mixed solution was added to the remaining precipitate and mixed. These processes were repeated 15 times, and then the mixed solution was replaced by water 5-6 times to obtain aqueous graphene-oxide (GO) slurry.

GO slurry is generally a material that is produced by acid treatment of graphite and purification processes, and thus GO slurry in the present invention may be a generally-known sheet-shaped graphene oxide or graphite oxide without limitation. In general, aqueous GO slurry has a solid content of 2 to 8 wt % based on centrifuged slurry.

##### (Preparation of Dispersion-treated GO)

The graphene oxide powder (GO) was added to ethanol and treated with an ultrasonic wave disperse (tip-shaped ultrasonic wave), or discharged into a fine nozzle with a high pressure (providing shear stress) to prepare dispersion-treated dispersion. Herein, a dispersing agent, BYK series was used.

#### Preparation Example 2

##### Preparation of Thermally Reduced Graphene

Reduced graphene oxide powder was prepared by adding hydrazine to the aqueous graphene oxide slurry according to

22

Preparation Example 1, reacting the mixture for 24 hours, and centrifuging/washing/drying a precipitate obtained therefrom.

##### (Preparation of Dispersion-Treated RGO)

5 The graphene powder (RGO) was added to ethanol and treated with an ultrasonic wave disperse (tip-shaped ultrasonic wave), or discharged into a fine nozzle with a high pressure (providing shear stress) to prepare dispersion-treated dispersion. Herein, a dispersing agent, BYK series 10 was used.

#### Preparation Example 3

##### Preparation of Chemically Reduced Graphene

15 Reduced graphene oxide powder was prepared by adding hydrazine to the aqueous graphene oxide slurry according to Preparation Example 1, reacting the mixture for 24 hours, and centrifuging/washing/drying a precipitate obtained 20 therefrom.

##### (Preparation of Dispersion-Treated RGO)

The graphene powder (RGO) was added to ethanol and treated with an ultrasonic wave disperse (tip-shaped ultrasonic wave), or discharged into a fine nozzle with a high pressure (providing shear stress) to prepare dispersion-treated dispersion. Herein, a dispersing agent, BYK series 25 was used.

#### Comparative Example 1

##### Preparation of Si(OH)<sub>4</sub> Typed SiO<sub>2</sub> Sol Solution

15 mg of the chemically reduced graphene preparation according to Example 3 was put in a 500 mL plastic bottle, 35 150 ml of IPA was added thereto, 20 g of PEG was added thereto, and the mixture was ultrasonication-dispersed for 10 minutes. Then, 100 ml of ethanol was added thereto, 10 ml of TMOS (tetramethyl orthosilicate) was added thereto, and the resulting mixture was agitated for greater than or equal 40 to 24 hours. Herein, the resultant maintained about pH 3.3 by using hydrochloric acid. The TMOS had a hydrolysis shape of Si (OH)<sub>4</sub> including no organic functional group.

##### (Preparation of Graphene-SiO<sub>2</sub> Hybrid Coating Film I)

The graphene-ceramic hybrid sol solution was spin-coated (rpm 800) on a glass substrate surface-treated with plasma. The spin-coated film was vacuum-dried at room temperature and heat-treated at a temperature of 80° C. for 45 1 hour in a heater, manufacturing a GP-SiO<sub>2</sub> hybrid-coating film.

50 The formation of the coating film may include spray coating, bar coating, knife coating, screen printing, dip coating, and the like,

The heat-treatment may include a vacuum heat treatment, an atmosphere heat treatment, an IR heat treatment, a convention heat treatment, a heat treatment using a heater, a heat treatment using an electromagnetic wave such as a laser and the like, a heat treatment using a microwave, and the like.

##### (Preparation of Graphene-SiO<sub>2</sub> Hybrid Coating Film II)

60 The graphene-ceramic hybrid sol solution was spray-coated on a PC (Polycarbonate) substrate surface-treated with plasma, vacuum-dried at a temperature of 50° C., and heat-treated on the surface by repetitively giving a instant thermal impact with an IR lamp. The heat treatment was 65 performed at a temperature of 300° C. for an exposure time of 3 seconds. The heat treatment and the expose process were repeated. The repetition of the heat treatment and the

23

expose process was performed after the substrate was substantially cooled down to room temperature, and the rear surface of the substrate was maintained at a temperature of 80° C. to 130° C. for the heat treatment, since this process is advantageous for a plastic substrate. The temperature may be further cooled down by cooling down a lower substrate lower (or air-cooled).

Referring to FIG. 5, the graphene-ceramic hybrid coating film formed of the graphene-ceramic hybrid sol solution includes about 1.8 wt % of graphene (carbon).

### Example 1

#### Preparation of $\text{Si}(\text{OH})_3\text{X}_1$ Type Graphene-Ceramic Hybrid Sol Solution

A  $\text{Si}(\text{OH})_3\text{X}_1$  type graphene-ceramic hybrid sol solution may be prepared in the following three methods depending on mixing.

1) A simply mixing method using a mechanical dispersion treatment method

50 mg of the graphene according to Preparation Example 3 was put in 100 ml of IPA, and the mixture was ultrasonic wave-dispersed for 10 minutes. After 1 hour, 1 ml of the outmost supernatant was taken therefrom, 100 ml of ethanol was added thereto, a solution obtained by dissolving 10 wt % to 40 wt % of glycidoxypolytrimethoxysilane (hereinafter, GT) in a mixed solvent of water and ethanol in a weight ratio of 1:1 was added thereto, and 20 wt % of LUDOX® (20 nm of silica sol, SIGMA-ALDRICH, USA) and nitric acid were added thereto adjust pH in a range of 2 to 4, and then, the resultant was agitated for 24 hours. After the reaction, an ethylene diamine hardener was added thereto in the same numbers of mols as those of the GT, and the mixture was stirring for 30 minutes, preparing a  $\text{Si}(\text{OH})_3\text{X}_1$  type graphene-ceramic hybrid sol solution. Its final film included graphene in an amount ranging from 0.04 wt % to 7.5 wt %.

2) A method of adding an aqueous dispersion graphene solution from the beginning for mixing

100 ml of ethanol was added to 1 ml of a commonly-used aqueous dispersion graphene (1% of a weight-containing solution), a solution obtained by dissolving 10 wt % to 40 wt % of glycidoxypolytrimethoxysilane (hereinafter, GT) in a mixed solvent of water and ethanol in a weight ratio of 1:1, 20 wt % of LUDOX® (20 nm of silica sol, SIGMA-ALDRICH, USA) and nitric acid were added thereto to adjust pH in a range of 2 to 4, and the mixture was agitated for 24 hours. After the reaction, an ethylene diamine hardener was added thereto in the same mols of those of the GT, and the resulting mixture was stirred for 30 minutes, preparing a  $\text{Si}(\text{OH})_3\text{X}_1$  type graphene-ceramic hybrid sol solution. Its final film included graphene in an amount of 0.06 wt % to 8.5 wt %.

When a kind of graphene is simply dispersed into water or alcohol, a process may be shortened. For example, graphene manufactured in a electrical stripping method, a graphene local oxidation method, and the like or graphene including a plurality of hydrophilic group on the surface may be in a small amount of about 0.01 wt % to 0.1 wt % during a sol reaction. Herein, an additive such as a binder, an inorganic powder, an organic additive, and the like may be used together to prevent agglomeration of the graphene.

#### 3) Mixing by Solvent Exchange Method

15 mg of each chemical reduction graphene according to Preparation Example 3 was put in a 500 mL plastic bottle, 150 ml of IPA was added thereto, 10 g of PEG was added

24

thereto, and the mixture was ultrasonic wave-dispersed for 10 minutes. Then, 100 ml of ethanol was added thereto, a solution obtained by dissolving 10 to 40 wt % of glycidoxypolytrimethoxysilane (hereinafter, GT) in a mixed solvent of water and ethanol in a weight ratio of 1:1 was added thereto, and then, the mixture was agitated for 24 hours by adding 20 wt % of LUDOX® (20 nm of a silica sol, SIGMA-ALDRICH, USA) and nitric acid thereto to adjust its pH in a range of 2 to 4. After the reaction, an ethylene diamine hardener was added thereto in the same number of mol as that of GT, and the mixture was stirred for 30 minutes, preparing a  $\text{Si}(\text{OH})_3\text{X}_1$  type graphene-ceramic hybrid sol solution.

#### (Manufacture of Coating Film)

15 A coating film was manufactured according to the same method as Comparative Example 1 except for using the  $\text{Si}(\text{OH})_3\text{X}_1$  type graphene-ceramic hybrid sol solution.

Referring to FIG. 5, the graphene-ceramic hybrid coating film formed of the graphene-ceramic hybrid sol solution according to Example 1 and maintaining sol stability included about 0.001 wt % to 10 wt % of graphene.

Since Example includes one organic functional group ( $\text{X}_1$ ) compared with Comparative Example 1, the maximum amount of graphene in a coating layer maintaining sol stability was in a range of 1.8 wt % to 10 wt %, which was greater than or equal to times improved.

When a highly dispersed graphene solution was simply mixed with a ceramic sol solution (a mechanical dispersion treatment), the maximum amount of graphene was improved up to about 7.5 wt %. In addition, when an aqueous dispersed graphene solution was added from the beginning, the maximum amount of graphene was improved up to about 8.5 wt %, and when the mixing was performed in a solvent exchange method, the maximum amount of graphene was improved up to about 10 wt %.

### Example 2

#### Manufacture of $\text{Si}(\text{OH})_3\text{X}_1+\text{Si}(\text{OH})_2\text{X}_1\text{X}_2$ Type Graphene-Ceramic Hybrid Sol Solution

1) Simple Mixing by Using Mechanical Dispersion Treatment

50 mg of graphene prepared in Preparation Example 3 was put in 100 ml of IPA and ultrasonic wave dispersed for 10 minutes. After one hour, 1 ml of an outmost supernatant not going down therein was taken from, 100 ml of ethanol was added thereto, a solution obtained by dissolving 10 to 40 wt % of a mixture of glycidoxypolytrimethoxysilane (hereinafter, GT) and diphenyldiethoxysilane (a weight ratio of 1:1) in a mixed solvent of water and ethanol in a ratio of 1:1, and then, the mixture was agitated for 24 hours by using 20 wt % of LUDOX® (20 nm of silica sol, SIGMA-ALDRICH, USA) and nitric acid to adjust its pH into 2 to 4. After the reaction, an ethylene diamine hardener was added thereto in the same number of mol as that of GT, and the mixture was stirred for 30 minutes, preparing a  $\text{Si}(\text{OH})_3\text{X}_1+\text{Si}(\text{OH})_2\text{X}_1\text{X}_2$  type graphene-ceramic hybrid sol solution. Its final film included graphene in an amount of about 0.08 wt % to 13.5 wt %.

2) Mixing by Adding Aqueous Dispersed Graphene Solution from the Beginning

100 ml of ethanol was added to 1 ml of aqueous dispersed graphene (1% of a weight content in a solution), a solution obtained by dissolving 10 wt % to 40 wt % of a mixture of glycidoxypolytrimethoxysilane (hereinafter, GT) and diphenyldiethoxysilane (1:1 of a weight ratio) in a mixed

25

solvent of water and ethanol in 1:1 of a weight ratio was added thereto, and then, the mixture was agitated for 24 hours by using 20 wt % of LUDOX® (15 nm of a silica sol, SIGMA-ALDRICH, USA) and nitric acid to adjust its pH into 2 to 4. After the reaction, an ethylene diamine hardener was added in the same number of mol as that of GT was added thereto, and the mixture was stirred for 30 minutes, preparing a  $\text{Si(OH)}_3\text{X}_1+\text{Si(OH)}_2\text{X}_1\text{X}_2$  type graphene-ceramic hybrid sol solution. Its final film included graphene in an amount of about 0.09 wt % to 14 wt %.

3) Mixing in Solvent Exchange Method

15 mg of the chemical reduction graphene according to Preparation Example 3 was put in a 500 mL plastic bottle, 150 ml of IPA was added thereto, and 10 g of PEG was added thereto, and the mixture was ultrasonic wave dispersed for 10 minutes. Then, 100 ml of ethanol was added thereto, a solution obtained by dissolving 10 to 40 wt % of a mixture of glycidoxypolytrimethoxysilane (hereinafter, GT) and diphenyldiethoxysilane (1:1 of a weight ratio) in a mixed solvent of water and ethanol in a ratio of 1:1.5 was added thereto, and then, the resulting mixture was reacted for 24 hours by adding 20 wt % of LUDOX® (15 nm of a silica sol, SIGMA-ALDRICH, USA) and nitric acid to adjust its pH into 2 to 4. After the reaction, an ethylene diamine hardener was added in the same number of mol of that of GT was added thereto, and the mixture was stirred for 30 minutes, preparing a  $\text{Si(OH)}_3\text{X}_1+\text{Si(OH)}_2\text{X}_1\text{X}_2$  type graphene-ceramic hybrid sol solution.

(Manufacture of Coating Film)

A coating film was formed in the same method as Comparative Example 1 except for using the  $\text{Si(OH)}_3\text{X}_1+\text{Si(OH)}_2\text{X}_1\text{X}_2$  type graphene-ceramic hybrid sol solution.

Referring to FIG. 5, the graphene-ceramic hybrid coating film formed of the graphene-ceramic hybrid sol solution according to Example 2 and maintaining sol stability included graphene (carbon) in an amount of about 0.001 wt % to 15 wt %.

Compared with Comparative Example 1, the maximum amount of graphene in a coating film including two organic functional groups ( $\text{X}_1\text{X}_2$ ) and maintaining sol stability was 8 times improved in an amount of 1.8 wt % to 15 wt %.

When a highly dispersed graphene solution was simply mixed with a ceramic sol solution (a mechanical dispersion treatment), the maximum amount of graphene was improved up to about 13.5 wt %. Further, when an aqueous dispersed graphene solution was added from the beginning, the maximum amount of graphene was improved up to about 14 wt %, and when the mixing was performed in a solvent exchange method, the maximum amount of graphene was improved up to about 15 wt %.

Herein, the amount of graphene was reduced to form a transparent coating layer, the graphene was included in an amount of about 5 wt % for transmittance of 50%, and the graphene was included in an amount of about 3 wt % for transmittance of 70%.

### Example 3

#### Manufacture of $\text{Si(OH)}_3\text{X}_1+\text{Si(OH)}_4$ Type and Hardener Type Organic/Inorganic Hybrid Sol

1) Simple Mixing in Mechanical Dispersion Treatment

50 mg of graphene according to Preparation Example 3 was added to 100 ml of IPA and ultrasonic wave-dispersed for 10 minutes. Then, 1 ml of an outmost supernatant not doing down after one hour was taken therefrom, 100 ml of ethanol was added thereto, 10 to 40 wt % of a solution

26

obtained by dissolving a mixture of glycidoxypolytrimethoxysilane (hereinafter, GT) and TMOS (1:1 of a weight ratio) in a mixed solvent of water and ethanol in 1:2 of a weight ratio was added thereto, and the mixture was reacted for 24 hours by adding 20 wt % of LUDOX® (15 nm of a silica sol, SIGMA-ALDRICH, USA) and nitric acid to adjust its pH in a range of 2 to 4. After the reaction, an ethylene diamine hardener was added thereto in the same number of mol as that of the GT, and the mixture was stirred for 30 minutes, preparing a  $\text{Si(OH)}_3\text{X}_1+\text{Si(OH)}_4$  type graphene-ceramic hybrid sol solution. Its final film included graphene in an amount of 0.03 wt % to 4.5 wt %.

2) Mixing by using Aqueous Dispersed Graphene Solution from the Beginning

100 ml of ethanol was added to 1 ml of commonly-used aqueous dispersed graphene (1% of a weight content in a solution), a solution obtained by dissolving 10 to 40 wt % of a mixture of glycidoxypolytrimethoxysilane (hereinafter, GT) and TMOS (1:1 of a weight ratio) in a mixed solvent of water and ethanol in a weight ratio of 1:2, and the mixture was reacted for 24 hours by adding 20 wt % of LUDOX® (15 nm of a silica sol, SIGMA-ALDRICH, USA) and nitric acid to adjust pH in a range of 2 to 4. After the reaction, an ethylene diamine hardener was added thereto in the same number of mol as that of the GT, and the mixture was stirred for 30 minutes, preparing a  $\text{Si(OH)}_3\text{X}_1+\text{Si(OH)}_4$  type graphene-ceramic hybrid sol solution. Its final film included graphene in an amount of 0.07 wt % to 5 wt %.

3) Mixing by Solvent Exchange Method

15 mg of the chemical reduction graphene of Preparation Example 3 was put in a 500 mL plastic bottle, 150 ml of IPA was added thereto, 10 g of PEG was added thereto, and the mixture was ultrasonic wave-dispersed for 10 minutes. Then, 100 ml of ethanol was added thereto, a solution obtained by dissolving 10 to 40 wt % of a mixture of glycidoxypolytrimethoxysilane (hereinafter, GT) and TMOS (1:1 of a weight ratio) in a mixed solvent of water and ethanol in 1:2 of a weight ratio, and then, the mixture was reacted for 24 hours by adding 20 wt % of LUDOX® (15 nm of a silica sol, SIGMA-ALDRICH, USA) and nitric acid to adjust its pH in a range of 2 to 4. After the reaction, an ethylene diamine hardener was added thereto in the same number of mol as that of GT, and the mixture was stirred for 30 minutes, preparing a  $\text{Si(OH)}_3\text{X}_1+\text{Si(OH)}_4$  type graphene-ceramic hybrid sol solution.

(Manufacture of Coating Film)

A coating film was formed in the same method as Comparative Example 1 except for using the  $\text{Si(OH)}_3\text{X}_1+\text{Si(OH)}_4$  type graphene-ceramic hybrid sol solution.

50 The graphene-ceramic hybrid coating film formed of the graphene-ceramic hybrid sol solution according to Example 3 and maintaining sol stability included graphene (carbon) in an amount of about 0.01 wt % to 5 wt %.

The result may be caused from a reason that a coating film 55 maintaining sol stability compared with Comparative Example 1 has a 2 to 3 times improved maximum amount of graphene.

### Examples 4 to 6

#### Addition of Polymer

##### Example 4

65 A graphene-ceramic hybrid sol solution and a coating film formed thereof were manufactured according to the same method as Example 1 except for adding 10 parts by weight

27

of PVA based on 100 parts by weight of a graphene-solvent-hydrate precursor before adding a hardener thereto during manufacture of the graphene-ceramic hybrid sol solution.

The coating film maintaining sol stability included graphene in up to about 35 wt % improved maximum amount.

The dispersion stability of graphene was increased as an organic component was increased on the interface of ceramic-graphene.

#### Example 5

A graphene-ceramic hybrid sol solution and a coating film formed thereof were manufactured according to the same method as Example 2 except for adding 10 parts by weight of PVA (polyvinyl alcohol) based on 100 parts by weight of a graphene-solvent-hydrate precursor solution before adding a hardener thereto during manufacture of the graphene-ceramic hybrid sol solution.

Referring to FIG. 5, the coating film maintaining sol stability included graphene in up to about 50 wt % improved maximum amount.

#### Example 6

A graphene-ceramic hybrid sol solution and a coating film formed thereof were manufactured according to the same method as Example 3 except for using 10 parts by weight of PVA (polyvinyl alcohol) based on 100 parts by weight of a graphene-solvent-hydrate precursor before adding a hardener thereto during manufacture of the graphene-ceramic hybrid sol solution.

The coating film maintaining sol stability included graphene in up to about 15 wt % improved maximum amount.

#### Comparative Example 2 and Example 7

##### Addition of Silica Particle

##### Comparative Example 2

A  $\text{Si(OH)}_3\text{X}_1$  type sol solution and a coating film formed thereof were manufactured by agitating 50 ml of IPA and 50 ml of  $\text{Si(OH)}_3\text{X}_1$  for greater than or equal to 30 minutes, 10 ml of water, 10 g of PEG (polyethylene glycol), and LUDOX® (20 nm of a silica sol, SIGMA-ALDRICH, USA) and 1 ml of HCl thereto and uniformly reacting the for 90 minutes as being agitated.

#### Example 7

A graphene-ceramic hybrid sol solution and a coating film formed thereof were manufactured according to the same method as Example 4 except for using 0.1 parts by weight of silver nanowire and 0.1 parts by weight of silver nanoparticle based on 100 parts by weight of a graphene-solvent-hydrate precursor solution instead of the polyvinyl alcohol. Evaluation 1: Uniformity (Stability) of Graphene-Containing Hybrid Sol Solution

FIG. 6 shows the results of adding uniformly dispersed graphene to be 10 wt % in a coating film formed of a graphene-containing sol solution as a resulting material to each sol solution according to Example 1 and Comparative Example 1. Referring to FIG. 6, the sol solution according to Example 1 showed excellent dispersion stability, while the solution according to Comparative Example 1 was mostly precipitated. In particular, a transparent brown part of a supernatant in the sol solution according to Comparative

28

Example 1 showed that the amount of graphene was saturated, and herein, the amount of graphene was in a range of 0.001 to 1.8 wt % in a coating film obtained from the supernatant.

- 5 Examples 2 to 4 showed a similar phenomenon to that of FIG. 6. A dispersion prepared according exemplary embodiments of the present invention had a high concentration and thus showed greater than or equal to about 1 month of stability (maintained greater than or equal to about 1 month of stability in refrigeration and thermal impact at a temperature of 60° C.), which is improved stability not found in a conventional graphene dispersion. The amount of graphene in a dispersion is presently reported in a range of about 1 to 2 wt %.
- 10 Evaluation 2: Stability of Graphene-Containing Hybrid Coating Film

FIG. 7 shows the result of a film obtained by coating each coating liquid according to Comparative Example 1 and Example 1 on a PC substrate and drying it.

- 20 The film obtained in Comparative Example 1 was easily stripped like being crumbled, but the film obtained in Example 1 according to an exemplary embodiment the present invention had a smooth and transparent surface and showed satisfactory coating property.

Evaluation 3: Transmittance of Graphene-Containing Hybrid Coating Film

FIG. 8 shows the transmittance evaluation result of the graphene-containing ceramic hybrid coating film according to Example 2 measured with a UV-Vis spectrophotometer (V-530, Jasco analytical Instruments) by coating a sol solution including 0.03 wt % of graphene on a head lamp (made of a PC material).

FIG. 8 is a graph showing transmittance of a graphene-containing coating film according to an exemplary embodiment of the present invention.

Referring to FIG. 8, the head lamp made of a bare-PC material showed transmittance of 87.4% at a wave length of 550 nm, but a coating film according to the present invention showed improved transmittance of 90.6%. The transmittance was improved, since organic/inorganic hybrid components were well bonded for example, at an interface junction and the like as described above, and thus formed a sufficient quality film and changed an index [NOTE: please describe the "index"].

Evaluation 4: Thermal Conductivity of Graphene-Containing Hybrid Coating Film

Thermal conductivity of a graphene-containing hybrid coating film according to the present invention was evaluated by using a thermal conductivity measuring equipment (home-made).

The equipment for measuring the thermal conductivity of the graphene-containing ceramic hybrid coating film was fabricated by heating a thermocouple, the center of a PC (poly carbonate) substrate (a size of 10 cm×10 cm, a thickness of 2 mm) with a halogen lamp as a heating source (heating shape and diameter: circle and 5 cm) up to a temperature of about 120° C., and measuring a temperature at the thermocouple (TC2) and simultaneously, measuring a temperature at the edge of the substrate temperature (TC1).

FIG. 8 shows the thermal conductivity results measured by using the equipment.

FIG. 9 is a graph showing the thermal conductivity effect of the graphene-containing coating film according to an exemplary embodiment of the present invention.

On the other hand, a coating film manufactured by using only pure GT (a ceramic sol) on a common PC substrate according to Comparative Example 2 showed about 2.8° C.

increased effect per hour, but the coating film including graphene according to Example 1 showed 9.6° C. increased effect per hour and a larger thermal conductivity effect. The reason is that the graphene was uniformly dispersed in the coating film, so that properties of the graphene were well realized. However, when the graphene was unstably dispersed and brought about an interface delamination phenomenon, a thermal conductivity effect of around 2.8° C. and less than or equal to 2.8° C. was obtained just like a coating film including only a ceramic sol.

When graphene was included in a minimum amount of 0.001 wt % in the present invention, thermal conductivity was improved about twice as much as when graphene was not included.

The coating film of Example 2 showed the highest thermal conductivity of about 12.5° C.

#### Evaluation 5: Surface Function of Graphene-Containing Hybrid Coating Film Depending on Additive

FIG. 10 shows the waterdrop contact angle result of a graphene-containing organic-inorganic ceramic hybrid coating film according to an exemplary embodiment of the present invention.

FIG. 10 shows the waterdrop contact angle results of a coating film formed of a coating liquid according to Comparative Example 2, a coating film formed of a coating liquid according to Comparative Example 1, and a coating film formed of a coating liquid according to Example 1.

Referring to FIG. 10, the contact angle was reduced, as graphene was more included, and when a silica nanoparticle was further added, the contact angle was further reduced. When the contact angle was reduced, surface hydrophilic characteristics were increased.

FIG. 11 is a TEM (Transmission Electron Microscope) photograph showing the graphene-containing organic-inorganic ceramic hybrid coating film according to an exemplary embodiment of the present invention.

Referring to FIG. 11, graphene (a two dimension sheet-shaped material), silver nanowire (an one dimension linear material), and silver nanoparticle (a zero-dimension particle-shaped material) were well fused among sol matrix. Herein, since variously-shaped solid-phased materials were used, a polymer binder may be used to well bond them.

In Evaluations 4 and 5, the present exemplary embodiment sufficiently showed a thermal conductivity effect and a surface contact angle effect (a surface functionality) due to 45 graphene.

#### Evaluation 6: Heat Treatment of Graphene-Containing Coating Film

The coating film obtained in Example 2 was heat-treated at a temperature of 200° C. in the air, at a temperature of 50 500° C. under an oxygen atmosphere, and at a temperature of 900 ° C. under a nitrogen atmosphere, and the results as provided in FIG. 12.

Referring to FIG. 12, graphene having a two dimensional carpet was vividly maintained by using a coating solution including a polymer, a silver nano wire, a silver nanoparticle, and the like.

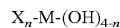
These exemplary embodiments show that an organic component may be required to well bond graphene-ceramic components as aforementioned, and accordingly, an organic functional group may be importantly designed to be included in a ceramic precursor from an initial step. In addition, a moiety oxidized earlier than graphene may be necessarily required to prevent oxidization of the graphene during realization of graphene properties and firing, and accordingly, additives, that is, a reagent capable of M(OH)<sub>4</sub>-shaped hydrolysis, a polymer additive, a dispersing agent,

an organic material additive, a one dimensional nano material, a zero-dimension nanomaterial were added but realized new properties.

While this invention has been described in connection with what is presently considered to be practical exemplary embodiments, it is to be understood that the invention is not limited to the disclosed embodiments, but, on the contrary, is intended to cover various modifications and equivalent arrangements included within the spirit and scope of the 10 appended claims.

What is claimed is:

1. A graphene-containing coating film, comprising:  
at least one hydrate represented by Chemical Formula 1;  
a graphene positioned on the surface of the hydrate  
represented by Chemical Formula 1; and  
a silica particle positioned on the surface of the hydrate of  
Chemical Formula 1 and positioned on the surface of  
the graphene in a shape of discontinuous island,  
wherein the silica particle include agglomeration of a  
plurality of silica nanoparticles:



[Chemical Formula 1]

wherein, in Chemical Formula 1,  
M is selected from the group consisting of Si, Ti, Ag, Sn,  
In, and Zn, and a combination thereof,  
X is:

- a) a C1 to C30 alkyl group substituted or unsubstituted  
with at least one functional group selected from the  
group consisting of an epoxy group, a glycidoxyl group,  
a vinyl group, an acryl group, a methacryl group, a  
carboxyl group, an amino group, a thiol group, a  
phosphoric acid group, a fluoro group, a chloro group,  
a bromo group, an iodine group, a hydroxy group, a  
substituted or unsubstituted C1 to C10 alkoxy group, a  
substituted or unsubstituted C1 to C10 ketone group, a  
substituted or unsubstituted C1 to C10 amine group, a  
substituted or unsubstituted C1 to C10 sulfur group, a  
substituted or unsubstituted C1 to C10 ester group, and  
a substituted or unsubstituted C1 to C10 silyl group;
- b) a C1 to C30 alkenyl group substituted or unsubstituted  
with at least one functional group selected from the  
group consisting of an epoxy group, a glycidoxyl group,  
a vinyl group, an acryl group, a methacryl group, a  
carboxyl group, an amino group, a thiol group, a  
phosphoric acid group, a fluoro group, a chloro group,  
a bromo group, an iodine group, a hydroxy group, a  
substituted or unsubstituted C1 to C10 alkoxy group, a  
substituted or unsubstituted C1 to C10 ketone group, a  
substituted or unsubstituted C1 to C10 amine group, a  
substituted or unsubstituted C1 to C10 sulfur group, a  
substituted or unsubstituted C1 to C10 ester group, and  
a substituted or unsubstituted C1 to C10 silyl group; or
- c) a C1 to C30 alkynyl group substituted or unsubstituted  
with at least one functional group selected from the  
group consisting of an epoxy group, a glycidoxyl group,  
a vinyl group, an acryl group, a methacryl group, a  
carboxyl group, an amino group, a thiol group, a  
phosphoric acid group, a fluoro group, a chloro group,  
a bromo group, an iodine group, a hydroxy group, a  
substituted or unsubstituted C1 to C10 alkoxy group, a  
substituted or unsubstituted C1 to C10 ketone group, a  
substituted or unsubstituted C1 to C10 amine group, a  
substituted or unsubstituted C1 to C10 sulfur group, a  
substituted or unsubstituted C1 to C10 ester group, and  
a substituted or unsubstituted C1 to C10 silyl group,

n is an integer of 1 to 3.

## 31

2. The graphene-containing coating film of claim 1, wherein the graphene-containing coating film comprises: a first region including the hydrate represented by Chemical Formula 1 and the silica particle bound with each other; and a second region including the hydrate represented by Chemical Formula 1, the graphene and the silica particle bound with one another.

3. The graphene-containing coating film of claim 2, wherein an average diameter of the silica particle of the first region is from about 5 nm to about 50 nm, and an average diameter of the silica particle of the second region is from about 5 nm to about 25 nm.

4. The graphene-containing coating film of claim 1, wherein an average diameter of the silica nanoparticle is from about 5 nm to about 30 nm.

5. The graphene-containing coating film of claim 1, wherein a thickness of the graphene is from about 0.4 nm to about 5 nm.

6. The graphene-containing coating film of claim 1, wherein a major axis length of the graphene is from about 100 nm to about 10,000 nm, and a minor axis length of the graphene is about from 100 nm to about 900 nm.

7. The graphene-containing coating film of claim 1, wherein an amount of the graphene is from about 0.001 wt % to about 50 wt % based on the total weight of the hydrate represented by Chemical Formula 1, the graphene, and the silica nanoparticle.

8. The graphene-containing coating film of claim 1, wherein when transmittance is greater than or equal to about 70%, the an amount of the graphene is from about 0.001 wt % to about 3 wt % based on the total weight of the hydrate represented by Chemical Formula 1, the graphene, and the silica nanoparticle.

9. The graphene-containing coating film of claim 1, wherein the graphene-containing coating film has a thickness of about 100 nm to 2  $\mu$ m.

10. The graphene-containing coating film of claim 1, wherein when transmittance is greater than or equal to about 70%, the graphene-containing coating film has a thickness of about 200 nm to 500 nm.

11. The graphene-containing coating film of claim 1, wherein the Chemical Formula 1 is represented by one of Chemical Formulae 1-1 to 1-3:



wherein, in Chemical Formulae 1-1 to 1-3, M is selected from the group consisting of Si, Ti, Ag, Sn, In, and Zn, and a combination thereof,

$X^1$ ,  $X^2$  and  $X^3$  are each independently:

a) a C1 to C30 alkyl group substituted or unsubstituted with at least one functional group selected from the group consisting of an epoxy group, a glycidoxyl group, a vinyl group, an acryl group, a methacryl group, a carboxyl group, an amino group, a thiol group, a phosphoric acid group, a fluoro group, a chloro group, a bromo group, an iodine group, a hydroxy group, a substituted or unsubstituted C1 to C10 alkoxy group, a substituted or unsubstituted C1 to C10 ketone group, a substituted or unsubstituted C1 to C10 amine group, a substituted or unsubstituted C1 to C10 sulfur group, a substituted or unsubstituted C1 to C10 ester group, and a substituted or unsubstituted C1 to C10 silyl group;

## 32

b) a C1 to C30 alkenyl group substituted or unsubstituted with at least one functional group selected from the group consisting of an epoxy group, a glycidoxyl group, a vinyl group, an acryl group, a methacryl group, a carboxyl group, an amino group, a thiol group, a phosphoric acid group, a fluoro group, a chloro group, a bromo group, an iodine group, a hydroxy group, a substituted or unsubstituted C1 to C10 alkoxy group, a substituted or unsubstituted C1 to C10 ketone group, a substituted or unsubstituted C1 to C10 amine group, a substituted or unsubstituted C1 to C10 sulfur group, a substituted or unsubstituted C1 to C10 ester group, and a substituted or unsubstituted C1 to C10 silyl group; or

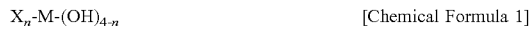
c) a C1 to C30 alkynyl group substituted or unsubstituted with at least one functional group selected from the group consisting of an epoxy group, a glycidoxyl group, a vinyl group, an acryl group, a methacryl group, a carboxyl group, an amino group, a thiol group, a phosphoric acid group, a fluoro group, a chloro group, a bromo group, an iodine group, a hydroxy group, a substituted or unsubstituted C1 to C10 alkoxy group, a substituted or unsubstituted C1 to C10 ketone group, a substituted or unsubstituted C1 to C10 amine group, a substituted or unsubstituted C1 to C10 sulfur group, a substituted or unsubstituted C1 to C10 ester group, and a substituted or unsubstituted C1 to C10 silyl group.

12. The graphene-containing coating film of claim 1, wherein the M is Si or Ti.

13. The graphene-containing coating film of claim 1, wherein the graphene-containing coating film further comprises an additive selected from the group consisting of an inorganic powder, an organic additive, and a combination thereof.

14. The graphene-containing coating film of claim 12, wherein the inorganic powder has an average diameter of about 5 nm to 50 nm.

15. A method of preparing a graphene-containing coating film comprising dispersing a graphene; mixing and dispersing a silica nanoparticle and the precursor of the hydrate represented by Chemical Formula 1 in a hydrophilic solvent and mixing the same with the dispersed graphene; performing hydrolysis and condensation reactions of the mixed dispersed solution to prepare a graphene-containing sol solution; coating the graphene-containing sol solution on a substrate and drying the same at a temperature of about 25° C. to 400° C.; and heat-treating the dried film at a temperature of about 50° C. to 900° C.,



wherein, in Chemical Formula 1, M is selected from the group consisting of Si, Ti, Ag, Sn, In, and Zn, and a combination thereof,

X is: a) a C1 to C30 alkyl group substituted or unsubstituted with at least one functional group selected from the group consisting of an epoxy group, a glycidoxyl group, a vinyl group, an acryl group, a methacryl group, a carboxyl group, an amino group, a thiol group, a phosphoric acid group, a fluoro group, a chloro group, a bromo group, an iodine group, a hydroxy group, a substituted or unsubstituted C1 to C10 alkoxy group, a substituted or unsubstituted C1 to C10 ketone group, a substituted or unsubstituted C1 to C10 amine group, a substituted or unsubstituted C1 to C10 sulfur group, a substituted or unsubstituted C1 to C10 ester group, and a substituted or unsubstituted C1 to C10 silyl group;

33

- substituted or unsubstituted C1 to C10 ester group, and a substituted or unsubstituted C1 to C10 silyl group; b) a C1 to C30 alkenyl group substituted or unsubstituted with at least one functional group selected from the group consisting of an epoxy group, a glycidoxy group, a vinyl group, an acryl group, a methacryl group, a carboxyl group, an amino group, a thiol group, a phosphoric acid group, a fluoro group, a chloro group, a bromo group, an iodine group, a hydroxy group, a substituted or unsubstituted C1 to C10 alkoxy group, a substituted or unsubstituted C1 to C10 ketone group, a substituted or unsubstituted C1 to C10 amine group, a substituted or unsubstituted C1 to C10 sulfur group, a substituted or unsubstituted C1 to C10 ester group, and a substituted or unsubstituted C1 to C10 silyl group; or c) a C1 to C30 alkynyl group substituted or unsubstituted with at least one functional group selected from the group consisting of an epoxy group, a glycidoxy group, a vinyl group, an acryl group, a methacryl group, a carboxyl group, an amino group, a thiol group, a phosphoric acid group, a fluoro group, a chloro group, a bromo group, an iodine group, a hydroxy group, a substituted or unsubstituted C1 to C10 alkoxy group, a substituted or unsubstituted C1 to C10 ketone group, a substituted or unsubstituted C1 to C10 amine group, a substituted or unsubstituted C1 to C10 sulfur group, a substituted or unsubstituted C1 to C10 ester group, and a substituted or unsubstituted C1 to C10 silyl group, and

n is an integer of 1 to 3.

**16.** A vehicle part comprising a graphene-containing coating film of claim 1.

**17.** The vehicle part of claim 16 is a head lamp.

**18.** A vehicle comprising a vehicle part of claim 16.

**19.** The method of claim 15, wherein the silica nanoparticle is present in an amount of about 5 to 20 wt % based on the total amount of the mixed dispersed solution;

the precursor of the hydrate represented by Chemical Formula 1 is present in an amount of about 10 to 40 wt % based on the total amount of the mixed dispersed solution;

the highly dispersed graphene is present in an amount of about 0.001 to 15 wt % based on the total amount of the mixed dispersed solution; and

the hydrophilic solvent is present in a balance amount.

34

**20.** The method of claim 15, wherein the graphene is dispersed by mechanical disperse treatment, or a solvent exchange method.

**21.** The method of claim 20, wherein the solvent exchange method comprises:

preparing a dispersion by mixing a graphene powder, a first dispersing agent and a first non-aqueous based solvent;

preparing a mixture by adding a second non-aqueous based solvent and a precursor of the hydrate to the dispersion; and

preparing a graphene-containing sol solution by mixing the mixture with a second dispersing agent and water.

**22.** The method of claim 15, wherein in mixing and dispersing of the silica nanoparticle and the precursor of the hydrate represented by Chemical Formula 1 in a hydrophilic solvent and mixing the same with the highly dispersed graphene, an additive selected from the group consisting of an inorganic powder, an organic additive, and a combination thereof are further included.

**23.** The method of claim 22, wherein the inorganic powder is mixed in an amount of about 5 parts by weight to 30 parts by weight based on 100 parts by weight of the mixed dispersed solution.

**24.** The method of claim 22, wherein the organic additive is mixed in an amount of about 0.01 parts by weight to 10 parts by weight based on 100 parts by weight of the mixed dispersed solution.

**25.** The method of claim 15, wherein the precursor of the hydrate represented by Chemical Formula 1 is selected from the group consisting of trimethoxysilane, triethoxysilane, methyltrimethoxysilane, methyltriethoxysilane, ethyltrimethoxysilane, ethyltriethoxysilane, propyltrimethoxysilane, propyltriethoxysilane, isobutyltriethoxysilane, glycidoxypyropyltrimethoxysilane, glycidoxypyropyltriethoxysilane, cyclohexyltrimethoxysilane, phenyltrimethoxysilane, phenyltriethoxysilane, vinyltrimethoxysilane, vinyltriethoxysilane, allyltrimethoxysilane, allyltriethoxysilane, dimethylidimethoxysilane, dimethyldiethoxysilane, diphenyldimethoxysilane, (N,N-dimethylaminopropyl)trimethoxysilane, (N,N-dimethylaminopropyl)triethoxysilane, and N,N-{(2-aminoethyl) (3-aminopropyl)}trimethoxysilane, or a combination thereof.

\* \* \* \* \*



US010483012B1

(12) **United States Patent**  
**Al-Harthi et al.**(10) **Patent No.:** US 10,483,012 B1  
(45) **Date of Patent:** Nov. 19, 2019(54) **PROCESS FOR FORMING A NANOCOMPOSITE FILM**(71) Applicant: **King Fahd University of Petroleum and Minerals**, Dhahran (SA)(72) Inventors: **Mamdouh Ahmed Al-Harthi**, Dhahran (SA); **Osamah Awadh Bin-Dahman**, Dhahran (SA)(73) Assignee: **King Fahd University of Petroleum and Minerals**, Dhahran (SA)

(\*) Notice: Subject to any disclaimer, the term of this patent is extended or adjusted under 35 U.S.C. 154(b) by 0 days.

(21) Appl. No.: **16/455,825**(22) Filed: **Jun. 28, 2019****Related U.S. Application Data**

(60) Division of application No. 16/102,337, filed on Aug. 13, 2018, now Pat. No. 10,395,792, which is a (Continued)

(51) **Int. Cl.****H01B 1/24** (2006.01)  
**B29C 41/12** (2006.01)

(Continued)

(52) **U.S. Cl.**CPC ..... **H01B 1/24** (2013.01); **B29C 39/003** (2013.01); **B29D 7/01** (2013.01); **C08J 3/215** (2013.01);

(Continued)

(58) **Field of Classification Search**

CPC ..... H01B 1/02; H01B 1/20–24; H01B 3/002–006; G02B 2270/121;

(Continued)

(56)

**References Cited**

## U.S. PATENT DOCUMENTS

7,976,950 B2 7/2011 Okai et al.  
8,585,934 B2 11/2013 Shah

(Continued)

## FOREIGN PATENT DOCUMENTS

KR 10-2010-0055766 A 5/2010  
KR 10-1209293 B1 12/2012

(Continued)

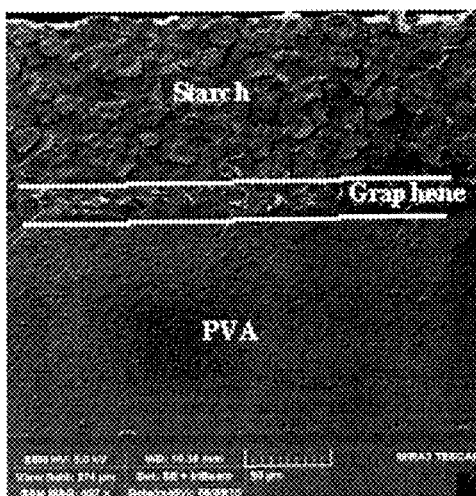
## OTHER PUBLICATIONS

G. Chakraborty, et al., "Activation behavior and dielectric relaxation in polyvinyl alcohol and multiwall carbon nanotube composite films", Solid State Communications, vol. 151, Issue 10, May 2011, pp. 754-758.

(Continued)

*Primary Examiner* — Z. Jim Yang(74) *Attorney, Agent, or Firm* — Oblon, McClelland, Maier & Neustadt, L.L.P.(57) **ABSTRACT**

Nanocomposite films comprising carbon nanotubes dispersed throughout a polymer matrix and further comprising at least two surfaces with differing amounts of carbon nanotubes and differing electrical resistivity values are provided. Nanocomposite films comprising a polymer layer, a conductive nanofiller layer, and a polysaccharide layer having antistatic properties are provided. In particular, nanocomposites comprising polyvinyl alcohol as the polymer, graphene as the conductive nanofiller and starch as the polysaccharide are provided. In addition, processes for forming the nanocomposites, methods for characterizing the nanocomposites as well as applications in or on electrical and/or electronic devices are provided.

**8 Claims, 3 Drawing Sheets**

**Related U.S. Application Data**

continuation of application No. 15/067,796, filed on Mar. 11, 2016, now Pat. No. 10,090,078.

(60) Provisional application No. 62/280,459, filed on Jan. 19, 2016.

**(51) Int. Cl.**

**B29C 39/00** (2006.01)  
**C08J 5/18** (2006.01)  
**B29D 7/01** (2006.01)  
**C08J 3/215** (2006.01)  
**H01B 1/04** (2006.01)  
**B29K 29/00** (2006.01)  
**B29L 7/00** (2006.01)  
**B29K 105/00** (2006.01)  
**B29K 105/16** (2006.01)  
**B29K 507/04** (2006.01)

**(52) U.S. Cl.**

CPC ..... **C08J 5/18** (2013.01); **H01B 1/04** (2013.01); **B29C 41/12** (2013.01); **B29K 2029/04** (2013.01); **B29K 2105/0073** (2013.01); **B29K 2105/162** (2013.01); **B29K 2105/167** (2013.01); **B29K 2507/04** (2013.01); **B29K 2995/0005** (2013.01); **B29K 2995/006** (2013.01); **B29L 2007/008** (2013.01); **B32B 2307/21** (2013.01); **C08J 2329/04** (2013.01); **C08J 2403/02** (2013.01); **G02B 2207/121** (2013.01)

**(58) Field of Classification Search**

CPC ..... B32B 2307/21; C08L 1/00–1/32; C08L 3/00–20; C08L 5/00–16

See application file for complete search history.

**(56) References Cited****U.S. PATENT DOCUMENTS**

9,162,896	B2	10/2015	Kranbuehl
9,382,392	B2	7/2016	Al-Harthi
9,899,123	B2	2/2018	Alden
2008/0044651	A1	2/2008	Douglas
2009/0029125	A1	1/2009	Nakahira
2010/0221508	A1	9/2010	Huang
2010/0301278	A1	12/2010	Hirai
2011/0088931	A1	4/2011	Lettow
2011/0135884	A1	6/2011	Lettow
2011/0281070	A1	11/2011	Mittal
2012/0003467	A1	1/2012	Suzuki
2013/0032765	A1	2/2013	Ermolov
2014/0050903	A1	2/2014	Lettow
2014/0203214	A1	7/2014	Hamad
2014/0284083	A1	9/2014	Srinivas
2015/0200037	A1	7/2015	Inoue

2015/0221411	A1	8/2015	Nakamura
2015/0305212	A1	10/2015	Sarto
2015/0368108	A1	12/2015	Sone
2016/0012936	A1	1/2016	Wu
2016/0035456	A1	2/2016	Sauro
2016/0118156	A1	4/2016	Kawaguchi
2016/0133349	A1	5/2016	Cho
2016/0137854	A1	5/2016	Heintz
2016/0276056	A1	9/2016	Stolyarov
2016/0322133	A1	11/2016	Kim
2017/0103826	A1	4/2017	Al-Harth I
2017/0125136	A1	5/2017	Park
2017/0206997	A1	7/2017	Al-Harth I
2017/0229668	A1	8/2017	Stapleton
2017/0345965	A1	11/2017	Seo

**FOREIGN PATENT DOCUMENTS**

KR	10-1374273	B1	3/2014
KR	10-1391158	B1	5/2014

**OTHER PUBLICATIONS**

Priscilla P. Peregrino, et al., "Thermal and electrical properties of starch-graphene oxide nanocomposites improved by photochemical treatment", Carbohydrate Polymers, vol. 106, Jun. 15, 2014, pp. 305-311.

Yuxi Xu, et al., "Strong and ductile poly(vinyl alcohol)/graphene oxide composite films with a layered structure", Carbon, vol. 47, 2009, pp. 3538-3543.

Xin Zhao, et al., "Enhanced Mechanical Properties of Graphene-Based Poly(vinyl alcohol) Composites", Macromolecules, vol. 43, No. 5, 2010, pp. 2357-2363.

Chen Wang, et al., "Preparation and Characterization of Graphene Oxide/Poly(vinyl alcohol) Composite Nanofibers via Electrospinning", Journal of Applied Polymer Science, 2013, pp. 3026-3032.

Sunil G. Rathod, et al., "Thermal, Mechanical and Dielectric Properties of Poly(vinyl alcohol)/Graphene Oxide Composites", AIP Conference Proceedings, vol. 1591, p. 1769, Apr. 2014 (Abstract only).

Jiajia Liang, et al., "Molecular-Level Dispersion of Graphene into Poly(vinyl alcohol) and Effective Reinforcement of their Nanocomposites", Advanced Functional Materials, vol. 19, 2009, pp. 1-6.

Henry Kuo Feng Cheng, et al., "Poly(vinyl alcohol) Nanocomposites Filled with Poly(vinyl alcohol)—Grafted Graphene Oxide", ACS Applied Materials & Interfaces, vol. 4, 2012, pp. 2387-2394.

Pandele et al., Synthesis, characterization, and in vitro studies of graphene oxide/chitosan-polyvinyl alcohol films, Carbohydrate Polymers, vol. 102, 2014, p. 813-820 (Year: 2014).

Layek et al., Graphene sulphonic acid/chitosan nano biocomposites with tunable mechanical and conductivity properties, Polymer, vol. 53, 2012, p. 2265-2273 (Year: 2012).

Jose et al., Effect of graphene loading on thermomechanical properties of poly(vinyl alcohol)/starch blend, Journal of Applied Polymer Science, p. 41827 (Year: 2015).

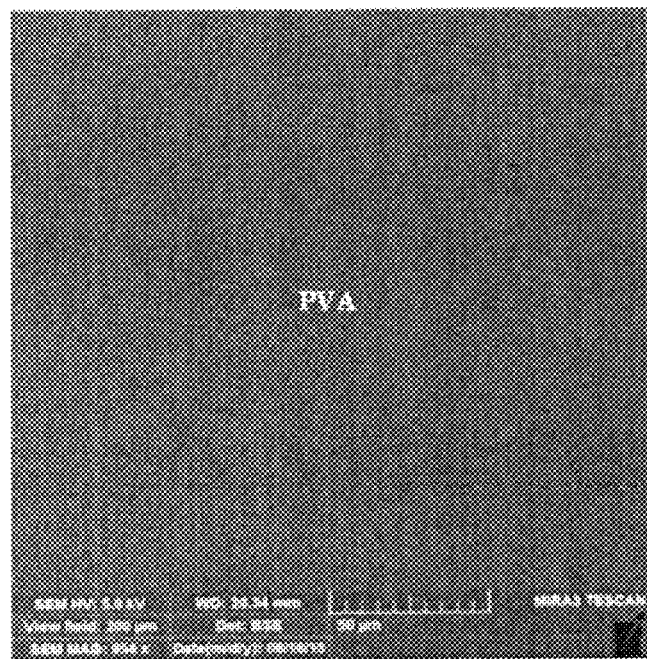


FIG. 1A

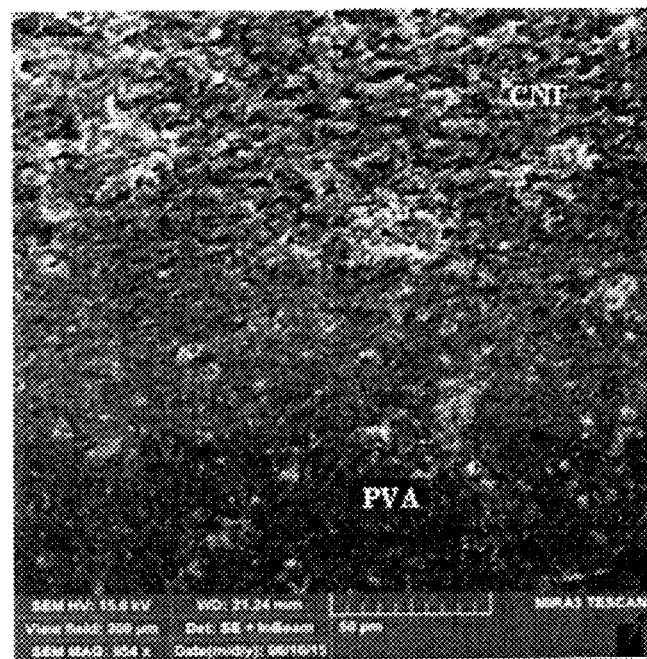


FIG. 1B

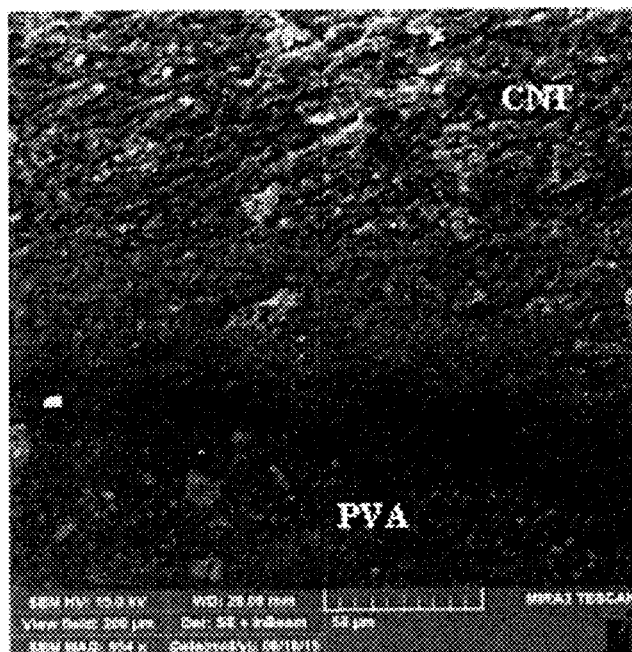


FIG. 1C

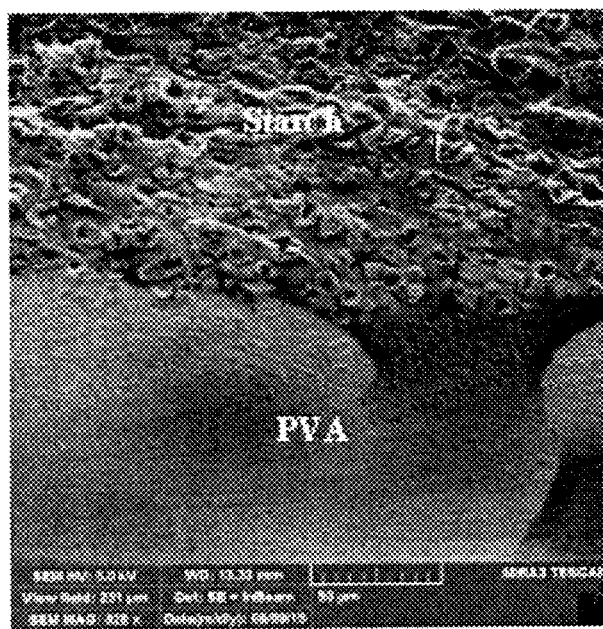


FIG. 2A

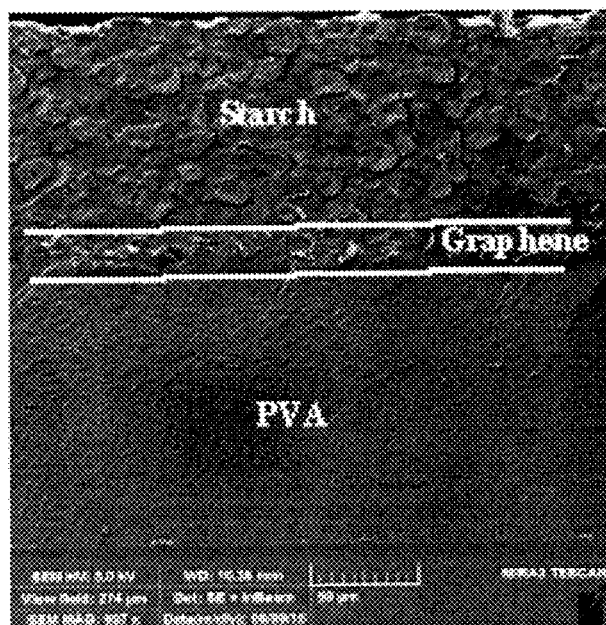


FIG. 2B

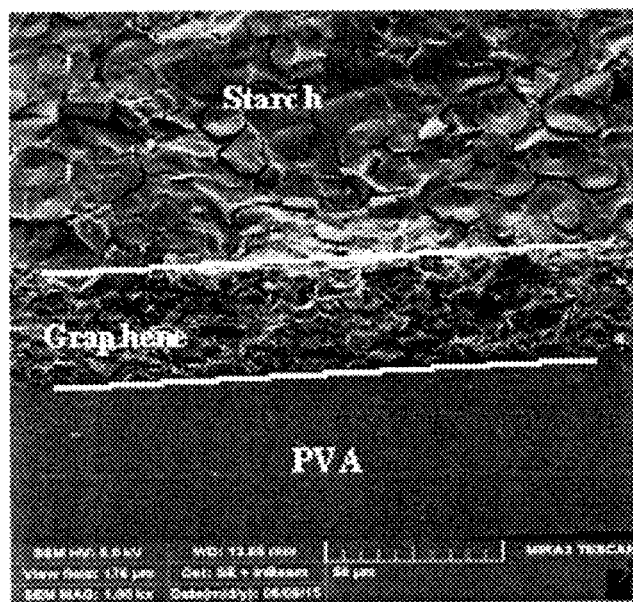


FIG. 2C

1

**PROCESS FOR FORMING A  
NANOCOMPOSITE FILM**

**CROSS REFERENCE TO RELATED  
APPLICATIONS**

The present application is a Divisional of U.S. application Ser. No. 16/102,337, now allowed, having a filing date of Aug. 13, 2018 which is a Continuation of U.S. application Ser. No. 15/067,796, now U.S. Pat. No. 10,090,078, having a filing date of Mar. 11, 2016 which claims benefit of priority to U.S. Provisional Application No. 62/280,459 having a filing date of Jan. 19, 2016 which is incorporated herein by reference in its entirety. Further, this application is related to U.S. application Ser. No. 14/877,623 now U.S. Pat. No. 10,049,784, having a filing date of Oct. 7, 2015, the entire contents of which are incorporated herein by reference.

**BACKGROUND OF THE INVENTION**

**Technical Field**

The present disclosure relates to a nanocomposite film comprising a polymer matrix and conductive carbon nanotubes dispersed in the matrix having a first surface with a first resistivity and a second surface with a second resistivity, a process for producing the nanocomposite film and an electronic device comprising the nanocomposite film. The present disclosure also relates to a nanocomposite film comprising a polymer layer, a polysaccharide layer and a conductive nanofiller layer sandwiched between the polymer layer and the polysaccharide layer, a process for producing the nanocomposite film and an electronic device comprising the electronic film.

**Description of the Related Art**

The “background” description provided herein is for the purpose of generally presenting the context of the disclosure. Work of the presently named inventors, to the extent it is described in this background section, as well as aspects of the description which may not otherwise qualify as prior art at the time of filing, are neither expressly or impliedly admitted as prior art against the present invention.

The shortage in petroleum resources and the rapid increase in the usage of non-biodegradable polymers pose a great risk to the environment. Development of polymer composites from biodegradable and renewable materials has attracted wide attention in scientific and technological communities owing to their interesting properties. Polymer composites filled by nanostructures have attracted significant attention as a result of their unique mechanical, electric and optical properties. Nano-scale conductive fillers can create a seamlessly interconnected percolative network within the polymer matrix altering the energy storing and transporting properties of the composite while reinforcing the native polymer and enhancing its mechanical strength.

Polyvinyl alcohol (PVA) is a synthetic, water soluble and biodegradable polymer that has been used in numerous applications including water soluble packaging films, drug delivery, paper coating, textile sizing, etc. PVA is well known for its biocompatibility and non-toxicity. PVA can easily be blended with a wide range of natural polymers and fillers to make biodegradable composites with outstanding properties. PVA has excellent properties such as biocompatibility, barrier properties to gases and liquids, hydrophilicity and chemical resistance [M. I. Baker, S. P. Walsh, Z.

2

Schwartz, and B. D. Boyan, “A review of polyvinyl alcohol and its uses in cartilage and orthopedic applications,” *J. Biomed. Mater. Res. B. Appl. Biomater.*, vol. 100, no. 5, pp. 1451-7, July 2012.—incorporated herein by reference in its entirety].

- Carbon nanotubes (CNTs) have attracted a great interest since they were discovered in 1991 [S. Iijima, “Helical microtubules of graphitic carbon,” *Nature*, vol. 354, no. 6348, pp. 56-58, November 1991.—incorporated herein by reference in its entirety]. They have a cylindrical structure of carbon atoms with excellent mechanical, electrical, thermal, optical and chemical properties. The Young’s modulus and the tensile strength of carbon nanotubes are approximately 5 times and 50 times higher than those of steel, respectively. 10 The thermal conductivity of carbon nanotubes is in the range of 1800-200 W/m-K [F. D. S. Marquis and L. P. F. Chibante, “Improving the heat transfer of nanofluids and nanolubricants with carbon nanotubes,” *JOM*, vol. 57, no. 12, pp. 32-43, December 2005.—incorporated herein by reference 15 in its entirety]. In recent years, many studies have been carried out on the preparation and characterization of biopolymer nanocomposites based on CNTs [M. C. Paiva, B. Zhou, K. A. S. Fernando, Y. Lin, J. M. Kennedy, and Y.-P. Sun, “Mechanical and morphological characterization of polymer-carbon nanocomposites from functionalized carbon nanotubes,” *Carbon N. Y.*, vol. 42, no. 14, pp. 2849-2854, January 2004; and S.-I. Moon, F. Jin, C. Lee, S. Tsutsumi, and S.-H. Hyon, “Novel Carbon Nanotube/Poly(L-lactic acid) Nanocomposites; Their Modulus, Thermal Stability, 20 and Electrical Conductivity,” *Macromol. Symp.*, vol. 224, no. 1, pp. 287-296, April 2005; and W. Chen and X. Tao, “Production and characterization of polymer nanocomposite with aligned single wall carbon nanotubes,” *Appl. Surf. Sci.*, vol. 252, no. 10, pp. 3547-3552, March 2006; and J. T. Yoon, 25 Y. G. Jeong, S. C. Lee, and B. G. Min, “Influences of poly(lactic acid)-grafted carbon nanotube on thermal, mechanical, and electrical properties of poly(lactic acid),” *Polym. Adv. Technol.*, vol. 20, no. 7, pp. 631-638, July 2009; and W.-M. Chiu, Y.-A. Chang, H.-Y. Kuo, M.-H. Lin, and H.-C. Wen, “A study of carbon nanotubes/biodegradable plastic polylactic acid composites,” *J. Appl. Polym. Sci.*, vol. 108, no. 5, pp. 3024-3030, June 2008; and S. W. Ko, M. K. Hong, B. J. Park, R. K. Gupta, H. J. Choi, and S. N. Bhattacharya, “Morphological and rheological characterization of multi-walled carbon nanotube/PLA/PBAT blend nanocomposites,” *Polym. Bull.*, vol. 63, no. 1, pp. 125-134, April 2009; and S. Chen, G. Wu, Y. Liu, and D. Long, “Preparation of Poly(acrylic acid) Grafted Multiwalled Carbon Nanotubes by a Two-Step Irradiation Technique,” *Macromolecules*, vol. 39, no. 1, pp. 330-334, January 2006; and Y.-L. Liu, W.-H. Chen, and Y.-H. Chang, “Preparation and properties of chitosan/carbon nanotube nanocomposites using poly(styrene sulfonic acid)-modified CNTs,” *Carbohydr. Polym.*, vol. 76, no. 2, pp. 232-238, March 2009; and 30 F. Mai, Y. Habibi, J.-M. Raquez, P. Dubois, J.-F. Feller, T. Peijs, and E. Biliti, “Poly(lactic acid)/carbon nanotube nanocomposites with integrated degradation sensing,” *Polymer (Guildf.)*, vol. 54, no. 25, pp. 6818-6823, November 2013; and J. Jose, S. K. De, M. A. AlMa’adeed, J. B. Dakua, 35 P. A. Sreekumar, R. Sougrat, and M. A. Al-Harthi, “Compatibilizing role of carbon nanotubes in poly(vinyl alcohol)/starch blend,” *Starch/Stärke*, vol. 66, pp. 1-7, October 2014.—each incorporated herein by reference in its entirety]. 40 Starch is a natural biodegradable polymer and has several benefits such as availability, its low cost compared to synthetic polymers, and its full compostability without leaving

ing any toxic residue [F. Xie, E. Pollet, P. J. Halley, and L. Avérous, "Starch-based nano-biocomposites," *Prog. Polym. Sci.*, vol. 38, no. 10-11, pp. 1590-1628, October 2013.—incorporated herein by reference in its entirety]. Starch can be used to enhance the properties as well as to decrease the cost of products incorporating it [M. Maiti, B. S. Kaith, R. Jindal, and A. K. Jana, "Synthesis and characterization of corn starch based green composites reinforced with *Saccharum spontaneum* L graft copolymers prepared under microwave and their effect on thermal, physio-chemical and mechanical properties," *Polym. Degrad. Stab.*, vol. 95, no. 9, pp. 1694-1703, September 2010.—incorporated herein by reference in its entirety]. However, the films formed from native starch have certain shortcomings such as brittleness and high water absorption [B. Chatterjee, N. Kulshrestha, and P. N. Gupta, "Electrical properties of starch-PVA biodegradable polymer blend," *Phys. Scr.*, vol. 90, no. 2, p. 025805, February 2015.—incorporated herein by reference in its entirety]. Blends of polyvinyl alcohol with starch have been widely studied in the literature [P. Sreekumar, M. a. Al-Harthi, and S. De, "Reinforcement of starch/polyvinyl alcohol blend using nano-titanium dioxide," *J. Compos. Mater.*, vol. 46, no. 25, pp. 3181-3187, February 2012; and P. A. Sreekumar, M. A. Al-Harthi, and S. K. De, "Effect of glycerol on thermal and mechanical properties of polyvinyl alcohol/starch blends," *J. Appl. Polym. Sci.*, vol. 123, no. 1, pp. 135-142, 2012; and P. A. Sreekumar, M. A. Al-Harthi, and S. K. De, "Studies on compatibility of biodegradable starch/polyvinyl alcohol blends," *Polym. Eng. Sci.*, vol. 52, no. 10, pp. 2167-2172, October 2012; and S. P. Appu, S. K. De, M. J. Khan, and M. A. Al-Harthi, "Natural weather ageing of starch/polyvinyl alcohol blend: effect of glycerol content," *J. Polym. Eng.*, vol. 33, no. 3, pp. 1-7, January 2013.—each incorporated herein by reference in its entirety].

Graphene has a two-dimensional structure of carbon atoms in a hexagonal lattice with sheets having a thickness of just one atom (0.33 nm). The graphene has a layered crystal structure, in which the carbon atoms are strongly bonded on a two-dimensional network consisting of hexagons. Graphene combines the layered structure of clays with the excellent mechanical, thermal and electrical properties of carbon nanotubes to provide unique functional properties in final products. Since the isolation of a single sheet of graphene [K. S. Novoselov, A. K. Geim, S. V Morozov, D. Jiang, Y. Zhang, S. V Dubonos, I. V Grigorieva, a a Firsov, *Science*, vol. 306, no. 5696 (2004) 666-669.—incorporated herein by reference in its entirety], graphene has attracted the attention of researchers pursuing novel nanocomposites. Recently, it has received a substantial interest compared to the conventional nanofillers such as nanoclays and carbon nanotubes because of its exceptional electrical and mechanical properties, high aspect ratio, and low density [O. C. Compton and S. T. Nguyen, "Graphene oxide, highly reduced graphene oxide, and graphene: versatile building blocks for carbon-based materials," *Small*, vol. 6, no. 6, pp. 711-23, March 2010; and S. Sheshmani, A. Ashori, and M. A. Fashapoyeh, "Wood plastic composite using graphene nanoplatelets," *Int. J. Biol. Macromol.*, vol. 58, pp. 1-6, July 2013; and S. Sheshmani and R. Amini, "Preparation and characterization of some graphene based nanocomposite materials," *Carbohydr. Polym.*, vol. 95, no. 1, pp. 348-59, June 2013.—each incorporated herein by reference in its entirety].

Graphene is known to be combined as a few layers (graphite) and different types of graphite nanoplatelets such as thermally expanded graphite, graphene oxide (GO) and

chemically modified graphene have been used to make functional polymer nanocomposites [H. Kim, A. Abdala, C. W. Macosko, *Macromolecules* 43 (2010) 6515; and C. Gomez-Navarro, J. C. Meyer, R. S. Sundaram, A. Chuvilin, S. Kurasch, M. Burghard, K. Kern, U. Kaiser, *Nano Lett.* 10 (2010) 1144; and J. T. Robinson, F. K. Perkins, E. S. Snow, Z. Wei, P. E. Sheehan, *Nano Lett.* 8 (2008) 3137; and Y. Zhu, S. Murali, W. Cai, X. Li, J. W. Suk, J. R. Potts, R. S. Ruoff, *Adv. Mater.* 22 (2010) 3906.—each incorporated herein by reference in its entirety]. The initial development of graphene from graphite was via acid treatment (Hummer's reaction) to exfoliate graphene sheets [W. S. Hummers, R. E. Offeman, *J. Am. Chem. Soc.* 80 (1958) 1339.—incorporated herein by reference in its entirety].

Making nanocomposites with unique functional properties from polyvinyl alcohol and graphene has attracted significant attention from researchers [Y. Xu, W. Hong, H. Bai, C. Li, and G. Shi, "Strong and ductile poly(vinyl alcohol)/graphene oxide composite films with a layered structure," *Carbon* N. Y., vol. 47, no. 15, pp. 3538-3543, December 2009; and J. Liang, Y. Huang, L. Zhang, Y. Wang, Y. Ma, T. Guo, and Y. Chen, "Molecular-Level Dispersion of Graphene into Poly(vinyl alcohol) and Effective Reinforcement of their Nanocomposites," *Adv. Funct. Mater.*, vol. 19, no. 14, pp. 2297-2302, July 2009; and H. K. F. Cheng, N. G. Sahoo, Y. P. Tan, Y. Pan, H. Bao, L. Li, S. H. Chan, and J. Zhao, "Poly(vinyl alcohol) nanocomposites filled with poly(vinyl alcohol)-grafted graphene oxide," *ACS Appl. Mater. Interfaces*, vol. 4, no. 5, pp. 2387-94, May 2012; and X. Zhao, Q. Zhang, D. Chen, and P. Lu, "Enhanced Mechanical Properties of Graphene-Based Poly(vinyl alcohol) Composites," *Macromolecules*, vol. 43, no. 5, pp. 2357-2363, March 2010; and H.-D. Huang, P.-G. Ren, J. Chen, W.-Q. Zhang, X. Ji, and Z.-M. Li, "High barrier graphene oxide nanosheet/poly(vinyl alcohol) nanocomposite films," *J. Memb. Sci.*, vol. 409, no. 410, pp. 156-163, August 2012; and C. Wang, Y. Li, G. Ding, X. Xie, and M. Jiang, "Preparation and characterization of graphene oxide/poly(vinyl alcohol) composite nanofibers via electrospinning," *J. Appl. Polym. Sci.*, vol. 127, no. 4, pp. 3026-3032, February 2013; and Y.-S. Ye, M.-Y. Cheng, X.-L. Xie, J. Rick, Y.-J. Huang, F.-C. Chang, and B.-J. Hwang, "Alkali doped polyvinyl alcohol/graphene electrolyte for direct methanol alkaline fuel cells," *J. Power Sources*, vol. 239, pp. 424-432, October 2013; and H.-L. Ma, Y. Zhang, Q.-H. Hu, S. He, X. Li, M. Zhai, and Z.-Z. Yu, "Enhanced mechanical properties of poly(vinyl alcohol) nanocomposites with glucose-reduced graphene oxide," *Mater. Lett.*, vol. 102-103, pp. 15-18, July 2013.—each incorporated herein by reference in its entirety].

For example, Xu et al. reported the preparation of a PVA/graphene oxide nanocomposite that was shown to be strong and ductile in comparison to the pristine polymer. Liang et al. have also prepared PVA/graphene oxide nanocomposites by a simple solution mixing in water and casting method. The molecular level dispersion of graphene (only 0.7 wt. % of graphene oxide) in the polymer matrix significantly improved the mechanical strength properties in comparison to the native polymer.

Furthermore, Cheng et al. used PVA/graphene/graphene oxide instead of pristine graphene oxide alone to further improve the properties of PVA nanocomposites. The results showed a 88% increase in tensile strength, a 150% increase in Young's modulus and a 225% increase in elongation at break compared to the native polymer with only a 1% by weight loading of filler. Zhao et al. prepared a staple dispersion of graphene oxide in water with the aid of sodium dodecyl benzene sulfonate (SDBS) via sonication. The

results demonstrated a 150% increase in tensile strength with the addition of 1.8% by weight graphene to the native polymer.

In addition, Huang et al. prepared PVA/graphene oxide nanosheet composites by a simple solution mixing process. A significant change was noted in the barrier property and the results lead to applications in the packaging industry. Wang et al. reported the characterization and preparation of PVA/graphene oxide nanocomposites via electrospinning methods. The results showed a decrease in decomposition temperature as well as a significant increase (42x) in tensile strength with a very low loading (0.02 wt. % of graphene oxide) in the PVA matrix.

Recently, Ye et al. demonstrated significant improvements in ionic conductivity and methanol crossover for a PVA membrane reinforced with graphene leading to fuel cell applications. Ma et al. prepared nanocomposite films of PVA and a glucose-reduced graphene oxide (rGO) by a solution blending method. The aqueous suspension stability of rGO was investigated by adding sodium dodecyl benzene sulfonate (SDBS) and poly(N-vinyl-2-pyrrolidone) (PVP). The results showed that PVP enhanced the dispersion of rGO in water significantly better than SDBS. Furthermore, the results showed an increased tensile strength and an increased Young's modulus for the nanocomposite films compared to the native PVA polymer.

In view of the forgoing, one aspect of the present disclosure is to design and provide nanocomposites with a non-uniform dispersion of carbon nanotubes in a polymeric matrix to introduce non-uniform electrical conductivity. It is envisioned that by this manner nanocomposites having the same or different local and bulk electrical resistivities can be produced. Another aspect of the present disclosure is nanocomposite films comprising a polymer layer, a conductive nanofiller layer, and a polysaccharide layer having antistatic properties at both the polymer layer and the polysaccharide layer. In addition, processes for forming the nanocomposites, methods for characterizing the nanocomposites as well as applications in or on electrical and/or electronic devices are provided.

#### BRIEF SUMMARY OF THE INVENTION

According to a first aspect, the present disclosure relates to a nanocomposite film comprising i) a polymer matrix, ii) carbon nanotubes having an average outer diameter of 5-75 nm and an average inner diameter of 0.5-50 nm dispersed in the matrix, iii) a first surface having a first content of carbon nanotubes and a first resistivity, and iv) a second surface having a second content of conductive nanofiller and a second resistivity, wherein the second content of carbon nanotubes is greater than or equal to the first content of carbon nanotubes, and wherein the second resistivity is less than or equal to the first resistivity.

In one embodiment, the nanocomposite film comprises up to 25 weight percent of the carbon nanotubes relative to the total weight of the nanocomposite film.

In one embodiment, the nanocomposite film has an average thickness of 0.1-1.0 mm.

In one embodiment, the polymer matrix comprises polyvinyl alcohol.

In one embodiment, the carbon nanotubes are at least one selected from the group consisting of multi walled carbon nanotubes, single walled carbon nanotubes and hybrid nanotubes.

In one embodiment, the nanocomposite film comprises 0.01-0.75 weight percent of the carbon nanotubes relative to

the total weight of the nanocomposite film and the first surface is insulating and has a first resistivity of greater than  $10^8 \text{ ohm}\cdot\text{cm}^2$  and the second surface is insulating and has a second resistivity of greater than  $10^8 \text{ ohm}\cdot\text{cm}^2$ .

5 In one embodiment, the nanocomposite film comprises 1.0-7.0 weight percent of the carbon nanotubes relative to the total weight of the nanocomposite film and the first surface is insulating and has a first resistivity of greater than  $10^8 \text{ ohm}\cdot\text{cm}^2$  and the second surface is antistatic and has a second resistivity of  $10^4\text{-}10^8 \text{ ohm}\cdot\text{cm}^2$ .

10 In one embodiment, the nanocomposite film comprises greater than 7.5 weight percent of carbon nanotubes relative to the total weight of the nanocomposite film and the first surface is insulating and has a first resistivity of greater than  $10^8 \text{ ohm}\cdot\text{cm}^2$  and the second surface is semiconducting and/or conducting and has a second resistivity of less than  $10^4 \text{ ohm}\cdot\text{cm}^2$ .

15 According to a second aspect, the present disclosure relates to a process for forming the nanocomposite film comprising i) sonicating a solution of carbon nanotubes to form a stable dispersion of carbon nanotubes, ii) mixing the dispersion of carbon nanotubes with a solution of polymer to form a reaction mixture, and iii) casting the reaction mixture and drying to form the nanocomposite film.

20 According to a third aspect, the present disclosure relates to an electronic device comprising the nanocomposite film, wherein the nanocomposite film is present in or on said device.

25 According to a fourth aspect, the present disclosure relates to a nanocomposite film comprising i) a polymer layer, ii) a conductive nanofiller layer, iii) a polysaccharide layer, iv) a surface of the polysaccharide layer having a first resistivity, and v) a surface of the polymer layer having a second resistivity, wherein the conductive nanofiller layer is sandwiched between and in continuous contact with the polymer layer and the polysaccharide layer, and wherein the second resistivity is less than or equal to the first resistivity.

30 In one embodiment, the nanocomposite film comprises a weight ratio between the polymer layer and the polysaccharide layer is in the range of 80:20 to 60:40.

35 In one embodiment, the nanocomposite film comprises up to 25 weight percent of the conductive nanofiller layer relative to the total weight of the nanocomposite film.

40 In one embodiment, the conductive nanofiller layer comprises graphene in the form of nanosheets having an average longest dimension of 1-75  $\mu\text{m}$  and an average thickness of 0.5-300 nm or in the form of nanoplatelets having an average diameter of 1-75  $\mu\text{m}$  and an average thickness of 0.5-300 nm.

45 In one embodiment, the polymer layer comprises polyvinyl alcohol.

50 In one embodiment, the polysaccharide layer comprises starch.

55 In one embodiment, the nanocomposite film has an average thickness of 0.1-1.0 mm.

60 In one embodiment, the surface of the polysaccharide layer is antistatic and has a first resistivity in the range of  $10^6\text{-}10^8 \text{ ohm}\cdot\text{cm}^2$  and the surface of the polymer layer is antistatic and has a second resistivity in the range of  $10^6\text{-}10^8 \text{ ohm}\cdot\text{cm}^2$ .

65 According to a fifth aspect, the present disclosure relates to a process for forming the nanocomposite film comprising i) sonicating a solution of conductive nanofiller to form a stable dispersion of conductive nanofiller, ii) mixing the dispersion of conductive nanofiller with a solution compris-

ing polymer and polysaccharide to form a reaction mixture, and iii) casting the reaction mixture and drying to form the nanocomposite film.

According to a sixth aspect, the present disclosure relates to an electronic device comprising the nanocomposite film, wherein the nanocomposite film is present in or on said device.

#### BRIEF DESCRIPTION OF THE DRAWINGS

A more complete appreciation of the disclosure and many of the attendant advantages thereof will be readily obtained as the same becomes better understood by reference to the following detailed description when considered in connection with the accompanying drawings, wherein:

FIG. 1A is a field emission scanning electron microscopy (FESEM) image of a control pure polyvinyl alcohol (PVA) film.

FIG. 1B is a FESEM image of the prepared polyvinyl alcohol and carbon nanotube nanocomposite film comprising 7.0 weight percent of carbon nanotubes relative to the total weight of the nanocomposite film.

FIG. 1C is a FESEM image of the prepared polyvinyl alcohol and carbon nanotube nanocomposite film comprising 10.0 weight percent of carbon nanotubes relative to the total weight of the nanocomposite film.

FIG. 2A is a FESEM image of a control pure polyvinyl alcohol (PVA) and starch blend film.

FIG. 2B is a FESEM image of the prepared polyvinyl alcohol, starch and graphene nanocomposite film comprising 1.0 weight percent of graphene relative to the total weight of the nanocomposite film.

FIG. 2C is a FESEM image of the prepared polyvinyl alcohol, starch and graphene nanocomposite film comprising 5.0 weight percent of graphene relative to the total weight of the nanocomposite film.

#### DETAILED DESCRIPTION OF THE EMBODIMENTS

Referring now to the drawings.

According to a first aspect, the present disclosure relates to a nanocomposite film including a polymer matrix and carbon nanotubes dispersed in the matrix.

As used herein, "composite" refers to a combination of two or more distinct constituent materials into one. The individual components, on an atomic level, remain separate and distinct within the finished structure. The materials may have different physical or chemical properties, that when combined, produce a material with characteristics different from the original components. A composite is understood to consist of a bulk phase, termed the matrix, enclosing a reinforcing phase, termed the filler. In a preferred embodiment, the filler is carbon nanotubes.

Nanocomposites are nanomaterials where a nano-object is dispersed into a matrix or phase. A nanocomposite is a multiphase solid material where one of the phases, the nano-object, has one, two or three dimensions of less than 100 nm, or structures having nano-scale repeat distances between the different phases that make up the material. In the broadest sense this definition can include porous media, colloids, gels and copolymers, but is more usually taken to mean the solid combination of a bulk matrix and one or more nanodimensional filler phases differing in properties due to dissimilarities in structure and chemistry. In general, the mechanical, electrical, thermal optical, electrochemical and

catalytic properties of the nanocomposite will differ from that of the component materials.

Nanocomposites differ from conventional composite materials due to the exceptionally high surface to volume ratio of the filler phase and/or its exceptionally high aspect ratio. The aspect ratio of a nanofiller (i.e. carbon nanotubes) is defined as the length of the major (long) axis divided by the width of the minor (short) axis. The area of interface between matrix and filler phase or phases is typically an order of magnitude greater than for conventional composite materials.

A polymer nanocomposite is a multiphase system consisting of a polymer or copolymer having nanofillers (i.e. carbon nanotubes) dispersed in the polymer matrix. These nanofillers may be of different shapes and sizes and comprise particles, sheets and/or fibers, but at least one dimension must be in the range of less than 100 nm. Appropriately adding nanomaterial to a polymer matrix can enhance its performance by capitalizing on the nature and properties of the nanoscale filler. This strategy is particularly effective in yielding high performance composites when the properties of the nanoscale filler are substantially different or better than those of the matrix. Nanoscale dispersion of filler or controlled nanostructures into a composite can introduce new physical properties and novel behaviors that are absent in the unfilled matrices, effectively changing the nature of the original matrix.

A polymer is a large molecule, or macromolecule, composed of many repeated subunits. Polymers, both natural and synthetic are created via polymerization of many small molecules, termed monomers. When two or more different monomers unite together to polymerize it is termed a copolymer and the process is termed copolymerization. The consequently large molecular mass of polymers relative to small molecule compounds produce unique physical properties including toughness, viscoelasticity, and a tendency to form semicrystalline structures rather than crystals. The polymer of the polymer matrix of the present disclosure may be a homopolymer (one monomer) or a copolymer (more than one monomer) and mixtures thereof.

Copolymers can be classified based on how their constituent monomeric units are arranged along the chain. Alternating copolymers have regular alternating monomeric units. Periodic copolymers have monomeric units arranged in a repeating sequence. Statistical copolymers have a sequence of monomer residues following a statistical rule. Random copolymers have the probability of finding a given type of monomer unit at a particular point in the chain equal to the mole fraction of that monomer in the chain. Block copolymers comprise two or more homopolymer subunits linked by covalent bonds and may require an intermediate non-repeating subunit or junction block. In gradient copolymers the monomer composition changes gradually along the chain. The polymer of the polymer matrix of the present disclosure may be a homopolymer, an alternating copolymer, a periodic copolymer, a statistical copolymer, a block copolymer, a gradient copolymer or mixtures thereof.

Polymers can be classified based on their origin and occurrence in nature. Polymers which occur in nature are called natural polymers, also known as biopolymers. Examples of such polymers include, but are not limited to natural rubber, natural silk, shellac, amber, cellulose, starch, alginate, chitosan, collagen, keratin, gelatin, fibrin, polypeptides, polysaccharides, nucleic acids, proteins, etc. Semisynthetic polymers are chemically modified natural polymers and include hydrogenated natural rubber, cellulosic, cellulose nitrate, methyl cellulose, etc. A polymer which has been

synthesized in a laboratory is known as a synthetic polymer or manmade polymers. Examples of such polymers include synthetic rubber, polyvinyl alcohol, polyethylene, polyethylene glycol, polystyrene, polyvinyl chloride (PVC or vinyl), polypropylene, polyacrylonitrile, polyvinyl butyral (PVB), polysulfone, polycaprolactone (PCL), polyglycerol sebacate (PGS), poly(lactic-co-glycolic acid), phenol formaldehyde resin (Bakelite), neoprene, nylon, silicone etc. The polymer of the polymer matrix of the present disclosure may be a natural polymer, a semisynthetic polymer or a synthetic polymer or copolymers and mixtures thereof.

Polymers can be classified based on their thermal response. Thermoplastic polymers can be softened or plasticized repeatedly upon the application of thermal energy without much change in properties if treated with certain precautions. Examples of such polymers include polyolefins, nylons, linear polyesters and polyethers, poly(vinyl chloride), sealing wax, etc. Thermosetting polymers undergo certain chemical changes on heating and convert themselves into an infusible mass. The curing or setting process involves chemical reaction leading to further growth and cross linking of the polymer chain molecules and producing giant molecules. Examples of such polymers include phenolic resins, urea, epoxy resins, diene rubbers, etc. The polymer of the polymer matrix of the present disclosure may be a thermoplastic polymer, a thermosetting polymer or copolymers and mixtures thereof.

Polymers can be classified based on their mode of formation. Addition polymers are formed from olefinic, diolefinic, vinyl and related monomers. They are formed from simple addition of monomer molecules to each other in quick succession by a chain mechanism. This process is called addition polymerization. Examples of such polymers include polyethylene, polypropylene, polystyrene. Condensation polymers are formed from intermolecular reactions between bifunctional or polyfunctional monomer molecules having reactive functional groups such as —OH, —COOH, —NH<sub>2</sub>, —NCO, etc. The polymer of the polymer matrix of the present disclosure may be an addition polymer, a condensation polymer or copolymers and mixtures thereof.

Polymers can be classified based on their structure or line structure. If the monomer units are joined in a linear fashion the polymer is said to be a linear polymer. If the monomer units are joined in a branched manner the polymer is said to be a branched polymer. If the monomer units are joined together in a chain fashion the polymer is said to be a cross linked polymer. A graft copolymer is a special type of branched copolymer where the side chains are structurally distinct from the main chain. The individual chains of a graft copolymer may be homopolymers or copolymers. The polymer of the polymer matrix of the present disclosure may be a linear homopolymer (one monomer), a linear copolymer (more than one monomer), a branched homopolymer, a branched copolymer, a cross linked homopolymer, a cross linked copolymer, a graft copolymer or mixtures and copolymers thereof.

Polymers can be classified based on their application and physical properties depending on the ultimate form and use of the polymer. Rubbers (elastomers) are high molecular weight polymers with long flexible chains and weak intermolecular forces. They typically exhibit tensile strength in the range of 300-3000 psi and elongation at break in the range of 300-1000% and examples include natural and synthetic rubber. Plastics are relatively tough substances with high molecular weight that can be molded with (or without) the application of heat. These are usually much stronger than rubbers. They typically exhibit tensile strength

in the range of 4000-15000 psi and elongation at break in the range of 20-200% and examples include polyethylene, polypropylene, poly(vinyl chloride), polystyrene, etc. Fibers are long chain polymers characterized by highly crystalline regions resulting mainly from secondary forces. They have a much lower elasticity than plastics and elastomers. They typically also have high tensile strength ranging between 20,000-150,000 psi, are light weight and possess moisture absorption properties. The polymer of the polymer matrix of the present disclosure may be a rubber, a plastic, a fiber or copolymers and mixtures thereof.

Polymers can be classified based on their tacticity or structure. Tacticity may be defined as the geometric arrangement (orientation) of the characteristic group (side group) of monomer units with respect to the main chain (backbone) of the polymer. An isotactic polymer is the type of polymer in which the characteristic groups are arranged on the same side of the main chain. A syndiotactic polymer is the type of polymer in which the characteristic groups are arranged in an alternating fashion. An atactic polymer is the type of polymer in which the characteristic groups are arranged in irregular fashion (randomness) around the main chain. The polymer of the polymer matrix of the present disclosure may be isotactic, syndiotactic, atactic or copolymers and mixtures thereof.

In a preferred embodiment, the polymer matrix is polyvinyl alcohol (PVA). Polyvinyl alcohol (PVA, PVOH or PVAI) is a water-soluble synthetic polymer. It has the idealized chemical formula [CH<sub>2</sub>CH(OH)]<sub>n</sub>. Polyvinyl alcohol, like most polymers, is an electrical insulator. It is white (colorless) and odorless, exhibits crystallinity and can be supplied as beads or as solutions in water. PVA is biocompatible, non-toxic, resistant to oil, grease and solvents and has a high tensile strength and flexibility. Additionally, PVA has excellent film forming, emulsifying and adhesive properties.

Polyvinyl alcohol (PVA) has a relatively simple chemical structure with a pendant hydroxyl group. Unlike most vinyl polymers, PVA is not prepared by polymerization of the corresponding monomer. The monomer, vinyl alcohol, does not exist in a stable form, but rather rearranges to its tautomer, acetaldehyde. PVA instead is prepared by the polymerization of vinyl acetate to polyvinyl acetate (PVAc), followed by hydrolysis of PVAc to PVA. Other precursor polymers are sometimes used, with formate or chloroacetate groups instead of acetate. The conversion of the polyesters is usually conducted by base-catalyzed transesterification with ethanol. The hydrolysis reaction does not go to completion resulting in polymers with a certain degree of hydrolysis that depends on the extent of the reaction. In essence, PVA is always a copolymer of PVA and PVAc.

Polyvinyl alcohol is an atactic material, defined as a macromolecule where the substituents are placed randomly along the chain. The percentage of meso diads is between 1 and 99%. In terms of microstructure, it is composed mainly of 1,3-diol linkages [—CH<sub>2</sub>—CH(OH)—CH<sub>2</sub>—CH(OH)—] but a few percent of 1,2 diols [—CH<sub>2</sub>—CH(OH)—CH(OH)—CH<sub>2</sub>—] occur, depending on the conditions for the polymerization of the vinyl ester precursor.

Several properties of the polyvinyl alcohol polymer depend on the amount of residual ester groups. The content of acetate groups, or degree of hydrolysis, has an effect on the chemical properties, solubility and crystallizability of PVA. Residual hydrophobic acetate groups weaken the intra- and intermolecular hydrogen bonding of adjoining

## 11

hydroxyl groups. Generally, PVA grades with high degrees of hydrolysis have a lower solubility in water and are more difficult to crystallize.

In one embodiment, the polyvinyl alcohol of the present disclosure has a hydrolysis value of at least 60%, preferably at least 65%, preferably at least 70%, preferably at least 75%, preferably at least 80%, preferably at least 85%, preferably at least 90%, preferably at least 91%, preferably at least 92%, preferably at least 93%, preferably at least 94%, preferably at least 95%, preferably at least 96%, preferably at least 97%, preferably at least 98%, preferably at least 99%, where a value of 100% is complete hydrolysis and 0% is no hydrolysis.

Polyvinyl alcohol is produced by free radical polymerization and subsequent hydrolysis resulting in a wide molecular weight distribution. In one embodiment, the polyvinyl alcohol of the present disclosure has an average molecular weight of 5-200 kDa, preferably 10-150 kDa, preferably 10-100 kDa, preferably 10-75 kDa, more preferably 10-50 kDa, preferably 20-35 kDa.

Dispersity is a measure of the heterogeneity of sizes of molecules or particles in a mixture. The polydispersity index (PDI or heterogeneity index) is a measure of the distribution of molecular mass in a given polymer sample. The PDI is calculated as the weight average molecular weight divided by the number average molecular weight. Typically, dispersities vary based on the mechanism of polymerization and can be affected by a variety of reaction conditions such as reactant ratios, how close the polymerization went to completion, etc. Generally, a decreasing molecular weight distribution increases water solubility and increase flexibility. It can further affect properties of PVA including crystallizability, adhesion, mechanical strength and diffusivity. In one embodiment, the polyvinyl alcohol of the present disclosure has a PDI of up to 6, preferably up to 5, preferably up to 3, preferably up to 2.5, preferably up to 2, preferably up to 1.5, preferably up to 1.25.

The degree of polymerization (DP) is defined as the number of monomeric units in a macromolecule or polymer. In one embodiment, the polyvinyl alcohol of the present disclosure has a degree of polymerization of 100-2500, preferably 100-1500, preferably 100-750, preferably 100-300.

General grades of polyvinyl alcohol include ultra-low viscosity (DP<300 and average molecular weight <23 kDa), low viscosity (DP=350-650 and average molecular weight=31-50 kDa), medium viscosity (DP=1000-1500 and average molecular weight=85-124 kDa) and high viscosity (DP=1600-2200 and average molecular weight=146-186 kDa). In the present disclosure, polyvinyl alcohol may refer to PVA that is ultra-low viscosity, low viscosity, medium viscosity, high viscosity or mixtures thereof.

It is envisioned that other polymeric materials may be used in lieu of polyvinyl alcohol as the polymer matrix of the nanocomposite film of the present disclosure. Although the selection of a polymer is not viewed as particularly limiting, the polarity of the polymer should be compatible with the carbon nanotubes. Suitable polymers may be selected from the group including, but not limited to, polyacrylates, acrylics, poly(acrylic acid), poly(acrylonitrile), poly(2-hydroxyethylmethacrylate), sodium polyacrylate, ethylene glycol dimethacrylate, polystyrenes, high impact polystyrene, poly(vinyl pyridine), poly(methyl acrylate), polymethacrylates, poly(methyl methacrylate), polychloroprene, polyacrylamide, poly(N-isopropylacrylamide), poly(tetrafluoroethylene) (PTFE), poly(N-vinyl pyrrolidone), poly(vinyl pyrrolidone), poly(vinyl pyridine), polyethylenes, low-density poly-

## 12

(ethylene), high-density poly(ethylene), chlorinated polyethylene (CPD), poly(propylene), poly(isobutylene), poly(butylene), polyvinyl chlorides (PVC), polyvinyl chloride acetate, polyacrylonitriles, poly(ethyl acetate), poly(vinyl acetate), polyvinylacetates, polyvinyl acetate phthalate, ethylene vinyl acetates, poly(ethylene glycol), polyphenylene ethers, poly(ethylene vinyl alcohol), poly(vinylidene fluoride), poly(p-phenylenevinylene), poly(benzoxazole), polyphenylenebenzobisoxazole (PBO), polyaryletherketones, poly(ether ether ketones), polyphenylenesulfides, polyamide imides, polyarylates, polyarylsulphones, poly(styrene-co-acrylonitrile), ethyl-vinyl-alcohol copolymers, copolymers of ethylene and 1-alkenes, polybutene-1, polymethylpentene, amorphous poly-alpha-olefins (APAO), terephthalates, polyacetylene, polyethylene oxides, polycycloolefins, polyisoprenes, polystyrene-polyisoprene diblock copolymers, polyamides, poly(ethylene terephthalate), poly(trimethylene terephthalate), poly(butylene terephthalate), polycarbonates, polychlorotrifluoroethylene, polyvinylidifluoride, polyperfluoroalkoxy, poly(ethylene oxide), ethylene oxide copolymers, poly(ethylene imine), poly(dimethyl siloxane), silicones, fluorosilicones, fluoropolymers, polybutadienes, butadiene copolymers, epoxidized natural rubbers, epoxy polymer resins, poly(cis-1,4-isoprene), poly(trans-1,4-isoprene), viton, phenolic resins, acrylic resins, vinylacetate resins, polyurethanes, polyurethane-urea, thermosetting polyimides, thermoplastic polyimides, poly(amic acid), polysulfones, polyetherimides, polyethersulfones, chlorosulfonates, polyoxymethylene, polyphenylene oxide, polyphenylenes, perfluorinatedpolyethylenepropylene, polyvinylidene chloride, fluoropoly(ether-imide), polyolefins, aromatic polyamides (Aramid, para-aramid), polyesters, conducting and conjugated polymers, liquid crystal polymers, liquid crystalline polyesters, vectran, biodegradable thermoplastic polyesters and their copolymers, thermosetting polyesters, unsaturated polyesters, acetals, fluorinated elastomers, rubbers, styrene butadiene rubbers, bismaleimides, copolymer rubbers, styrene-isoprene-styrenes, styrene-butadiene-styrenes, ethylene-propylene, ethylene-propylene-diene monomers (EPDM), nitrile-butadienes, acrylonitrile butadiene styrene (ABS), polyethylene/acrylonitrile butadiene styrene, polycarbonate/acrylonitrile butadiene styrene, nylons, thermoplastic continuous and discontinuous fiber composites, thermosetting continuous and discontinuous fiber composites, specialty polymers, etc. and blends, mixtures, alloys and copolymers thereof.

Intrinsically conducting polymers (ICPs) are organic polymers that conduct electricity. They can have metallic conductivity or can be semiconductors. They offer high electrical conductivity but do not show similar mechanical properties to other available polymers. Their electrical properties can be fine-tuned using the methods of organic synthesis and advanced dispersion techniques.

In one embodiment, it is envisioned that the polymer matrix of the nanocomposite film may be adapted to incorporate an intrinsically conducting polymer. Examples of intrinsically conducting polymers include, but are not limited to, poly(fluorene)s, polyphenylenes, polypyrenes, polyazulenes, polynaphthalenes, poly(acetylene)s (PAC), poly(p-phenylene vinylene) (PPV), poly(pyrrole)s (PPY), polycarbazoles, polyindoles, polyazepines, polyanilines (PANT), poly(thiophene)s (PT), poly(3,4-ethylenedioxythiophene) (PEDOT), poly(p-phenylene sulfide) (PPS) and copolymers and mixtures thereof.

In one embodiment, the polymer matrix is envisioned to be comprised of polyvinyl alcohol copolymers including, but not limited to, poly(vinyl alcohol-co-ethylene) ethylene,

13

poly(acrylic acid)-co-poly(vinyl alcohol) copolymer, poly(vinyl butyral)-co-poly(vinyl alcohol copolymer, poly(vinyl acetate)-co-poly(vinyl alcohol) copolymer, poly(vinyl chloride)-co-poly(vinyl alcohol) and mixtures thereof.

In one embodiment, the polymer matrix is envisioned to be comprised of polyvinyl alcohol doped with additives including, but no limited to, crosslinkers, defoamers, dispersants, biocides and plasticizers.

In one embodiment, the nanocomposite of the present disclosure includes carbon nanotubes comprising at least one selected from the group consisting of single-walled carbon nanotubes, multi-walled carbon nanotubes, and hybrid nanotubes dispersed in the matrix.

Carbon nanotubes (CNTs) are allotropes of carbon with a cylindrical nanostructure with a significantly large length-to-diameter ratio (up to 100,000,00:1). These cylindrical carbon molecules have unusual properties, which are valuable for nanotechnology, electronics, optics and other fields of materials science and technology. In particular owing to their extraordinary thermal conductivity and mechanical and electrical properties, carbon nanotubes find applications as additives to various structural materials.

Nanotubes are members of the fullerene structural family. The name refers to their long, hollow structure with the "walls" formed by one-atom-thick sheets of carbon, called graphene. These sheets are rolled at specific and discrete ("chiral") angles, and the combination of the rolling angle and radius determines the nanotube properties. Individual nanotubes naturally align themselves into "ropes" held together by van der Waals forces and pi-stacking. Nanotubes are categorized as single-walled nanotubes (SWNTs) and multi-walled nanotubes (MWNTs).

Single-walled nanotubes typically have a diameter of close to 1 nm and a tube length of up to many millions of times longer. The structure of a single-walled nanotube can be conceptualized by wrapping a one-atom-thick layer of graphite called graphene into a seamless cylinder. In practice, the way the graphene sheet is wrapped is represented by a pair of indices (n, m). The integers n and m denote the number of unit vectors along two directions in the honeycomb crystal lattice of graphene. If m=0, the nanotubes are called zigzag nanotubes, and if n=m, the nanotubes are called armchair nanotubes. Otherwise they are called chiral.

Multi-walled nanotubes consist of multiple rolled layers (concentric tubes) of graphene. There are two models that can be used to describe the structures of multi-walled nanotubes. In the Russian Doll model, sheets of graphite are arranged in concentric cylinders, for example, a single-walled nanotube within a larger single-walled nanotube. In the Parchment model, a single sheet of graphite is rolled in around itself, resembling a scroll of parchment or a rolled newspaper. The interlayer distance in multi-walled nanotubes is close to the distance between graphene layers in graphite. The Russian Doll structure is observed more commonly, its individual shells can be described as SWNTs. Hybrid carbon nanotubes refer to hybrids of MWCNTs and, for example, Silica. They are designed to open the tubes of MWCNTs as a sheet instead of a tube.

In one embodiment, the nanocomposite comprises carbon nanotubes with an average outer diameter of 5-75 nm, preferably 8-60 nm, preferably 10-50 nm, preferably 20-40 nm and an average inner diameter of 0.5-50 nm, preferably 0.75-30 nm, preferably 0.8-20, preferably 1.0-10 nm dispersed in the matrix. In one embodiment, the carbon nanotubes have an average length of 1-100 µm, preferably 2-80 µm, preferably 5-60 µm, preferably 10-50 µm. In one embodiment, the carbon nanotubes have a length to diameter

14

ratio in the range of 100,000:1 to 10:1, preferably 50,000:1 to 50:1, preferably 20,000:1 to 100:1, preferably 10,000:1 to 500:1, preferably 5,000:1 to 1,000:1.

In one embodiment, the carbon nanotubes of the nanocomposite are multi-walled carbon nanotubes. The multi-walled carbon nanotubes can adopt the Russian Doll model or the Parchment model or mixtures thereof.

In one embodiment, the carbon nanotubes of the nanocomposite comprise substantially multi-walled carbon nanotubes. The ratio of MWCNTs to SWCNTs is preferably greater than 2:1, preferably greater than 5:1, preferably greater than 10:1, preferably greater than 15:1, preferably greater than 20:1, preferably greater than 25:1, preferably greater than 50:1, preferably greater than 75:1, and preferably greater than 100:1.

The Brunauer-Emmet-Teller (BET) theory aims to explain the physical adsorption of gas molecules on a solid surface and serves as the basis for an important analysis technique for the measurement of the specific surface area of a material. Specific surface area is a property of solids which is the total surface area of a material per unit of mass, solid or bulk volume, or cross sectional area. In one embodiment, the raw carbon nanotubes of the nanocomposite have a BET surface area of at least 50 m<sup>2</sup>/g, preferably at least 75 m<sup>2</sup>/g, preferably at least 100 m<sup>2</sup>/g, preferably at least 150 m<sup>2</sup>/g, preferably at least 200 m<sup>2</sup>/g, preferably at least 250 m<sup>2</sup>/g, such as for example, 50-300 m<sup>2</sup>/g, preferably 100-280 m<sup>2</sup>/g, preferably 150-260 m<sup>2</sup>/g, preferably 200-240 m<sup>2</sup>/g.

In addition to single-walled carbon nanotubes and multi-walled carbon nanotubes it is envisaged that the present invention may be adapted to incorporate other types and related structures of carbon nanotubes including, but not limited to, a carbon nanotorus, a carbon nanobud, a 3D macroscopic carbon nanotube architecture, graphenated carbon nanotubes (g-CNTs), nitrogen-doped carbon nanotubes, a carbon peapod, cup-stacked carbon nanotubes, extreme carbon nanotubes and mixtures thereof.

In one embodiment, the carbon nanotubes of the present disclosure are "raw" or lacking any surface functionalization or modifications. In addition, it is envisaged that the present invention may be adapted to incorporate surface functionalized and/or surface modified carbon nanotubes. These surface modifications may be covalent, non-covalent or mixtures thereof. Examples of functional groups on the carbon nanotubes include alcoholic, carboxylic, aldehydic, ketonic and esteric oxygenated functional groups. Alternatively, the carbon nanotubes of the present disclosure may be surface modified with amine functionality or other functionality that is proton absorbing or basic.

In one embodiment, the raw carbon nanotubes may be treated with an acid such as HNO<sub>3</sub>, HF, HCl and H<sub>2</sub>SO<sub>4</sub>. The acid treatment may affect the pore size and/or surface characteristics of the carbon nanotubes. Alternatively, the raw carbon nanotubes may be treated with a base such as NaOH. The base treatment may affect the pore size and/or surface characteristics of the carbon nanotubes.

As used herein, "impregnated" describes being completely or partially filled throughout, saturated, permeated and/or infused. In one embodiment, the carbon nanotubes of the nanocomposite may be impregnated with nanoparticles, such as metal oxide nanoparticles. The nanoparticles may be affixed inside of and/or on an outer surface of the carbon nanotubes. The nanoparticles may be affixed on one or more surfaces of the carbon nanotubes. The nanoparticles may be affixed to carbon nanotubes in any reasonable manner, such as affixed to one or more surfaces of the carbon nanotubes or alternately, at least partially embedded within the tubular

15

cavity of the carbon nanostructure and/or additional pore spaces. In one embodiment, from 10-90% of the total volume and/or total surface area of the nanoparticles may be embedded within the tubular cavity of the carbon nanotube, preferably 25-80%, preferably 40-60%.

In one embodiment, greater than 10% of the surface area (i.e. surface and pore spaces) of the carbon nanotubes are covered by nanoparticles and preferably greater than 15%, preferably greater than 20%, preferably greater than 25%, preferably greater than 30%, preferably greater than 35%, preferably greater than 40%, preferably greater than 45%, preferably greater than 50%, preferably greater than 55%, preferably greater than 60%, preferably greater than 65%, preferably greater than 70%, preferably greater than 75%, preferably greater than 80%, preferably greater than 85%, preferably greater than 90%, preferably greater than 95%, preferably greater than 96%, preferably greater than 97%, preferably greater than 98%, preferably greater than 99%.

Nanoparticles are particles between 1 and 100 nm in size. A particle is defined as a small object that behaves as a whole unit with respect to its transport and properties. Nanoparticles are named for the real-world shapes that they appear to represent. These morphologies sometimes arise spontaneously as an effect of the synthesis or from the innate crystallographic growth patterns of the materials themselves. Some of these morphologies may serve a purpose, such as bridging an electrical junction. In one embodiment, the nanoparticles of the present disclosure can be synthesized and formed into a variety of morphologies and may refer to nanoparticles, nanocrystals, nanospheres, nanoplatelets, nanowires, nanorods, nanotubes, nanocylinders, nanoboxes, nanostars, tetrapods, nanobelts, nanoflowers, etc. and mixtures thereof.

In one embodiment, it is envisaged that the present invention may be adapted to incorporate carbon nanotubes impregnated with nanoscale metals. Examples of possible metals include, but are not limited to, silver, gold, copper, nickel, iron, aluminum zinc, palladium, platinum, magnesium, zirconium, titanium, vanadium, rhodium, rhenium, uranium, silicon, molybdenum, thorium, chromium, manganese, cerium, germanium, tantalum, lead, cadmium, calcium, antimony, tin, bismuth, cobalt, tungsten, indium, silicon, brass, bronze, white brass, stainless steel and alloys or mixtures thereof.

In one embodiment, the nanocomposite of the present disclosure includes carbon nanotubes impregnated with metal oxide nanoparticles comprising at least one selected from the group consisting of aluminum oxide, iron oxide and zinc oxide. In addition to aluminum oxide, iron oxide and zinc oxide, it is envisaged that the present invention may be adapted to incorporate carbon nanotubes impregnated with other metal oxide nanoparticles as a part of the nanocomposite. Exemplary metal oxides include, but are not limited to, oxides of copper, nickel, magnesium, zirconium, titanium, vanadium, rhodium, rhenium, silicon, molybdenum, thorium, chromium, manganese, cerium, silver, lead, cadmium, calcium, antimony, tin, bismuth, cobalt and tungsten and alloys or mixtures thereof. In one embodiment, the carbon nanotubes may comprise up to 15% metal oxide nanoparticles by weight relative to the total weight of the carbon nanotubes, preferably up to 12%, preferably up to 10% by weight relative to the total weight of the carbon nanotubes. In one embodiment, the nanocomposite comprises carbon nanotubes impregnated with metal oxide nanoparticles with a crystal nanoparticle morphology and an average particle size of 5-40 nm, preferably 10-35 nm, preferably 15-30 nm. In one embodiment, the modification

16

of carbon nanotubes with impregnated metal oxide nanoparticles may increase the BET surface area of the carbon nanotubes by at least 100%, preferably by at least 125%, preferably by at least 150%, preferably by at least 175%, more preferably by at least 200% or within said ranges.

An electrical conductor is an object or type of material that allows the flow of electrical current in one or more directions. Metals, such as copper, typify conductors. Traditionally, most metals are good electrical conductors, most non-metals are not. In metals, the movable charged particles are electrons, but positive charges may also be mobile. Conductor implies that the outer electrons of the atoms are loosely bound and free to move through the material.

A semiconductor material has an electrical conductivity value falling between that of a conductor and an insulator. Semiconducting materials exist in two types, elemental materials and compound materials. The properties of a semiconductor rely on the unique arrangement of the crystal lattice and the movement of electrons and holes within the crystal lattice. Current conduction in a semiconductor occurs through the movement of free electrons and "holes", known collectively as charge carriers. Adding impurity atoms to a semiconducting material ("doping") can greatly increase the number of charge carriers within it.

An antistatic material or dissipative material is one which prevents, inhibits, eliminates, or reduces the accumulation of static electricity. In antistatic or dissipative materials the initial charges are suppressed (antistatic) or there is no or low initial charges (dissipative) and discharge to or from human contact is prevented. They represent a slight or minimum amount of conductivity that prevents the buildup of electric charge by dissipating or promoting the decay of the static electricity.

An electrical insulator is a material whose internal electric charges do not flow freely, and therefore make it very hard to conduct an electric current under the influence of an electric field. Most non-metallic solids are said to be good insulators, having very high resistance to the flow of charge through them. Most atoms hold on to their electrons tightly and are insulators. The property that distinguishes an insulator is its resistivity; insulators have higher resistivity than semiconductors or conductors.

Electrical resistivity (resistivity, specific electrical resistance or volume resistivity) is an intrinsic property that quantifies how strongly a given material opposes the flow of electric current. A low resistivity indicates that a material readily allows the movement of electric charge. Electrical conductivity (specific conductance) is the reciprocal of electrical resistivity, and measures a material's ability to conduct an electric current. As used in the present disclosure, an insulator is a material having a resistivity of greater than  $10^8$  ohm·cm<sup>2</sup>, preferably in the range of  $10^8$ - $10^{17}$  ohm·cm<sup>2</sup>, a semiconductor and/or conductor is a material having a resistivity of less than  $10^4$  ohm·cm<sup>2</sup>, preferably less than  $0.5 \times 10^4$  ohm·cm<sup>2</sup> and a antistatic material is a material having an intermediate resistivity in the range of  $10^4$ - $10^8$  ohm·cm<sup>2</sup>, preferably  $10^5$ - $10^8$  ohm·cm<sup>2</sup>.

According to its first aspect, the present disclosure relates to a nanocomposite film further including a first surface and a second surface. The first surface has a first content of carbon nanotubes and a first resistivity. The second surface has a second content of carbon nanotubes and a second resistivity. Additionally, the second content of carbon nanotubes is greater than or equal to the first content of carbon nanotubes, and the second resistivity is less than or equal to the first resistivity.

The nanocomposite film of the present disclosure may have various shapes and sizes. In one embodiment, the nanocomposite film may be horizontally oriented with a longitudinal axis. The first surface and second surface may be parallel to each other and the longitudinal axis. The first and second surface may also be opposing across the longitudinal axis and the vertical distance between the first surface and second surface may define the thickness of the nanocomposite film. In one embodiment, the film is double sided and the first and second surface are not adjoining. In terms of the present disclosure, the carbon nanotubes may be oriented parallel to the longitudinal axis, perpendicular to the longitudinal axis, or in orientations that are not exactly parallel or perpendicular to the longitudinal axis.

In a preferred embodiment, the carbon nanotubes of the second surface may be in such a quantity and dispersed in such a manner to effectively form one or more seamlessly interconnected infinite conductive networks. Percolation threshold refers to a mathematical concept related to the formation of long-range connectivity in random systems. Below the threshold a giant connected component does not exist; while above it, there exists a giant component of the order of the system size. In one embodiment, the second surface of the nanocomposite film of the present disclosure has a percolation threshold of less than less 10% carbon nanotubes by weight relative to the total weight of the nanocomposite film, preferably less than 7%, preferably less than 5%, more preferably less than 3%.

As used herein, "surface" refers to the outermost part or most outside layer or boundary of a material, here the nanocomposite film. It includes both a continuous set of points with length and width providing an exterior face to the nanocomposite and also may have a thickness and depth and be described as a layer. A surface, as used herein, is in complete and continuous contact with an external environment of the nanocomposite film of the present disclosure as well as the nanocomposite film itself. In one embodiment, the nanocomposite film of the present disclosure comprises a first and second surface. It is further envisaged that the present disclosure may be adapted to incorporate a third surface, a fourth surface, a fifth surface, etc. or a plurality of surfaces with defined content of carbon nanotubes and defined electrical resistivity.

As used herein, "core" refers to the portion of the nanocomposite that is neither the first surface nor the second surface. The core may have characteristics of the first surface, the second surface, both and/or neither. In a preferred embodiment, the first and second surface form distinct layers with distinct and identifiable interfaces between the two surfaces or each surface and the nanocomposite core. In one embodiment, the first and second surfaces form distinct layers, although the interface between the two surfaces or each surface and the nanocomposite core is a mixture of both the first and second surface, a mixture of the first surface and the nanocomposite core, a mixture of the second surface and the nanocomposite core, or a mixture of the first surface, the second surface and the nanocomposite core. The nanocomposite film described herein is singular comprising a first surface, a second surface, a core and their interfaces. The film is not formed by conjoining multiple films and has no internal film-to-film interfaces.

In one embodiment, the core of the nanocomposite film may have a carbon nanotube content gradient. Generally, the core will have a content of carbon nanotubes greater than the first surface and less than the second surface. In one embodiment, the content of the carbon nanotubes in the core may increase at greater distances from the first surface and

smaller distances towards the second surface. Conversely, the content of carbon nanotubes in the core may decrease at greater distances from the second surface and smaller distances towards the first surface.

5 In one embodiment, the nanocomposite film has up to 25% carbon nanotubes by weight relative to the total weight of the nanocomposite film, preferably up to 20%, preferably up to 15%, preferably up to 10%, preferably up to 9%, preferably up to 8%, preferably up to 7%, preferably up to 6%, preferably up to 5%, preferably up to 4%, preferably up to 3%, preferably up to 2%, preferably up to 1%, preferably up to 0.75%, preferably up to 0.5%, preferably up to 0.25%, preferably up to 0.2%, preferably up to 0.15%, preferably up to 0.1%, preferably up to 0.01%.

10 In one embodiment, the nanocomposite film is at least 75% polymer matrix by weight relative to the total weight of the nanocomposite film, preferably at least 80%, preferably at least 85%, preferably at least 90%, preferably at least 91%, preferably at least 92%, preferably at least 93%, 15 preferably at least 94%, preferably at least 95%, preferably at least 96%, preferably at least 97%, preferably at least 98%, preferably at least 99%, preferably at least 99.5%, preferably at least 99.75%.

20 In one embodiment, the first surface has less than 50% of the total mass of carbon nanotubes in the nanocomposite film, preferably less than 40%, preferably less than 30%, preferably less than 25%, preferably less than 20%, preferably less than 15%, preferably less than 10%, preferably less than 5%.

25 In one embodiment, the second surface has greater than 50% of the total mass of carbon nanotubes in the nanocomposite film, preferably greater than 60%, preferably greater than 70%, preferably greater than 75%, preferably greater than 80%, preferably greater than 85%, preferably greater than 90%, preferably greater than 95%.

30 In one embodiment, the nanocomposite film of the present disclosure has a total average thickness of 0.1-1.0 mm, preferably 0.2-0.8 mm, preferably 0.3-0.7 mm, preferably 0.4-0.6 mm or about 0.5 mm.

35 In one embodiment, the first surface of the present disclosure may encompass up to 70% of the total thickness of the nanocomposite film, preferably up to 60%, preferably up to 50%, preferably up to 40%, preferably up to 30%, preferably up to 25%, preferably up to 20%, preferably up to 15%, preferably up to 10%, preferably up to 5% of the total thickness of the nanocomposite film.

40 In one embodiment, the first surface of the present disclosure has a total average thickness of up to 0.5 mm, preferably up to 0.4 mm, preferably up to 0.3 mm, preferably up to 0.25 mm, preferably up to 0.2 mm, preferably up to 0.15 mm, preferably up to 0.1 mm, preferably up to 0.05 mm.

45 In one embodiment, the second surface of the present disclosure may encompass up to 70% of the total thickness of the nanocomposite film, preferably up to 60%, preferably up to 50%, preferably up to 40%, preferably up to 30%, preferably up to 25%, preferably up to 20%, preferably up to 15%, preferably up to 10%, preferably up to 5% of the total thickness of the nanocomposite film.

50 In one embodiment, the second surface of the present disclosure has a total average thickness of up to 0.5 mm, preferably up to 0.4 mm, preferably up to 0.3 mm, preferably up to 0.25 mm, preferably up to 0.2 mm, preferably up to 0.15 mm, preferably up to 0.1 mm, preferably up to 0.05 mm.

55 The mechanical properties of the nanocomposite film of the present disclosure are also of interest. Tensile strength is

the maximum stress that a material can withstand while being stretched or pulled before failing or breaking. Young's modulus (tensile modulus, E-modulus or elastic modulus) is a measure of a material's stiffness or its resistance to being deformed elastically (non-permanently) when a force is applied and can be thought of as the ratio of stress to strain. In one embodiment, the nanocomposite film of the present disclosure has a tensile strength in the range of 5-75 MPa, more preferably 10-60 MPa, more preferably 15-50 MPa. The inclusion of carbon nanotubes may increase the tensile strength by at least 20%. In one embodiment, the nanocomposite film of the present disclosure has a Young's modulus in the range of 2-80 MPa, preferably 10-70 MPa, preferably 15-60 MPa, more preferably 20-50 MPa. The inclusion of carbon nanotubes may increase the tensile strength by at least 15%.

In one embodiment, the nanocomposite film comprises from 0.01-0.75% carbon nanotubes by weight relative to the total weight of the nanocomposite film, preferably 0.01-0.7%, preferably 0.01-0.60%, preferably 0.01-0.50%, preferably 0.01-0.40%, preferably 0.01-0.30%, preferably 0.01-0.25% by weight relative to the total weight of the nanocomposite film.

In one embodiment, the nanocomposite film has a first surface that is insulating and a second surface that is insulating. The first surface is insulating and has a first resistivity of greater than  $10^8$  ohm·cm<sup>2</sup>, preferably greater than  $1.25 \times 10^8$ , preferably greater than  $1.5 \times 10^8$ , preferably greater than  $1.75 \times 10^8$ , preferably greater than  $2.0 \times 10^8$ , preferably greater than  $2.5 \times 10^8$ , preferably greater than  $3 \times 10^8$ , preferably greater than  $3.5 \times 10^8$ , preferably greater than  $4.0 \times 10^8$ , preferably greater than  $5.0 \times 10^8$  ohm·cm<sup>2</sup>. The second surface is insulating and has a second resistivity of greater than  $10^8$  ohm·cm<sup>2</sup>, preferably greater than  $1.25 \times 10^8$ , preferably greater than  $1.5 \times 10^8$ , preferably greater than  $1.75 \times 10^8$ , preferably greater than  $2.0 \times 10^8$ , preferably greater than  $2.5 \times 10^8$ , preferably greater than  $3 \times 10^8$ , preferably greater than  $3.5 \times 10^8$ , preferably greater than  $4.0 \times 10^8$ , preferably greater than  $5.0 \times 10^8$  ohm·cm<sup>2</sup>.

In one embodiment, the nanocomposite film comprises from 1.0-7.0% of carbon nanotubes by weight relative to the total weight of the nanocomposite film, preferably 1.0-6.0%, preferably 1.0-5.0%, preferably 1.0-4.0%, preferably 1.0-3.5%, preferably 1.0-3.0%, preferably 1.0-2.5%, preferably 1.0-2.25%, preferably 1.0-2.0% by weight relative to the total weight of the nanocomposite film.

In one embodiment, the nanocomposite film has a first surface that is insulating and a second surface that is antistatic. The first surface is insulating and has a first resistivity of greater than  $10^8$  ohm·cm<sup>2</sup>, preferably greater than  $1.25 \times 10^8$ , preferably greater than  $1.5 \times 10^8$ , preferably greater than  $1.75 \times 10^8$ , preferably greater than  $2.0 \times 10^8$ , preferably greater than  $2.5 \times 10^8$ , preferably greater than  $3 \times 10^8$ , preferably greater than  $3.5 \times 10^8$ , preferably greater than  $4.0 \times 10^8$ , preferably greater than  $5.0 \times 10^8$  ohm·cm<sup>2</sup>. The second surface is antistatic and has a second resistivity of  $10^4$ - $10^8$  ohm·cm<sup>2</sup>, preferably  $10^4$ - $10^7$ , preferably  $10^4$ - $10^6$ , preferably  $10^4$ - $7.5 \times 10^5$ , preferably  $10^4$ - $5.0 \times 10^5$ , preferably  $10^4$ - $2.5 \times 10^5$ , preferably  $10^4$ - $10^5$ , preferably  $10^4$ - $0.5 \times 10^5$ , preferably  $10^4$ - $0.25 \times 10^5$  ohm·cm<sup>2</sup>.

In one embodiment, the nanocomposite film comprises greater than 7.5% carbon nanotubes by weight relative to the total weight of the nanocomposite film, preferably greater than 8.0%, preferably greater than 8.5%, preferably greater than 9%, preferably greater than 9.5%, preferably greater than 9.75%, preferably greater than 10% by weight relative to the total weight of the nanocomposite film.

In one embodiment, the nanocomposite film has a first surface that is insulating and a second surface that is semiconducting and/or conducting. The first surface is insulating and has a first resistivity of greater than  $10^8$  ohm·cm<sup>2</sup>, preferably greater than  $1.25 \times 10^8$ , preferably greater than  $1.5 \times 10^8$ , preferably greater than  $2.0 \times 10^8$ , preferably greater than  $2.5 \times 10^8$ , preferably greater than  $3 \times 10^8$ , preferably greater than  $3.5 \times 10^8$ , preferably greater than  $4.0 \times 10^8$ , preferably greater than  $5.0 \times 10^8$  ohm·cm<sup>2</sup>. The second surface is semiconducting and/or conducting and has a second resistivity of less than  $10^4$  ohm·cm<sup>2</sup>, preferably less than  $7.5 \times 10^3$ , preferably less than  $5.0 \times 10^3$ , preferably less than  $4.0 \times 10^3$ , preferably less than  $3.5 \times 10^3$ , preferably less than  $3.0 \times 10^3$ , preferably less than  $2.5 \times 10^3$ , preferably less than  $2.0 \times 10^3$ , preferably less than  $1.5 \times 10^3$ , preferably less than  $1.0 \times 10^3$ , preferably less than  $0.75 \times 10^3$ , preferably less than  $0.5 \times 10^3$  ohm·cm<sup>2</sup>.

Thus, the nanocomposite film of the present disclosure may be insulating in the bulk or at one surface but additionally present an antistatic, semiconducting and/or conducting surface. Thus, a single material is presented that can fulfill the function of both an electrical insulator and an electrical semiconductor and/or conductor depending on which surface is engaged.

According to a second aspect, the present disclosure relates to a process for forming the polymer and carbon nanotube nanocomposite films of the present disclosure, in one or more of their embodiments.

In a preferred embodiment, the polymer and carbon nanotube nanocomposite film of the present disclosure is formed by a solution processing or solution mixing and casting technique. The process is described as wet chemistry and is considered simple and cost effective compared to other processes for manufacturing polymer nanocomposites. In general, solution processing refers to the dispersion of conductive carbon nanotubes into a solvent followed by mixing with a polymer solution and subsequent vaporization of the solvent to form the desired nanocomposite.

In one embodiment, the solution processing begins with dispersion of the carbon nanotubes into a liquid solution by energetic mixing. The certain amount of carbon nanotubes is determined by the desired weight percent of the final nanocomposite. In one embodiment, the ratio of polymer matrix to carbon nanotubes may be 85:1, 90:1, 93:1, 95:1, 97:1, 99:1, 99.5:1, 99.75:1. This mixing may include, but is not limited to, mechanical mixing, magnetic agitation, mild sonication, high-energy ultrasonication, shear mixing, refluxing and mixtures thereof. The process of mixing to form a stable dispersion may last as little as 2 hours, preferably 1.5 hours, preferably 1 hour, preferably 30 minutes, preferably 15 minutes, preferably 10 minutes, preferably 5 minutes. In one embodiment, the dispersion of carbon nanotubes may occur directly in a polymeric solution, in another embodiment the carbon nanotubes are dispersed in a solvent and then mixed with an independent polymer solution that may be in the same solvent or a different solvent.

In one embodiment, once combined in a reaction mixture the dispersed carbon nanotube solution and the polymer solution are further mixed by the means discussed previously, preferably heating, magnetic agitation and ultrasonication, preferably magnetic stirring at 400-1000 rpm, preferably 500-800 rpm, preferably 550-650 rpm or about 600 rpm. In one embodiment the reaction mixture is mixed at elevated temperature of at least 40° C., preferably at least 60° C., preferably at least 70° C., preferably at least 80° C. The process of mixing the reaction mixture may last as little

as 2 hours, preferably 1.5 hours, preferably 1 hour, preferably 30 minutes, preferably 15 minutes. In one embodiment, following the mixing the reaction mixture is degassed to remove any traces of air from the solution with inert gas. The process of degassing may last as little as 2 min, preferably 5 min, preferably 10 min, preferably 15 min. Finally, the mixture is poured on a leveled flat surface and allowed to dry at room temperature. The dried films may then be peeled from the surface they were poured and cast on and kept in a desiccator to avoid moisture uptake. In one embodiment, the nanocomposite films are cast and dried in plastic petri dishes. In one embodiment, the drying is done at elevated temperature up to 200° C., preferably up to 150° C., preferably up to 100° C., preferably up to 75° C., preferably up to 50° C. The drying may also be performed at room temperature of 20-40° C., preferably 25-30° C. The drying time may take up to 160 hours, preferably up to 100 hours, preferably up to 80 hours, preferably up to 60 hours, preferably up to 48 hours, preferably up to 24 hours, preferably up to 12 hours, preferably up to 8 hours, preferably up to 4 hours, preferably up to 2 hours.

The nature of the carbon nanotube/polymer ratio and fabrication conditions including, but not limited to temperatures, sonication, step durations and casting and drying conditions are what allow for control of the size, shape and non-uniform dispersion of the carbon nanotubes in the nanocomposite film. Thus, variations in the above process give rise to a nanocomposite film comprising a first surface and a second surface. The first surface has a first content of carbon nanotubes and a first resistivity. The second surface has a second content of carbon nanotubes and a second resistivity. The second content of carbon nanotubes is greater than or equal to the first content of carbon nanotubes, and the second resistivity is less than or equal to the first resistivity.

In one embodiment, the polymerization by solution processing is carried out in a liquid solvent that may include polar protic solvents, aprotic polar solvents and non-polar solvents. Suitable polar protic solvents may include, but are not limited to, water, nitromethane, and short chain alcohols such as methanol, ethanol, propanol, isopropanol, butanol or the like and mixtures thereof. Suitable aprotic polar solvents may include, but are not limited to, propylene carbonate, ethylene carbonate, butyrolactone, acetonitrile, benzonitrile, nitromethane, nitrobenzene, sulfolane, dimethylformamide, N-methylpyrrolidone or the like and mixtures thereof. Suitable non-polar solvents may include, but are not limited to, cyclohexane, octane, heptane, hexane, benzene, toluene, xylene, methylene chloride, carbon tetrachloride, diethyl ether or the like and mixtures thereof. In one embodiment, co-solvents may also be used. In a most preferred embodiment, the liquid solvent is water.

In one embodiment, the reaction mixture of the present process may contain one or more additional additives to change the properties of the nanocomposites and/or to improve the process of producing the nanocomposites. Exemplary additives include, but are not limited to, surfactants, antifoaming agents or defoamers, a scale inhibitor, a corrosion inhibitor, a colorant, a thermal stabilizer, a dopant, a coolant additive, a polymerization catalyst, a hardener, a Lewis base, a plasticizer and mixtures thereof.

In one embodiment, the nanocomposite film may further undergo one or more manufacturing steps after formation to instill any desired properties. Techniques or processes including, but not limited to, vulcanization, grafting, cross-linking, injection molding, hot pressing, drawing, extrusion, autoclaving, annealing, heat treating, sintering, compression

molding, machining, welding, adhesively bonding, thermo-forming, coating, vacuum forming, blow molding, stretch blow molding, transfer molding, calendaring, compounding, orienting, tape laying with in situ consolidation, diaphragm forming, rotational molding, centrifugal molding, fiber spinning, filament winding, foam blowing, pultruding and the like are considered to be within the scope of the present method.

In another embodiment, the polymer and carbon nanotube 10 nanocomposite film of the present disclosure is formed by in situ polymerization. In general, the carbon nanotubes are mixed with monomers or pre-polymers and then the nanocomposite is formed by polymerizing the monomers or 15 pre-polymers. This method may further encompass the use of metallocene-based catalyst, anchoring agents such as methylaluminoxane and/or a hardener. This polymerization process is usually accompanied by a viscosity increase that hinders manipulation and limits load fraction. Additionally, 20 solvents may be necessary and may need to be removed, similarly to solution processing.

In another embodiment, the polymer and carbon nanotube 25 nanocomposite film of the present disclosure is formed by melt blending. This method is generally applied to polymers that are insoluble and is particularly useful for dealing with thermoplastic polymers. The technique capitalizes on the fact that thermoplastic polymers soften when heated. Amorphous polymers are heated above their glass transition temperature and semi-crystalline polymers are heated above their melt temperature to induce sufficient softening. Carbon 30 nanotubes can then be mixed into the melt by conventional blending equipment such as shear mixing or a twin screw extruder and bulk samples can be further fabricated by techniques such as compression molding, injection molding, and/or extrusion. In other embodiments, the polymer and 35 carbon nanotube nanocomposite film of the present disclosure is further envisioned to be produced by novel methods including, but not limited to, solid-state mechanochemical pulverization, coagulation spinning and/or latex fabrication methods.

40 In a preferred embodiment, the polymer matrix is poly (vinyl alcohol). In one embodiment, the carbon nanotubes can be formed by conventional methods known to those of ordinary skill in the art. Techniques have been developed to produce carbon nanotubes in sizable quantities. Exemplary 45 techniques may include, but are not limited to, arc discharge, laser ablation, plasma torch, high pressure carbon monoxide disproportionation, chemical vapor deposition, and super growth carbon vapor deposition. In another embodiment, the nanocomposite film of the present disclosure may be formed by methods requiring a substrate, typically glass or plastic. Such methods include, but are not limited to chemical vapor 50 deposition (CVD), preferably microwave-assisted CVD, and spin coating.

According to a third aspect, the present disclosure relates 55 to an electrical or electronic device including the polymer and carbon nanotube nanocomposite films of the present disclosure, in one or more of their embodiments.

In one embodiment, the electrical or electronic device is 60 covered by the nanocomposite film by attaching the free-standing film to the device by any reasonable manner. The nanocomposite may be attached through surface coating interaction (e.g. glued, tacked, cemented, pasted, etc.), attached by highly connected or integral interactions (e.g. melted together, fused, amalgamated, etc.), or sandwiched 65 between a plurality of electronic components of the device. In another embodiment, the electrical or electronic device is covered by the nanocomposite film by first applying the

carbon nanotube/polymer reaction mixture to the device and then forming the nanocomposite on the device by drying. In another embodiment, the electrical device is covered by, attached to, wrapped or enclosed by a metal or alloy or ceramic substrate on which the nanocomposite is disposed.

In one embodiment, the nanocomposite film of the present disclosure may be transparent and find use as a transparent conductive film in photovoltaic cells, liquid crystal displays and touch panel devices. In another embodiment, the unique non-uniform electrical storage characteristics of the nanocomposite film of the present disclosure may find use in supercapacitors, Li—O<sub>2</sub> batteries, or Li-ion batteries.

In one embodiment, the nanocomposite film of the present disclosure is envisioned to find use as an electromagnetic shielding material. Electromagnetic (EM) shielding is the practice of reducing the electromagnetic field in a space by blocking the field with barriers made of conductive materials. Shielding is typically applied to enclosures for isolating electronic devices from the “outside world” and cables to isolate wire from the environment through which the cable runs. The nanocomposite film of the present disclosure may completely enclose an electronic product or a portion of that product and prevent the EM emission from an outside source from deteriorating its electronic performance. Conversely, it may also be used to prevent an external susceptible (electronic items or living organisms) from internal emissions of an instruments’ electronic circuitry. In one embodiment, the nanocomposite film of the present invention may be applied to plastics comprising sensitive electronic devices.

Exemplary non-limiting applications of the nanocomposite film as an electromagnetic shielding material include, but are not limited to, an EM shielding gasket, a shielded cable, protection of medical, laboratory and defense equipment from interfering signals including AM, FM, TV, emergency services, dispatch, pagers, cellular, ESMR and PCS, protection for computers and keyboards to prevent passive monitoring, and protection of secure data stored on RFID chips embedded in many devices.

According to a fourth aspect, the present disclosure relates to a nanocomposite film comprising a polymer layer, a conductive nanofiller layer, and a polysaccharide layer, wherein the conductive nanofiller layer is sandwiched between and in continuous contact with the polymer layer and the polysaccharide layer.

The polymer of the polymer layer of the present disclosure may be a homopolymer (one monomer) or a copolymer (more than one monomer) and mixtures thereof. The polymer of the polymer layer of the present disclosure may be a homopolymer, an alternating copolymer, a periodic copolymer, a statistical copolymer, a block copolymer, a gradient copolymer or mixtures thereof. The polymer of the polymer layer of the present disclosure may be a natural polymer, a semisynthetic polymer or a synthetic polymer or copolymers and mixtures thereof. The polymer of the polymer layer of the present disclosure may be a thermoplastic polymer, a thermosetting polymer or copolymers and mixtures thereof. The polymer of the polymer layer of the present disclosure may be an addition polymer, a condensation polymer or copolymers and mixtures thereof. The polymer of the polymer layer of the present disclosure may be a linear homopolymer (one monomer), a linear copolymer (more than one monomer), a branched homopolymer, a branched copolymer, a cross linked homopolymer, a cross linked copolymer, a graft copolymer or mixtures and copolymers thereof. The polymer of the polymer layer of the present disclosure may be a rubber, a plastic, a fiber or copolymers and mixtures

thereof. The polymer of the polymer layer of the present disclosure may be isotactic, syndiotactic, atactic or copolymers and mixtures thereof.

In a preferred embodiment, the polymer layer is polyvinyl alcohol (PVA). Polyvinyl alcohol (PVA, PVOH or PVAI) is a water-soluble synthetic polymer. It has the idealized chemical formula [CH<sub>2</sub>CH(OH)]<sub>n</sub>. In one embodiment, the polyvinyl alcohol of the present disclosure has a hydrolysis value of at least 60%, preferably at least 65%, preferably at least 70%, preferably at least 75%, preferably at least 80%, preferably at least 85%, preferably at least 90%, preferably at least 91%, preferably at least 92%, preferably at least 93%, preferably at least 94%, preferably at least 95%, preferably at least 96%, preferably at least 97%, preferably at least 98%, preferably at least 99%, where a value of 100% is complete hydrolysis and 0% is no hydrolysis.

In one embodiment, the polyvinyl alcohol of the present disclosure has an average molecular weight of 5-200 kDa, preferably 10-150 kDa, preferably 10-100 kDa, preferably 10-75 kDa, more preferably 10-50 kDa, preferably 20-35 kDa. In one embodiment, the polyvinyl alcohol of the present disclosure has a PDI of up to 6, preferably up to 5, preferably up to 3, preferably up to 2.5, preferably up to 2, preferably up to 1.5, preferably up to 1.25. In one embodiment, the polyvinyl alcohol of the present disclosure has a degree of polymerization of 100-2500, preferably 100-1500, preferably 100-750, preferably 100-300. In the present disclosure, polyvinyl alcohol may refer to PVA that is ultra-low viscosity, low viscosity, medium viscosity, high viscosity or mixtures thereof. In one embodiment, the polymer layer is envisioned to be comprised of polyvinyl alcohol doped with additives including, but no limited to, crosslinkers, defoamers, dispersants, biocides and plasticizers.

It is envisioned that other polymeric materials may be used in lieu of polyvinyl alcohol as the polymer layer of the nanocomposite film of the present disclosure. Although the selection of a polymer is not viewed as particularly limiting, the polarity of the polymer should be compatible with the conductive nanofiller. Suitable polymers may be selected from the group including, but not limited to, polyacrylates, acrylics, poly(acrylic acid), poly(acrylonitrile), poly(2-hydroxyethylmethacrylate), sodium polyacrylate, ethylene glycol dimethacrylate, polystyrenes, high impact polystyrene, poly(vinyl pyridine), poly(methyl acrylate), polymethacrylates, poly(methyl methacrylate), polychloroprene, polyacrylamide, poly(N-isopropylacrylamide), poly(tetrafluoroethylene) (PTFE), poly(N-vinyl pyrrolidone), poly(vinyl pyrrolidinone), poly(vinyl pyridine), polyethylenes, low-density poly(ethylene), high-density poly(ethylene), chlorinated polyethylene (CPD), poly(propylene), poly(isobutylene), poly(butylene), polyvinyl chlorides (PVC), polyvinyl chloride acetate, polyacrylonitriles, poly(ethyl acetate), poly(vinyl acetate), polyvinylacetates, polyvinyl acetate phthalate, ethylene vinyl acetates, poly(ethylene glycol), polyphenylene ethers, poly(ethylene vinyl alcohol), poly(vinylidene fluoride), poly(p-phenylenevinylene), poly(benzoxazole), polyphenylenebenzobisoxazole (PBO), polyaryletherketones, poly(ether ether ketones), polyphenylenesulfides, polyamide imides, polyarylates, polyarylsulphones, poly(styrene-co-acrylonitrile), ethyl-vinyl-alcohol copolymers, copolymers of ethylene and 1-alkenes, polybutene-1, polymethylpentene, amorphous poly-alpha-olefins (APAO), terephthalates, polyacetylene, polyethylene oxides, polycycloolefins, polyisoprenes, poly-styrene-polyisoprene diblock copolymers, polyamides, poly(ethylene terephthalate), poly(trimethylene terephthalate), poly(butylene terephthalate), polycarbonates, polychlorotri-

fluoroethylene, polyvinylidluoride, polyperfluoroalkoxy, poly(ethylene oxide), ethylene oxide copolymers, poly(ethylene imine), poly(dimethyl siloxane), silicones, fluorosilicones, fluoropolymers, polybutadienes, butadiene copolymers, epoxidized natural rubbers, epoxy polymer resins, poly (cis-1,4-isoprene), poly (trans-1,4-isoprene), viton, phenolic resins, acrylic resins, vinylacetate resins, polyurethanes, polyurethane-urea, thermosetting polyimides, thermoplastic polyimides, poly(amic acid), polysulfones, polyetherimides, polyethersulfones, chlorosulfonates, polyoxymethylene, polyphenylene oxide, polyphenylenes, perfluorinatedpolyethylenepropylene, polyvinylidene chloride, fluoropoly(ether-imide), polyolefins, aromatic polyamides (Aramid, para-aramid), polyesters, conducting and conjugated polymers, liquid crystal polymers, liquid crystalline polyesters, vectran, biodegradable thermoplastic polyesters and their copolymers, thermosetting polyesters, unsaturated polyesters, acetals, fluorinated elastomers, rubbers, styrene butadiene rubbers, bismaleimides, copolymer rubbers, styrene-isoprene-styrenes, styrene-butadiene-styrenes, ethylene-propylene, ethylene-propylene-diene monomers (EPDM), nitrile-butadienes, acrylonitrile butadiene styrene (ABS), polyethylene/acrylonitrile butadiene styrene, polycarbonate/acrylonitrile butadiene styrene, nylons, thermoplastic continuous and discontinuous fiber composites, thermosetting continuous and discontinuous fiber composites, specialty polymers, etc. and blends, mixtures, alloys and copolymers thereof.

Intrinsically conducting polymers (ICPs) are organic polymers that conduct electricity. They can have metallic conductivity or can be semiconductors. They offer high electrical conductivity but do not show similar mechanical properties to other available polymers. Their electrical properties can be fine-tuned using the methods of organic synthesis and advanced dispersion techniques.

In one embodiment, it is envisioned that the polymer layer of the nanocomposite film may be adapted to incorporate an intrinsically conducting polymer. Examples of intrinsically conducting polymers include, but are not limited to, poly (fluorene)s, polyphenylenes, polypyrenes, polyazulenes, polynaphthalenes, poly(acetylene)s (PAC), Poly(p-phenylene vinylene) (PPV), poly(pyrrole)s (PPY), polycarbazoles, polyindoles, polyazepines, polyanilines (PAM), poly (thiophene)s (PT), poly(3,4-ethylenedioxythiophene) (PEDOT), poly(p-phenylene sulfide) (PPS) and copolymers and mixtures thereof.

In one embodiment, the polymer layer is envisioned to be comprised of polyvinyl alcohol copolymers including, but not limited to, poly(vinyl alcohol-co-ethylene) ethylene, poly(acrylic acid)-co-poly(vinyl alcohol) copolymer, poly(vinyl butyral)-co-poly(vinyl alcohol copolymer, poly(vinyl acetate)-co-poly(vinyl alcohol) copolymer, poly(vinyl chloride)-co-poly(vinyl alcohol) and mixtures thereof.

As used herein, fillers are particles added to materials, such as polymers, to engender advantageous properties to the mixed material. Furthermore, fillers may affect the process by which a material or mixed material is processed, making production more efficient or more facile. In terms of the present disclosure the term "nanofiller" refers to added materials with at least one dimension of less than 100 nm that change the properties of the material to which they are added, or affect the process by which the mixed material is produced or manufactured. The nanofiller of the present invention may be selected from the group including, but not limited to, metallic, metal oxide, metal carbonate, ceramic, polymeric and carbonaceous nanomaterials.

In one embodiment, the nanofiller of the present disclosure may be of any shape that provides desired polymerization activity and desired properties in the resulting polymer/nanofiller nanocomposite. The nanocomposites can be classified according to their nanofillers. One-dimensional nanofillers have one dimension of less than 100 nm, generally thickness. Examples of one-dimensional nanofillers include nanosheets, nanoplatelets, nanolaminas and nanoshells. Two-dimensional nanofillers have two dimensions of less than 100 nm, generally including diameter. Examples of two-dimensional nanofillers include nanotubes, nanofibers and nanowiskers. Three-dimensional nanofillers have all dimensions of less than 100 nm, and generally encompass isodimensional nanoparticles. Examples of three-dimensional nanofillers include nanoparticles, nanogranules and nanometric silica beads. The nanofiller of the present disclosure may be one-dimensional, two-dimensional, three-dimensional or mixtures thereof.

As used herein, the nanofiller or nanoparticle is defined as a small object that behaves as a whole unit with respect to its transport and properties having at least one dimension of less than 100 nm. Nanoparticles are named for the real-world shapes that they appear to represent. These morphologies sometimes arise spontaneously as an effect of the synthesis or from the innate crystallographic growth patterns of the materials themselves. Some of these morphologies may serve a purpose, such as bridging an electrical junction.

In one embodiment, the nanofiller of the present invention may be synthesized and formed into a variety of morphologies and forms including, but not limited to, nanoparticles, nanosheets, nanoplatelets, nanocrystals, nanospheres, nanowires, nanofibers, nanoribbons, nanorods, nanotubes, nanocylinders, nanogranules, nanowiskers, nanoflakes, nanofoils, nanopowders, nanoboxes, nanostars, tetrapods, nanobelts, nanoflowers, etc. and mixtures thereof.

Nanofiller and nanocomposite characterization is necessary to establish understanding and control of nanoparticle and nanocomposite synthesis, assembly and application. In one embodiment, the nanofiller and nanocomposite are characterized by at least one technique. In another embodiment, it is envisioned that characterization is done using a variety of other techniques. Exemplary techniques include, but are not limited to, electron microscopy (TEM, SEM), atomic force microscopy (AFM), dynamic light scattering (DLS), X-ray photoelectron spectroscopy (XPS), X-ray fluorescence (XRF), powder X-ray diffraction (XRD), energy-dispersive X-ray spectroscopy (EDX), thermogravimetric analysis (TGA), Fourier transform infrared spectroscopy (FTIR), matrix-assisted laser desorption/ionization time-of-flight mass spectrometry (MALDI-TOF), ultraviolet-visible spectroscopy, Rutherford backscattering spectrometry (RBS), dual polarization interferometry and nuclear magnetic resonance (NMR).

In one embodiment, the nanofiller of the present disclosure is a conductive nanofiller. A conductive nanofiller refers to any nanometer sized material that is, or contains at least one material that is, electronically conductive i.e. has a non-zero flow of internal electric charges.

In one embodiment, the conductive nanofiller is an inexpensive carbonaceous nanomaterial such as carbon black (e.g., furnace black and Ketjen black), active carbon, carbon nanorods, carbon nanotubes, carbon fibers, graphene, graphite, expandable graphite, graphene oxide, exfoliated graphite nanoplatelets, thermally reduced graphene oxide, chemically reduced graphene oxide and mixtures thereof, more preferably graphene, graphite, graphene oxide and mixtures thereof, most preferably graphene.

In a preferred embodiment, the conductive nanofiller is graphene. Graphene is an allotrope of carbon in the form of a two-dimensional, atomic-scale hexagonal lattice in which one atom forms each vertex. Graphene is approximately 200 times stronger than steel by weight and conducts heat and electricity with great efficiency. It is the basic structural element of other allotropes including graphite, charcoal, carbon nanotubes and fullerenes. Carbon nanotubes are formed by rolling up a graphene sheets into a tubular structure and graphite is formed by stacking multiple graphene sheets.

Structurally, graphene is a crystalline allotrope of carbon with 2-dimensional properties. As used herein, graphene is a sheet of six membered carbon rings that do not form a closed surface. Its carbon atoms are densely packed in a regular atomic-scale "chicken wire" (hexagonal) pattern. Each atom has four bonds, one 6-bond with each of its three neighbors and one  $\pi$ -bond that is oriented out of the plane. Graphene's hexagonal lattice can be regarded as two inter-leaving triangular lattices.

Graphene's stability is due to its tightly packed carbon atoms and each carbon atom in a graphene sheet having a  $sp^2$  orbital hybridization and delocalized electrons present at opposite surfaces of the graphene sheet. The  $sp^2$  hybridization is a combination of orbitals  $S$ ,  $P_x$  and  $P_y$  that constitute the  $\sigma$ -bond, the final  $P_z$  electron makes up the  $\pi$ -bond. The  $\pi$ -bonds hybridize together to form the  $\pi$ -band and the  $n^*$ -band. These bands are responsible for most of graphene's notable electronic properties, via the half-filled band that permits free-moving electrons. Graphene is a zero-gap semiconductor. Graphene is also the only form of carbon (or solid material) in which every atom is available for chemical reaction from two sides (due to the 2D structure).

In one embodiment, the graphene conductive nanofiller of the present disclosure may be present as a one-atom thick (~0.33 nm) single layer, or monolayer. As used herein the monolayer is termed a "nanosheet". In another embodiment, the graphene may be present as a bilayer (two atom thick layer) or trilayer (three atom thick layer). In another embodiment, the graphene of the present disclosure may be present as several stacked graphene layers. Thus, in one embodiment the graphene layer may have a thickness greater than one atom and up to 200 atoms, preferably up to 100 atoms, preferably up to 50 atoms, preferably up to 10 atoms, preferably up to 5 atoms, preferably up to 4 atoms, preferably up to 3 atoms.

In very basic terms graphene could be described as a single, one atom thick layer of the commonly found mineral graphite; as used herein "graphite" is essentially made up of hundreds, preferably thousands of layers of graphene. Graphene nanoplatelets have "platelet" morphology, meaning they have a very thin but wide aspect ratio. As used herein a "nanoplatelet" consists of several sheets of graphene with an overall thickness. In one embodiment, the graphene nanoplatelets overlap one another to form a multilayer structure. The graphene of the conductive nanofiller of the present disclosure may be nanosheet graphene, nanoplatelet graphene, and/or mixtures thereof.

Multilayer graphene is a material consisting of two or more layers of graphene. Multilayer graphene can exist in the AB, or Bernal-stacked form, where half of the atoms lie directly over the center of a hexagon in the lower graphene sheet, and half of the atoms lie over an atom. Multilayer graphene can also exist in the AA form in which the layers are exactly aligned. Multilayer graphene can also be found in a twisted configuration. The graphene of the conductive

nanofiller of the present disclosure may be multilayer graphene in the AB form, the AA form, the twisted form and mixtures thereof.

In one embodiment, the graphene nanosheets or nanoplatelets of the present disclosure may have wrinkled and/or rippled morphologies. The height of these wrinkles or ripples from the basal plane of the graphene nanosheets or nanoplatelets may range from less than 0.25 nm to about 5 nm, preferably from 0.3-2.5 nm, preferably from 0.5-2 nm, preferably from 1-1.5 nm. The number and frequency of these wrinkles or ripples can vary depending on the chemical size and structure of the nanosheet or nanoplatelet. In another embodiment, the nanosheets or nanoplatelets may be substantially corrugated leading to substantially increased surface area relative to non-corrugated nanosheets or nanoplatelets of comparable size.

In one embodiment, the graphene nanosheets or nanoplatelets of the present disclosure may form sandwich structures such as a sandwich of graphene-polymer-graphene or polymer-graphene-polymer, and so on to more complex multilayer structures with repeating layers of graphene and polymer layer. In one embodiment, the graphene nanosheets or nanoplatelets of the present disclosure may form sandwich structures such as a sandwich of graphene-polysaccharid-graphene or polysaccharide-graphene-polysaccharide, and so on to more complex multilayer structures with repeating layers of graphene and polysaccharide layer.

In one embodiment, the inter-planar distance of the graphene is less than 10 Å, preferably less than 7.5 Å, preferably less than 5 Å, preferably less than 4 Å, preferably less than 3 Å, preferably less than 2.5 Å, preferably less than 2 Å, preferably less than 1.5 Å, preferably less than 1 Å. In one embodiment, the graphene of the present disclosure is in the form of nanoplatelets or nanosheets having an average thickness of 0.5-300 nm, preferably 1-250 nm, preferably 10-200 nm, preferably 20-150 nm, preferably 25-125 nm, preferably 50-100 nm. In one embodiment, the graphene of the present disclosure is in the form of nanoplatelets or nanosheets having an average diameter or width of 1-75 µm, preferably 2.5-50 µm, preferably 5-45 µm, preferably 10-40 µm, preferably 20-30 µm. In one embodiment, the graphene of the present disclosure is in the form of nanoplatelets or nanosheets having an aspect ratio of 200-2000, preferably 500-1500, more preferably 900-1200. In one embodiment, the graphene of the present disclosure is in the form of nanoplatelets or nanosheets having a surface area in the range of 10-2500 nm<sup>2</sup>, preferably 25-2000 nm<sup>2</sup>, more preferably 50-1500 nm<sup>2</sup>, more preferably 75-1250 nm<sup>2</sup>, more preferably 100-1000 nm<sup>2</sup>, more preferably 150-750 nm<sup>2</sup>, or more preferably 200-500 nm<sup>2</sup>. In one embodiment, the graphene of the present disclosure is in the form of nanoplatelets or nanosheets having a specific surface area of 2.5-750 m<sup>2</sup>/g, preferably 5-500 m<sup>2</sup>/g, preferably 7.5-300 m<sup>2</sup>/g, preferably 10-150 m<sup>2</sup>/g, preferably 12-120 m<sup>2</sup>/g, preferably 15-100 m<sup>2</sup>/g.

In one embodiment, the graphene comprising the conductive nanofiller of the present disclosure has not been chemically modified, it is pristine graphene and a pure carbonaceous material having a purity of greater than 90%, preferably greater than 95%, preferably greater than 96%, preferably greater than 97%, preferably greater than 98%, preferably greater than 99%. In one embodiment, the graphene comprising the conductive nanofiller of the present disclosure has an oxygen content of less than 5%, preferably less than 4%, preferably less than 3%, preferably less than 2%, preferably less than 1%. In one embodiment, the graphene comprising the conductive nanofiller of the present

disclosure has a C/O ratio of at least 10, preferably at least 20, preferably at least 30, preferably at least 40, preferably at least 50, preferably at least 75, preferably at least 100, preferably at least 150, preferably at least 200.

In one embodiment, the graphene comprising the conductive nanofiller of the present disclosure may be chemically modified; graphene is commonly modified with nitrogen and oxygen containing functional groups (e.g. graphene oxide). Exposed carbon on the edges of nanosheets or nanoplatelets often reacts with the atmosphere to form hydroxyls, carboxyls, lactones, pyrones, alcohols, carbonyls, imines and/or amines. These modifications may be covalent, non-covalent or mixtures thereof. Examples of functional groups on graphene include, but are not limited to, alcoholic, carboxylic, aldehydic, ketonic and esteric oxygenated functional groups. Alternatively, the graphene may be chemically modified with amine or imine functionality. Chemical functionalization of the graphene may aid the manufacturing of the graphene polymer polysaccharide nanocomposite or improve the interface between the conductive nanofiller and the polymer layer, the polysaccharide layer or both.

In one embodiment, the graphene comprising the conductive nanofiller of the present invention has been chemically modified such that it has a C/O ratio of less than 10, preferably less than 5, preferably less than 4, preferably less than 3, preferably less than 2. In another embodiment, the graphene comprising the conductive nanofiller of the present invention has been chemically modified such that it has a C/N ratio of less than 50, preferably less than 40, preferably less than 30, preferably less than 20, preferably less than 20.

In one embodiment, it is envisaged that the present invention may be adapted to incorporate nanoscale metals as the conductive nanofiller. Examples of possible metals include, but are not limited to, silver, gold, copper, nickel, iron, aluminum zinc, palladium, platinum, magnesium, zirconium, titanium, vanadium, rhodium, rhenium, uranium, silicon, molybdenum, thorium, chromium, manganese, cerium, germanium, tantalum, lead, cadmium, calcium, antimony, tin, bismuth, cobalt, tungsten, indium, silicone, brass, bronze, white brass, stainless steel and alloys or mixtures thereof.

In one embodiment, it is envisaged that the present invention may be adapted to incorporate nanoscale metal oxides as the conductive nanofiller. Examples of possible metal oxides include, but are not limited to oxides of iron, copper, zinc, magnesium, vanadium, nickel, rhodium, rhenium, molybdenum, thorium, chromium, manganese, cerium, silver, lead, cadmium, calcium, antimony, tin, bismuth, cobalt, tungsten, titanium dioxide (anatase, rutile), alumina ( $\text{Al}_2\text{O}_3$ ), antimony-tin-oxide (ATO), silica (diatomite, pyrogenic silica, silica fume), ruthenium dioxide ( $\text{RuO}_2$ ), bismuth ruthenate ( $\text{Bi}_2\text{Ru}_2\text{O}_7$ ), bismuth iridate ( $\text{Bi}_2\text{Ir}_2\text{O}_7$ ), indium oxide ( $\text{In}_2\text{O}_3$ ), lanthanum chromite ( $\text{LaCr}_2\text{O}_4$ ), zirconia ( $\text{ZrO}_2$ ), titania, iron oxide, silica-alumina, mica, ferrite and mixtures thereof.

In another embodiment, the conductive nanofiller may be additional inorganic materials such as boehmite, a mineral aluminum oxide hydroxide ( $\gamma\text{-AlO(OH)}$ ) orthorhombic dipyramidal crystal. It can be obtained naturally or from chemical synthesis from saturated solutions. In another embodiment, the conductive nanofiller may be metal carbonates including, but not limited to magnesium carbonate, potassium carbonate, sodium carbonate, barium carbonate, calcium carbonate and mixtures thereof.

In one embodiment, it is envisaged that the present invention may be adapted to incorporate nanoscale fillers of natural or synthetic clays as well as phosphates of transition

metals as the conductive nanofiller. The nanoscale clays are classified according to their crystalline structures and also to the quantity and position of the ions within their simplest atomic geometric pattern. The most widely used nanoscale 5 clays are phyllosilicates (smectites) having a shell-shaped crystalline structure with nanometer thickness but also include polysilicates and double lamellar hydroxides. Examples of possible nanoclays include, but are not limited to, montmorillonite (MMT), kaolinite, smectite (Talc, Mica, 10 MMT), sepiolite, chlorite, saponite, bentonite, kenyaite, magadiite, kanemite, ilerite, silhydrite, zeolite, fluorohectorite, hydrotalcite and mixtures thereof.

In one embodiment, it is envisaged that the present 15 invention may be adapted to include nanoscale ceramics as the conductive nanofiller. Representative examples of ceramics include carbides such as silicon carbide ( $\text{SiC}$ ), chromium carbide ( $\text{Cr}_3\text{C}_2$ ), titanium carbide ( $\text{TiC}$ ), zirconium carbide ( $\text{ZrC}$ ), boron carbide ( $\text{B}_4\text{C}$ ) and diamond ( $\text{C}$ ), nitrides such as silicon nitrides ( $\text{SiN}$ ,  $\text{Si}_3\text{N}_4$ ), boron nitride 20 ( $\text{BN}$ ), zirconium nitride ( $\text{ZrN}$ ), niobium nitride ( $\text{NbN}$ ), and titanium nitride ( $\text{TiN}$ ), borides such as titanium boride ( $\text{TiB}$ ), zirconium boride ( $\text{ZrB}$ ), tantalum boride ( $\text{TaB}$ ), vanadium boride ( $\text{VB}_2$ ), and lanthanum boride ( $\text{LaB}_6$ ) and silicides such as titanium silicide ( $\text{TiSi}$ ), tantalum silicide ( $\text{TaSi}$ ), 25 molybdenum silicide ( $\text{MoSi}$ ), and tungsten silicide ( $\text{WSi}_2$ ).

In one embodiment, it is envisaged that the present 30 invention may be adapted to include nanoscale electroceramics as the conductive nanofiller. Representative examples of electroceramics include zirconium barium titanate, strontium titanate (ST), calcium titanate (CT), magnesium titanate (MT), calcium magnesium titanate (CMT), zinc titanate (ZT), lanthanum titanate (TLT), lithium lanthanum titanate (LLT), neodymium titanate (TNT), barium zirconate (BZ), calcium zirconate (CZ), lead magnesium niobate (PMN), 35 lead zinc niobate (PZN), lithium niobate (LN), barium stannate (BS), calcium stannate (CS), layered silicates, magnesium aluminum silicate, magnesium silicate, barium tantalite, titanium dioxide, niobium oxide, sapphire, beryllium oxide, barium titanate, zirconia, silica, zirconium tin titanate and mixtures thereof.

In one embodiment, it is envisaged that the present 40 invention may be adapted to include nanoscale silsesquioxanes as the conductive nanofiller. A silsesquioxane is an organosilicon compound with the empirical formula  $\text{RSiO}_{3/2}$  where R is hydrogen or an alkyl, alkene, aryl, arylene or organo-functional group. Silsesquioxanes can have a cage-like structure, most commonly in the form of a cube, hexagonal prism, octagonal prism, decagonal prism, dodecahedral prism, or opened cage-like structure. The high three-dimensional symmetry and nanometer size make silsesquioxanes building blocks for nanocomposites. The diversity of possible functional groups along with their controlled orientation in three-dimensional space allows for highly tailored nanometer-by-nanometer construction in all three 45 dimensions. Examples of possible silsesquioxanes include, but are not limited to, polyhedral oligosilsesquioxanes (POSS), octasilsesquioxanes of the  $[\text{ROSiO}_{1.5}]_8$  type and its polymeric derivatives and the  $[\text{R-phenylSiO}_{1.5}]_8$  type and its polymeric derivatives.

As used herein, polysaccharides are polymeric carbohydrate molecules composed of long chains of monosaccharide units bound together by glycosidic linkages. They may range in structure from linear to highly branched. Examples include storage polysaccharides such as starch and glycogen and structural polysaccharides such as cellulose and chitin. Polysaccharides are often quite heterogeneous, containing slight modifications of the repeating unit. Depending on the 50

structure, these macromolecules can have distinct properties from their monosaccharide building blocks. They may be amorphous or even insoluble in water. When all the monosaccharides in a polysaccharide are the same type, the polysaccharide is called a homopolysaccharide or homoglycan, when more than one type of monosaccharide is present they are called heteropolysaccharides or heteroglycans.

Natural saccharides are generally of simple carbohydrates called monosaccharides with the general formula  $(CH_2O)_n$ , wherein n is three or more. Examples of monosaccharides include glucose, fructose and glyceraldehyde. Polysaccharides, meanwhile have a general formula of  $C_x(H_2O)_y$ , wherein x is usually a larger number in the range of 100-3000, preferably 200-2500, preferably 500-200. Considering that the repeating units in the polymer backbone are often six carbon monosaccharides, the general formula can also be represented as  $(C_6H_{10}O_5)_n$ , wherein n is in the range of 10-5000, preferably 20-4000, preferably 40-3000. In general, polysaccharides contain more than ten monosaccharide units. Definitions of how large a carbohydrate must be to fall into the categories of polysaccharides or oligosaccharides may vary.

In terms of the present disclosure, the polysaccharide may be a structure polysaccharide (chitin, arabinoxylans, pectins, cellulose) or a storage polysaccharide (starches, glycogen). Additional exemplary polysaccharides include, but are not limited to, callose, laminarin, chrysotaminarin, xylan, arabinoxylan, mannan, fucoidan and galactomannan. In a preferred embodiment, the polysaccharide comprises starch.

As used herein, starch or amylose is a carbohydrate consisting of a large number of glucose units joined by glycosidic bonds. Starch is a glucose polymer in which glucopyranose units are bonded by alpha linkages. It consists of two types of molecules, the linear and helical amylose and the branched amylopectin. Amylose consists of a linear chain of several hundred glucose molecules and amylopectin is a branched molecule made of several thousand glucose units (approximately every chain of 20-40, preferably 22-35, preferably 24-30 glucose units is one unit of amylopectin). In a preferred embodiment, the starch of the present disclosure comprises 10-30% amylose by weight relative to the total weight of the starch, preferably 12-28%, preferably 15-25% amylose by weight relative to the total weight of the starch. In a preferred embodiment, the starch of the present disclosure comprises 70-90% amylopectin by weight relative to the total weight of the starch, preferably 72-88%, preferably 75-85% amylopectin by weight relative to the total weight of the starch.

According to its fourth aspect, the present disclosure relates to a nanocomposite film further including a surface of the polysaccharide layer and a surface of the polymer layer. The polysaccharide layer surface has a first resistivity. The polymer layer surface has a second resistivity. Additionally, the second resistivity is less than or equal to the first resistivity.

The nanocomposite film of the present disclosure may have various shapes and sizes. In a preferred embodiment, the nanocomposite film may be horizontally oriented with a longitudinal axis. The polymer layer and polysaccharide layer may be parallel to each other and the longitudinal axis and the longitudinal axis may run through the conductive nanofiller layer sandwiched between and in continuous contact with both the polymer layer and the polysaccharide layer. The polymer layer and the polysaccharide layer may also be opposing across the longitudinal axis and the vertical distance between the polymer layer surface and polysaccharide layer surface may define the thickness of the nanocom-

posite film. In one embodiment, the film is double sided and the polymer layer surface and polysaccharide layer surface are not adjoining. In terms of the present disclosure, the conductive nanofiller layer is oriented parallel to the polymer layer and the polysaccharide layer.

As used herein, "surface" refers to the outermost part or most outside layer or boundary of a material, here the nanocomposite film. It includes both a continuous set of points with length and width providing an exterior face to the nanocomposite and also may have a thickness and depth and be described as a layer. A surface, as used herein, is in complete and continuous contact with an external environment of the nanocomposite film of the present disclosure as well as the nanocomposite film itself. In one embodiment, the nanocomposite film of the present disclosure comprises a first (polysaccharide) and second (polymer) surface. It is further envisaged that the present disclosure may be adapted to incorporate a third surface, a fourth surface, a fifth surface, etc. or a plurality of surfaces with defined content of polymer, polysaccharide and conductive nanofiller and defined electrical resistivity.

As used herein, the conductive nanofiller layer refers to the portion of the nanocomposite that is neither the polymer layer nor the polysaccharide layer. The conductive nanofiller layer may have characteristics of the polymer layer, the polysaccharide layer, both and/or neither. In a preferred embodiment, the polymer layer and the polysaccharide layer form distinct layers with distinct and identifiable interfaces between each layer and the conductive nanofiller layer. In one embodiment, the polymer and polysaccharide layers form distinct layers, although the interface between each layer and the conductive nanofiller layer may be a mixture of both the polymer layer and the conductive nanofiller layer, a mixture of the polysaccharide layer and the conductive nanofiller layer, or a mixture of the polymer layer, the polysaccharide layer and the conductive nanofiller layer. The nanocomposite film described herein is singular comprising a polymer layer, a polysaccharide layer, a conductive nanofiller layer, a polymer layer surface, and a polysaccharide layer surface, and their interfaces. The film is not formed by conjoining multiple films and has no internal film-to-film interfaces.

In one embodiment, the conductive nanofiller layer of the nanocomposite film may have a conductive nanofiller content gradient. Generally, the conductive nanofiller layer will have a content of conductive nanofiller greater than the polymer layer and greater than the polysaccharide layer. In one embodiment, the content of the conductive nanofiller layer may increase at greater distances from the polymer layer and greater distances from the polysaccharide layer. Conversely, the content of conductive nanofiller in the conductive nanofiller layer may decrease at shorter distances from the polymer layer and shorter distances from the polysaccharide layer.

In one embodiment, the nanocomposite film of the present disclosure has a total average thickness of 0.1-1.0 mm, preferably 0.2-0.8 mm, preferably 0.3-0.7 mm, preferably 0.4-0.6 mm or about 0.5 mm.

In one embodiment, the polymer layer of the present disclosure may encompass up to 70% of the total thickness of the nanocomposite film, preferably up to 60%, preferably up to 50%, preferably up to 40%, preferably up to 30%, preferably up to 25%, preferably up to 20%, preferably up to 15%, preferably up to 10%, preferably up to 5% of the total thickness of the nanocomposite film. In one embodiment, the polymer layer of the present disclosure has a total average thickness of up to 0.5 mm, preferably up to 0.4 mm,

preferably up to 0.3 mm, preferably up to 0.25 mm, preferably up to 0.2 mm, preferably up to 0.15 mm, preferably up to 0.1 mm, preferably up to 0.05 mm.

In one embodiment, the polysaccharide layer of the present disclosure may encompass up to 70% of the total thickness of the nanocomposite film, preferably up to 60%, preferably up to 50%, preferably up to 40%, preferably up to 30%, preferably up to 25%, preferably up to 20%, preferably up to 15%, preferably up to 10%, preferably up to 5% of the total thickness of the nanocomposite film. In one embodiment, the polysaccharide layer of the present disclosure has a total average thickness of up to 0.5 mm, preferably up to 0.4 mm, preferably up to 0.3 mm, preferably up to 0.25 mm, preferably up to 0.2 mm, preferably up to 0.15 mm, preferably up to 0.1 mm, preferably up to 0.05 mm.

In one embodiment, the nanocomposite film has up to 25% conductive nanofiller by weight relative to the total weight of the nanocomposite film, preferably up to 20%, preferably up to 15%, preferably up to 10%, preferably up to 9%, preferably up to 8%, preferably up to 7%, preferably up to 6%, preferably up to 5%, preferably up to 4%, preferably up to 3%, preferably up to 2%, preferably up to 1%, preferably up to 0.75%, preferably up to 0.5%, preferably up to 0.25%, preferably up to 0.2%, preferably up to 0.15%, preferably up to 0.1%, preferably up to 0.01%.

In one embodiment, the nanocomposite film is at least 50% polymer by weight relative to the total weight of the nanocomposite film, preferably at least 55%, preferably at least 60%, preferably at least 65%, preferably at least 66%, preferably at least 67%, preferably at least 68%, preferably at least 69%, preferably at least 70%. In one embodiment, the nanocomposite film is at least 20% polysaccharide by weight relative to the total weight of the nanocomposite film, preferably at least 25%, preferably at least 30%, preferably at least 35%, preferably at least 36%, preferably at least 37%, preferably at least 38%, preferably at least 39%, preferably at least 40%. In one embodiment, the nanocomposite film comprises a weight ratio between the polymer and the polysaccharide in the range of 80:20 to 60:40, preferably 75:25 to 65:45, preferably 72:23 to 67:48, or about 70:30.

The mechanical properties of the nanocomposite film of the present disclosure are also of interest. Tensile strength is the maximum stress that a material can withstand while being stretched or pulled before failing or breaking. Young's modulus (tensile modulus, E-modulus or elastic modulus) is a measure of a material's stiffness or its resistance to being deformed elastically (non-permanently) when a force is applied and can be thought of as the ratio of stress to strain. In one embodiment, the nanocomposite film of the present disclosure has a tensile strength in the range of 5-75 MPa, more preferably 10-60 MPa, more preferably 15-50 MPa. The inclusion of conductive nanofiller may increase the tensile strength by at least 20%. In one embodiment, the nanocomposite film of the present disclosure has a Young's modulus in the range of 2-80 MPa, preferably 10-70 MPa, preferably 15-60 MPa, more preferably 20-50 MPa. The inclusion of conductive nanofiller may increase the tensile strength by at least 15%.

In one embodiment, the nanocomposite film comprises from 0.1-10.0% of conductive nanofiller by weight relative to the total weight of the nanocomposite film, preferably 0.25-7.0%, preferably 0.5-5.0%, preferably 1.0-3.0% by weight relative to the total weight of the nanocomposite film. In one embodiment, the nanocomposite film has a polymer layer that is antistatic and a polysaccharide layer that is

antistatic. The polymer layer is antistatic and has a second resistivity of  $10^4$ - $10^8$  ohm·cm<sup>2</sup>, preferably  $10^4$ - $10^7$ , preferably  $10^4$ - $10^6$ , preferably  $10^4$ - $7.5\times 10^5$ , preferably  $10^4$ - $5.0\times 10^5$ , preferably  $10^4$ - $2.5\times 10^5$ , preferably  $10^4$ - $10^5$ , preferably  $10^4$ - $0.5\times 10^5$ , preferably  $10^4$ - $0.25\times 10^5$  ohm·cm<sup>2</sup>. The polysaccharide layer is antistatic and has a second resistivity of  $10^4$ - $10^8$  ohm·cm<sup>2</sup>, preferably  $10^4$ - $10^7$ , preferably  $10^4$ - $10^6$ , preferably  $10^4$ - $7.5\times 10^5$ , preferably  $10^4$ - $5.0\times 10^5$ , preferably  $10^4$ - $2.5\times 10^5$ , preferably  $10^4$ - $10^5$ , preferably  $10^4$ - $0.5\times 10^5$ , preferably  $10^4$ - $0.25\times 10^5$  ohm·cm<sup>2</sup>.

According to a fifth aspect, the present disclosure relates to a process for forming the polymer, polysaccharide and conductive nanofiller nanocomposite films of the present disclosure, in one or more of their embodiments.

In a preferred embodiment, the nanocomposite film of the present disclosure is formed by a solution processing or solution mixing and casting technique. The process is described as wet chemistry and is considered simple and cost effective compared to other processes for manufacturing polymer nanocomposites. In general, solution processing refers to the dispersion of conductive nanofiller into a solvent followed by mixing with a polymer solution and a polysaccharide solution and subsequent vaporization of the solvent to form the desired nanocomposite.

In one embodiment, the solution processing begins with dispersion of the conductive nanofiller into a liquid solution by energetic mixing. The certain amount of conductive nanofiller is determined by the desired weight percent of the final nanocomposite. In one embodiment, the ratio of polymer and polysaccharide to conductive nanofiller may be 85:1, 90:1, 93:1, 95:1, 97:1, 99:1, 99.5:1, 99.75:1. This mixing may include, but is not limited to, mechanical mixing, magnetic agitation, mild sonication, high-energy ultrasonication, shear mixing, refluxing and mixtures thereof. The process of mixing to form a stable dispersion may last as little as 2 hours, preferably 1.5 hours, preferably 1 hour, preferably 30 minutes, preferably 15 minutes, preferably 10 minutes, preferably 5 minutes, preferably 2 minutes. In one embodiment, the dispersion of nanofiller may occur directly in a polymeric and polysaccharide solution, in another embodiment the nanofiller is dispersed in a solvent and then mixed with an independent polymer and polysaccharide solution that may be in the same solvent or a different solvent.

In one embodiment, once combined in a reaction mixture the dispersed conductive nanofiller solution and the polymer and polysaccharide solution are further mixed by the means discussed previously, preferably heating, magnetic agitation and ultrasonication, preferably magnetic stirring at a speed of at least 100 rpm, preferably at least 200 rpm, preferably at least 400 rpm. In one embodiment the reaction mixture is mixed at elevated temperature of at least 40° C., preferably at least 60° C., preferably at least 70° C., preferably at least 80° C. Alternatively the reaction mixture is mixed at room temperature, 20-30° C. The process of mixing the reaction mixture may last as little as 6 hours, preferably 4 hours, preferably 2 hours, preferably 1.5 hours, preferably 1 hour, preferably 30 minutes, preferably 15 minutes. In one embodiment, following the mixing the reaction mixture is degassed to remove any traces of air from the solution with inert gas. The process of degassing may last as little as 2 min, preferably 5 min, preferably 10 min, preferably 15 min. Finally, the mixture is poured on a leveled flat surface and allowed to dry at room temperature. The dried films may then be peeled from the surface they were poured and cast on and kept in a desiccator to avoid moisture uptake. In one embodiment, the nanocomposite films are cast and dried in

glass plates. In one embodiment, the drying is done at elevated temperature up to 200° C., preferably up to 150° C., preferably up to 100° C., preferably up to 75° C., preferably up to 50° C. The drying time may take up to 48 hours, preferably up to 24 hours, preferably up to 12 hours, preferably up to 8 hours, preferably up to 4 hours, preferably up to 2 hours.

The nature of the conductive nanofiller/polymer/polysaccharide ratio and fabrication conditions including, but not limited to temperatures, sonication, step durations and casting and drying conditions are what allow for control of the size, shape and dispersion of the conductive nanofiller in the nanocomposite film. Thus, variations in the above process give rise to a nanocomposite film comprising a polymer layer, a conductive nanofiller layer and a polysaccharide layer.

In one embodiment, the polymerization by solution processing is carried out in a liquid solvent that may include polar protic solvents, aprotic polar solvents and non-polar solvents. Suitable polar protic solvents may include, but are not limited to, water, nitromethane, and short chain alcohols such as methanol, ethanol, propanol, isopropanol, butanol or the like and mixtures thereof. Suitable aprotic polar solvents may include, but are not limited to, propylene carbonate, ethylene carbonate, butyrolactone, acetonitrile, benzonitrile, nitromethane, nitrobenzene, sulfolane, dimethylformamide, N-methylpyrrolidone or the like and mixtures thereof. Suitable non-polar solvents may include, but are not limited to, cyclohexane, octane, heptane, hexane, benzene, toluene, xylene, methylene chloride, carbon tetrachloride, diethyl ether or the like and mixtures thereof. In one embodiment, co-solvents may also be used. In a most preferred embodiment, the liquid solvent is water or a solution comprising glycerol and water, preferably less than 10% glycerol by weight relative to the total weight of the solution, preferably less than 8% glycerol, preferably less than 6% glycerol, preferably less than 4% glycerol, preferably less than 2% glycerol.

In one embodiment, the reaction mixture of the present process may contain one or more additional additives to change the properties of the nanocomposites and/or to improve the process of producing the nanocomposites. Exemplary additives include, but are not limited to, surfactants, antifoaming agents or defoamers, a scale inhibitor, a corrosion inhibitor, a colorant, a thermal stabilizer, a dopant, a coolant additive, a polymerization catalyst, a hardener, a Lewis base, a plasticizer and mixtures thereof.

In one embodiment, the nanocomposite film may further undergo one or more manufacturing steps after formation to instill any desired properties. Techniques or processes including, but not limited to, vulcanization, grafting, cross-linking, injection molding, hot pressing, drawing, extrusion, autoclaving, annealing, heat treating, sintering, compression molding, machining, welding, adhesively bonding, thermo-forming, coating, vacuum forming, blow molding, stretch blow molding, transfer molding, calendaring, compounding, orienting, tape laying with in situ consolidation, diaphragm forming, rotational molding, centrifugal molding, fiber spinning, filament winding, foam blowing, pultruding and the like are considered to be within the scope of the present method.

In another embodiment, the polymer nanocomposite film of the present disclosure is formed by in situ polymerization. In general, the conductive nanofiller and polysaccharide are mixed with monomers or pre-polymers and then the nanocomposite is formed by polymerizing the monomers or pre-polymers. This method may further encompass the use

of metallocene-based catalyst, anchoring agents such as methylaluminoxane and/or a hardener. This polymerization process is usually accompanied by a viscosity increase that hinders manipulation and limits load fraction. Additionally, solvents may be necessary and may need to be removed, similarly to solution processing.

In another embodiment, the polymer nanocomposite film of the present disclosure is formed by melt blending. This method is generally applied to polymers that are insoluble and is particularly useful for dealing with thermoplastic polymers. The technique capitalizes on the fact that thermoplastic polymers soften when heated. Amorphous polymers are heated above their glass transition temperature and semi-crystalline polymers are heated above their melt temperature to induce sufficient softening. Conductive nanofiller and polysaccharide can then be mixed into the melt by conventional blending equipment such as shear mixing or a twin screw extruder and bulk samples can be further fabricated by techniques such as compression molding, injection molding, and/or extrusion. In other embodiments, the polymer nanocomposite film of the present disclosure is further envisioned to be produced by novel methods including, but not limited to, solid-state mechanochemical pulverization, coagulation spinning and/or latex fabrication methods.

In a preferred embodiment, the conductive nanofiller is graphene, the polysaccharide is starch and the polymer is polyvinyl alcohol. In one embodiment, the graphene can be prepared from exfoliation of graphite. As used herein, "exfoliation" refers to cleavage or coming apart of a material shed from a surface in scales or layers. The exfoliation may be by mechanical cleavage means such as adhesive tape, shearing or wedge based mechanical exfoliation. The exfoliation may also be by direct sonication cleavage such as solvent-aided sonication, solvent/surfactant aided sonication and immiscible liquid aided sonication. In one embodiment, the graphene can be prepared from graphite oxide or graphene oxide via thermal (~2000° C./s) or chemical (hydrazine) reduction followed by or preceded by exfoliation.

In another embodiment, the graphene may be produced by epitaxy. Epitaxy refers to the deposition of a crystalline overlayer on a crystalline substrate, ideally coupled weakly enough to retain the two dimensional electronic band structure of isolated graphene. Suitable substrates include, but are not limited to silicon carbide, metals such as ruthenium, iridium, nickel or copper. The graphene conductive nanofiller of the present disclosure is envisioned to be produced by a variety of techniques including, but not limited to, the sugar method, sodium ethoxide pyrolysis, roll-to-roll manufacturing, silicon/germanium/hydrogen chemical vapor deposition, nanotube slicing, carbon dioxide reduction, spin coating, supersonic spray, intercalation, CO<sub>2</sub> infrared laser, and microwave assisted oxidation.

In another embodiment, the nanocomposite film of the present disclosure may be formed by methods requiring a substrate, typically glass or plastic. Such methods include, but are not limited to chemical vapor deposition (CVD), preferably microwave-assisted CVD, and spin coating.

According to a sixth aspect, the present disclosure relates to an electrical or electronic device including the polymer, polysaccharide and conductive nanofiller nanocomposite films of the present disclosure, in one or more of their embodiments.

In one embodiment, the electrical or electronic device is covered by the nanocomposite film by attaching the free-standing film to the device by any reasonable manner. The nanocomposite may be attached through surface coating interaction (e.g. glued, tacked, cemented, pasted, etc.),

37

attached by highly connected or integral interactions (e.g. melted together, fused, amalgamated, etc.), or sandwiched between a plurality of electronic components of the device. In another embodiment, the electrical or electronic device is covered by the nanocomposite film by first applying the conductive nanofiller/polymer/polysaccharide reaction mixture to the device and then forming the nanocomposite on the device by drying. In another embodiment, the electrical device is covered by, attached to, wrapped or enclosed by a metal or alloy or ceramic substrate on which the nanocomposite is disposed.

In one embodiment, the nanocomposite film of the present disclosure is envisioned to find use as an antistatic agent or electrostatic discharge material. An antistatic agent is a compound used for the treatment of materials or their surfaces in order to reduce or eliminate the buildup of static electricity. The role of the antistatic agent is to make the surface of the material itself slightly conductive. Antistatic devices reduce static electricity that can damage electrical components such as computer hard drives, cause bodily injury, or ignite flammable liquids and gases. Exemplary non-limiting applications of the nanocomposite film as an antistatic agent or component of an antistatic device include, but are not limited to, antistatic bags used to contain devices, such as graphics cards or hard disk drives, often during transport, antistatic garments such as gloves or shoes used in many industries such as electronics, communication, telecommunication and defense applications, antistatic mats, antistatic straps and antistatic bars used to ground many sensitive processes and systems.

In one embodiment, the nanocomposite film of the present disclosure is envisioned to find use as an electromagnetic shielding material. Electromagnetic (EM) shielding is the practice of reducing the electromagnetic field in a space by blocking the field with barriers made of conductive materials. Shielding is typically applied to enclosures for isolating electronic devices from the “outside world” and cables to isolate wire from the environment through which the cable runs. The nanocomposite film of the present disclosure may completely enclose an electronic product or a portion of that product and prevent the EM emission from an outside source from deteriorating its electronic performance. Conversely, it may also be used to prevent an external susceptible (electronic items or living organisms) from internal emissions of an instruments’ electronic circuitry. In one embodiment, the nanocomposite film of the present invention may be applied to plastics comprising sensitive electronic devices.

Exemplary non-limiting applications of the nanocomposite film as an electromagnetic shielding material include, but are not limited to, an EM shielding gasket, a shielded cable, protection of medical, laboratory and defense equipment from interfering signals including AM, FM, TV, emergency services, dispatch, pagers, cellular, ESMR and PCS, protection for computers and keyboards to prevent passive monitoring, and protection of secure data stored on RFID chips embedded in many devices.

The examples below are intended to further illustrate protocols for preparing and characterizing the nanocomposite films of the present disclosure described herein. Further, they are intended to illustrate assessing the morphology and electrical properties of these nanocomposite films, specifically resistivity. They are not intended to limit the scope of the claims.

38

## Example 1

## Chemicals

Polyvinyl alcohol (PVA) was purchased from Sigma Aldrich Company and utilized directly without further purification. Millipore MilliQ purified deionized water was used in all operations. Multiwall carbon nanotubes were procured from Nanostructure and Amorphous Material, Inc., USA and utilized directly without any further purification. Starch was obtained from ARASCO Corn products, Dammam, Saudi Arabia and utilized directly without any further purification. Graphene (Grafen®-iGP) of 96-99% purity was procured from Grafen Chemical Industries Co., Turkey and utilized directly without any further treatment or purification in the embodiments described herein.

## Example 2

## Preparation of Polyvinyl Alcohol (PVA) and Carbon Nanotube (CNT) Nanocomposite Blends

Blends of polyvinyl alcohol (PVA) and carbon nanotubes (CNT) were prepared via a solution mixing and evaporative casting method. First of all, 3 g of PVA was completely dissolved in deionized water (40 mL) at 98° C. under 600 rpm. Subsequently, a certain amount of carbon nanotubes, based on the formulations as shown in Table 1, was added to 35 mL of deionized water.

TABLE 1

Formulations used in preparing the polyvinyl alcohol and carbon nanotube blends	
Sample	Amount of carbon nanotubes (g)
PVA (control)	—
PVA/CNT (0.5 wt. %)	0.015
PVA/CNT (1.0 wt. %)	0.03
PVA/CNT (3.0 wt. %)	0.09
PVA/CNT (5.0 wt. %)	0.15
PVA/CNT (7.0 wt. %)	0.21
PVA/CNT (10.0 wt. %)	0.30

A stable dispersion of carbon nanotubes in water was prepared by ultra-sonication using the Ultrasonicator Probe (Ultrasonica Q 700) at an amplitude of 30% for 15 minutes. After that, the dispersion of water and carbon nanotubes was added to the PVA solution in water and stirring was continued for one hour with the use of a magnetic stirrer at 600 rpm and at a temperature of 80° C. The mixture was then degassed for 10 minutes to remove any traces of air from the solution. Finally, the mixture was poured into a plastic Petri dish placed on a leveled flat surface and allowed to dry at room temperature for six days. The dried films of approximately 0.5 mm in thickness were carefully peeled off from the plastic Petri dish and kept in a desiccator to avoid moisture uptake.

## Example 3

## Characterization of Polyvinyl Alcohol (PVA) and Carbon Nanotube (CNT) Nanocomposite Blends

Field emission scanning electron microscopy (FESEM) images were taken using MIRA3 TESCAN field emission SEM. The samples were cryo-fractured using liquid nitrogen before testing. The cross section of samples was coated with platinum (5 nm thickness) to make the surface conductive. The electrical resistances of the samples were measured using a digital source meter (Model 2400 Series, Keithley Instruments, Inc.). The calculated results of the electrical resistivity are reported in Table 2.

TABLE 2

Sample	Resistance measurements of polyvinyl alcohol and carbon nanotube blends	
	Surface Resistivity ( $\Omega \cdot \text{cm}^2$ ) Second Surface	Surface Resistivity ( $\Omega \cdot \text{cm}^2$ ) First Surface
PVA (control)	$>2.00 \times 10^8$	$>2.00 \times 10^8$
PVA/CNT (0.5 wt. %)	$>2.00 \times 10^8$	$>2.00 \times 10^8$
PVA/CNT (1.0 wt. %)	$5.67 \times 10^7$	$>2.00 \times 10^8$
PVA/CNT (3.0 wt. %)	$3.44 \times 10^5$	$>2.00 \times 10^8$
PVA/CNT (5.0 wt. %)	$1.27 \times 10^6$	$>2.00 \times 10^8$
PVA/CNT (7.0 wt. %)	$7.35 \times 10^4$	$8.11 \times 10^7$
PVA/CNT (10.0 wt. %)	$3.05 \times 10^3$	$1.02 \times 10^8$

FIG. 1A, FIG. 1B and FIG. 1C show scanning electron micrographs of pure PVA film (FIG. 1A), PVA/CNT (7%) (FIG. 1B), and PVA/CNT (10%) (FIG. 1C). Pure PVA film demonstrated one homogeneous phase (FIG. 1A), while the PVA/CNT nanocomposite films demonstrated by FESEM two phases (layers) were formed (FIG. 1B and FIG. 1C). One phase was rich with carbon nanotubes and the other contained little to no carbon nanotube content. At high loadings of carbon nanotubes, there was a clear distinction between the PVA and carbon nanotube phases.

The effect of carbon nanotube loading on the electrical surface resistivity of PVA/CNT bio-nanocomposites is reported in Table 2. The surface resistivity has been presented for both surfaces of the film, where the first surface has been considered as an “upper” surface and the other second surface as a “bottom” surface relative to and depending on location at the time of casting the nanocomposite film. Interestingly, there is a great difference in surface resistivity between the second and first surface of the films, especially in those with a high content of carbon nanotubes. The surface resistivity of the first surface falls under insulating at all loadings of carbon nanotubes, indicating that this surface is insulating in nature. However, the electrical surface resistivity of the second surface is found to decrease with increasing carbon nanotube loading in the nanocomposite. It is seen that the resistivity of the composites transitions from the insulating region ( $10^8 \text{ ohm}\cdot\text{cm}^2$  to  $10^{17} \text{ ohm}\cdot\text{cm}^2$ ) to the semiconductive/conductive region (below  $10^4 \text{ ohm}\cdot\text{cm}^2$ ) through the antistatic region ( $10^4 \text{ ohm}\cdot\text{cm}^2$  to  $10^8 \text{ ohm}\cdot\text{cm}^2$ ) depending on the loading of carbon nanotubes.

Thus, depending on the carbon nanotube loading one can generate composites with insulating-insulating surface (PVA control and 0.5 wt % carbon nanotube composite), insulating-antistatic surfaces (1.0 wt %, 3.0 wt %, 5.0 wt % and 7.0 wt % carbon nanotube composites) and insulating-semiconductive/conductive surfaces (10.0 wt % carbon nanotube composite). These types of composites have practical value due to their applicability in different electrical and electronic fields. The advantage of using these insulating-semiconducting materials is that they minimize the risk of an electrical shock due to one surface being insulating in nature.

#### Example 4

#### Preparation of Polyvinyl Alcohol (PVA), Graphene, and Starch Nanocomposite Blends

Nanocomposites of polyvinyl alcohol (PVA), graphene and starch were prepared via a solution mixing and evaporative casting method. The ratio between PVA and starch was kept constant at 70/30 (parts by weight). First of all, 4.2 g of PVA was completely dissolved in deionized water (50

mL) at 98° C. under stirring at 600 rpm. Next, 1.8 g of starch and 3.0 g of glycerol were mixed with deionized water (50 mL) at 80° C. under stirring at 400 rpm for 30 minutes. Subsequently, certain amounts of graphene, based on the compositions shown in Table 3, were added to 50 mL of deionized water.

TABLE 3

Sample	Formulations used in preparing the polyvinyl alcohol, graphene, and starch nanocomposite blends	
	Graphene (wt. %)	Amount of graphene (g)
PVA/S (control)	0.0	—
PVA/G/S (0.25 wt. %)	0.25	0.015
PVA/G/S (0.5 wt. %)	0.5	0.03
PVA/G/S (1.0 wt. %)	1.0	0.06
PVA/G/S (3.0 wt. %)	3.0	0.18
PVA/G/S (5.0 wt. %)	5.0	0.30
PVA/G/S (7.0 wt. %)	7.0	0.42
PVA/G/S (10.0 wt. %)	10.0	0.60

Stable dispersions of graphene in deionized water were prepared by ultra-sonication using the Ultrasonicator Probe (Ultrasonica Q 700) at an amplitude of 30% for 2 minutes. After that, the dispersions of starch and graphene were added to the PVA solution. The whole mixture was continuously stirred at 400 rpm for 4 hours. The mixture was then degassed for 10 minutes to remove any traces of air from the solution. Finally, the mixture was poured into a glass plate placed on a leveled flat surface and kept for drying at 50° C. in an air oven for 24 hours. The dried films of approximately 0.3 mm in thickness were carefully peeled off from the plates and preserved in a desiccator filled with silica gel to avoid the absorption of any moisture.

#### Example 5

#### Characterization of Polyvinyl Alcohol (PVA), Graphene, and Starch Nanocomposite Blends

Field emission scanning electron microscopy (FESEM) images were taken using MIRA3 TESCAN field emission SEM. The samples were cryo-fractured using liquid nitrogen before testing. The cross section of samples was coated with platinum (5 nm thickness) to make the surface conductive. The electrical resistances of the samples were measured using a digital source meter (Model 2400 Series, Keithley Instruments, Inc.). The calculated results of the electrical resistivity are reported in Table 4.

TABLE 4

Sample	Resistance measurements of polyvinyl alcohol, graphene and starch nanocomposite blends	
	Surface Resistivity ( $\Omega \cdot \text{cm}^2$ ) PVA Layer Surface	Surface Resistivity ( $\Omega \cdot \text{cm}^2$ ) Starch Layer Surface
PVA (control)	$2.0 \times 10^7$	$2.3 \times 10^7$
PVA/G/S (0.25 wt. %)	$1.7 \times 10^7$	$2.4 \times 10^7$
PVA/G/S (0.5 wt. %)	$2.2 \times 10^7$	$2.2 \times 10^7$
PVA/G/S (1.0 wt. %)	$1.8 \times 10^7$	$2.5 \times 10^7$
PVA/G/S (3.0 wt. %)	$6.9 \times 10^6$	$7.7 \times 10^6$
PVA/G/S (5.0 wt. %)	$5.5 \times 10^6$	$1.1 \times 10^7$
PVA/G/S (7.0 wt. %)	$4.7 \times 10^6$	$8.9 \times 10^6$
PVA/G/S (10.0 wt. %)	$3.4 \times 10^6$	$1.2 \times 10^7$

FIG. 2A, FIG. 2B and FIG. 2C show scanning electron micrographs of the PVA/Starch blend film (FIG. 2A) and PVA/Graphene/Starch nanocomposite blends. In the case of

**41**

the PVA and starch blend, there are two phases formed (FIG. 2A). However, in the case of the PVA/Graphene/Starch nanocomposite blends there are three phases formed of distinctly PVA, graphene and starch (FIG. 2B and FIG. 2C). The graphene phase was formed between the PVA and starch. The thickness of the graphene layer depends on the amount of graphene in the samples. It increased with increasing graphene content as shown in FIG. 2C.

The electrical surface resistivities for the PVA/Starch blend and PVA/Starch/Graphene nanocomposite blends are presented in Table 4. The surface resistivities for both surfaces of the PVA/Starch and PVA/Graphene/Starch films have been reported in Table 4. Based on the casting of the film, the starch layer surface has been considered as an "upper" surface and the other PVA layer surface as a "bottom" surface. It is clear that the surface resistivities of the upper starch layer surface and bottom PVA layer surface of all the prepared films fall within the antistatic zone ( $10^8$  ohm·cm $^2$  to  $10^4$  ohm·cm $^2$ ). The semiconductive/conductive layer of graphene is sandwiched between the polyvinyl alcohol and starch layers.

Thus, the foregoing discussion discloses and describes merely exemplary embodiments of the present invention. As will be understood by those skilled in the art, the present invention may be embodied in other specific forms without departing from the spirit or essential characteristics thereof. Accordingly, the disclosure of the present invention is intended to be illustrative, but not limiting of the scope of the invention, as well as other claims. The disclosure, including any readily discernible variants of the teachings herein, defines, in part, the scope of the foregoing claim terminology such that no inventive subject matter is dedicated to the public.

The invention claimed is:

1. A process for forming a nanocomposite film, comprising:  
sonicating a solution of a conductive nanofiller to form a stable dispersion of nanofiller,  
mixing the stable dispersion of nanofiller with a solution comprising a polymer and a polysaccharide to form a reaction mixture, and  
casting the reaction mixture and drying to form the nanocomposite film, wherein during the casting the mixture separates into a polymer phase containing a

5

10

15

20

25

30

40

**42**

majority of the polymer, a conductive nanofiller phase containing a majority of the conductive nanofiller, and a polysaccharide phase containing a majority of the polysaccharide,

wherein the nanocomposite film comprises:

a polymer layer comprising the polymer,  
a conductive nanofiller layer comprising the conductive nanofiller,  
a polysaccharide layer comprising the polysaccharide, wherein a surface of the polysaccharide layer has a first resistivity and a surface of the polymer layer has a second resistivity,  
wherein the conductive nanofiller layer is sandwiched between and in continuous contact with the polymer layer and the polysaccharide layer; and  
wherein the second resistivity is less than or equal to the first resistivity.

2. The process of claim 1, wherein a weight ratio between the polymer layer and the polysaccharide layer in the nanocomposite film is in the range of 80:20 to 60:40.

3. The process of claim 1, wherein the nanocomposite film comprises up to 25 weight percent of the conductive nanofiller layer relative to the total weight of the nanocomposite film.

4. The process of claim 1, wherein the conductive nanofiller is graphene in the form of nanosheets having an average longest dimension of 1-75  $\mu\text{m}$  and an average thickness of 0.5-300 nm or graphene in the form of nano-platelets having an average diameter of 1-75  $\mu\text{m}$  and an average thickness of 0.5-300 nm.

5. The process of claim 1, wherein the polymer is a polyvinyl alcohol.

6. The process of claim 1, wherein the polysaccharide is a starch.

7. The process of claim 1, wherein the nanocomposite film has an average thickness of 0.1-1.0 mm.

8. The process of claim 1, wherein the surface of the polysaccharide layer is antistatic and has a first product of electrical resistance and area (R·A) in the range of  $10^6$ - $10^8$  ohm·cm $^2$  and the surface of the polymer layer is antistatic and has a second product of electrical resistance and area (R·A) in the range of  $10^6$ - $10^8$  ohm·cm $^2$ .

\* \* \* \* \*

# Evaluation of Nanomechanical Properties of (Styrene–Methyl Methacrylate) Copolymer Composites Containing Graphene Sheets

Edreese H. Alsharaeh,<sup>\*,†</sup> Nadimul H. Faisal,<sup>‡,§</sup> Ali A. Othman,<sup>†</sup> and Rehan Ahmed<sup>‡,⊥</sup>

<sup>†</sup>Department of Chemistry and <sup>‡</sup>College of Engineering, Alfaisal University, P.O. Box 50927, Riyadh 11533, Saudi Arabia

<sup>§</sup>School of Engineering, Robert Gordon University, Garthdee Road, Aberdeen AB10 7GJ, U.K.

<sup>⊥</sup>School of Engineering and Physical Sciences, Heriot-Watt University, Edinburgh EH14 4AS, U.K.

**ABSTRACT:** The nanomechanical properties of polymers that contained (styrene–methyl methacrylate) copolymer (PS-PMMA) composites with reduced graphene oxide sheets (RGO) prepared by (i) *in situ* bulk polymerization and (ii) a microwave irradiation (MWI) method were compared. The nanomechanical properties such as the hardness and elastic modulus of these copolymers were analyzed using Berkovich nanoindentation. The results indicate that the composite obtained using the MWI method exhibited a better morphology and increased dispersion with enhanced thermal stability. As a result, the mechanical properties also improved due to increased mechanical interlocking between the graphene oxide (GO) nanofillers and the PS-PMMA matrix, which improved the mechanical strength. An average increase of 136% in hardness and 76% in elastic modulus were achieved through the addition of only 2.0 wt % of RGO composite obtained via the MWI method.

## 1. INTRODUCTION

The enhanced mechanical properties of copolymer composite materials can be a key performance criterion with respect to the durability of these materials in tribological applications. The asperity interactions at the nanoscale are dependent upon the structure property relationships. The mechanical properties of copolymers are therefore important parameters in the tribological design process. This work presents the preparation, characterization, and evaluation of the nanomechanical properties of a copolymer with reduced graphene oxide sheets to elucidate the structure–property relationships of the resulting composites with a view toward improving their mechanical properties.

Graphene is known as the thinnest one-atom-thick two-dimensional graphitic carbon ( $sp^2$ -bonded carbon sheets) material.<sup>1</sup> One of the advantages of graphene oxide (GO) is that it can be well-dispersed in water and physiological environments because of its abundant hydrophilic groups, such as hydroxyl, epoxide, and carboxylic groups, on its surfaces.<sup>2,3</sup> Graphene has recently attracted interest from researchers as a filler material in new composite polymers.<sup>4–15</sup> The structural, mechanical, tribological, thermal, optical, and electrical properties of graphene make it an excellent two-dimensional filler material for polymer composites that may find applications in numerous technological fields.<sup>4–8</sup>

Various techniques have been developed for the synthesis of such composite structures, including solution mixing, melt blending, *in situ* polymerization, and *in situ* polymerization using microwave irradiation (MWI).<sup>15–17</sup> The MWI method offers a fast and easy way to synthesize graphene-based materials. In MWI, dielectric heating energy is transferred directly to the reactants. Energy is supplied to the molecules faster than they are able to relax, which creates high instantaneous temperatures and increases the yield and quality of the products.<sup>18–21</sup> The copolymer of methyl methacrylate and styrene (PS-PMMA) is an important polymeric material that has numerous applications

in medicine (e.g., as bone cement), dentistry (e.g., dentures), and the paper, paint, and automotive industries.<sup>22–25</sup>

This paper reports on the nanomechanical characterization of copolymers PS-PMMA containing reduced graphene oxide sheets to provide an understanding of the influence of manufacturing method on the structure property relationship. Among other techniques, nanomechanical characterization is an important methodology in the design of a variety of materials. Nanomechanical characterization includes investigations of nanoindentation properties (hardness and elastic modulus). To the authors' knowledge, this is the first report of the nanomechanical properties of reduced graphene oxide-based copolymer RGO/(PS-PMMA) composite materials.

## 2. EXPERIMENTAL SECTION

**2.1. Materials.** Extra pure graphite powder (>99.5%) was purchased from Merck, and hydrazine hydrate (HH, 80%) was obtained from Loba Chemi. Pvt. Ltd. Styrene (S) and methyl methacrylate (MMA) monomers (Acros Chemical Co., 99%) were kept in a refrigerator and used as received. Benzoyl peroxide (BP) (BDH Chemicals Ltd.) was used as an initiator. Potassium permanganate ( $KMnO_4$ , >99%) and hydrogen peroxide ( $H_2O_2$ , 30%) were obtained from Merck. Other solvents and chemicals were of analytical grade and used without further purification.

**2.2. Preparation of Graphene Oxide (GO).** GO was synthesized from the oxidation of graphite powder via the Hummers and Offeman method.<sup>26</sup> Natural graphite (3.5 g) was added to 100 mL of 98%  $H_2SO_4$  at 0 °C under vigorous stirring.  $KMnO_4$  (10 g) was slowly added, and the temperature was maintained below 20 °C. The stirring was continued for 2 h at 35 °C. Then, the content of the flask was poured into 500 mL of deionized

Received: July 25, 2013

Revised: October 4, 2013

Accepted: November 27, 2013

Published: November 27, 2013



**Table 1.** List of Copolymer and RGO–Copolymer Composite Specimens

Sl. no.	specimen type	GO (wt %)	RGO (wt %)	S monomer (mmol)	MMA monomer (mmol)	BP initiator (wt %)	specimen thickness ( $\mu\text{m}$ )
1	PS-PMMA			24	25	5	500
2	2% RGO-(PS-PMMA)		2	24	25	5	250
3	2% R-(GO-(PS-PMMA))		2	24	25	5	500

water, and a sufficient amount of  $\text{H}_2\text{O}_2$  (20 mL of a 30% aqueous solution) was added to destroy any excess permanganate. Upon treatment with the peroxide, the suspension turned bright yellow. The product was thoroughly washed with dilute HCl and then hot water to remove the residual sulfate ions yielding a yellow-brown filter cake. After the resulting yellowish-brown cake was washed with hot water, the GO was dried at 80 °C overnight.

**2.3. Preparation of Reduced Graphene Oxide (RGO).** The dried GO (400 mg) was sonicated in 20 mL of deionized water until a homogeneous yellow dispersion was obtained. The solution was placed inside a conventional microwave after the addition of 400  $\mu\text{L}$  of the HH reducing agent. The microwave oven (KenWood MW740) was operated at full power (900 W) in 30 s cycles (on for 10 s and off and stirring for 20 s) for a total reaction time of 2 min.<sup>18</sup> The yellow dispersion of GO gradually changed to a black color indicating the completion of the chemical reduction to RGO. Then RGO was separated with the use of a centrifuge (Centurion Scientific Ltd.) operated at 5000 rpm for 15 min, and dried at 80 °C overnight.

**2.4. In Situ Preparation of RGO-(PS-PMMA) Composites.** RGO powder 2.0 (wt/wt %) was added to the S and MMA (1:1 wt %) mixture, stirred, and sonicated for 1 h. Then the mixture was maintained at 60 °C for 20 h after the addition of 5.0% BP initiator to promote *in situ* free radical bulk polymerization. The neat PS-PMMA was prepared for comparison using the same procedure, but no RGO was added.

**2.5. Preparation of R-(GO-(PS-PMMA)) Composites via MWI.** GO powder 2.0 (wt/wt %) was added to the S and MMA (1:1 wt %) mixture, stirred, and sonicated for 1 h. The GO was then polymerized after the addition of 5.0% BP by the *in situ* bulk polymerization method as in the previous section, to produce GO-(PS-PMMA) composites. A mixture of 0.40 g of GO-(PS-PMMA) was dissolved in solvent, then reduced using MWI after the addition of 400  $\mu\text{L}$  HH, and then centrifuged and dried.

**2.6. Structural Characterization.** The FTIR (Thermo Scientific Nicolet-iS10) spectra of the composites were recorded in the range of 4000–500  $\text{cm}^{-1}$ . The  $^1\text{H}$  and  $^{13}\text{C}$  NMR of the solution was recorded on a Bruker Avance (III) at 400 MHz using  $\text{CDCl}_3$  as the solvent, and the composites were macerated in solvent for 1 day. The XPS measurements were carried out by using a SPECS GmbH X-ray photoelectron spectrometer. Prior to analysis, the samples were degassed under vacuum inside the load lock for 16 h. X-ray diffraction (Philips-Holland, PW 1729) of the composites were investigated with Cu radiation (30 kV, 40 mA,  $\text{K}\alpha$  radiation ( $\lambda = 1.54430 \text{\AA}$ )) between  $2\theta$  of 5° and 100°. A scanning electron microscope (SEM, FEI Quanta 200, FEI, Hillsboro, USA) was employed to study the morphology of the composites after they were mounted on the composite slabs and coated with gold via a sputtering system (Polaron E6100, Bio-Rad, UK). High resolution transmission electron microscopy (HRTEM) was carried out by using (JEOL JSM-2100F, Japan) and was operated at 200 kV. A drop of the composite dispersed in ethanol was placed on copper grids and dried for studies. The thermogravimetric analyses (TGA) of the composites were performed under an  $\text{N}_2$  atmosphere at a heating rate

of 10 °C per minute from 25 to 800 °C using a NETZCH 209 F1 thermogravimetric analyzer. Differential scanning calorimetry (DSC, NETZCH 204 F1) measurements were employed to estimate the glass-transition temperature ( $T_g$ ) of each composite. The composites were heated from –25 to 100 °C at a heating rate of 10 °C per min. Then, a double run was performed after cooling at a heating rate of 2 °C per min from 25 to 350 °C. The  $T_g$  was taken as the midpoint of the transition.

**2.7. Nanoindentation Tests.** Nanoindentation testing and measurements (e.g., hardness and elastic modulus) were performed using a calibrated NanoTest system (Micro Materials, UK) with a standard diamond Berkovich indenter (included angle of 142.3° with a centerline-to-face angle of 65.3°).<sup>27</sup> For each loading–unloading cycle, the loading and unloading lasted 10 s, respectively, and the dwell time at each peak load was 5 s. Five measurements were performed on each specimen (Table 1) in load-controlled mode at 100  $\mu\text{N}$ . The indentations were made in a vertical column with a spacing of 25 between the indentations. Further details of the testing instrument and measurement technique are provided elsewhere.<sup>28</sup> The  $P$ – $h$  profiles were analyzed using standard methods with the area function for the Berkovich indenter, which was determined by indentations into fused silica with an elastic modulus of 69.9 GPa. The raw data ( $P$ – $h$  profile) were used to evaluate the hardness ( $H$ ) and the reduced elastic modulus ( $E_r$ ) using the Oliver and Pharr method.<sup>29</sup> The elastic modulus ( $E_i$ ) and Poisson ratio ( $\nu_i$ ) of the diamond indenter were taken as 1140 GPa and 0.07, respectively, whereas the Poisson ratio ( $\nu_s$ ) of the specimen was taken as 0.34 (considering the  $\nu_s$  as 0.33 (PMMA) and 0.35 (PSTY), respectively<sup>30–32</sup>) for the calculations of the elastic modulus ( $E_s$ ).

In preparation for the nanoindentation test, the polymer specimens with different thicknesses (Table 1) were mounted onto the substrate base (steel disc) using cyanoacrylate adhesive (super glue). The evaluation of the hardness and elastic modulus of a copolymer requires the careful assessment of test parameters because the measured property may represent a combination of the properties of the copolymer film/substrate instead of those of the film. However, a general rule for the penetration depth is 1/10th the film thickness, as recommended by Haanappel et al.,<sup>33</sup> although a 1/20th rule has also been suggested.<sup>34</sup> Chudoba et al.<sup>35</sup> have indicated that these rules are often not practicable for films with a thickness less than 1  $\mu\text{m}$ . Because polymers have both strain-dependent and strain-rate-dependent properties and show substantially different behaviors when the indentations are produced under different contact conditions,<sup>30</sup> the viscoelastic–plastic response of these materials generally provides hardness and elastic moduli values that are a function of the contact conditions (e.g., the indenter geometry, the penetration depth, the loading rate, and the ambient temperature). Therefore, in the current investigation, a fixed nanoindentation test load of 100  $\mu\text{N}$  (0.1 mN) was used to allow relative comparisons of material performance; this test load corresponded to a low penetration depth of 1/80th the copolymer film thickness (e.g., 2% R-(GO-(PS-PMMA))). Nanoindentation tests on all specimens were conducted in air at room temperature (23 °C) in a temperature-controlled environment using a PID-controlled

chamber.<sup>30</sup> The surface roughnesses of these polymer specimens were sufficiently smooth for nanoindentation testing (e.g., for PS-PMMA, the  $R_a$  varied between 8 and 10 nm).

### 3. RESULTS

**3.1. Specimen Characterization.** FTIR spectral analysis was performed to confirm the chemical structure of all composites. Figure 1 shows the FTIR spectra of GO, RGO,

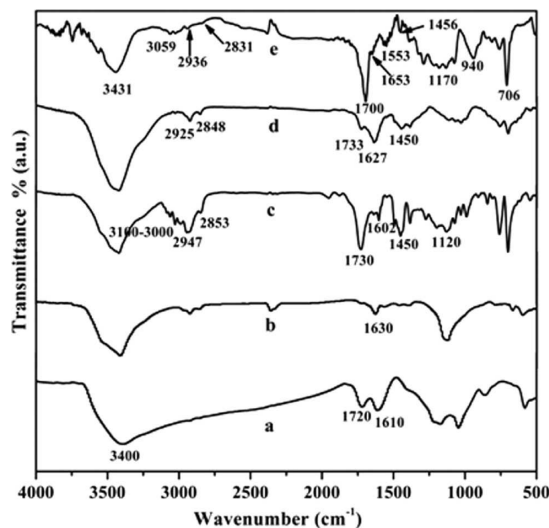


Figure 1. FTIR spectra of (a) GO, (b) RGO, (c) PS-PMMA, (d) 2% RGO-(PS-PMMA), and (e) 2% R-(GO-(PS-PMMA)) composites.

PS-PMMA, RGO-(PS-PMMA), and R-(GO-(PS-PMMA)) composites. The characteristic FTIR features of GO (Figure 1a) include the presence of different types of oxygen functionalities, which have been confirmed by the bands at 3400, 1720, 1610, and 1220  $\text{cm}^{-1}$ , which corresponds with the O—H, C=O, carbonyl/carboxyl, C=C aromatic, and C—O in the epoxide groups, respectively.<sup>36</sup> For RGO (Figure 1b), the spectrum shows the bands at 3430, 1630, and 1139  $\text{cm}^{-1}$  that correspond to O—H, C=C, and C—O groups, respectively. For the neat PS-PMMA (Figure 1c), the spectrum shows the typical characteristic bands for PS-PMMA at 2947, 2853, 1680–2000, and 1602, 1730, and 1160–1120  $\text{cm}^{-1}$  which correspond to the aliphatic C—H, —CH<sub>2</sub>, aromatic C=C stretching, C=O stretching vibrations of ester carbonyl, and C—O—C stretching vibrations, respectively. Finally, four peaks in the region 3000–3100  $\text{cm}^{-1}$  correspond to Ar—H and =C—H stretching. For RGO-(PS-PMMA) composites (Figure 1d) the spectrum shows the presence of the characteristic bands of RGO and PS-PMMA. The bands at 3412, 1733, 1627, and 1170–1114  $\text{cm}^{-1}$  that correspond with the O—H, C=O, C=C, and C—O—C groups, respectively. In the case of R-(GO-(PS-PMMA)) composites (Figure 1e), the spectrum shows bands at 3431, 3000–3100, and 1653, 1700  $\text{cm}^{-1}$  that correspond with the O—H, Ar—H, and C=C, C=O, and C—O—C groups, respectively.

Another structural-evidence can be obtained from <sup>1</sup>H NMR and <sup>13</sup>C NMR. Figure 2 display <sup>1</sup>H NMR spectra of neat PS-PMMA, RGO-(PS-PMMA), and R-(GO-(PS-PMMA)) composites. The peaks at  $\delta$  = ~0.6–1.0 ppm represented —CH<sub>3</sub> (for MMA unit) and those between  $\delta$  = ~1.3 and 2 ppm corresponded to —CH<sub>2</sub> (for both S and MMA units) and —CH (for S unit). It was reported that S shows a peak at  $\delta$  = 7.1 ppm and MMA at  $\delta$  = 2.8–3.6 ppm corresponding to the phenyl ring

(—C<sub>6</sub>H<sub>5</sub>) and the methoxy ester linkage (—COOCH<sub>3</sub>), respectively.<sup>37</sup> These peaks were identified in all copolymers composites. The relative peak areas due to phenyl and methoxy protons have been used to calculate copolymer composition.<sup>38</sup> The composition of all composites is very close to the amounts of (S-MMA) (0.96 mol %) in monomers feed. The <sup>13</sup>C NMR spectra of neat PS-PMMA, RGO-(PS-PMMA), and R-(GO-(PS-PMMA)) composites are shown in (Figure 3). The corresponding band of chemical shifts at around 128 ppm has been observed in PS-PMMA, RGO-(PS-PMMA), and R-(GO-(PS-PMMA)) composites, and it has been assigned to carbon—carbon bonds in condensed aromatic structures. The <sup>13</sup>C spectra of RGO-(PS-PMMA) and R-(GO-(PS-PMMA)) composites also show essentially complete elimination of all epoxides (60 ppm region), almost as large a decrease in the alcohol content (70 ppm region), and the apparent elimination of any esters (again, much less intensity near 167 ppm). The peak around 176 ppm is related to the carbon from aromatic carboxylic acids; (Figure 3b) also indicated C=C bonds in the 126 ppm region as well as the existence of carbonyl groups in the final product. The resonance at ~134 ppm belongs to the unoxidized sp<sup>2</sup> carbons of the graphene network.<sup>36,39</sup> This signal for graphitic sp<sup>2</sup> carbon dominates both the RGO-(PS-PMMA) and R-(GO-(PS-PMMA)) composites spectra (Figures 3b, 3c). This corresponds well with <sup>1</sup>H NMR findings.

X-ray photoelectron spectroscopy (XPS) is a useful tool used in the detection of the different oxygenated functionalities that form on the carbon surface during the chemical oxidation and reduction of graphite and GO, respectively. Figure 4 represents the XPS spectra of the graphite, GO, and RGO. The C1s XPS spectrum of GO (Figure 5) shows two typical peaks at 284.5 and 286.6 eV which are associated with C—C and C=C, and C—O (epoxy and hydroxyl groups), respectively. After HH reduction via MWI, the XPS of RGO (Figure 5) shows a C1s peak at 284.4 eV which is associated with C—C and C=C groups.

XRD analyses were used to study the structural changes of the composites after the loading of 2% RGO. Figure 6a shows the characteristic XRD peak ( $2\theta$ ) of GO at 9.34°, which corresponds to a *d*-spacing of 0.948 nm. After GO was reduced with HH (Figure 6b), the *d*-spacing decreased: the peak appeared at  $2\theta$  = 12.42° with a *d*-spacing of 0.714 nm. The characteristic diffraction peak of the PS-PMMA (Figure 6c) indicated an amorphous structure with a peak at  $2\theta$  = 27.20° and a *d*-spacing of 0.328 nm. After 2% RGO was loaded into the copolymer matrix, the XRD peak of the resulting 2% RGO-(PS-PMMA) composite (Figure 6d) appeared at  $2\theta$  = 27.85° with a *d*-spacing of 0.321 nm. Finally, the 2.0% R-(GO-(PS-PMMA)) composite (Figure 6e) shows  $2\theta$  = 28.56° with a *d*-spacing of 0.313 nm.

The morphology of composites were studied by SEM. Figure 7a shows a SEM micrograph of raw graphite. The particles have plate-like shapes with average sizes of 1–10  $\mu\text{m}$ . The platelets of GO (Figure 7b) were not fully exfoliated and consisted of close, thick multilayer stacks. The SEM image of the RGO (Figure 7c) shows randomly aggregated, thin, wrinkled reduced graphene oxide flakes closely associated with each other. The SEM micrograph of neat PS-PMMA (Figure 7d) reveals stacks of lamellae. The SEM image of the RGO-(PS-PMMA) (Figure 7e) shows very uneven surfaces as well as protrusions from the edges. The image of the R-(GO-(PS-PMMA)) composite (Figure 7f) shows a well established parallel-orientated lamellar structure.

The morphology of the copolymer and RGO-based copolymer composites was further studied using HR-TEM. The HR-TEM image of RGO (Figure 8a) shows the typical image of the

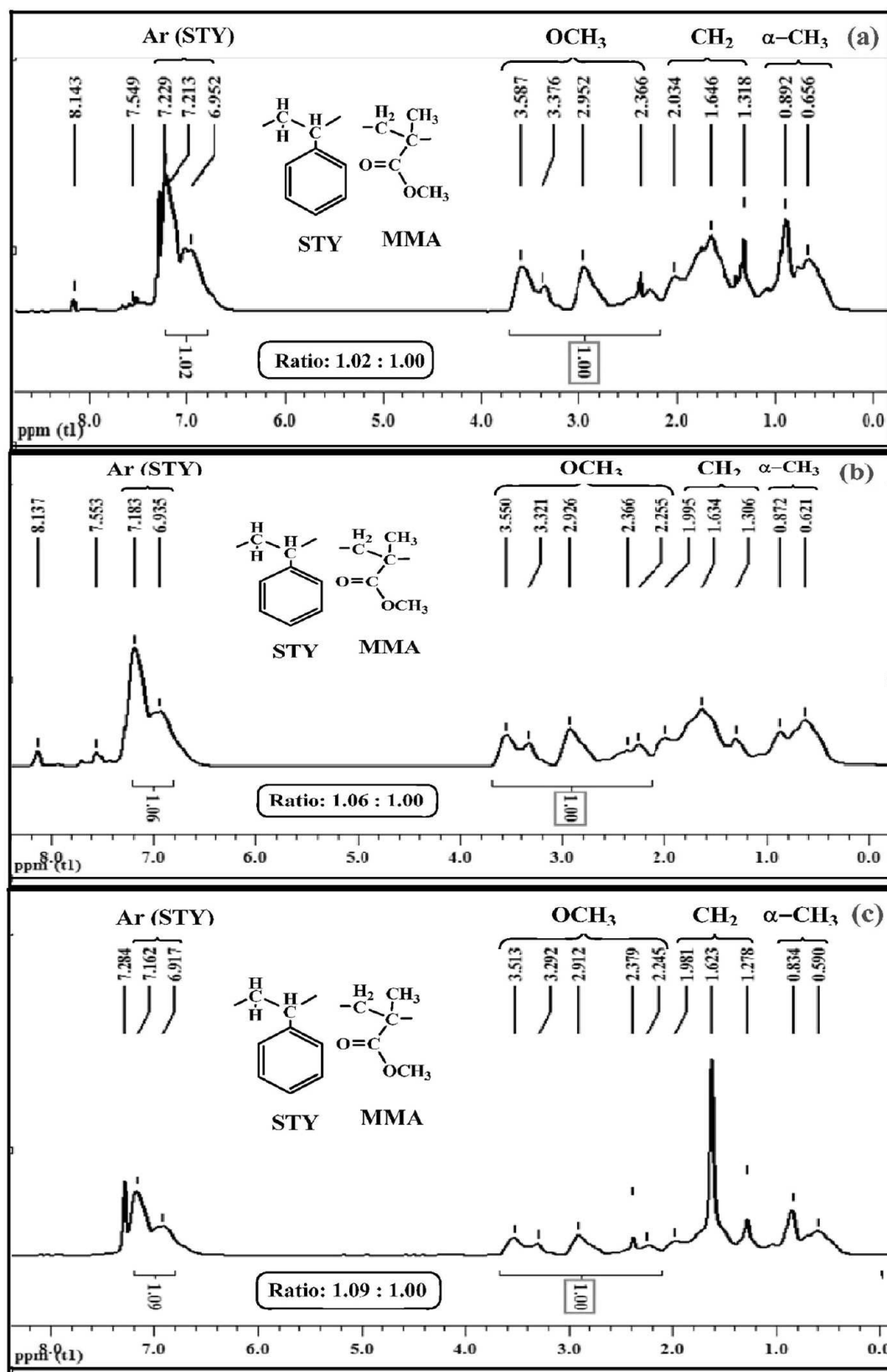


Figure 2. <sup>1</sup>H NMR spectra of (a) PS-PMMA, (b) 2% RGO-(PS-PMMA), and (c) 2% R-(GO-(PS-PMMA)) composites/using CDCl<sub>3</sub> solvent.

exfoliated RGO sheets. For neat PS-PMMA (Figure 8b), the image shows a uniform gray level with different stack lamellae, which indicates a miscible PS-PMMA copolymer matrix. The HR-TEM image of the RGO-(PS-PMMA) composite (Figure 8c)

shows dark regions of RGO platelets dispersed within the copolymer matrix. However, the R-(GO-(PS-PMMA)) HR-TEM image (Figure 8d) shows dark regions and visible boundaries between the RGO platelets and the PS-MMA

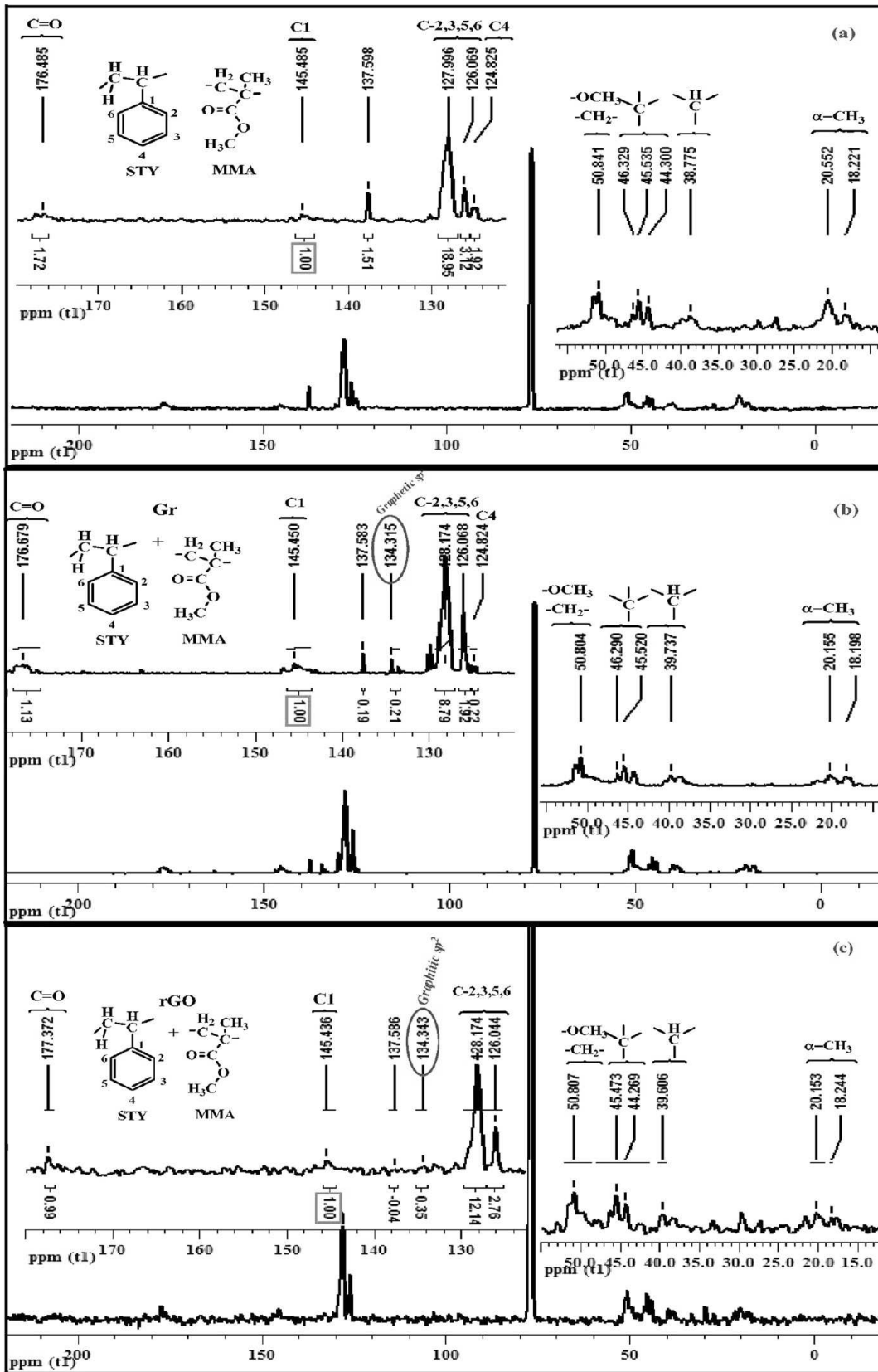


Figure 3.  $^{13}\text{C}$  NMR spectra of (a) PS-PMMA, (b) 2% RGO-(PS-PMMA), and (c) 2% R-(GO-(PS-PMMA)) composites/using  $\text{CDCl}_3$  solvent.

copolymer matrix; the layers clearly maintained their common orientation.

The TGA results of the composites are displayed in Figure 9 and summarized in Table 2. GO and RGO show that the thermal

degradation temperatures ( $T_d$ ) were 160 and 210 °C, respectively. The  $T_d$  of neat PS-PMMA was 405 °C. After 2.0% RGO was loaded via the *in situ* method, the  $T_d$  of the 2% RGO-(PS-PMMA) composite was 407 °C. In the case of 2% R-(GO-(PS-PMMA))

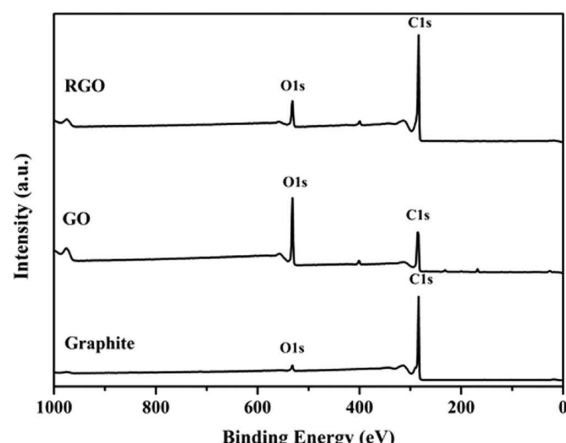


Figure 4. XPS spectra of graphite, GO, and RGO.

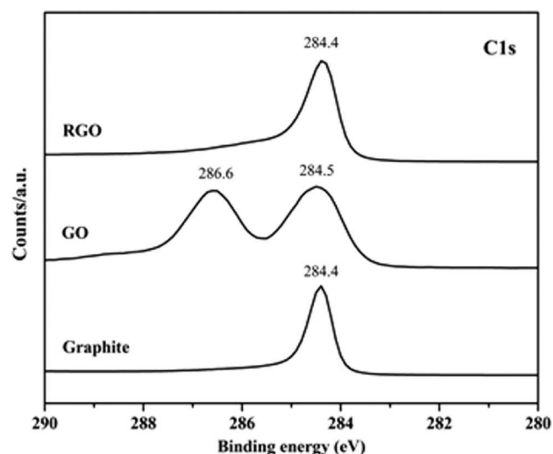


Figure 5. C1s spectra of graphite, GO, and RGO.

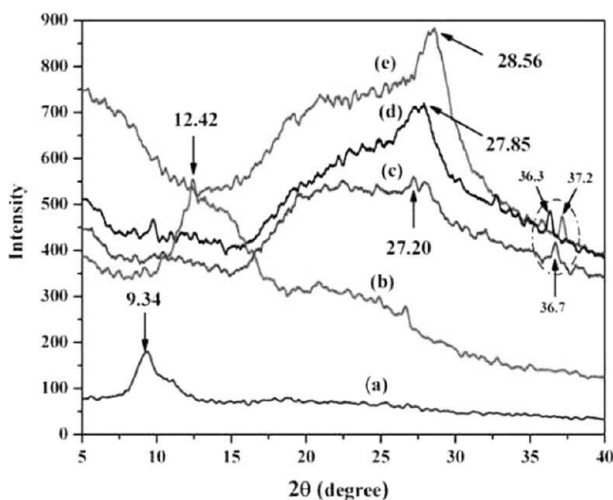


Figure 6. X-ray diffraction patterns of (a) GO, (b) RGO, (c) PS-PMMA, (d) 2% RGO-(PS-PMMA), and (e) 2% R-(GO-(PS-PMMA)) composites.

prepared via MWI showed a degradation temperature ( $T_d$ ) of 393 °C. The glass-transition temperature ( $T_g$ ) of the neat copolymers and RGO-copolymer composites are also displayed in Figure 10 and summarized in Table 2. The  $T_g$  values of neat PS-PMMA was 93 °C. The composite loaded with 2.0% RGO (i.e., the 2% RGO-(PS-PMMA) composite) showed a  $T_g$  of

89.5 °C, whereas when the MWI was used, the  $T_g$  of the 2% R-(GO-(PS-PMMA)) composite was 119 °C.

**3.2. Nanoindentation Results.** The measured values of hardness ( $H$ ) and elastic modulus ( $E_s$ ) determined from the  $P-h$  profiles are shown in Figure 11. An average of five values was determined for each set of measurements. With the addition of 2.0 wt % RGO to PS-PMMA, the average hardness values (34%) as well as the average elastic modulus values (22%) decreased. However, an overall increase of 136% in the average hardness and an overall increase of 76% in the average elastic modulus was achieved through the addition of 2.0 wt % of the RGO composites obtained using the MWI method.

#### 4. DISCUSSION

**4.1. Microstructure.** The FTIR,  $^1\text{H}$  NMR, and  $^{13}\text{C}$  NMR microstructural characterization results show the presence of the characteristic peaks of RGO within the neat PS-PMMA copolymer matrix. These results confirm the chemical reduction of GO via MWI and the successful preparation of R-(GO-(PS-PMMA)) and R-(GO-(PS-PMMA)) composites. This is in agreement with the C1s XPS spectra where the disappearing of the peak at 286.6 eV (Figure 5) which is assigned to the epoxy functional groups confirmed a successful reduction of GO into RGO.

The XRD patterns displayed in Figures 6a and 6b confirm the chemical reduction of the GO and the formation of reduced graphene oxide sheets when HH was used as a reducing agent.<sup>40,41</sup> In addition, a broad peak formed at  $2\theta = 12.42^\circ$  after the GO was reduced with HH. This result indicates the removal of a large number of oxygen-functionalities and the formation of much more disordered reduced graphene oxide sheets as well as a change in the hybridization of the reduced carbon atoms from tetrahedral  $\text{sp}^3$  to planar  $\text{sp}^2$ .<sup>42,43</sup> Only one broad diffraction peak related to the PS-PMMA in the composites (Figures 6c, 6d, and 6e) was observed, which indicates an amorphous structure. When the MWI method was used, the XRD pattern of the R-(GO-(PS-PMMA)) composites indicated  $d$ -spacing smaller than that of the composites; this result suggests more extensive stacking in the layers of the R-(GO-(PS-PMMA)) composites and reduced attractive interactions within the reduced graphene oxide-(PS-PMMA) copolymer matrix. These combined effects enable their exfoliation into individual sheets. A similar trend related to the changes in  $d$ -spacing can be observed for peaks at  $2\theta = 36.7^\circ$ , where the  $2\theta$  value decreased for the RGO-(PS-PMMA) composite and increased for the R-(GO-(PS-PMMA)) composite. Moreover, the absence of the characteristic peaks of GO and RGO in the composites indicate that the RGO platelets in composites were exfoliated.<sup>44,45</sup> The relative level of crystallinity was greater for the R-(GO-(PS-PMMA)) composite because the peak width (e.g., at  $2\theta = 28.56^\circ$ ) decreased in comparison to the width of the same peak in the pattern of RGO-(PS-PMMA) at  $2\theta = 27.85^\circ$ . Similarly, the XRD patterns of both composite polymers showed sharper peak in comparison to that of the (PS-PMMA), e.g., at  $2\theta = 27.20^\circ$ .

Direct evidence of exfoliation of the reduced graphene oxide in the final polymer composites can be obtained from SEM and HR-TEM; also it provides images of dispersion of RGO layers into neat PS-PMMA copolymer matrix. Figure 7a shows an SEM image of the natural graphite sheet flakes in which the sizes of the graphite particles are shown to be in the micrometer range. The particle size of the graphite sheets was reduced considerably due to the effect of the oxidation process (Figure 7b). Figure 7c reveals that the RGO consists of randomly aggregated, thin,

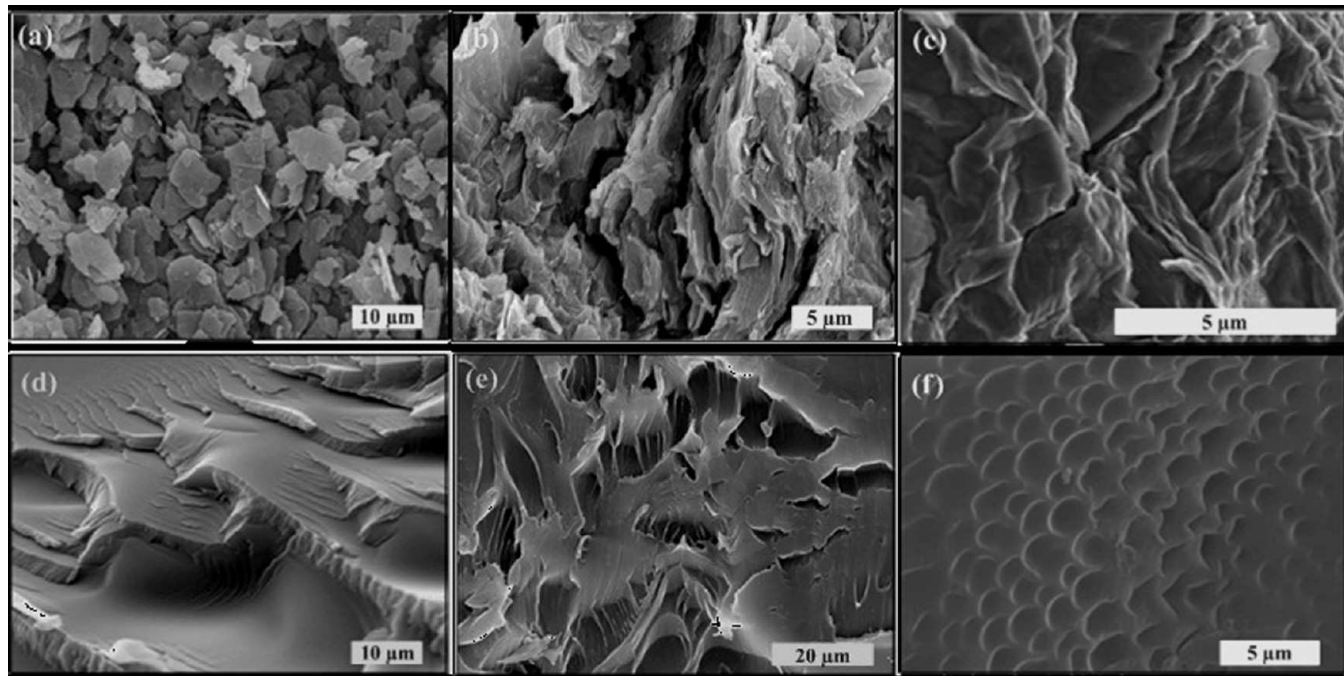


**Figure 7.** SEM micrographs of (a) graphite, (b) GO, (c) RGO, (d) PS-PMMA, (e) 2% RGO-(PS-PMMA), and (f) 2% R-(GO-(PS-PMMA)) composites.

crumpled sheets that are closely associated with each other. A comparison of the micrographs in Figure 7e and Figure 8c,e with Figure 7f and Figure 8d,f clearly indicates an improvement in the morphology of composite polymer, referred here as “better morphology” to aid the discussion. This improvement in the morphology of 2% R-(GO-(PS-PMMA)) in comparison to 2% RGO-(PS-PMMA) originates from two sources, that is, better uniformity of the microstructure both (i) in terms of distribution of RGO within the composite microstructure and (ii) in terms of the atomic level interactions of RGO sheets (bonding quality) with the neighboring polymer matrix in the composite microstructure. The former can be appreciated from the SEM and HRTEM observations (Figures 7 and 8), whereas the latter is best represented by nanoindentation elastic modulus measurements as discussed in the next section. A comparison of Figure 7e and Figure 8c,e with Figure 7f and Figure 8d,f indicates that for the 2% R-(GO-(PS-PMMA)) the microstructure represents a uniform distribution of graphene sheets within the polymer matrix and a needle-like structure (Figure 8d,f) can be observed in the HRTEM observation, which manifests itself as a uniformly distributed morphology in Figure 7f. Contrary to this, the HRTEM observation in Figure 8c,e for 2% RGO-(PS-PMMA) indicates islands of RGO which do not represent a uniform distribution of RGO in the polymer matrix. This is akin to a bimodal microstructure where the islands of RGO interconnect with a polymer matrix in the composite microstructural instead of a truly needle-like composite microstructure observed in the case of 2% R-(GO-(PS-PMMA)).

High resolution transmission electron microscopy (HR-TEM) was employed to determine if the RGO-based sheets were indeed present in the composites as single exfoliated sheets or as multilayered sheets. Figure 8 displays HR-TEM images of the RGO, neat PS-PMMA, 2.0% RGO-(PS-PMMA), and 2% R-(GO-(PS-PMMA)) composites. The HR-TEM image of *in situ* composites (Figure 8c) shows that RGO is not randomly dispersed. In contrast, the HR-TEM image of the R-(GO-(PS-PMMA))

composite (Figure 8d) shows that the RGO platelets, whose electron-beam transparency is better compared to those prepared via the *in situ* mixing method (Figure 8c), are finely dispersed in the matrix of the PS-PMMA copolymer and are oriented to a specific direction; in addition, the channels in this sample are more diffused. Interestingly the HRTEM images of RGO-(PS-PMMA) show dark regions in comparison with R-(GO-(PS-PMMA)). To investigate this, a high magnification HR-TEM were carried out for both composites and displayed in Figure 8 panels e and f, respectively. Figure 8e shows black heterogeneous regions that are visible; these regions may indicate the presence of thick layers composed of several RGO platelets or it may be attributed to polymer brushes as has been reported by other groups with different polymers.<sup>46–48</sup> These results indicate that delamination of the RGO platelets were effectively induced by the copolymerization and were effectively reduced by MWI to yield exfoliated RGO-(PS-PMMA) composites. These results also indicate that MWI can improve the dispersion of RGO in the matrix.

In the current work, the TGA and DSC measurements were performed on all three copolymer composites to examine the effect of the RGO content on the thermal stability. The TGA and DSC results are displayed in Figures 9 and 10, and summarized in Table 2. These results indicate that the approach of intercalating the RGO into PS-PMMA copolymer matrix using the MWI method clearly enhances the thermal properties of these copolymers. The shift in the  $T_g$  values has previously been attributed to the presence of so-called “interphase” copolymer networking, which arises due to the interaction of the chains with the reduced graphene oxide platelet surface; these interactions can restrict the mobility of the chains and create an enormous volume of matrix copolymer with increased  $T_g$ . Percolation of this network of interphase copolymer could then manifest as a large shift in the  $T_g$  of the copolymer composites,<sup>49–51</sup> as observed in the current investigation.

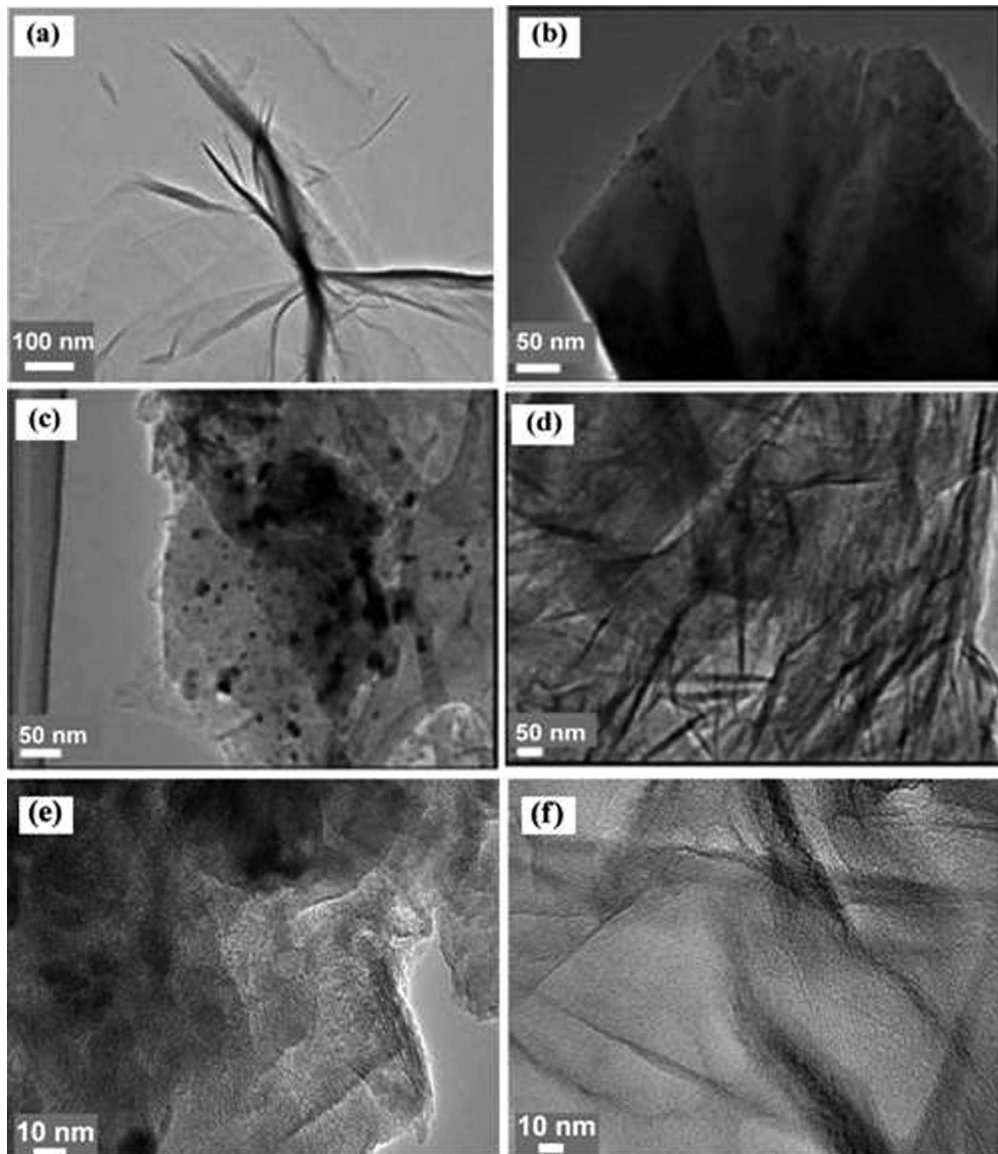


**Figure 8.** HR-TEM images of (a) RGO, (b) PS-PMMA, (c, e) 2% RGO-(PS-PMMA), and (d, f) 2% R-(GO-(PS-PMMA)) composites.

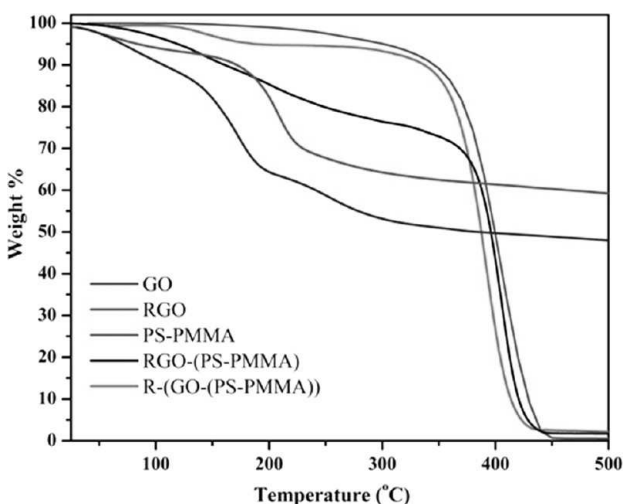


**Figure 9.** TGA thermograms of neat copolymer and RGO-copolymer composites prepared by *in situ* and via MWI.

**Table 2. Summary of Thermal Behavior Data Obtained from TGA and DSC Measurements**

Sl. no.	specimen type	$T_{\text{degradation}}^a$ (°C)	$T_g$ (°C)
1	GO	160	
2	RGO	210	
3	PS-PMMA	405	93.0
4	2% RGO-(PS-PMMA)	407	89.5
5	2% R-(GO-(PS-PMMA))	393	119.0

<sup>a</sup>The maximum degradation temperature in the decomposition stage obtained from the DrTG (derivative thermogram).

In the case of composites that show a decrease in  $T_g$  (Figure 10 and Table 2), the reduced  $T_g$  indicates that RGO did not disperse well into the copolymer matrix, which resulted in a weak interaction between the reduced graphene oxide and the copolymer interphase region. The decrease in  $T_g$  has been associated with an increase in mobility of the copolymer chains that results from an increase in free surfaces and repulsive interfaces.<sup>49,51,52</sup> The observed increase in  $T_g$  in the current

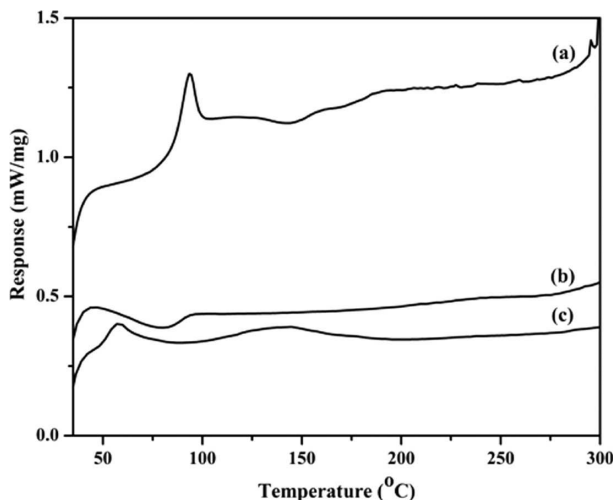


**Figure 10.** DSC curves of (a) PS-PMMA, (b) 2% RGO-(PS-PMMA), and (c) 2% R-(GO-(PS-PMMA)) composites.

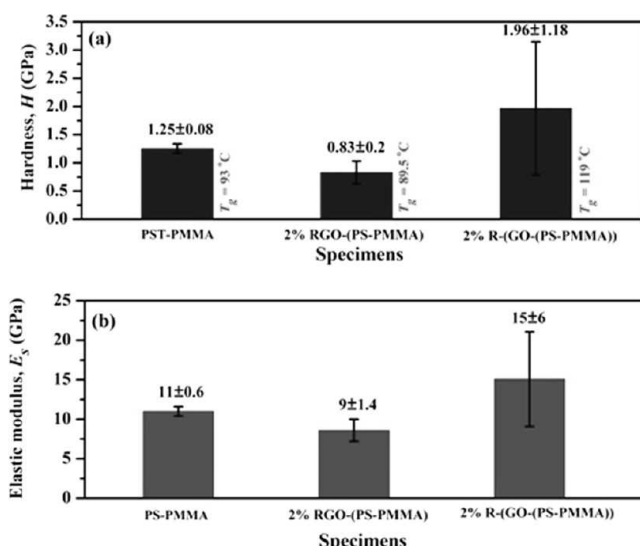


**Figure 11.** Nanoindentation (Berkovich) results under a  $100 \mu\text{N}$  load for the copolymer and RGO-copolymer composite specimens: (a) hardness,  $H$  and (b) elastic modulus,  $E_s$  ( $T_g$  is the glass-transition temperature).

investigation suggests that good compatibility and better dispersion were achieved between reduced graphene oxide and PS-PMMA copolymer when the MWI method was used.

**4.2. Nanoindentation Properties.** The volume of published literature in the area of copolymers that contain graphene sheets, and particularly in the area related to improvements in their mechanical properties using nano-indentation, is limited. Briscoe et al.<sup>30</sup> investigated the influence of penetration depth and loading rate on the hardness and elastic modulus of a range of commercially available polymeric materials using micrometer and submicrometer indentations. In the current investigation, the addition of 2.0 wt % RGO to PS-PMMA resulted in a reduction in hardness as well as a reduction in the elastic modulus values (Figure 11). In cases where composites showed both a decrease in  $T_g$  (e.g., 2.0% RGO-(PS-PMMA), Table 2) and decreases in hardness and elastic modulus (Figure 11), the RGO did not disperse well in the copolymer matrix and resulted in weak interactions between the reduced graphene oxide and the copolymer interphase region. These properties can also be due

to microstructural features (Figure 7e) that resulted in a disordered material that could accommodate strain under the indenter.

An average increase in hardness and elastic modulus (Figure 11) was achieved through the addition of 2.0 wt % of RGO to composites that were obtained using the MWI method. The high dispersibility and interfacial interactions between the GO nanofiller and the PS-PMMA matrix were responsible for the mechanical improvements,<sup>53</sup> as indicated by the presence of well established lamellae structures with a parallel orientation (Figure 7f). These improvements in the mechanical properties could be attributed to the stiffness of copolymers that arises from the amount of entanglements and covalent bonds within the network. Extra physical entanglements, introduced through cross-linking, result in an increase in the overall stiffness. Thus, the MWI method facilitated efficient load transfer between the GO and the PS-PMMA matrix, and it was used as a compatibilizer to reduce the difference in interfacial energy between the nanofiller and the matrix to increase chemical adhesion and mechanical interlocking. These results indicate that a quantitative measure of a copolymer's quality can also be benchmarked, for example, to investigate the influence of the weight percent of reduced graphene oxide through analysis of nanoindentation measurements.

The standard deviation of 2% R-(GO-(PS-PMMA)) in comparison to 2% RGO-(PS-PMMA) is higher albeit the similar chemical composition. To understand this difference we need to look at the "measured property" itself which is the elastic modulus. It represents the bonding mechanism between the elemental species within the composite structure. Having similar chemical composition of 2% R-(GO-(PS-PMMA)) in comparison to 2% RGO-(PS-PMMA) therefore does not mean that the quality and quantity of primary and secondary bonds will be similar just because they have similar chemical composition, as both materials are prepared by completely different manufacturing methods. Hence the higher standard deviation of R-(GO-(PS-PMMA)) here represents the fact that there are certain elastic bonds in the material structure which are much stronger, whereas other areas of the material represent bonding which is similar to the level observed in 2% RGO-(PS-PMMA). However, the quantity of these stronger bonds in a given volume fraction of material is still lower in comparison to the bonds in the rest of the material, and hence the standard deviation is higher, with a higher average value. Hence the higher standard deviation and average value observed here for 2% R-(GO-(PS-PMMA)) is a clear reflection of the microstructure produced by the microwave method and indicates an improvement in quality. The same argument can be extended to the hardness values represented in Figure 11.

**4.3. The Role of Structure and the Influence on the Materials Failure.** There is no simple relationship between the structure of a copolymer and its influence on degradation and failure during its potential applications. However, the work presented here provides an ability to relate the role of structure–property relationships to degradation and failure at the nanoscale, which otherwise would be difficult to ascertain using conventional techniques. Given the different types of failure (plastic deformation, sudden fracture) during nanomechanical testing, a copolymer with greater chemical adhesion, greater mechanical interlocking strength and a controlled composition is required for durability. Nanoindentation tests in association with other characterization techniques can potentially be used to obtain a better understanding of the mechanical properties of such copolymers.

## 5. CONCLUSIONS

This investigation considered the relative changes in mechanical properties of composites in which RGO was used as a nanofiller.

The findings of this research can be summarized as follows: (1) The composite obtained using MWI exhibited a better morphology and increased dispersion with enhanced thermal stability. As a result, the mechanical properties also improved due to increased mechanical interlocking between the GO nanofiller and the PS-PMMA matrix. (2) An overall increase of 136% in hardness and an overall increase of 76% in elastic modulus were achieved through the addition of only 2.0 wt % of RGO to composites that were obtained using the microwave irradiation (MWI) method.

## AUTHOR INFORMATION

### Corresponding Author

\*E-mail: ealsharaeh@alfaisal.edu. Tel: +966-1-215 7739.

### Notes

The authors declare no competing financial interest.

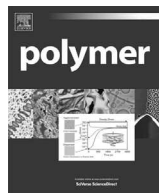
## ACKNOWLEDGMENTS

This study is part of research Project No. 405010901101 and the authors gratefully acknowledge the continued support from Alfaisal University and its Office of Research and Graduate Studies (ORGS).

## REFERENCES

- (1) Geim, A. K.; Novoselov, K. S. The rise of graphene. *Nat. Mater.* **2007**, *6*, 183–191.
- (2) Liu, Z.; Robinson, J. T.; Sun, X.; Dai, H. PEGylated nanographene oxide for delivery of water-insoluble cancer drugs. *J. Am. Chem. Soc.* **2008**, *130*, 10876–10877.
- (3) Sun, X.; Liu, Z.; Welsher, K.; Robinson, J.; Goodwin, A.; Zaric, S.; Dai, H. Nano-graphene oxide for cellular imaging and drug delivery. *Nano Res.* **2008**, *1*, 203–212.
- (4) Zhang, Y.; Tan, Y.-W.; Stormer, H. L.; Kim, P. Experimental observation of the quantum Hall effect and Berry's phase in graphene. *Nature* **2005**, *438*, 201–204.
- (5) Lee, C.; Wei, X. D.; Kysar, J. W.; Hone, J. Measurement of the elastic properties and intrinsic strength of monolayer graphene. *Science* **2008**, *321*, 385–388.
- (6) Balandin, A. A. Thermal properties of graphene and nanostructured carbon materials. *Nat. Mater.* **2011**, *10*, 569–581.
- (7) Balandin, A. A.; Ghosh, S.; Bao, W. Z.; Calizo, I.; Teweldebrhan, D.; Miao, F.; Lau, C. N. Superior thermal conductivity of single-layer graphene. *Nano Lett.* **2008**, *8*, 902–907.
- (8) Park, S.; Ruoff, R. S. Chemical methods for the production of graphenes. *Nat. Nanotechol.* **2009**, *4*, 217–224.
- (9) Stankovich, S.; Dikin, D. A.; Domke, G. H. B.; Kohlhaas, K. M.; Zimney, E. J.; Stach, E. A.; Piner, R. D.; Nguyen, S. T.; Ruoff, R. S. Graphene-based composite materials. *Nature* **2006**, *442*, 282–286.
- (10) Ramanathan, T.; Abdala, A. A.; Stankovich, S.; Dikin, D. A.; Herrera-Alonso, M.; Piner, R. D.; Adamson, D. H.; Schniepp, H. C.; Chen, X.; Ruoff, R. S.; Nguyen, S. T.; Aksay, I. A.; Prud'homme, R. K.; Brinson, L. C. Functionalized graphene sheets for polymer nanocomposites. *Nat. Nanotechol.* **2008**, *3*, 327–331.
- (11) Dikin, D. A.; Stankovich, S.; Zimney, E. J.; Piner, R. D.; Domke, G. H. B.; Evmenenko, G.; Nguyen, S. T.; Ruoff, R. S. Preparation and characterization of graphene oxide paper. *Nature* **2007**, *448*, 457–460.
- (12) Park, S.; Lee, K.-S.; Bozoklu, G.; Cai, W.; Nguyen, S. T.; Ruoff, R. S. Graphene oxide papers modified by divalent ions—Enhancing mechanical properties via chemical cross-linking. *ACS Nano* **2008**, *2*, 572–578.
- (13) Chen, H.; Müller, M. B.; Gilmore, K. J.; Wallace, G. G.; Li, D. Mechanically strong, electrically conductive, and biocompatible graphene paper. *Adv. Mater.* **2008**, *20*, 3557–3561.
- (14) Singh, V.; Joung, D.; Zhai, L.; Das, S.; Khondaker, S. I.; Seal, S. Graphene based materials: Past, present and future. *Prog. Mater. Sci.* **2011**, *56*, 1178–1271.
- (15) Huang, X.; Yin, Z. Y.; Wu, S. X.; Qi, X. Y.; He, Q. Y.; Zhang, Q. C.; Yan, Q. Y.; Boey, F.; Zhang, H. Graphene-based materials: synthesis, characterization, properties, and applications. *Small* **2011**, *7*, 1876–1902.
- (16) El-Shall, M. S.; Abdelsayed, V.; Khder, A. E. R. S.; Hassan, H. M. A.; El-Kaderi, H. M.; Reich, T. E. Metallic and bimetallic nanocatalysts incorporated into highly porous coordination polymer MIL-101. *J. Mater. Chem.* **2009**, *19*, 7625–7631.
- (17) Aldosari, M.; Othman, A.; Alsharaeh, E. Synthesis and characterization of the in situ bulk polymerization of PMMA containing graphene sheets using microwave irradiation. *Molecules* **2013**, *18*, 3152–3167.
- (18) Hassan, H. M. A.; Abdelsayed, V.; Khder, A.; AbouZeid, K. M.; Terner, J.; El-Shall, M. S.; Al-Resayes, S. I.; El-Azhary, A. A. Microwave synthesis of graphene sheets supporting metal nanocrystals in aqueous and organic media. *J. Mater. Chem.* **2009**, *19*, 3832–3837.
- (19) Zedan, A. F.; Sappal, S.; Moussa, S.; El-Shall, M. S. Ligand-controlled microwave synthesis of cubic and hexagonal CdSe nanocrystals supported on graphene. Photoluminescence quenching by graphene. *J. Phys. Chem. C* **2010**, *114*, 19920–19927.
- (20) Siamaki, A. R.; Khder, A. E. R. S.; Abdelsayed, V.; El-Shall, M. S.; Gupton, B. F. Microwave-assisted synthesis of palladium nanoparticles supported on graphene: A highly active and recyclable catalyst for carbon–carbon cross-coupling reactions. *J. Catal.* **2011**, *279*, 1–11.
- (21) Herring, N.; Almahoudi, S.; Olson, C.; El-Shall, M. S. Enhanced photocatalytic activity of ZnO–graphene nanocomposites prepared by microwave synthesis. *J. Nano. Res.* **2012**, *14*, 1–13.
- (22) Matusinovic, Z.; Rogosic, M.; Sipusic, J. Synthesis and characterization of poly(styrene-co-methyl methacrylate)/layered double hydroxide nanocomposites via in situ polymerization. *Polym. Deg. Stab.* **2009**, *94*, 95–101.
- (23) Pasupuleti, S.; Madras, G. Ultrasonic degradation of poly(styrene-co-alkyl methacrylate) copolymers. *Ultra. Sonochem.* **2010**, *17*, 819–826.
- (24) Sikka, M.; Pellegrini, N. N.; Schmitt, E. A.; Winey, K. I. Modifying a polystyrene/poly(methyl methacrylate) interface with poly(styrene-co-methyl methacrylate) random copolymers. *Macromolecules* **1997**, *30*, 445–455.
- (25) Coskun, M.; Seven, P. Synthesis, characterization and investigation of dielectric properties of two-armed graft copolymers prepared with methyl methacrylate and styrene onto PVC using atom transfer radical polymerization. *Reac. Funct. Polym.* **2011**, *71*, 395–401.
- (26) Hummers, W. S.; Offeman, R. E. Preparation of graphitic oxide. *J. Am. Chem. Soc.* **1958**, *80*, 1339–1339.
- (27) Faisal, N. H.; Ahmed, R.; Fu, Y. Q.; Elakwah, Y. O.; Alhosha, M. Influence of indenter shape on DLC film failure during multiple load cycle nanoindentation. *Mater. Sci. Technol.* **2012**, *28*, 1186–1197.
- (28) Beake, B. D.; Vishnyakov, V. M.; Valizadeh, R.; Colligon, J. S. Influence of mechanical properties on the nanoscratch behaviour of hard nanocomposite TiN/Si<sub>3</sub>N<sub>4</sub> coatings on Si. *J. Phys. D: Appl. Phys.* **2006**, *39*, 1392.
- (29) Oliver, W. C.; Pharr, G. M. An improved technique for determining hardness and elastic modulus using load and displacement sensing indentation experiments. *J. Mater. Res.* **1992**, *7*, 1564–1583.
- (30) Briscoe, B. J.; Fiori, L.; Pelillo, E. Nano-indentation of polymeric surfaces. *J. Phys. D: Appl. Phys.* **1998**, *31*, 2395.
- (31) Mott, P. H.; Dorgan, J. R.; Roland, C. M. The bulk modulus and Poisson's ratio of "incompressible" materials. *J. Sound Vib.* **2008**, *312*, 572–575.
- (32) Tjong, S. C. Structural and mechanical properties of polymer nanocomposites. *Mater. Sci. Eng., R* **2006**, *53*, 73–197.
- (33) Haanappel, V. A. C.; Vendel, D. v. d.; Metselaar, H. S. C.; van Corbach, H. D.; Fransen, T.; Gellings, P. J. The mechanical properties of thin alumina films deposited by metal–organic chemical vapour deposition. *Thin Solid Films* **1995**, *254*, 153–163.
- (34) Lao, J.; Han, Z.; Tian, J.; Li, G. Mechanical property investigation of AlN/VN nanomultilayers with microindentation technique. *Mater. Lett.* **2004**, *58*, 859–862.

- (35) Chudoba, T.; Schwarzer, N.; Richter, F. Determination of elastic properties of thin films by indentation measurements with a spherical indenter. *Surface Coat. Technol.* **2000**, *127*, 9–17.
- (36) Li, D.; Mueller, M. B.; Gilje, S.; Kaner, R. B.; Wallace, G. G. Processable aqueous dispersions of graphene nanosheets. *Nat. Nanotechnol.* **2008**, *3*, 101–105.
- (37) Morejon, L.; Mendizabal, E.; Delgado, J. A.; Davidenko, N.; Lopez-Dellamary, F.; Manriquez, R.; Ginebra, M. P.; Gil, F. J.; Planell, J. A. Synthesis and characterization of poly(methyl methacrylate-styrene) copolymeric beads for bone cements. *Lat. Am. Appl. Res.* **2005**, *35*, 175–182.
- (38) Titelman, G. I.; Gelman, V.; Bron, S.; Khalfin, R. L.; Cohen, Y.; Bianco-Peled, H. Characteristics and microstructure of aqueous colloidal dispersions of graphite oxide. *Carbon* **2005**, *43*, 641–649.
- (39) Gao, W.; Alemany, L. B.; Ci, L. J.; Ajayan, P. M. New insights into the structure and reduction of graphite oxide. *Nat. Chem.* **2009**, *1*, 403–408.
- (40) Gilje, S.; Han, S.; Wang, M.; Wang, K. L.; Kaner, R. B. A chemical route to graphene for device applications. *Nano Lett.* **2007**, *7*, 3394–3398.
- (41) Fan, X.; Peng, W.; Li, Y.; Li, X.; Wang, S.; Zhang, G.; Zhang, F. *Adv. Mater.* **2008**, *20*, 4490.
- (42) McAllister, M. J.; Li, J.-L.; Adamson, D. H.; Schniepp, H. C.; Abdala, A. A.; Liu, J.; Herrera-Alonso, M.; Milius, D. L.; Car, R.; Prud'homme, R. K.; Aksay, I. A. Single Sheet Functionalized Graphene by Oxidation and Thermal Expansion of Graphite. *Chem. Mater.* **2007**, *19*, 4396–4404.
- (43) Subrahmanyam, K. S.; Vivekchand, S. R. C.; Govindaraj, A.; Rao, C. N. R. A study of graphenes prepared by different methods: Characterization, properties and solubilization. *J. Mater. Chem.* **2008**, *18*, 1517–1523.
- (44) Zhang, R.; Hu, Y.; Xu, J. Y.; Fan, W. C.; Chen, Z. Y. Flammability and thermal stability studies of styrene-butyl acrylate copolymer/graphite oxide nanocomposite. *Polym. Degrad. Stab.* **2004**, *85*, 583–588.
- (45) Cao, Y.; Feng, J.; Wu, P. Preparation of organically dispersible graphene nanosheet powders through a lyophilization method and their poly(lactic acid) composites. *Carbon* **2010**, *48*, 3834–3839.
- (46) Fang, M.; Wang, K.; Lu, H.; Yang, Y.; Nutt, S. Single-layer graphene nanosheets with controlled grafting of polymer chains. *J. Mater. Chem.* **2010**, *20*, 1982–1992.
- (47) Yang, Y.; Wang, J.; Zhang, J.; Liu, J.; Yang, X.; Zhao, H. Exfoliated graphite oxide decorated by PDMAEMA chains and polymer particles. *Langmuir* **2009**, *25*, 11808–11814.
- (48) Paula, A. P.; Marques, G. G.; Cruz, S.; Almeida, N.; Singh, M. K.; Grácio, J.; Sousa, A. C. M. Functionalized graphene nanocomposites. In *Advances in Nanocomposite Technology*; InTech Janeza Trdine 9: Rijeka, Croatia, 2011; pp 256–257.
- (49) Priestley, R. D.; Ellison, C. J.; Broadbelt, L. J.; Torkelson, J. M. Structural relaxation of polymer glasses at surfaces, interfaces and in between. *Science* **2005**, *309*, 456–459.
- (50) Potts, J. R.; Dreyer, D. R.; Bielawski, C. W.; Ruoff, R. S. Graphene-based polymer nanocomposites. *Polymer* **2011**, *52*, 5–25.
- (51) Qiao, R.; Deng, H.; Putz, K. W.; Brinson, L. C. Effect of particle agglomeration and interphase on the glass transition temperature of polymer nanocomposites. *J. Polym. Sci. B, Polym. Phys.* **2011**, *49*, 740–748.
- (52) Ellison, C. J.; Torkelson, J. M. The distribution of glass-transition temperatures in nanoscopically confined glass formers. *Nat. Mater.* **2003**, *2*, 695–700.
- (53) Shin, K.-Y.; Hong, J.-Y.; Lee, S.; Jang, J. Evaluation of anti-scratch properties of graphene oxide/polypropylene nanocomposites. *J. Mater. Chem.* **2012**, *22*, 7871–7879.



# Microwave exfoliated reduced graphene oxide epoxy nanocomposites for high performance applications



Bindu Sharmila T.K.<sup>a, b, c</sup>, Ajalesh B. Nair<sup>b, d</sup>, Beena T. Abraham<sup>e</sup>, P.M. Sabura Beegum<sup>a</sup>, Eby Thomas Thachil<sup>b,\*</sup>

<sup>a</sup> Department of Applied Chemistry, Cochin University of Science and Technology, Kochi, 682022 Kerala, India

<sup>b</sup> Department of Polymer Science and Rubber Technology, Cochin University of Science and Technology, Kochi, 682022 Kerala, India

<sup>c</sup> Department of Chemistry, T.M. Jacob Memorial Govt. College Manimalakunnu, Olyapuram, 686679 Kerala, India

<sup>d</sup> BK21 Plus Haptic Polymer Composite Research Team, Department of Polymer-Nano Science and Technology, Jeonju 561-756, Republic of Korea

<sup>e</sup> Department of Chemistry, S.N.M. College Maliankara, Maliankara, 683516 Kerala, India

## ARTICLE INFO

### Article history:

Received 11 February 2014

Received in revised form

29 April 2014

Accepted 13 May 2014

Available online 22 May 2014

### Keywords:

Graphene

Epoxy resin

Nanocomposites

## ABSTRACT

Graphene has captured the attention of scientific community due to recently emerging high performance applications. Hence, studying its reinforcing effects on epoxy resin is a significant step. In this study, microwave exfoliated reduced graphene oxide (MERO) was prepared from natural graphite for subsequent fabrication of epoxy nanocomposites using triethylenetetramine (TETA) as a curing agent via *in-situ* polymerization. Thermogravimetric analysis (TGA), X-ray diffraction (XRD), Raman spectroscopy, Fourier transform infrared spectroscopy (FTIR), C<sup>13</sup> NMR spectroscopy, X-ray photoelectron spectroscopy (XPS) and ultraviolet-visible (UV-vis) spectroscopy were employed to confirm the simultaneous reduction and exfoliation of graphene oxide. The reinforcing effect of MERO on epoxy resin was explored by investigating its static mechanical properties and dynamic mechanical analysis (DMA) at MERO loadings of 0 to 0.5 phr. The micro-structure of epoxy/MERO nanocomposites was investigated using scanning electron microscope (SEM), transmission electron microscope (TEM) and XRD techniques. The present work reports an enhancement of 32%, 103% and 85% in tensile, impact and flexural strength respectively of epoxy by the addition of even 0.25 phr MERO. At this loading elastic and flexural moduli also increased by 10% and 65%, respectively. Single-edge-notch three-point-Bending (SEN-TPB) fracture toughness ( $K_{IC}$ ) measurements were carried out where a 63% increase was observed by the introduction of 0.25 phr MERO. The interfacial interactions brought about by graphene also benefited the dynamic mechanical properties to a large extent in the form of a significant enhancement in storage modulus and slightly improved glass transition temperature. Considerable improvements were also detected in dielectric properties. The epoxy nanocomposite also attained an ac conductivity of  $10^{-5}$  S/m and a remarkable increase in dielectric constant. The simple and cost effective way of graphene synthesis for the fabrication of epoxy/MERO nanocomposites may be extended to the preparation of other MERO based polymer nanocomposites. This remarkable class of materials has thrown open enormous opportunities for developing conductive adhesives and in microelectronics.

© 2014 Elsevier Ltd. All rights reserved.

## 1. Introduction

Carbon nanomaterials have a unique place in nanoscience owing to their exceptional electrical, thermal, chemical and mechanical properties [1]. They have found application in areas as diverse as composite materials, energy storage/conversion, sensors,

drug delivery, field emission devices and nanoscale electronic components [2]. Of all the carbon based nanofillers graphene is perhaps the newest and has grabbed wide attention since its discovery in 2004. This can be attributed to its novel electronic properties, absent in thicker carbon films or other carbon nanostructures [3] coupled with its unique mechanical and thermal properties. Graphene, a monolayer of sp<sup>2</sup> hybridized carbon atoms arranged in a two-dimensional honeycomb structure continues to invite the attention of the scientific community and industrial researchers [4]. Moreover it is the thinnest material and also, the strongest material ever subjected to measurement [5].

\* Corresponding author. Tel.: +91 (0)484 2575723; fax: +91 (0)484 2577747.

E-mail addresses: bindusharmilatk@gmail.com (B.S. T.K.), ethachil@cusat.ac.in, ethachil@gmail.com (E.T. Thachil).

Graphene can be prepared via various techniques [6], of which the most commonly researched route are via graphitic oxide (GO) [7] due to scalability and shows potential for the production of graphene sheets in bulk quantities required for the fabrication of polymer composites. Brodie, Staudemaier, Hummers and Tour group have proposed various methods for the synthesis of graphite oxide from graphite [8–11]. But graphene in its oxidized form is nonconductive and it is sensitive to higher temperature. By removing oxygen containing groups (reducing), it is possible to restore these properties. However the structure and electrical properties of reduced graphene oxide can be never fully restored to that of pristine graphene [12].

Chemical and thermal methods are frequently used to reduce graphitic oxide. Microwave assisted exfoliation is a simple yet versatile method to simultaneously achieve the exfoliation and reduction of graphitic oxide [13]. However, pristine graphene contains rare surface functional moieties and possesses limited dispersibility in solvents, seriously affecting its performance [14]. In contrast to pristine graphene, the graphene from the microwave exfoliation still contains some oxygen containing groups on the sheet surface. Due to the presence of residual functionalities, this material is referred to in this article as microwave exfoliated reduced graphene oxide (MERGO) instead of graphene. These functionalities not only allow good dispersion of graphene in polymer matrix, but also provide active sites to form chemical bonds between the graphene nanosheets and the polymer matrix [15]. The prepared graphene shows more thermal stability than that of graphene oxide precursor while its composites show good dielectric properties too.

Epoxy resins are a class of high performance thermosetting polymers having wide applications in adhesives, composites, laminates, coatings etc. [16]. However, epoxy resins are generally brittle which restrict their applications. Nanocomposite technology offers an interesting yet challenging alternative for the modification of polymer matrix properties. There are innumerable publications concerned with multifunctional epoxy nanocomposites based on layered silicates [17,18], single walled and multi walled carbon nanotubes (SWCNT & MWCNT) [19,20], natural graphite [21], carbon black [22] etc. The use of CNT in nanocomposites has been limited to date by challenges in processing, dispersion and their prohibitively high cost. Functionalized graphene holds great promise as an effective new filler [23] as it offers properties that are equivalent to or better than those of SWCNTs but with the advantages of scale and practicality associated with clay. Gallego et al. have evaluated comparison of filler percolation and mechanical properties in graphene and carbon nanotube filled epoxy nanocomposites and concluded that graphene sheet based epoxy nanocomposites offer a wider range of improvement than MWCNT [24]. Yang et al. investigated the synergistic effects between multi-graphene platelets (MGP) and chemically functionalized multi-walled carbon nanotubes (GD400-MWCNTs) on epoxy thermosets [25]. It was found that Stacking of individual MGPs was effectively inhibited by the introduction of GD 400-MWCNT, which lead to impressive enhancement in mechanical and thermal properties. Moreover, graphene fillers at even very low loadings have the potential to match or exceed the performance of large quantities of traditional composite fillers. The exploitation of this class of materials has lead to an enormous range of applications in hi-tech and microelectronics [26]. Zhaman et al. reported developing epoxy/graphene nanocomposites with enhanced toughness through the surface modification of graphene sheets [27]. Wang et al. found that graphene could enhance the properties of epoxy thermosets on functionalizing with organosilane [28]. Feng et al. have probed the reinforcing effect of graphene on spirocyclic phosphazene based epoxy resin [29] and the studies demonstrated that the

incorporation of graphene lead to considerable increase in Tg, mechanical and conductive properties.

In this investigation, we have prepared graphene through microwave exfoliation of graphene oxide which in turn was synthesized from graphite by the method suggested by the Tour group. Various techniques have been employed for monitoring the simultaneous reduction and exfoliation of graphene oxide. The simple, easy and cost effective technique of microwave exfoliation produces functionalized graphene sheets (FGS) which provide superb polymer particle interactions during subsequent fabrication of epoxy nanocomposites. Considerable potential exhibited by graphene based nanocomposites and the promises they hold for future, novel FGS based nanocomposites are constantly being sought. This makes MERGO a prime candidate for developing high performance light weight composites that can be tailored to individual applications. The microwave exfoliated reduced graphene oxide epoxy nanocomposites obtained are mechanically robust with good thermo-mechanical properties and improved electrical properties. The dielectric response of the epoxy nanocomposites studied herein also holds promise for the development of new polymer composites with excellent dielectric properties. For these reasons, the present initiative represents an advance over previous work. No literature regarding fabrication of microwave exfoliated reduced graphene oxide epoxy nanocomposites or their static and dynamic mechanical properties as well as dielectric properties have come to the attention of the authors.

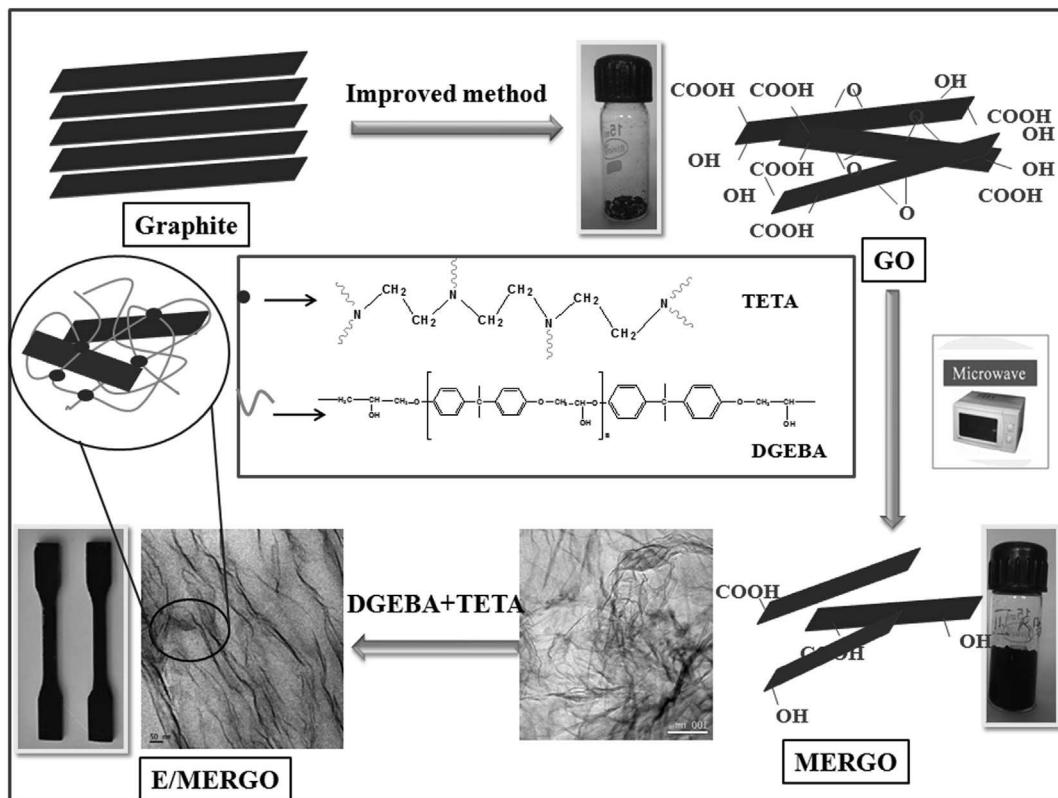
## 2. Experimental section

### 2.1. Materials

The matrix used in the present study was epoxy resin Araldite GY 250 based on diglycidyl ether of bisphenol A (DGEBA) (epoxy equivalent 187 g/eq) and triethylenetetramine (TETA) hardener under the commercial name HY 951 and was purchased from Emax Glass Fibre and Accessories Pvt. Ltd., Chennai. Graphite powder, sulfuric acid ( $H_2SO_4$ , 98 wt%), phosphoric acid ( $H_3PO_4$ , 85 wt%) potassium permanganate ( $KMnO_4$ ), hydrogen peroxide ( $H_2O_2$ , 30 Vol%), hydrochloric acid (HCl, 35%), ether and ethanol were used for the preparation of graphene oxide. They were purchased from Sigma Aldrich, Bangalore, India. All the chemicals were used as received without further purification.

### 2.2. Preparation of epoxy/microwave exfoliated reduced graphene oxide (E/MERGO) nanocomposites

The fabrication strategy of E/MERGO nanocomposites is shown in Scheme 1. The graphite platelets were first exfoliated to form graphene oxide using the improved method of Tour group [11]. In a typical process a 9:1 mixture of concentrated  $H_2SO_4/H_3PO_4$  (360:40 ml) was added to a mixture of graphite (3.0 g, 1 wt equiv) and  $KMnO_4$  (18.0 g, 6 wt equiv) producing a slight rise in temperature to 35–40 °C. The reactants were heated to 50 °C and stirred for 12 h. The mixture was cooled to room temperature and poured onto ice (~400 ml). 30%  $H_2O_2$  was slowly added into the mixture until the solution turned bright yellow. The resulting yellowish brown mixture was centrifuged and the solid material was then washed in succession with 200 ml of water, 200 ml of 30% HCl and 200 ml of ethanol. After this multiple wash, it was coagulated with 200 ml of ether. The solid graphene oxide (GO) obtained after the evaporation of ether, was vacuum-dried overnight at room temperature. The dried GO powder was exfoliated in a microwave oven (T.D.S, Model MW73BD) at ambient conditions and 700 W for 1 min. Upon microwave irradiation, a large volume expansion of the GO powder, accompanied by ‘violent fuming’ was observed. As



**Scheme 1.** Fabrication strategy of E/MERGO nanocomposites.

can be seen from Scheme 1, the GO powder in the glass vial had dramatically expanded yielding black and fluffy MERGO.

The epoxy nanocomposite was prepared as follows. First the required quantity of MERGO was dispersed in acetone and it was added to the epoxy oligomer with mechanical stirring for 45 min followed by ultrasonication for another 30 min. The mixture was degassed at 40 °C under vacuum for 30 min to remove the solvent as well as air bubbles. Then 10 phr hardener was added to the epoxy resin, followed by 5 min mixing and degassing. After this, the mixture was transferred into Teflon molds of different shapes coated with a releasing agent and kept for 24 h at room temperature. This was followed by postcuring at 80 °C for 4 h. The cured samples were then demolded and trimmed and used for mechanical studies.

### 3. Characterization techniques

#### 3.1. X-ray diffraction analysis (XRD)

XRD patterns were employed to portray the graphitic structures of the graphite, GO, and MERGO. The patterns were obtained using a Bruker AXS D8 Advance X-ray powder diffractometer equipped with Cu K $\alpha$  radiation. The samples were scanned in the range of 2–25° 2 $\theta$  at increments of 0.020° at a wavelength of 1.541 Å operating at 40 KV and 35 mA.

#### 3.2. Raman spectrum

Raman spectroscopy has been utilized as powerful tools for the nondestructive characterization of graphitic structures. It was employed to confirm the structure of GO and MERGO. Raman spectra of GO and MERGO were recorded with Horiba Jobin Yvon

Lab Ram HR system at a resolution of 2 mm by using excitation of 514.5 nm of Argon ion laser.

#### 3.3. X-ray photoelectron spectroscopy

X-ray photoelectron spectroscopy (XPS) analysis was carried out on a Kratos Axis Ultra X-ray photoelectron spectrometer (UK) with Al K $\alpha$  radiation of 1486.6 eV.

#### 3.4. Thermogravimetric analysis

The thermogravimetric analysis of the samples was carried out under nitrogen atmosphere at a heating rate of 20 °C/min in a TGA Q 50 Thermal Analyser (TA Instruments). In all cases the sample weights were between 5 and 10 mg. Thermograms (TG) were recorded for the range from room temperature to 600 °C.

#### 3.5. Fourier transform infrared spectroscopy (FTIR) and UV-visible spectra

Fourier transform infrared spectra (FTIR) were recorded on a Jasco FT/IR-4100 instrument. UV-vis spectra were collected on an Evolution 201 UV-visible spectrophotometer. GO dispersion in water and MERGO dispersion in DMF thereafter prepared were diluted to an appropriate absorbance range, and their normalized spectra were compared.

#### 3.6. C<sup>13</sup> NMR spectroscopy

Solid-state Magic Angle Spinning Nuclear Magnetic Resonance analyses were performed with a 13C HPDEC MAS NMR spectrometer operating at 8 KHz.

### 3.7. Scanning electron microscopy

SEM observations of graphite, GO, MERGO and the fracture surface of neat epoxy and E/MERGO nanocomposites were examined using a JEOL Model JSM.6390 LV scanning electron microscope. The fracture surfaces were gold coated prior to SEM investigation to make them conductive.

### 3.8. Transmission electron microscopy (TEM)

The MERGO was dispersed in acetone by ultrasonicator, and some pieces were collected on carbon coated 200 mesh copper grids for TEM observation. For E/MERGO nanocomposite, the ultra thin TEM sample with a thickness of 70 nm was cut using a Leica Ultracut UCT Ultramicrotome at room temperature. Microtomed thin sections were collected on 200 mesh copper grids and examined by a JEM 2100 TEM at 200 kV in a bright field mode.

### 3.9. Mechanical properties

Tensile properties were tested using a Shimadzu Universal Testing Machine, equipped with a 10 KN load cell at a displacement rate of 5 mm/min at room temperature as per ASTM D 638. The flexural properties were determined using rectangular bars on the same machine, at a speed of 10 mm/min as per ASTM D 790. Impact strength was measured using unnotched samples according to ASTM D 4812-99 on a Ceast Resil Impact analyser (Junior) using a hammer of 4 J at a striking rate of 3.96 m/s. A single-edge-notch three-point-Bending (SEN-TPB) test was conducted to obtain the critical stress intensity factor toughness ( $K_{IC}$ ) of E/MERGO nanocomposites according to ASTM D 5045 by using the rectangular specimen [See Fig. 6(e)] at a crosshead speed of 10 mm/min. The notches were made first by the formation of saw-cut slots having rectangular shape with a width of ~1 mm in the midsection of specimens. Before testing the specimens were pre-cracked by inserting a fresh razor blade into the sawed notch and impacting with a hammer. The total notch length of SEN-TPB specimen was in such a way that ( $a/w$ ) should be in between 0.45–0.55, where ‘ $a$ ’ is the initial crack length (crack prenotch plus razor tapping notch) and ‘ $w$ ’ is the specimen width. Equations (1) and (2) were used to evaluate the fracture toughness of the intrinsically brittle epoxy and E/MERGO nanocomposites by taking ‘ $P$ ’ as the critical load for crack propagation and ‘ $B$ ’ as the specimen thickness.

$$K_{IC} = \frac{P}{BW^{1/2}} f\left(\frac{a}{w}\right), \quad (x = a/w) \quad (1)$$

$$f\left(\frac{a}{w}\right) = \left\{ 6x^{1/2} [1.99 - x(1-x)(2.15 - 3.93x + 2.7x^2)] \right\} / [(1+2x)(1-x)^{3/2}] \quad (2)$$

### 3.10. Dynamic mechanical analysis (DMA)

The dynamic mechanical thermal analysis was conducted using rectangular test specimens having a dimension of 60 mm × 4 mm × 2 mm with a dual cantilever clamp on a dynamic mechanical analyzer (Model Q 800, TA instruments). The tests were carried out by temperature sweep (temperature ramp from 35 °C to 130 °C at 3 °C/min) method at a constant frequency of 1 Hz to get the dynamic storage modulus ( $E'$ ) and loss modulus ( $E''$ ) of the samples.  $\tan \delta (E''/E')$  was calculated as the ratio.

### 3.11. Dielectric properties and DC electrical conductivity

The dielectric measurements were carried out at frequencies ranging from 20 Hz to 2 MHz using an impedance analyzer, Agilent E 4980 A Precision LCR Meter. Disc shaped samples having diameter 12 mm and thickness 2 mm were used for the measurements. The changes in AC conductivity, real permittivity ( $\epsilon'$ ), imaginary permittivity ( $\epsilon''$ ) and dielectric loss tangent ( $\tan \delta$ ) of E/MERGO nanocomposites with frequency were obtained from the instrument. The results were directly read on the monitor and recorded on a computer data sheet file. DC electrical conductivity measurements were done by a standard two-probe electrode using a Keithley 2400 source-measure unit in dry air at ambient temperature.

## 4. Results and discussion

### 4.1. Structural characterization of MERGO

The XRD pattern of pure graphite, GO and MERGO are shown in Fig. 1(a). Graphite shows a diffraction peak at 26.6° corresponding to a basal spacing ( $d_{002}$ ) of 3.35 Å. The pattern of GO, on the other hand, exhibits a  $d_{001}$  reflection at 8.67° having a basal spacing of 10.189 Å. Intense intercalation of graphite during oxidation is confirmed by the typical increase of  $d$  spacing from 3.35 to 10.189 Å. Nevertheless, the XRD pattern of MERGO does not demonstrate any diffraction peaks due to the disappearance of the long-term ordering graphitic structure.

The major Raman features of graphene and graphite are the so called G band and 2D band. The G band originates from in plane vibration of  $sp^2$  bonded carbon atoms that constitute graphene and is corresponding to the first order scattering of the  $E_{2g}$  vibration mode. The 2D band originates from a two phonon double resonance Raman process [30]. A third band known as the defect band (D band) is the result of a one phonon lattice vibrational process. This disorder band is also useful in graphene synthesis as its intensity is directly proportional to the level of defects in the sample [31]. Fig. 1(b) shows the Raman spectra of GO and MERGO. Pure graphite [Fig. 1(b) inset] exhibits an intense G band at 1580.76 cm<sup>-1</sup>, 2D band at 2687.99 cm<sup>-1</sup> and a very weak D band at 1351.9 cm<sup>-1</sup>. In the Raman spectrum of GO, D band at 1360 cm<sup>-1</sup> becomes the prominent feature indicating the creation of  $sp^3$  domains or the decrease of  $sp^2$  domains due to extensive oxidation [32]. Additionally, in GO, the G band is broadened and shifted to 1585.42 cm<sup>-1</sup> owing to the presence of isolated double bonds that resonated slightly at higher frequencies than pure graphite. In MERGO, G band and D band are at 1583.33 cm<sup>-1</sup> and at 1358 cm<sup>-1</sup> respectively. Here we got a D/G ratio of 1. Presence of D band and G band confirms the formation of graphene with some defects. This is in agreement with Jingquan et al., who reported that the graphene sheets prepared through oxidation-reduction methods usually retain significant level of defects and possess uncontrolled geometrical shapes due to the harsh oxidation condition [33].

Thermogravimetric and the corresponding differential thermal analysis curves are shown in Fig. 1(c) and (d) respectively. From the TGA curves it is clear that graphite has a good thermal stability on heating up to 900 °C, while GO is thermally unstable and starts to lose mass upon heating below 100 °C. Severe mass reduction at 190 °C is due to the pyrolysis of the labile oxygen containing functional groups, resulting in a rapid thermal expansion of the material. Compared to GO, which has a severe mass reduction at 200 °C [see Fig. 1(d)], MERGO displays a slight reduction in mass. It indicates that oxygen-containing functional groups still remain on the graphene sheets to a small extend after microwave exfoliation.

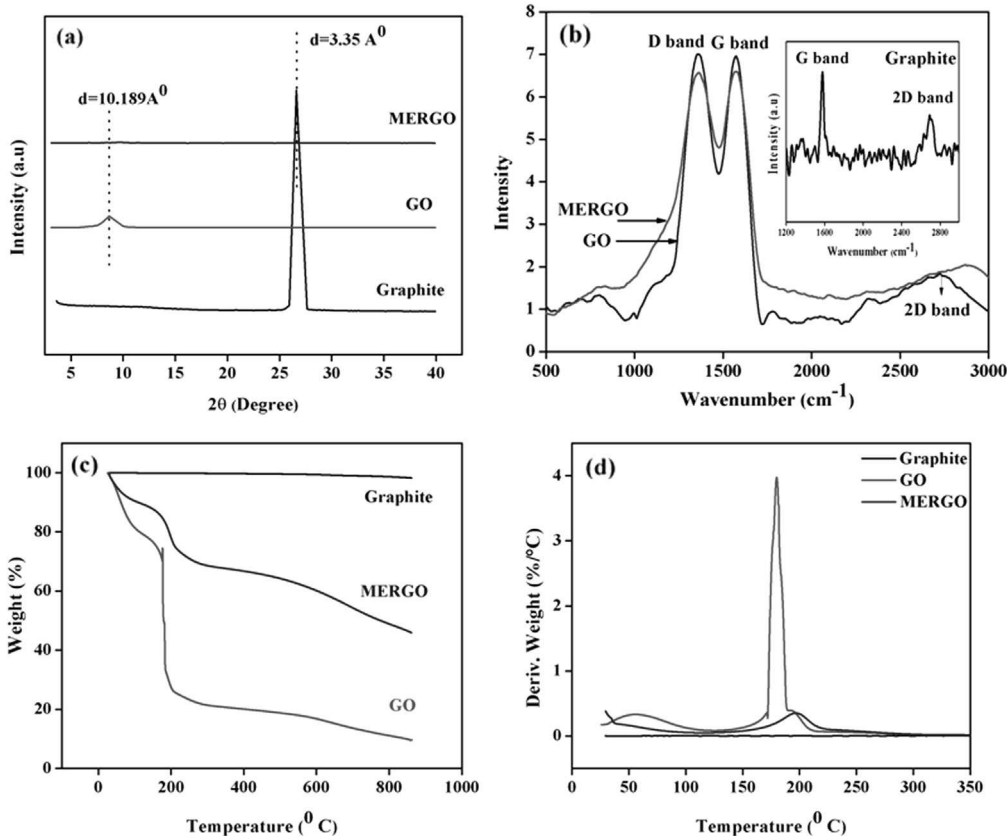


**Fig. 1.** (a) XRD patterns of pure graphite, GO and MERGO. (b) Raman spectra of GO & MERGO (inset-Raman spectrum of graphite). (c) TGA and (d) DTG curves of pure graphite, GO and MERGO.

Energy dispersive X-Ray spectroscopy (EDX) analysis of graphite, GO and MERGO are shown in Fig. 2(a,b,c). Only the element carbon (100 atom%) is present in pristine graphite as shown in Fig. 2(a). However, after chemical oxidation, the oxygen concentration drastically increased to 20.05 atom% in GO [Fig. 2(b)]. Compared with spectrum GO, the EDX spectrum of MERGO, [Fig. 2(c)] confirms the reduction process as the elemental oxygen presence decreased to 2.9 atom% with a corresponding increase in atom% of carbon to 97.1.

X-ray photoelectron spectroscopy (XPS) was conducted to investigate the surface elements present, for quantitative analysis

and to determine the extent of reduction to graphitic oxide. The corresponding spectra are shown in Fig. 3. Fig. 3(a) shows the wide scan spectra and in both GO and MERGO, C 1s and O 1s signals appear at 286 and 531 eV respectively. Clearly the peaks with binding energies higher than for sp<sup>2</sup> bonded carbon (284.5) are smaller for MERGO [Fig. 3(d)] than for the GO precursor [Fig. 3(c)]. The peaks between 286 and 289 eV are typically assigned to epoxide, hydroxyl and carboxyl groups [34].

The reactive groups of GO and MERGO are also reflected in the FTIR spectra shown in Fig. 4(a). The FTIR spectrum of graphite

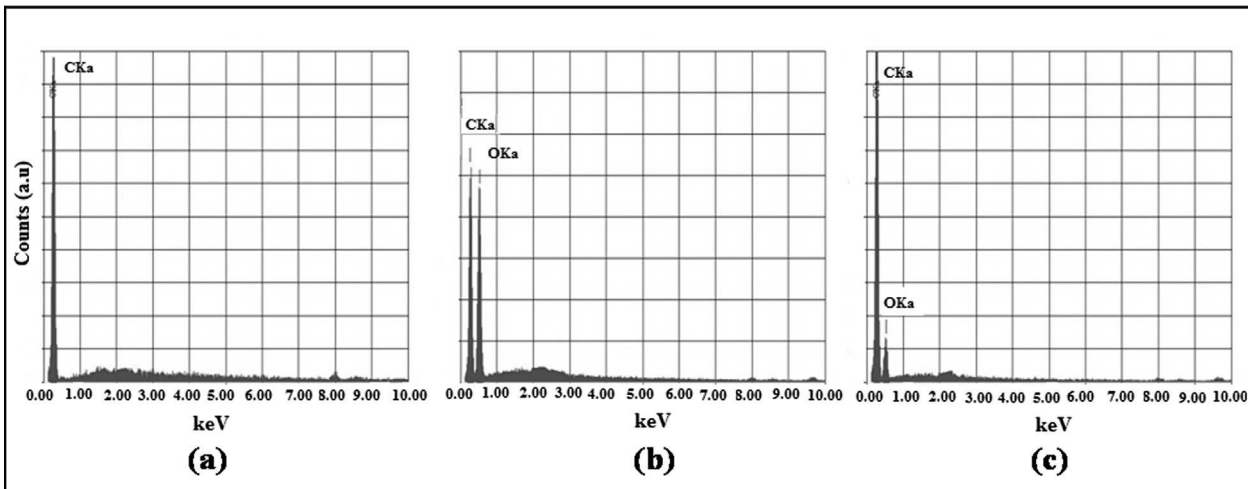


**Fig. 2.** Energy dispersive X-Ray spectroscopy (EDAX) analysis of (a) graphite, (b) GO and (c) MERGO.

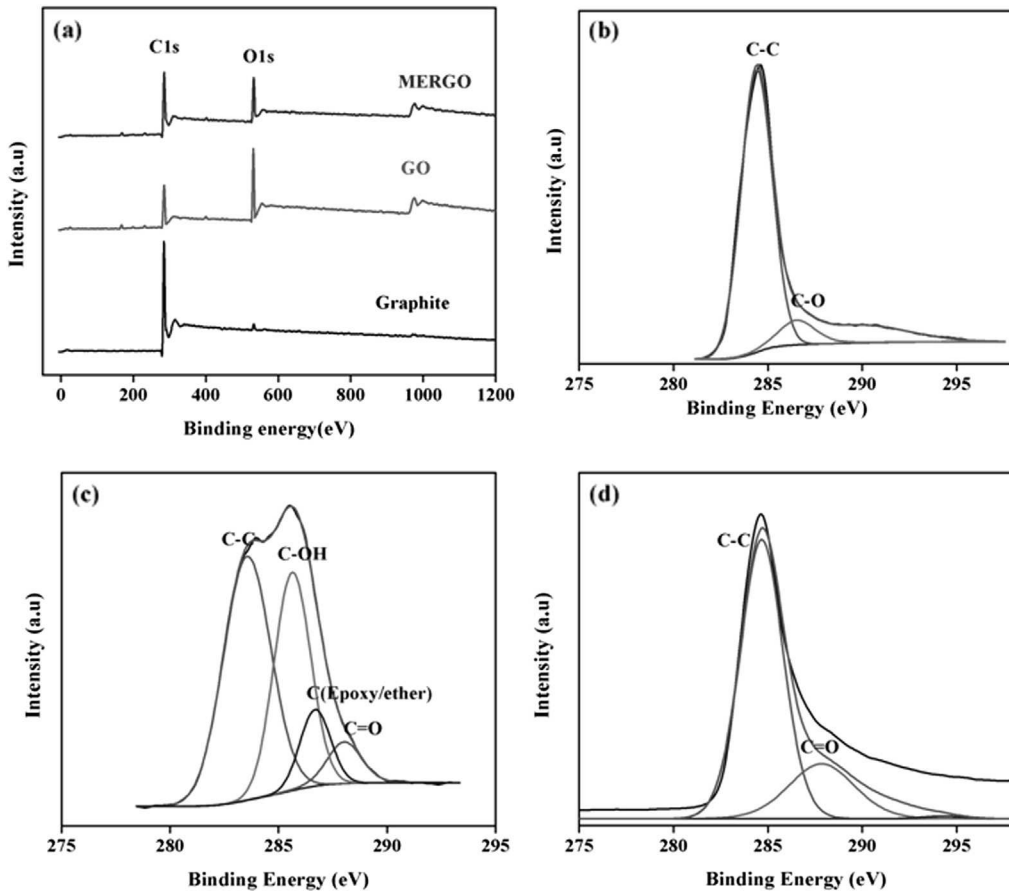


Fig. 3. (a) XPS wide scan spectra. XPS C 1S spectra of (b) Pure graphite, (c) GO and (d) MERGO.

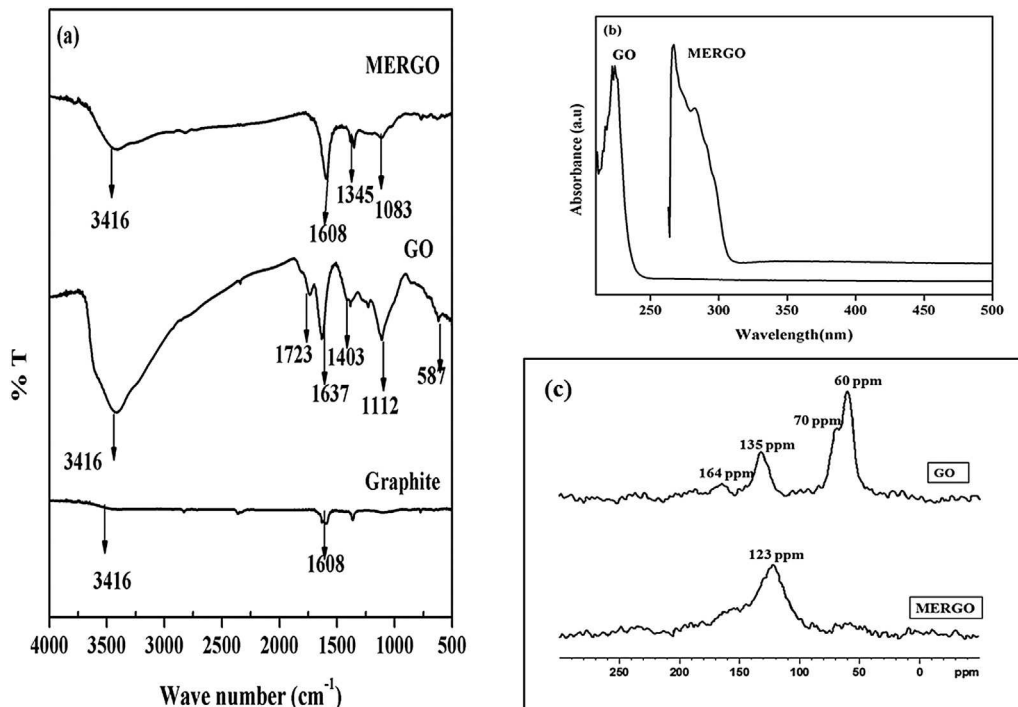


Fig. 4. (a) FTIR spectra of graphite, GO and MERGO, (b) Ultraviolet-visible spectra and (c) <sup>13</sup>C NMR spectra of GO and MERGO.

shows a vibrational peak of C=C at about  $1608\text{ cm}^{-1}$  and a weak shoulder at  $3416\text{ cm}^{-1}$ , due to the O–H stretching vibration of the moisture absorbed by the sample. In the case of GO the following functional groups can be identified: O–H stretching vibration at  $3416\text{ cm}^{-1}$ , C=O stretching vibration (carbonyl/carboxyl) at  $1723\text{ cm}^{-1}$ , from unoxidized  $\text{sp}^2$  C=C at  $1637\text{ cm}^{-1}$ , a peak at  $1403\text{ cm}^{-1}$  assigned to O–H bending deformation or C–O (carboxyl) vibration, and a C–O (alkoxyl) vibration at  $1112\text{ cm}^{-1}$ . This confirms the presence of hydroxyl, epoxide, and carbonyl functional groups in GO. However, in MERGO, intensity of O–H stretching vibration at  $3416\text{ cm}^{-1}$  gets decreased. C=C stretching at  $1608\text{ cm}^{-1}$ , low intensity band at  $1396\text{ cm}^{-1}$  assigned to O–H deformations of the C–OH groups and C–O stretching vibrations observed as a very low intensity band at  $1083\text{ cm}^{-1}$  are due to the remaining carbonyl groups after the reduction process.

The ultraviolet–visible spectra of GO exhibits a maximum absorption peak at about  $223\text{ nm}$  corresponding to  $\pi-\pi^*$  transition of aromatic C–C bonds. The absorption peak for MERGO had red shifted to  $267\text{ nm}$  which indicates that a substantial amount of GO reduction has taken place. This phenomenon of red shift from  $223$  to  $267\text{ nm}$  has been used as a monitoring tool for the reduction of GO or restoration of the conjugated  $\pi$  structure, demonstrated in Fig. 4(b). The weak shoulder around  $282\text{ nm}$  in MERGO is attributed to the  $n-\pi^*$  transition of C–O bonds embedded by the exfoliation and intercalation on the reduced graphene oxide.

$\text{C}^{13}$  NMR spectroscopy further substantiates the reduction of GO, in agreement with the above results. In  $\text{C}^{13}$  NMR spectroscopy (See Fig. 4(c)) the peaks at  $60$  and  $70\text{ ppm}$  in GO represent epoxide and hydroxyl groups. The peak at  $135\text{ ppm}$  corresponds to the presence of unoxidized  $\text{sp}^2$  carbon atoms. However in MERGO, the  $60\text{ ppm}$

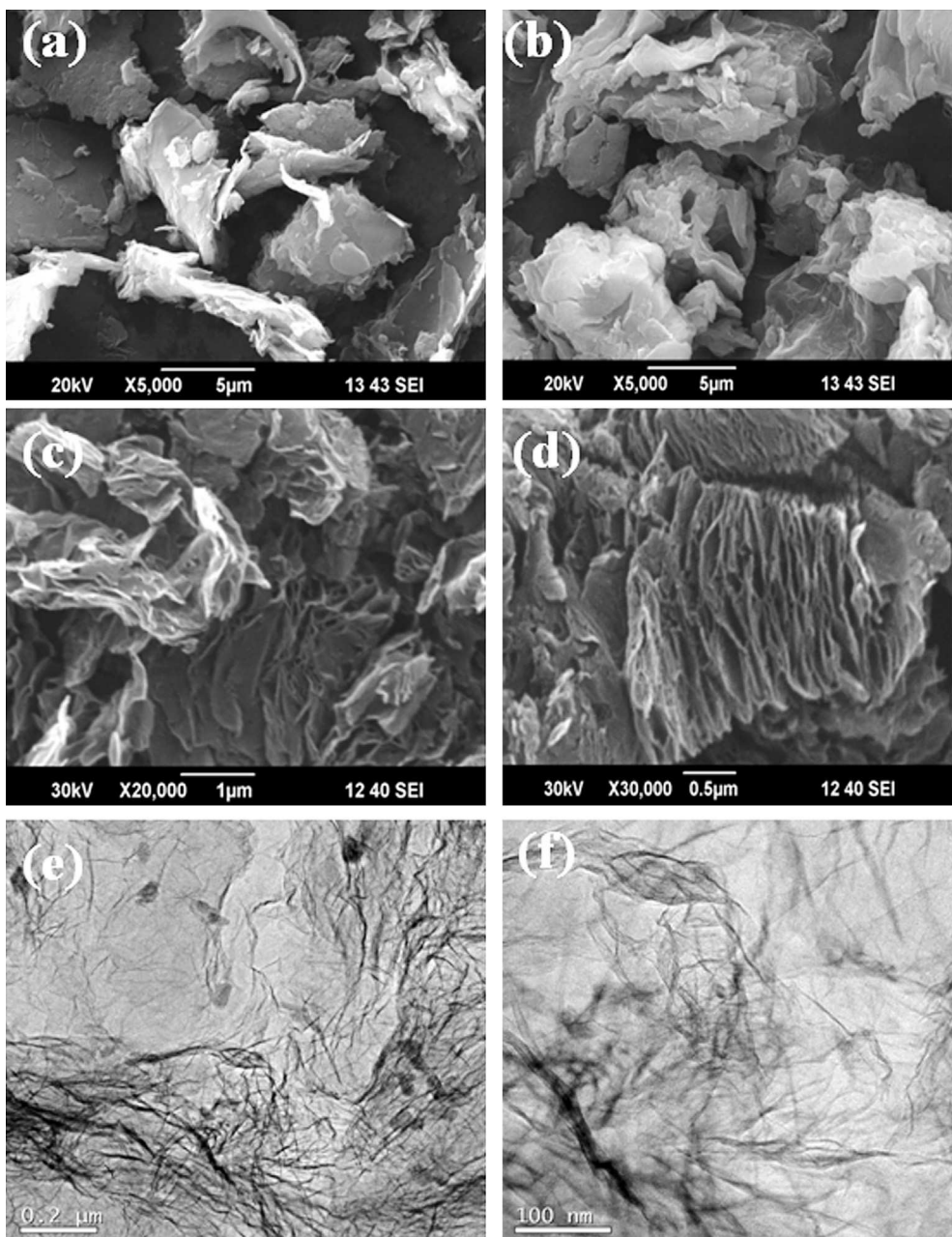


Fig. 5. SEM photograph of (a) graphite, (b) GO, (c) & (d) MERGO, (e) & (f) TEM images of MERGO.

and 70 ppm resonances have disappeared and the peak at 135 ppm shifted to 123 ppm because of the change in the chemical environment of the  $sp^2$  carbon.

Fig. 5(a) and (b) shows the SEM photographs of graphite and GO, which clearly reflect the morphologies of graphite sheets before and after oxidation. The graphite presented a typical multilayer structure whereas the stacking graphitic sheets were separated from one another after oxidation. Fig. 5(b) shows the random orientation and wavy appearance of GO. Fig. 5(c) and (d) represents the higher magnification image of MERGO. It is notable in Fig. 5(c) that the microwave exfoliated reduced graphene oxide exhibits a very small thickness having isolated layers. But in Fig. 5(d), formation of few layer graphene in some areas is also found. It is observed from TEM micrograph of Fig. 5(e and f) that the graphene obtained via microwave exfoliation has wrinkled surface and folds at the edges and has an irregular shape.

#### 4.2. Static mechanical properties of E/MERGO nanocomposites

The influence of MERGO on the mechanical performance of E/MERGO nanocomposites was evaluated in terms of the tensile, flexural and unnotched impact properties. Fig. 6(a) shows the

stress-strain curves of neat epoxy and its MERGO nanocomposites. Fig. 6(b), (c) and (d) shows the variation of flexural strength and strain, elastic and flexural moduli and impact strength of the nanocomposites respectively in which the reinforcing effect of the MERGO is clearly brought out.

Examination of these figures leads to the following findings. Tensile, impact and flexural properties present a considerable improvement when MERGO is incorporated into epoxy resin. Such an increasing trend persists with increase of MERGO content till 0.25 phr. At this concentration, the nanocomposite achieved about 32%, 103% and 85% increase in tensile, impact strength and flexural properties respectively, compared to pure epoxy. With the addition of MERGO the strain to failure decreases at higher loading. This is due to the hard and rigid fillers that restrict the elongation and hence the deformation. The E/MERGO nanocomposites exhibit an increasing trend in both elastic and flexural moduli and the highest rate of improvement is obtained at 0.25 phr MERGO loading and thereafter rate of improvement falls until a plateau is reached. The MERGO successfully enhances the interfacial properties upto a 0.25 phr concentration. As MERGO behaves as functionalized graphene, it can form chemical bonds with DGEBA. Epoxy functionalities of MERGO can also react with amine curing agent. Besides

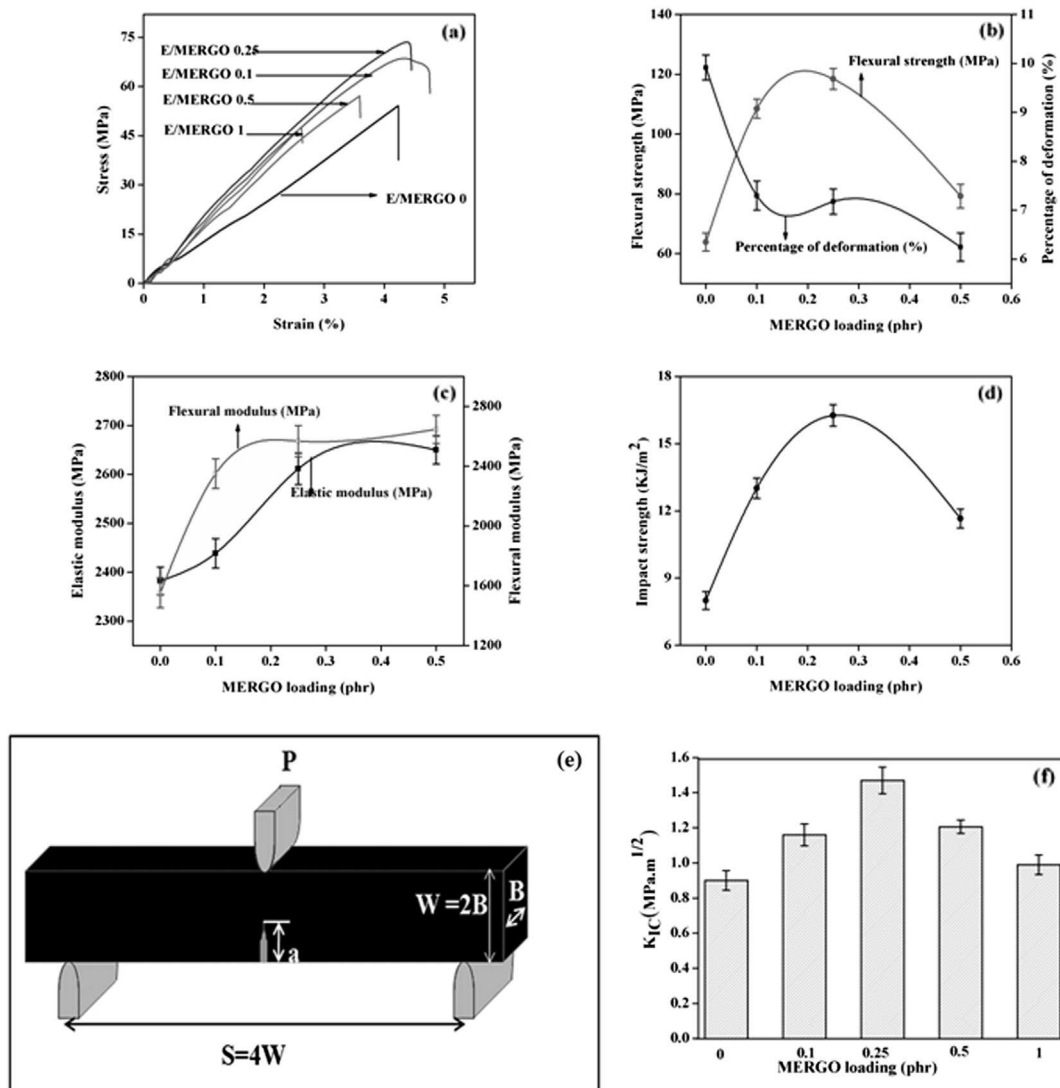


**Fig. 6.** Mechanical properties of E/MERGO nanocomposites. (a) Stress–strain curves. (b) Flexural strength. (c) Elastic & flexural modulus & (d) Impact strength versus MERGO loadings (phr). (e) Specimen geometry for SEN-TPB fracture toughness test. (f) Fracture toughness against MERGO loading.

chemical interactions, physical cross linking such as hydrogen bonding may also exists in E/MERGO nanocomposites. All the possible interactions are depicted in Scheme 2. In addition, wrinkled topology of MERGO would produce an enhanced mechanical interlocking and adhesion with the epoxy chains and consequently strengthens the interaction and load transfer between MERGO and the epoxy matrix.

When the distribution of the fillers is more homogeneous and no obvious agglomeration is observed, stress transfer between the fillers and the epoxy matrix is more effective [35]. The dispersion of MERGO is good at lower concentrations and at higher values due to excessive interfacial contacts between MERGO/MERGO weakens the mechanical properties of E/MERGO nanocomposites [36]. Moreover the microstructure of E/MERGO nanocomposites may change from fully exfoliated to partially exfoliated/intercalated structure at higher loading and which lead to decrease in mechanical properties as seen in layered polymer nanocomposites. SEM and TEM photographs give credence to the MERGO dispersion in the epoxy matrix, which will be discussed in the coming section.

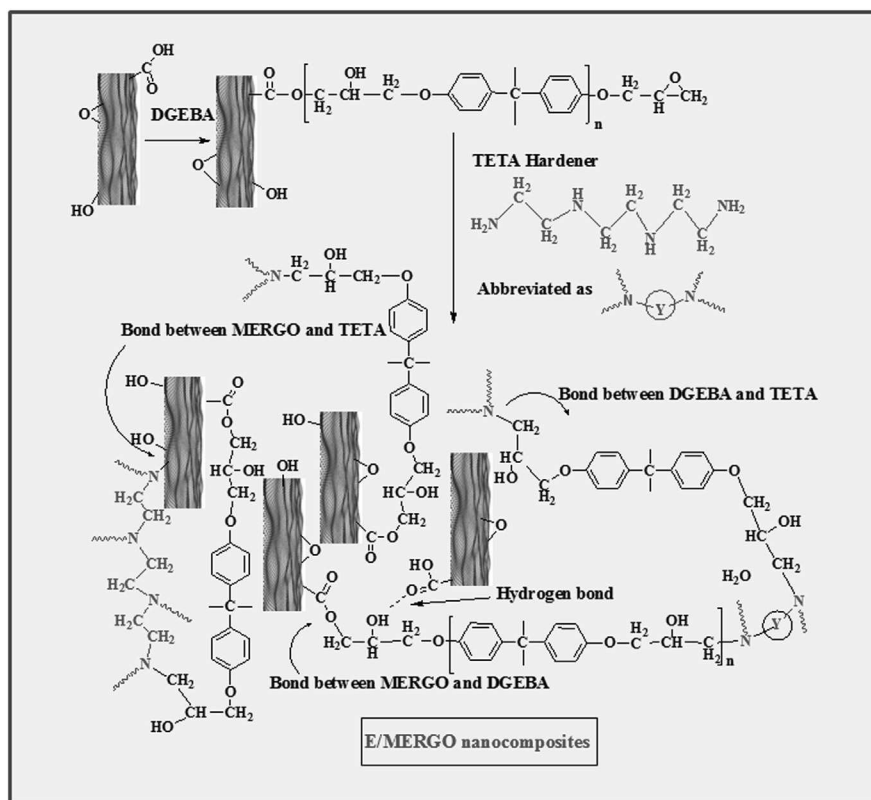
The SEN-TPB fracture specimens were prepared according to ASTM D 5045 as shown in Fig. 6 (e). Fig. 6 (f) illustrates the effect of the MERGO loading on the fracture toughness of the E/MERGO nanocomposites. The increment in fracture toughness of nanocomposites is believed to be due to the capability of the filler particles to resist the crack propagation before the fracture has taken place. The introduction of 0.25 phr MERGO into the epoxy matrix caused a sharp increase in  $K_{IC}$  value ( $1.47 \text{ MPa m}^{1/2} \pm 0.0762$ ), which corresponds to a 63% increase compared to pure epoxy. The exfoliated kind of dispersion and interfacial interactions are responsible for the improvement in fracture toughness. But as the MERGO loading increases further  $K_{IC}$  values decreases. This is because of decrease in the dispersion of the MERGO from exfoliated to

partially exfoliated. This will result in the reduction of the resistance of the composite against the crack propagation and subsequently deteriorate the fracture toughness of the composite. In this respect, a decrease in fracture toughness of the composites filled with relatively high MERGO loading is detected. However the  $K_{IC}$  value at 1 phr loading is still higher than that of pure epoxy.

#### 4.3. Microstructure of E/MERGO nanocomposites

The SEM image shown in Fig. 7 (a) represents neat epoxy resin, with a relatively smooth surface and occasional river patterns. The resistance of the material under crack propagation is minimal and leads to brittle failure, thus accounting for the low fracture toughness of the unfilled epoxy. Fig. 7(b) and (c) represents the failure surfaces of the nanocomposite containing 0.25 and 0.5 phr of MERGO respectively. Considerable difference is noticed between failure surface of neat epoxy and that of E/MERGO system. On the addition of 0.25 phr of MERGO [Fig. 7(b)] the failure surface becomes rough due to the uniform dispersion of graphene nanosheets in the epoxy matrix. The good compatibility between the nanosheets and the epoxy matrix makes crack propagation difficult and less prone to breakage at this particular loading. From Fig. 7(c), there is clear and irregular entanglement of nanosheets at higher MERGO content.

Morphological investigations of TPB fractured surfaces of pure epoxy and E/MERGO nanocomposites were also inspected by SEM and the corresponding micro photographs are shown in Fig. 7(d)–(i). The characteristic catastrophic brittleness and low fracture toughness of pure epoxy lead to smooth, fragile and mirror like fracture surfaces (Fig. 7(d)). In contrast to the pure epoxy, a rougher surface is observed in Fig. 7(e) indicating that the presence of MERGO forced the crack to propagate along a very tortuous path



**Scheme 2.** Schematic illustration of the formation of E/MERGO nanocomposites.

by the creation of matrix plastic deformation and localized shear yielding. Fig. 7 (f) clearly demonstrates the deflection of propagating crack front at 0.25 phr where an initial crack tilted when it encountered a rigid inclusion. This generates an increase in the total fracture surface area resulting in greater energy absorption. The bridge effect, which prevents crack opening, increased strength in the E/MERGO nanocomposites. MERGO sheets are embedded in the matrix and are held tightly by the epoxy resin as depicted in Fig. 7(g). However a dramatic change in morphology is observed at 1 phr loading with much coarser fracture surface [Fig. 7(h)] and its higher magnification image [Fig. 7(i)] shows single graphene or stacks of graphene with thickness of several nanometers protrude out of the fracture surface.

The morphology and the actual pattern of MERGO layer dispersion in the E/MERGO nanocomposites were investigated by TEM to corroborate with mechanical properties. TEM image of E/MERGO nanocomposite with 0.25 phr MERGO loading at different magnifications are shown in Fig. 8(a) and (b) to reveal the dispersion. The dark hair-like structures represent the cross section of the MERGO layers. The MERGO is dispersed well in the epoxy matrix as single or ultra thin sheets of thickness less than several nanometers

without the need for additional functionalization. The interfacial interactions brought by the presence of residual epoxy and hydroxyl sites present on the MERGO sheets and the epoxy matrix facilitate the dispersion of graphene nanosheets providing good bonding between MERGO and epoxy, resulting in an exfoliated nanoscale dispersion.

Selected area electron diffraction (SAED) pattern of E/MERGO nanocomposite with 0.25 phr [Fig. 8(c)] shows the amorphous nature of the nanocomposite. The exfoliated kind of dispersion at low loadings of MERGO is also reflected in the XRD analysis as demonstrated in Fig. 8(d). Pure epoxy exhibits a broad peak at  $18.5^{\circ}$ , reflecting its amorphous nature. The nanocomposites also possess only this peak and do not exhibit any other peak, which further confirms the effective dispersion of MERGO in the epoxy matrix.

#### 4.4. Dynamic mechanical analysis

Fig. 9(a), (b) and (c) shows the results of DMA tests including storage modulus ( $E'$ ), loss modulus ( $E''$ ), and damping factor ( $\tan \delta$ ) as a function of temperature from 35 to 140 °C for the cured pure epoxy and cured E/MERGO nanocomposites at different MERGO

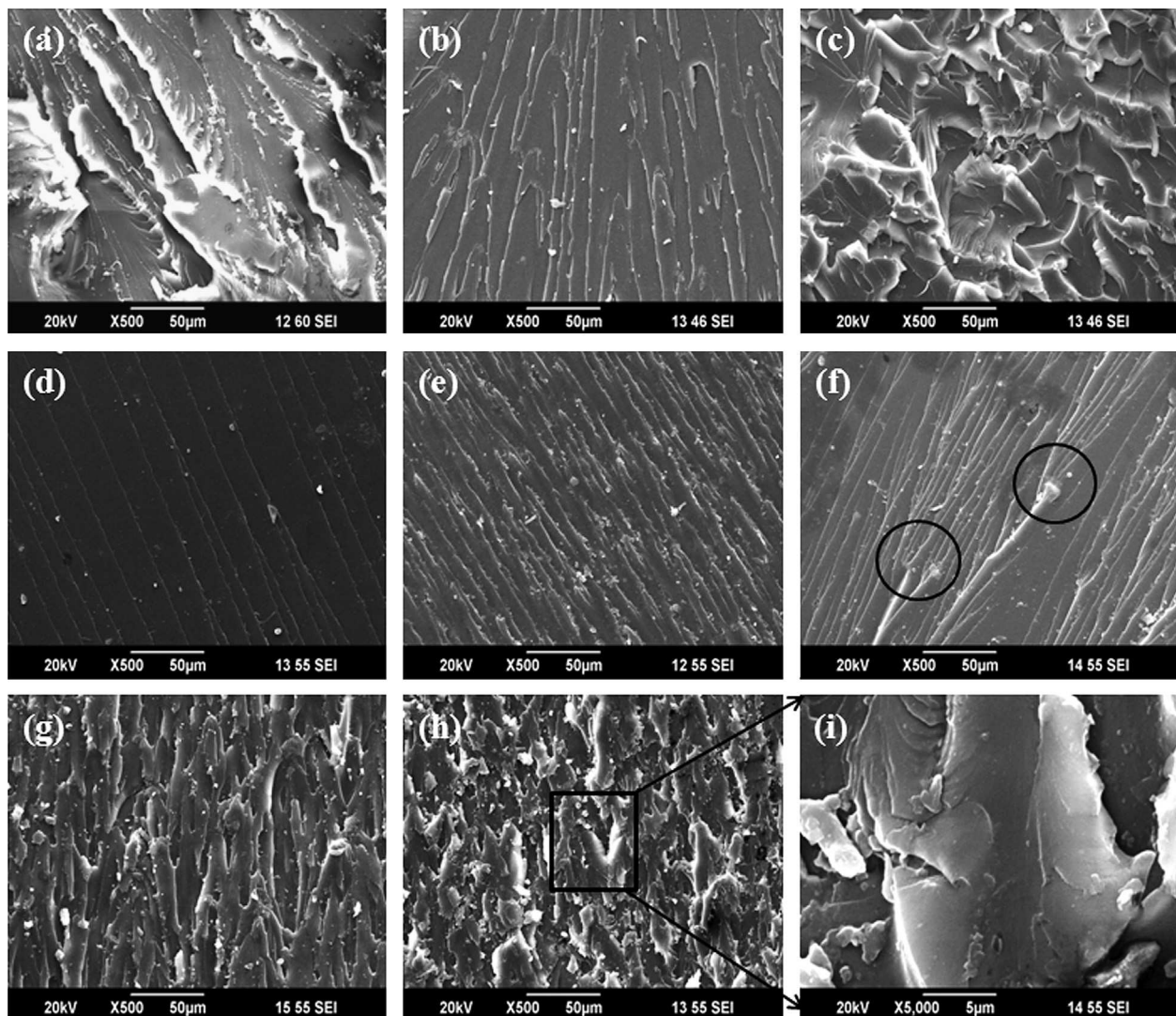


**Fig. 7.** SEM photographs. (a–c) Fractured surfaces of tensile test specimens of (a) pure epoxy, (b) E/MERGO at 0.25 phr, (c) E/MERGO at 0.5 phr. (d–i) Fractured surfaces of SEN-TPB test specimens of (d) pure epoxy, (e) E/MERGO at 0.1 phr, (f) E/MERGO at 0.25 phr, (g) E/MERGO at 0.5 phr (h & i) E/MERGO at 1 phr nanocomposites.

loadings. The  $E'$  values (Fig. 9(a)) of the epoxy filled with a MERGO loading of 0.1, 0.25 and 0.5 phr are 10.63%, 44.21%, and 50.81% respectively, higher than that of neat epoxy within the glassy state (at 40 °C) and only a slight change is visible within the rubbery state (at 120 °C). The highest rate of improvement in  $E'$  at 0.25 phr MERGO loading is ascribed to the stiffness enhancement of MERGO in the hosting epoxy matrix. The lower rate of improvement in  $E'$  at 0.5 phr MERGO loading is caused by the change in the microstructure of E/MERGO nanocomposites as explained in earlier sections.  $E''$  as a function of temperature also exhibits a similar trend to  $E'$  within the measured temperature scale. The maximum of  $E''$ , related to the motion of main chains of the epoxy networks at transition from the glassy state to the rubbery state for E/MERGO at 0.25 phr shift slightly to higher temperature compared with that (103 °C) of pure epoxy. This is because of the increased stiffness and constrained friction between polymer chains caused by the added MERGO [Fig. 9 (b)].

Fig. 9(c) shows the temperature dependent  $\tan \delta$  of cured pure epoxy and its MERGO composites. The  $\tan \delta$  is the ratio of  $E''$  to  $E'$  and the peak of  $\tan \delta$  is often used to determine the glass transition temperature ( $T_g$ ) of the material. As seen in Fig. 9(c), the  $T_g$  of E/MERGO 0.25 shifts slightly to a higher temperature (about 3–5 °C) compared to pure epoxy. This is because at optimum MERGO loading reinforcement of the polymer matrix is maximum and the flexibility of the epoxy matrix decreases. However there is no

change in  $T_g$  for the nanocomposite with 0.5 phr MERGO loading. For composites with more MERGO, the reaction between MERGO and amine curing agent also should easily occur during the curing process. This interfacial reaction leads to strongest interfacial interactions with epoxy resin, on the other hand it can change the stoichiometry of epoxy/TETA and microstructure of E/MERGO nanocomposites. As a result, the MERGO highly influences the molecular dynamics and cross linking density of epoxy matrix, thereby increase the storage modulus and reducing the  $T_g$  of the composites. Similar kinds of results have been observed by various authors [15,37,38]. The height of the  $\tan \delta$  peak is observed to decrease with increasing MERGO percentage which shows lower damping, enhanced stiffness and good MERGO-epoxy interaction. It was reported that the lowering of  $\tan \delta$  values are an indicative of improvement in the interfacial reinforcement of the nanocomposites [39,40]. Since the height depression in  $\tan \delta$  peak has been correlated with the chain mobility, a quantitative estimation of volume fraction of these constrained regions has been done by Rao and Pochan [41]. Reduced chain mobility due to the physical and chemical bonding of the epoxy chain segments to the MERGO surface caused a height reduction of  $\tan \delta$  peak during dynamic mechanical deformation. However the decrease in cross link density might be the reason for the  $T_g$  to remain unaffected at high MERGO loading. Reduction of  $T_g$  with high contents of graphene with simultaneous reduction of  $\tan \delta$  was reported by Feng et al. [29].

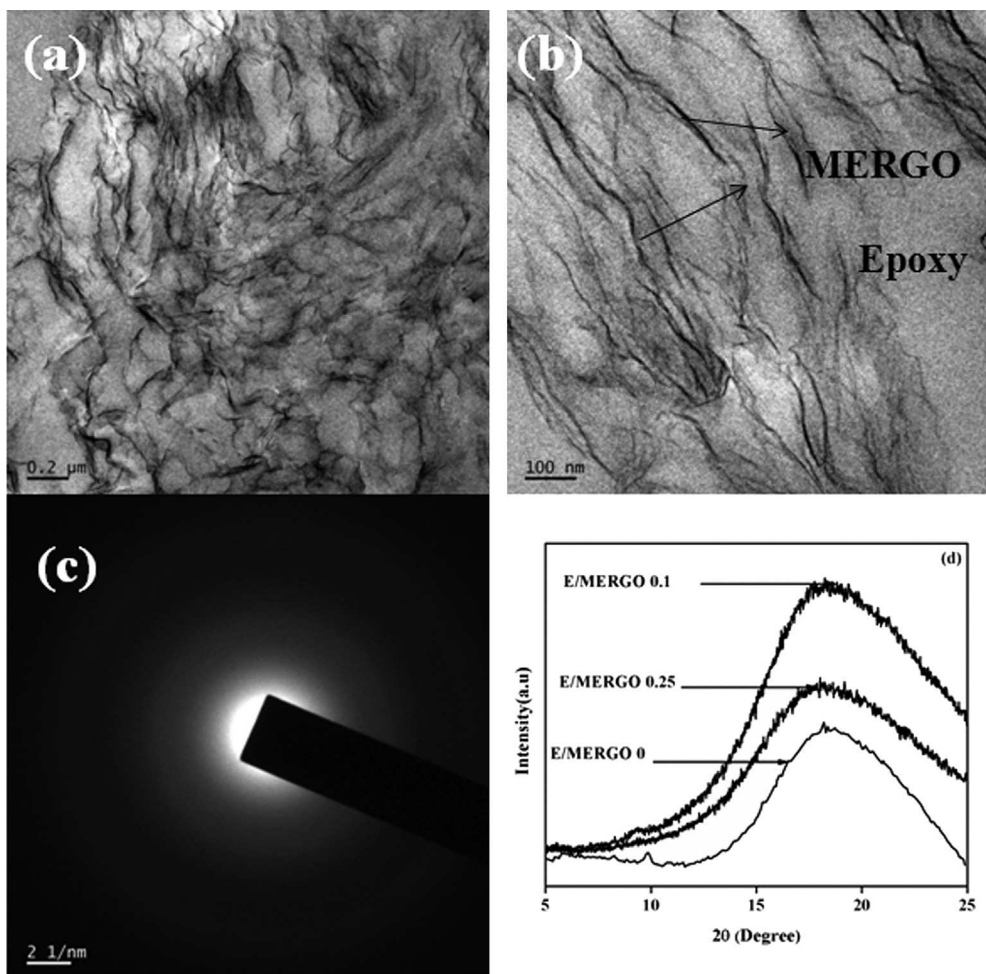


**Fig. 8.** (a & b) TEM image of E/MERGO nanocomposite with 0.25 phr MERGO loading at different magnification. (c) SAED pattern of E/MERGO at 0.25 phr loading. (d) XRD Pattern of pure epoxy and E/MERGO nanocomposites.

#### 4.5. Dielectric properties

The excellent dielectric properties with a low and stable dielectric constant within a wide range of frequencies make epoxy a favorite of the electronic industry [42]. However their applications are limited due to their low electrical conductivity. Moreover the molecular motions or dynamics of nanocomposites in response to various applied field have an intense connection with the macroscopic properties [43]. Again the dielectric property measurements can be used as a tool to understand the charge transport mechanism in conducting polymer composites. Hence these properties should be investigated in the case of E/MERGO nanocomposites. Fig. 10(a, b, d & e) shows the AC conductivity, real permittivity ( $\epsilon'$ ), imaginary permittivity ( $\epsilon''$ ) and dielectric loss tangent ( $\tan \delta = \epsilon''/\epsilon'$ ) as a function of the frequency (20 Hz–2 MHz) at room temperature for epoxy resin reinforced with different MERGO loadings. The AC conductivity is found to be increasing with increase in frequency [Fig. 10(a)]. Carbon materials such as graphene, CNTs, carbon fibers and carbon black are widely used to improve the electrical conductivity of composite materials [44–46].

The dependence of  $\epsilon'$  as a function of frequency ranging from 20 Hz to 2 MHz at room temperature for E/MERGO is plotted in Fig. 10(b). The  $\epsilon'$  for all samples exhibits a relatively large value at low frequency and remains nearly the same for a certain frequency range. The  $\epsilon'$  for neat epoxy and 0.1 phr MERGO loaded epoxy composites exhibits lower dielectric performance. For the other concentrations,  $\epsilon'$  increases with increase in loading and decreases with increase in frequency. At low frequencies, the dipole moments and the charge carriers can freely move within the E/MERGO nanocomposites and follow the varying electromagnetic field.

While at high frequencies dipole and charge carriers become unable to follow variations of the applied electric field resulting in a decrease in  $\epsilon'$ . In E/MERGO nanocomposites, the charges in conductive MERGO particles are easily delocalized, driven by the applied electric field. They accumulate at the interface of MERGO and epoxy insulator layers, leading to large scale polarization. As the MERGO content increases, Maxwell–Wagner (MW) polarization is significantly improved. Although the functional group present on the MERGO surface reduce the polarization process to some extent, the compatibility of MERGO/epoxy at the interface together with large surface area cause a 42% increase in  $\epsilon'$  at 0.5 phr MERGO loading.

Fig. 10(c) refers dielectric constant at different frequency with the MERGO loading. Variation of  $\epsilon'$  with MERGO loading is in agreement with Muradyan et al. [47]. Change in microstructure from fully exfoliated morphology of E/MERGO nanocomposites at lower loading to partially exfoliated or intercalated causes a decrease in interfacial polarization upto 2.5 phr. However with further loading, increase the number of intercalates, which decreases the thickness of dielectric spacers between conducting structures and increases the electrical capacitance. Moreover as the frequency of the applied electric field increases, gradually a situation arises, when dipoles present in the system can not reorient themselves fast enough to respond to applied field together with decreasing rate of interfacial polarization leads to a decrease in dielectric constant with increase in frequency.

The variation of  $\epsilon''$ , the imaginary part of complex permittivity and  $\tan \delta$  of E/MERGO nanocomposites with frequency is presented in Fig. 10(d) and (e) respectively. E/MERGO nanocomposites exhibit an initial decrease which may be due to some kind of relaxation and

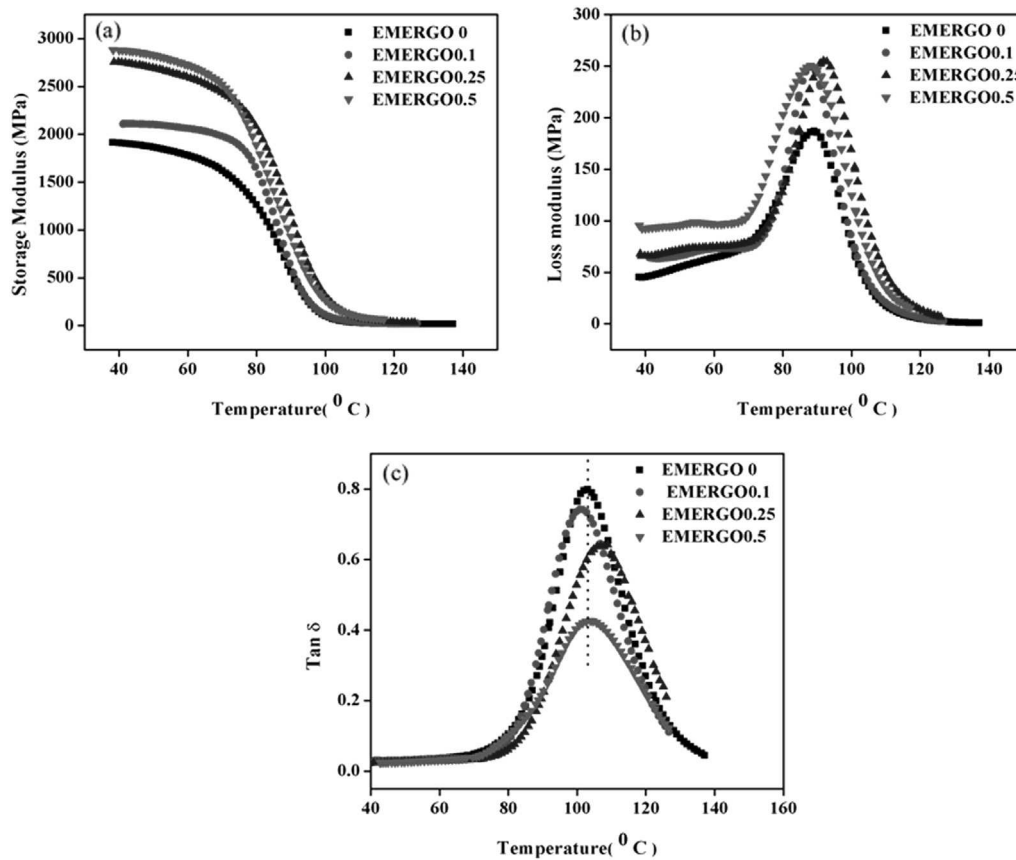


**Fig. 9.** Dynamic mechanical analysis, (a) storage modulus ( $E'$ ), (b) loss modulus ( $E''$ ), and (c) damping factor ( $\tan \delta$ ) for the pure epoxy and E/MERGO nanocomposites.

then increase of these properties with frequency. The dielectric behavior of composites depends up on the type of matrix, method of preparation, molecular structure, particle size and crystal structure. Dielectric loss arises due to the localized motion of charge carriers.

The electrical percolation network of the cured samples is also analyzed by measuring DC electrical conductivity depicted in Fig. 10(f). As we know, a sharp increase in the electrical conductivity of composites can be expected only when a continuous conductive network is formed by conductive nanoparticles. Moreover the filler need not be in direct contact for current flow, rather conduction can takes place via tunneling between thin polymer layers surrounding the filler particles [48]. It is well known that conductivity of a conductor–insulator composite follows the critical phenomenon around the percolation threshold which can be described by a scaling law in the form of  $\sigma \propto (p - p_c)^\beta$ , where  $\sigma$  is the composite

conductivity,  $p$  is the MERGO volume fraction,  $p_c$  is the percolation threshold and  $\beta$  is the critical exponent. The straight line graph from log–log plot of  $\sigma$  vs.  $(p - p_c/p_c)$  illustrated in the inset of Fig. 10(f) with  $p_c \sim 0.2696$  vol% (=0.5 phr) and  $\beta = 1.001$ , and a correlation factor of  $R^2 = 0.978$  gives a good fit to the data. The magnitude of increase of electrical conductivity in E/MERGO nanocomposites is lower compared to pristine graphene epoxy nanocomposites [49]. The functionalization disturbs the crystalline graphitic structure by reducing the number of  $\pi$  electrons and generating  $sp^3$  carbons, which do not cause such high electronic transport as  $\pi$  electrons in pristine graphene.

## 5. Conclusions

MERGO was synthesized from natural graphite through a simple, fast, and cost effective microwave exfoliation technique.

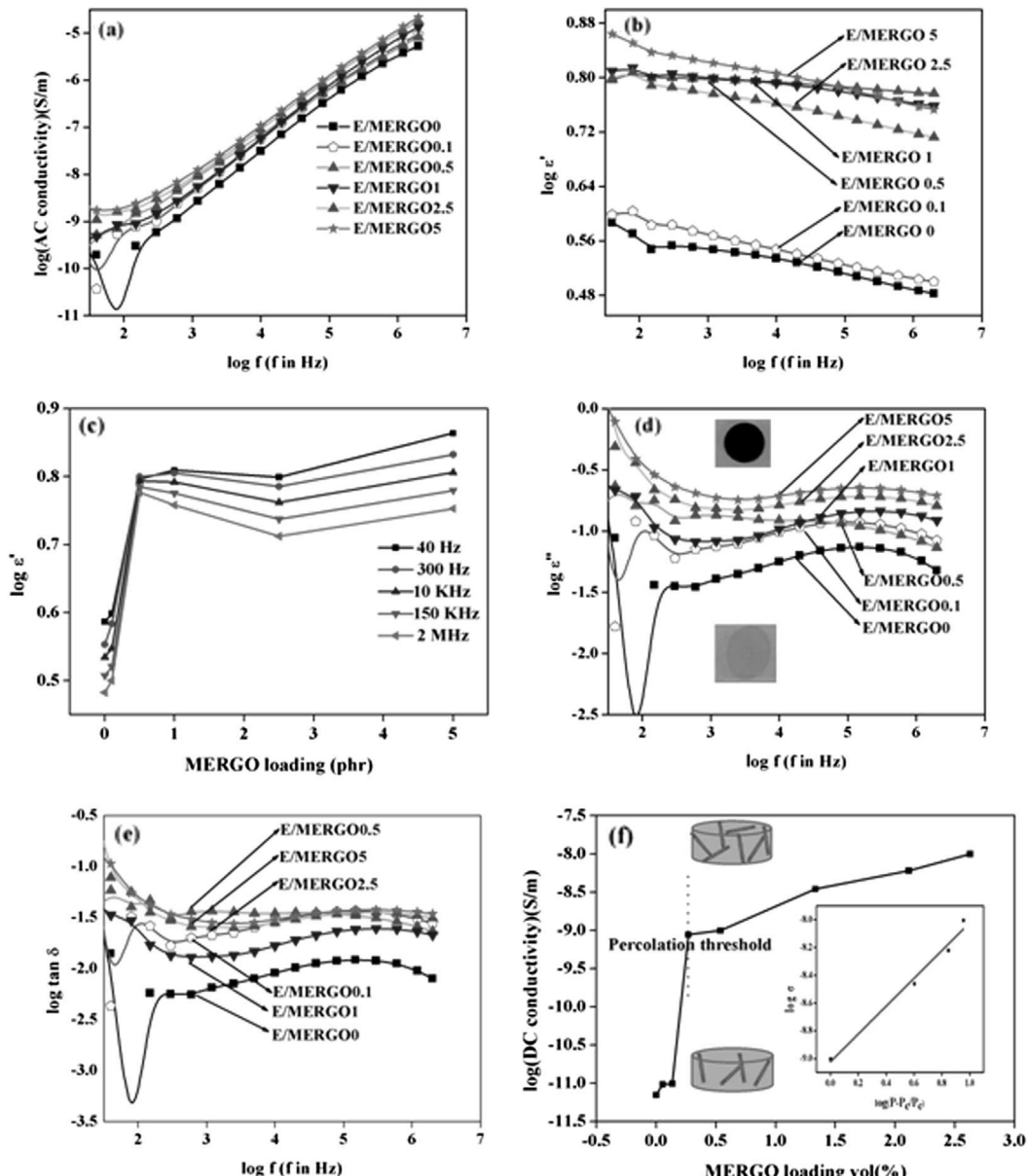


**Fig. 10.** Dielectric properties (a) AC conductivity, (b) Real permittivity ( $\epsilon'$ ), (c) Variation of real permittivity with MERGO loading, (d) Imaginary permittivity ( $\epsilon''$ ) [inset shows the samples for dielectric measurements] and (e) Dielectric loss tangent as a function of the frequency (20 Hz–2 MHz) at room temperature for pure epoxy and E/MERGO nanocomposites. (f) Variation of DC conductivity with MERGO loading [inset shows log–log plot of  $\sigma$  vs.  $(p - p_c/p_c)$ . Schematics of dispersion of MERGO in epoxy before (below) and at percolation (above) are also shown in inset].

Various techniques such as XRD, Raman, EDX, TGA, XPS, FTIR, C<sup>13</sup>NMR, SEM, TEM and UV-vis were adopted to establish the occurrence of simultaneous reduction and exfoliation during microwave exfoliation. E/MERGO nanocomposites were fabricated by incorporating conductive filler MERGO into the epoxy matrix. Static mechanical, dynamic mechanical and dielectric properties of the epoxy resin reinforced with MERGO were conducted. XRD, SEM and TEM were done to analyze the quality and quantity of micro structural distribution of MERGO in the epoxy matrix. The E/MERGO nanocomposites with 0.25 phr MERGO loading showed an enhancement of 32% in tensile strength, 103% in impact strength and 85% in flexural strength compared to pure epoxy. The 0.25 phr MERGO sheets incorporated into the epoxy matrix effectively disturbed the development of crack growth and prevented crack propagation and lead to a significant increase in stress intensity factor  $K_{IC}$  upto 63%. Morphological characterization such as SEM and TEM were performed on the E/MERGO nanocomposites and correlated with their mechanical performance. The storage modulus ( $E'$ ) of E/MERGO nanocomposites was higher than that of neat epoxy within the glassy state. Tg of E/MERGO 0.25 shifts slightly to a higher temperature (about 3–5 °C). The E/MERGO nanocomposite attained an ac conductivity of 10<sup>-5</sup> S/m and the dielectric constant was also remarkably increased. The combination of good processing properties with enhanced mechanical and dielectric properties makes MERGO great candidate to develop multifunctional polymer nanocomposites which has sought extensive application in Electromagnetic interference shielding (EMI), conductive adhesives and for thermal conductivity enhancement.

## References

- [1] Jeena JK, Narasimha Murthy HN, Rai KS, Krishna M, Sreejith M. *Polym Plast Technol Eng* 2010;49:1207–13.
- [2] Moazzami GM, Sharif F. *Express Polym Lett* 2012;6:1017–31.
- [3] Mildred Q, Ester V, Maurizio P. *Acc Chem Res* 2013;46:138–48.
- [4] Geim AK, Novoselov KS. *Nat Mater* 2007;6:183–90.
- [5] Liang-Xu D, Qiang C. *Front Mater Sci China* 2010;4(1):45–51.
- [6] Veerappan M, Shen MC, Bih SL. *Int J Electrochem Sci* 2013;8:11641–60.
- [7] Daniel RB, Erika GH, Ignacio MG. *Macromolecules* 2012;45:238–45.
- [8] Brodie BC. *Annales des Chimie et des Physique* 1860;59:466.
- [9] Staudenmaier L. *Verfahren zur L, Graphitsaure DD, Deutschen BD, Gesellschaft C* 1898;31:1481.
- [10] Hummers WS, Offeman RE. *J Am Chem Soc* 1958;80:1339.
- [11] Daniela CM, Dmitry V, Kosynkin, Jacob MB, Alexander S, Zhengzong S, et al. *ACS Nano* 2010;4:4806–14.
- [12] Dorsa P, Sriya D, Ahmed THS, Fahmida I, Sanjoy B, Micah JG. *ACS Nano* 2012;6: 8857–67.
- [13] Yanwu Z, Shanthi M, Meryl DS, Aruna V, Richard DP, Rodney SR. *Carbon* 2010;48:2118–22.
- [14] Li Y, Diyuan P, Shoubin CQ, Wang, Guangqin P, Wang T. *Mater Des* 2013;47: 850–6.
- [15] Chen Li, Songgang C, Kai L, Nanying N, Jian G, Qianfa L, et al. *ACS Appl Mater Interfaces* 2012;4:4398–404.
- [16] Alamri H, Low IM, Alothman Z. *Compos Part B* 2012;43:2762–71.
- [17] Park J, Jana SC. *Polymer* 2004;45:7673–9.
- [18] Narteh AT, Hosur M, Triggs E, Peter Owuor P, Jelaani S. *Polym Degrad Stab* 2014;101:81–91.
- [19] Gojny Florian H, Schulte K. *Compos. Sci Technol* 2004;64:2303–8.
- [20] Vennerberg D, Rueger Z, Kessler MR. *Polymer* 2014;55:1854–65.
- [21] Serra N, Maeder T, Ryser P. *Sens Actuators A Phys* 2012;186:198–202.
- [22] Liang Q, Nyugen MT, Moon KS, Watkins K, Morato LT, Wong CP. *J Electron Mater* 2013;42:1114–21.
- [23] Julia AK, Danielle RK, Ibrahim M, Greg MO. *J Appl Polym Sci* 2013;128: 4217–23.
- [24] Gallego MM, Bernal MM, Hernandez M, Verdejo R, Lopez-Manchado MA. *Eur Polym J* 2013;49:1347–53.
- [25] Yang SY, Lin WN, Huang YLi, Tien HW, Wang JY, Ma CCM, et al. *Carbon* 2011;49:793–803.
- [26] Zhang X, Alloul O, He Q, Zhu J, Verde MJ, Li Y, et al. *Polymer* 2013;54: 3594–604.
- [27] Zaman I, Phan TT, Kuan HC, Meng Q, Bao La LT, Luong LY, et al. *Polymer* 2011;52:1603–11.
- [28] Wang X, Xing W, Zhang P, Song L, Yang H, Hu Y. *Compos Sci Technol* 2012;72: 737–43.
- [29] Feng H, Wang X, Wu D. *Ind Eng Chem Res* 2013;52:10160–71.
- [30] Ni Z, Wang Y, Yu T, Shen Z. *Nano Res* 2008;1:273–91.
- [31] Joe Hodkiewicz. *Thermo scientific Application note 51946*.
- [32] Guo Y, Chenlu B, Song L, yuan B, Hu Y. *Ind Eng Chem Res* 2011;50:7772–83.
- [33] Liu J, Tang J, Goodling JJ. *J Mater Chem* 2012;22:12435–52.
- [34] Shi WM, Li J, Jun BD, Sheng XZ. *J Mater Sci* 2013;48:156–61.
- [35] Saw SWP, Mariatti M. *J Mater Sci Mater Electron* 2012;23:817–24.
- [36] Li Z, Young RJ, Wang R, Yang F, Hao L, Jiao W, et al. *Polymer* 2013;54:5821.
- [37] Wang L, Wang K, Chen L, Zhang Y, He C. *Compos Part A* 2006;37:1890–6.
- [38] Ma PC, Kim JK, Tang BZ. *Compos Sci Technol* 2007;67:2965–72.
- [39] Idicula M, Malhotra SK, Joseph K, Thomas S. *Compos Sci Technol* 2005;65: 1077–87.
- [40] Bindu P, Thomas S. *J Phys Chem B* 2013;117:12632–48.
- [41] Rao YQ, Pochan JM. *Macromolecules* 2007;40:290–6.
- [42] Sinh LH, Son BT, Trung NN, Lim DG, Shin SJ, Bae Y. *React Funct Polym* 2012;72: 542.
- [43] Sadashivuni KK, Ponnamma D, Thomas S, Grohens Y. *Prog Polym Sci* 2014;39: 749–80.
- [44] Kim H, Miura Y, Macosko CW. *Chem Mater* 2010;22:3441–50.
- [45] Long YZ, Chen ZJ, Zhang XT, Zhang J, Liu ZF. *Appl Phys Lett* 2004;85:1796–8.
- [46] Hu N, Masuda Z, Yan C, Yamamoto G, Fukunaga H, Hashida T. *Nanotechnology* 2008;19:215701.
- [47] Muradyan VE, Sokolov EA, Piven NP, Babenko SD, Allayarov SR. *Tech Phys Lett* 2010;36(12):1115–7.
- [48] Potts JR, Dreyer DR, Bielawski CW, Ruoff RS. *Polymer* 2011;52:5–25.
- [49] Lianga J, Wanga Y, Huangya Y, Maa Y, Liua Z, Caib J, et al. *Carbon* 2009;47: 922–5.



Cite this: RSC Adv., 2017, 7, 21918

# The influence of epitaxial crystallization on the mechanical properties of a high density polyethylene/reduced graphene oxide nanocomposite injection bar

Guibin Yao,<sup>a</sup> Tianchen Duan,<sup>a</sup> Minfang An,<sup>a</sup> Haojun Xu,<sup>a</sup> Feng Tian<sup>bc</sup> and Zongbao Wang <sup>\*a</sup>

High density polyethylene (HDPE)/reduced graphene oxide (RGO) nanocomposite bars were prepared by injection molding and the effects of RGO on the HDPE matrix were investigated. Differential scanning calorimetry results demonstrated that RGO was an effective nucleation agent for HDPE. Two dimensional wide angle X-ray diffraction (2D WAXD) results showed that the incorporation of RGO enhanced the degree of orientation of HDPE crystals in the flow direction but had no influence on the crystal structure of HDPE. Two dimensional small angle X-ray scattering (2D SAXS) results confirmed that the orientation of HDPE chains in the flow direction was enhanced with the increase of RGO content, which was attributed to the fact that RGO obstructed the motion of polymer chains. These results indicated that the incorporation of RGO can enhance the crystallization and orientation of the HDPE matrix, resulting in the improvement of mechanical properties.

Received 6th March 2017  
 Accepted 13th April 2017

DOI: 10.1039/c7ra02742g  
[rsc.li/rsc-advances](http://rsc.li/rsc-advances)

## 1. Introduction

Due to its excellent characteristics such as good physical and mechanical properties, chemical resistivity, gas barrier property, easy processing, and its low cost, HDPE has been widely used for film products, plastic products, hollow products, pipe products, fiber products, cable products *etc.*<sup>1–3</sup> However, further extension of the applications of HDPE has been limited by its mechanical properties.<sup>4–6</sup> Therefore, improving the mechanical properties of HDPE is an issue to be solved urgently.<sup>5,6</sup>

Nanocomposite materials in the past decades have attracted scientists' great attention as a promising novel class of materials, which can enhance properties significantly at very low loadings owing to their unique properties and numerous potential applications with greatly increased specific interfacial area.<sup>7–11</sup> It is well known that carbon based fillers, such as diamond and graphite, can particularly enhance the crystallization, orientation and mechanical properties of semi-crystalline polymer.<sup>12</sup> Drzal group showed that nanoparticle was a potential nano-reinforcement and it, as a 0 dimensional (0 D) point, could interact with the polymer matrix in improving the

mechanical properties.<sup>13–15</sup> Carbon nano tube (CNT), as 1 dimensional (1 D) material of graphite family, has also been proved that it could spectacularly reinforce the mechanical properties of HDPE matrix.<sup>16–18</sup> However, using carbon nanotubes in nanocomposite still contains many unresolved issues such as low interfacial interactions with the polymeric matrix.<sup>19</sup>

Graphene as the first 2D counterpart of graphite with single sheet was widely used.<sup>20–24</sup> It can also work as filler.<sup>25</sup> It is also found to be the strongest material up to now.<sup>26</sup> A lot of studies showed that graphene could improve the mechanical properties of polymers.<sup>27–29</sup> It is well known that the mechanical properties of polymer/nanofiller composites strongly depend on the interaction between polymer and nanofiller. Great efforts have been devoted to improve the interaction between graphene and polymer matrix.<sup>30–32</sup> However, most researches still use the common methods of other polymer/inorganic nanocomposites to improve the interface adhesion,<sup>33</sup> seldom make the best use of the structure character of graphene and its matching relationship with polymer structure. The researches using nondestructive physical modification methods to increase the interface adhesion between polymer and graphene are less, and the studies about interfacial crystallization to enhanced interaction of polymer/graphene nanocomposites are much less. Petermann *et al.* reported that epitaxial interfaces with strong adherence were responsible for the improvement of the mechanical properties of semicrystalline polymers.<sup>34–36</sup> Fukumaru<sup>52</sup> reported that effective interfacial interaction between the polybenzoxazole and CNT could improve the mechanical

<sup>a</sup>Ningbo Key Laboratory of Specialty Polymers, Faculty of Materials Science and Chemical Engineering, Ningbo University, Ningbo 315211, PR China. E-mail: wangzongbao@nbu.edu.cn

<sup>b</sup>Shanghai Institute of Applied Physics, Chinese Academy of Sciences, Shanghai 201204, PR China

<sup>c</sup>State Key Laboratory of Polymer Materials Engineering, Sichuan University, Chengdu 610065, PR China



properties of polymer matrix.<sup>37</sup> In our previous work, the yield strength and Young's modulus of poly(*e*-caprolactone) (PCL)/RGO nanocomposites with epitaxial interaction were improved compared with pure PCL.<sup>38,39</sup>

It is well known that epitaxial crystallization of polymers onto various polymeric substrates, since the early 1980s, has been an extremely active subject in the field of polymer science.<sup>40–42</sup> It is generally accepted that the occurrence of polymer epitaxy is based on some certain crystallographic matches, *e.g.*, a coincidence of unit cell dimensions, and the highest limit for the occurrence of the epitaxial growth is assumed to be 15%.<sup>43</sup> Previous literature showed that polyethylene could epitaxial crystallized on graphene surface, and the mismatch rate was –5.0%.<sup>44</sup> Moreover the melting point of HDPE is much higher than that of PCL, which may resulting in different enhancement of mechanical properties. Therefore HDPE was chosen as a model polymer to study the epitaxial crystallization on RGO.

In this work, we take advantage of the polymer epitaxial crystallization on RGO to improve the interfacial interaction between RGO and HDPE, and study the influence of epitaxial crystallization on the mechanical properties of polymer matrix. The WAXD and SAXS measurements were used to investigate the reinforcement effect and structural mechanism.

## 2. Experimental

### 2.1. Materials

HDPE was purchased from Dow Chemical Company, with average weight  $M_n = 15\ 820\ g\ mol^{-1}$  and polydispersity index  $M_w/M_n = 4.9$ . Natural flake graphite was purchased from Qingdao Jiuyi graphite Co., Ltd. (Shandong, China) with mean particle size of 50  $\mu m$ . Hydrochloric acid (HCl) (37%), sulfuric acid ( $H_2SO_4$ ) (98%), potassium nitrate ( $KNO_3$ ), potassium permanganate ( $KMnO_4$ ), hydrogen peroxide ( $H_2O_2$ ) (35%), *n*-hexanol and chloroform were purchased from Sinopharm Chemical Reagent Co., Ltd. (Shanghai, China). All reagents were used as received without further purification.

### 2.2. Sample preparation

GO was exfoliated by ultra-sonication from graphite oxide which was produced by modified Hummers' method.<sup>45</sup> RGO was prepared by thermal exfoliation and reduction of GO.<sup>46</sup> The standard bars of HDPE/RGO nanocomposites of 50 mm  $\times$  4 mm  $\times$  2 mm in size with different RGO contents (0, 0.1, 0.5 and 1.0 wt%) were melt mixed using HAAKE MiniLab. The melt temperature, the screw speed, mold temperature and injection pressure were preset at 180 °C, 80 °C, 80 °C and 650 bar, respectively.

### 2.3. Analytical methods

Tensile test was performed on Instron 5567 at a tensile rate of 50 mm min<sup>-1</sup>. Five standard bars for each sample were measured and the average values were calculated.

Differential scanning calorimetry (DSC) measurements were performed with Perkins Elmer DSC8000 under nitrogen

atmosphere. All samples were first heated to 180 °C at a heating rate of 10 °C min<sup>-1</sup>, and equilibrated at 180 °C for 5 min to remove thermal history. Subsequently, the samples were cooled to 30 °C at a cooling rate of 10 °C min<sup>-1</sup>. The crystallinity of the HDPE in mass fraction,  $X_c$ , was calculated as follow:

$$X_c = \frac{\Delta H}{\Delta H_m^0} \times 100\% \quad (1)$$

where  $\Delta H$  is the melting enthalpy of per gram of sample and  $\Delta H_m^0$  is the enthalpy of crystallization per gram of 100% crystalline HDPE, which is equal to 293 J g<sup>-1</sup>.

2D WAXD experiments were carried out on the BL16B1 beam-line in the Shanghai Synchrotron Radiation Facility (SSRF). WAXD curves were collected from the 2D WAXD patterns. The wavelength of the monochromatic X-ray was 1.24 Å. The 2D diffraction patterns were recorded in transmission mode at room temperature.

2D SAXS experiments were carried out on the BL16B1 beam-line in the SSRF. The 2D patterns were recorded in transmission mode at room temperature and the sample-to-detector distance was 2000 mm.

The SAXS and WAXD data analysis were performed out by using the Fit2d software package.<sup>47</sup> The lamellae parameters derived from the SAXS data is named the long period  $L$ . It can be calculated according to the Bragg equation:

$$L = \frac{2\pi}{q^*} \quad (2)$$

$q^*$  represents the peak position in the scattering curves.

## 3. Results and discussion

### 3.1. Mechanical properties

In order to investigate the influence of epitaxial crystallization on the mechanical properties of polymer matrix, tensile test was employed. Fig. 1 shows the stress-strain curves of pure HDPE and HDPE/RGO nanocomposites with different RGO contents and the inset shows the magnification around the yield point. It can be observed that the composite sample tends to reach the upper yield point with the increase of RGO contents. The effect

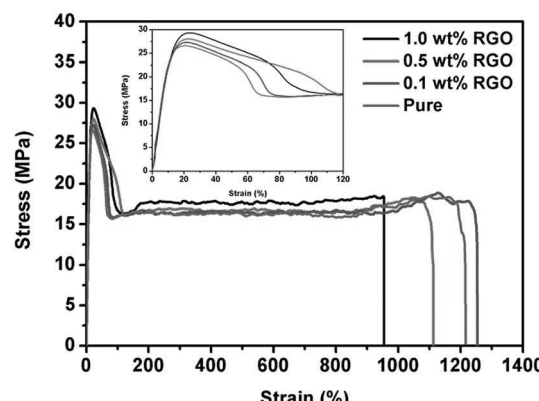


Fig. 1 Stress–strain curves of pure HDPE and its nanocomposites with various RGO contents.



of RGO content on the mechanical properties is shown in Fig. 2. Compared to pure HDPE, yield strength increases from  $26.7 \pm 0.3$  to  $29.6 \pm 0.1$  MPa and Young's modulus increases from  $244.9 \pm 6.1$  to  $379.4 \pm 6.1$  MPa for HDPE/RGO nanocomposites with 1.0 wt% RGO, which achieves 10.9 and 54.9% increase, respectively. This result is consistent with that of our previous work which showed the enhancement of PCL mechanical properties by RGO.<sup>38</sup>

### 3.2. Crystallization and orientation of HDPE/RGO nanocomposites

The DSC heating curves of neat iPP and iPP/RGO nanocomposites with different RGO loadings are shown in the Fig. 3a. The degree of crystallinity calculated from formula (1) is 62.5%, for pure HDPE, but the values increase to 56.1%, 57.0% and 58.4% as the RGO contents from 0.1 to 0.5, 1.0 wt%. These results are not agree with our previous work.<sup>39</sup> For the degree of crystallization decrease with 0.1 wt% RGO contents compare with the pure HDPE, we speculate that the incorporation of RGO destroys HDPE original lamellae and form smaller lamellae. While HDPE chains can be absorbed on the RGO surface and

grow into crystals at the cooling process because of epitaxial crystallization. With the increase of RGO contents, the orientation degree of HDPE chains is enhanced. And the degree of crystallization of nanocomposite increases. The DSC cooling curves of pure HDPE and HDPE/RGO nanocomposites with different RGO contents are presented in Fig. 3b. The crystallization temperature ( $T_c$ ) is around 110 °C for pure HDPE, while the  $T_c$  progressively shifts to high temperature with the increase of RGO contents from 0.1 wt% to 1.0 wt%. For example, it increases to 113 °C for HDPE/RGO-1.0 nanocomposites. These results indicate that RGO can significantly enhance the non-isothermal melt crystallization of HDPE.

### 3.3. WAXD analysis

The final properties of the injection molded bars are closely linked with the orientation of the lamellae in the nanocomposites. Fig. 4 gives the 2D WAXD patterns of injection-molded bars of pure HDPE and HDPE/RGO nanocomposites. From inner to outward, the diffraction circles are designated to the (110) and (200) crystal planes of polyethylene crystals, respectively. The corresponding WAXD curves of samples

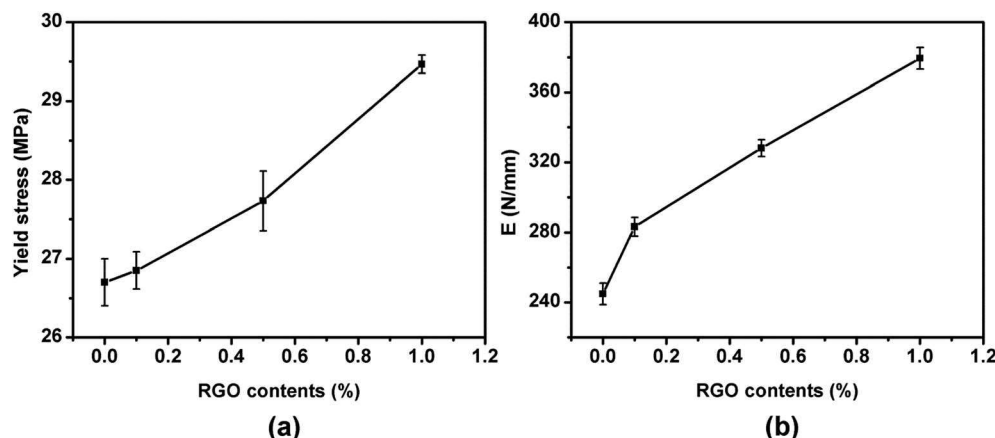


Fig. 2 The effect of RGO content on the mechanical properties: (a) yield stress (b) Young's modulus ( $E$ ).

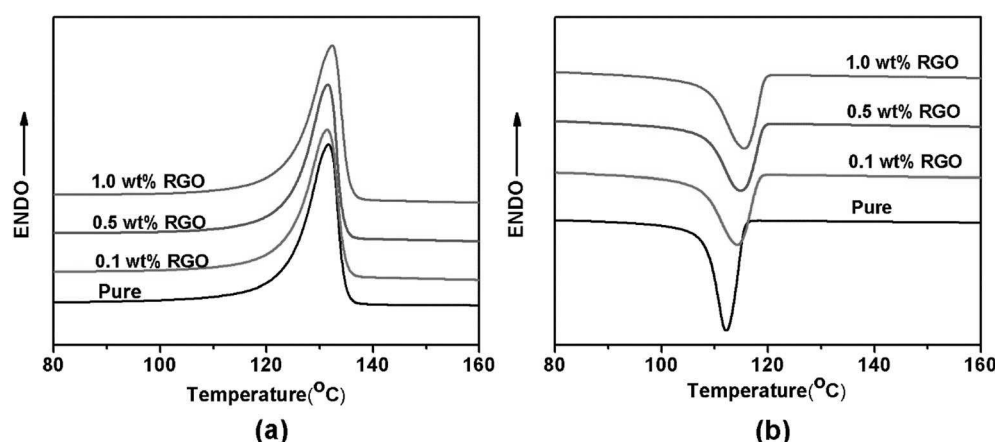


Fig. 3 Nonisothermal DSC scans of neat iPP and iPP/RGO nanocomposites with different RGO loadings (a) heating, (b) cooling.

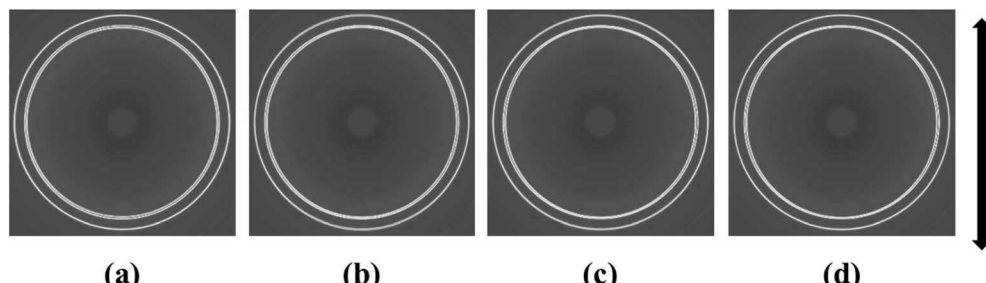


Fig. 4 2D WAXD patterns of pure HDPE (a) and its nanocomposites with different RGO contents: (b) 0.1 wt%, (c) 0.5 wt% and (d) 1.0 wt% (the arrow represents the orientation of the bars).

collected from 2D WAXD patterns shown in Fig. 5, which present the same two typical diffraction peaks at  $2\theta = 17.2^\circ$  and  $19.2^\circ$  corresponding to (110) and (200) crystal planes, respectively, suggesting that the crystal structure of HDPE remains unchanged despite the presence of RGO in the HDPE/RGO nanocomposites. It can be found in Fig. 4 that two isotropic circles are observed for pure HDPE, while two weakly focused diffraction focused arcs are found in the HDPE/RGO nanocomposites. The differences in the patterns demonstrate an enhancement of the crystalline orientation and an improvement of anisotropic degree of diffraction arcs with the increase of RGO content. It can be observed more clearly the influence of RGO on the crystallization of HDPE through 3D WAXD patterns shown in Fig. 6. With the increase of RGO content, the intensity of the two crystal plane diffraction rings are strengthened perpendicular to the sample injection flow direction and became less parallel to the injection flow direction. The differences in the 3D WAXD patterns indicate that the strong interaction between RGO and HDPE leads to more chain orientation and crystallization and the increase of RGO contents may hinders the relaxation of chains between HDPE and RGO during the orientation and crystallization process.

The 2D SAXS patterns from melt-crystallized isotropic samples typically display a strong scattering ring and one or two higher orders of much lower intensity. The SAXS pattern of an oriented sample typically displays strong two-point patterns

with a maximum in the draw or flow direction or within certain angle about the reference direction.<sup>48</sup> Fig. 7 shows 2D SAXS patterns of pure HDPE and its nanocomposites. An almost isotropic reflection circle and two small scattering spots are observed in pure HDPE (Fig. 7a). For HDPE/RGO nanocomposites, small scattering spots gradually become bulb-shape lobes in the meridian direction with the increase of RGO. Moreover, the scattering disks change from circular ring for pure HDPE to elliptical ring for HDPE/RGO nanocomposites. It is different from our previous work that the PCL/RGO nanocomposites have no periodic structure in center part.<sup>38</sup> The result seems to indicate that more HDPE chains can epitaxial crystallize on the RGO surface than PCL. We can clearly observe the periodic structure at the center of the patterns for HDPE/RGO nanocomposites. The center of pure HDPE has no periodic structure, but with the increase of RGO contents, scattering pattern of direction in the equator and meridian direction the periodic structure are both enhanced. The changes of two parts of pure HDPE and its nanocomposites can be observed through 3D SAXS patterns (Fig. 8). Obviously, the scattering intensity of both ends is enhanced at the flow direction, at the same time the scattering intensity of the center is strengthened with the increase of RGO contents.

In order to investigate the orientation and periodic structure of HDPE matrix, SAXS intensity profiles of pure HDPE and its nanocomposites are further presented. Fig. 9a shows azimuthally integrated profiles of all samples. It can be observed that two weak peaks in pure HDPE parallel to the sample injection flow direction, which implies that the flow field can promote the orientation of HDPE crystals. The orientation degree of HDPE chains is enhanced significantly in the meridian direction and increased with the increase of RGO content. Fig. 9b shows the radially integrated profiles of meridian direction, the sharp peaks reflect the center part in the 2D SAXS patterns and the flat peaks reflect the scattering outer ring which are used to calculate the long period of HDPE matrix using the eqn (2). Apparently, for the two bulb-shape lobes all samples have the same long period calculated to be about 22.4 nm, suggesting regular aligned crystal lamellae in HDPE matrix. The  $q$  value of intensity valley (solid line in Fig. 9b) increases with the addition of RGO. These results indicate that the orientation of polymer chains is enhanced with the incorporation of RGO and the thickness of periodic structure increase.

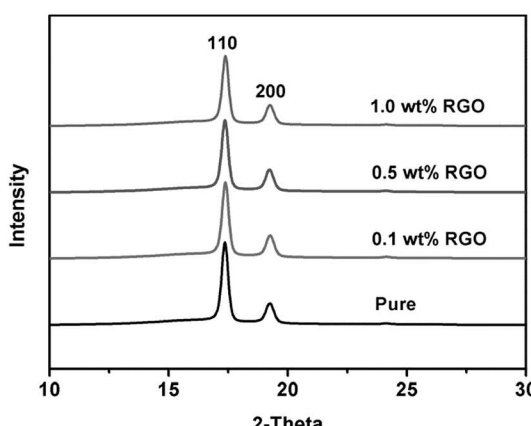
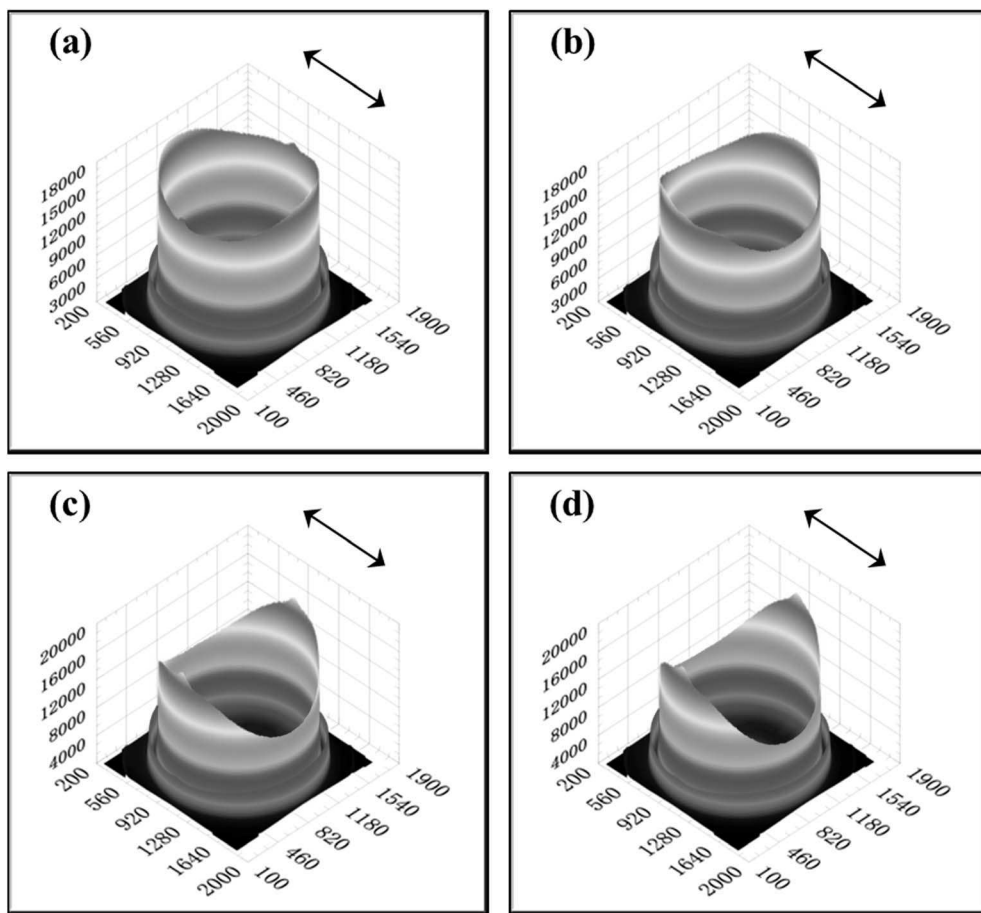
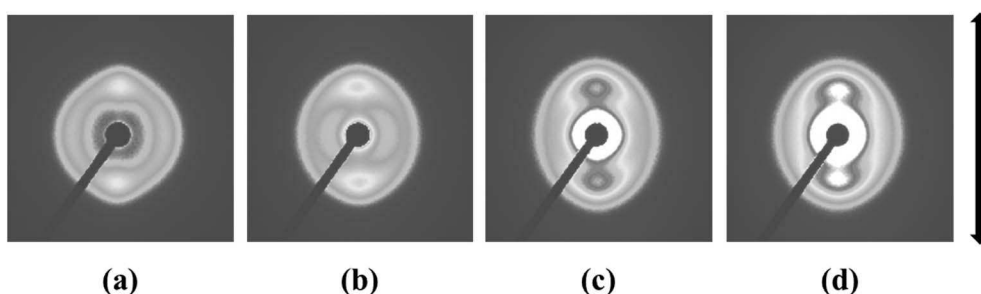


Fig. 5 WAXD curves of pure HDPE and HDPE/RGO nanocomposites with various RGO contents.





**Fig. 6** 3D WAXD patterns of pure HDPE (a) and its nanocomposites with different RGO contents: (b) 0.1 wt%, (c) 0.5 wt% and (d) 1.0 wt% (the arrows represent the orientation of the bars).



**Fig. 7** 2D SAXS patterns of pure HDPE (a) and its nanocomposites with different RGO contents: (b) 0.1 wt%, (c) 0.5 wt% and (d) 1.0 wt% (the arrow represents the orientation of the bars).

In our previous work, Wang *et al.* proved that RGO could induce PCL chain epitaxial crystallization on the surface, and the chains in the epitaxial crystallized lamellae were parallel to the flow direction in injection process.<sup>38</sup> On the basis of the aforementioned results in this paper, it can be concluded that the similar structural results are obtained in HDPE/RGO nanocomposites. Chen *et al.* reported that in the polymer/CNT composites, the CNT could preferentially orient parallel to the drawing direction in the stretched.<sup>49,50</sup> Similarly, the RGO sheets could orientation in the flow direction, during injection

process. The mechanism is thought to be similar to that of PCL/RGO nanocomposites in our previous work and it can be sketched as follows. Intensive shear flow during injection process not only leads 2D layered RGO sheets to the parallel orientation along flow direction but also stretches HDPE chains to high orientation even to extended form along same direction. Hu *et al.* proved that the relaxation of polymer chains would induce the loss in mechanical properties.<sup>51</sup> Paralleled 2D layered RGO sheets restrict the rapid mobility of HDPE chains resulting in delayed relaxation of oriented polymer chains.

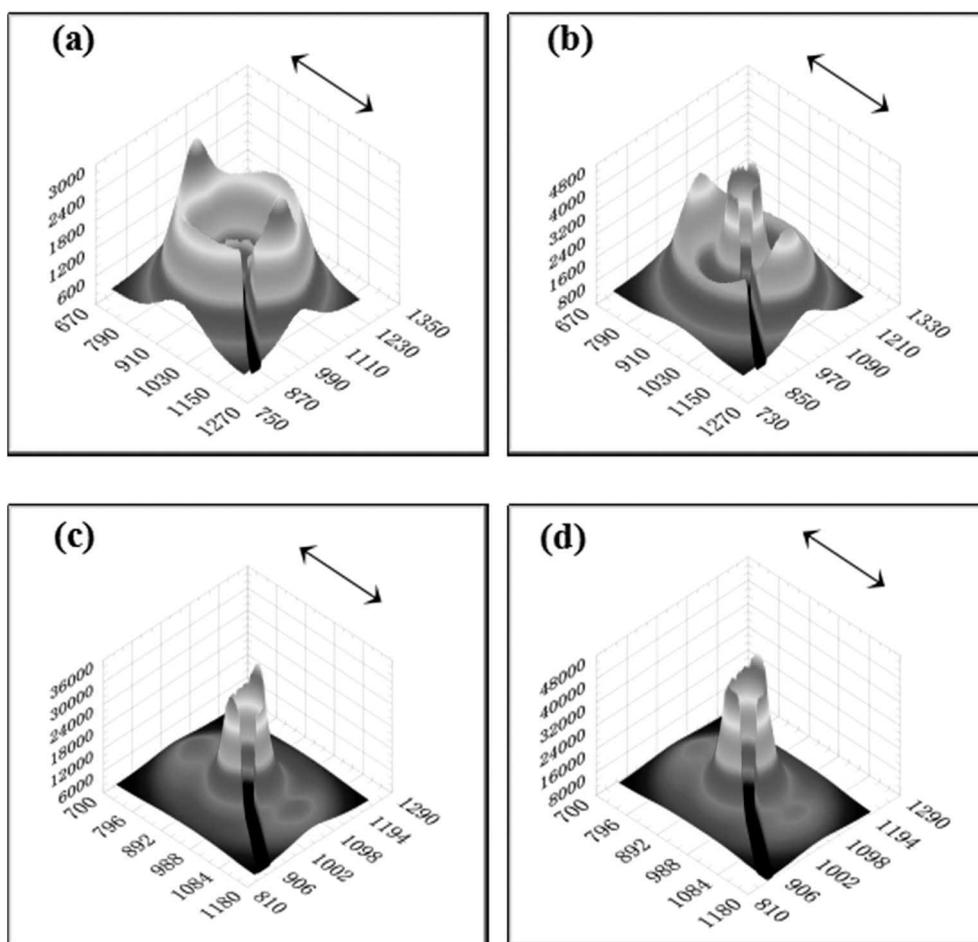


Fig. 8 3D SAXS patterns of pure HDPE (a) and its nanocomposites with different RGO contents: (b) 0.1 wt%, (c) 0.5 wt% and (d) 1.0 wt% (the arrows represent the orientation of the bars).

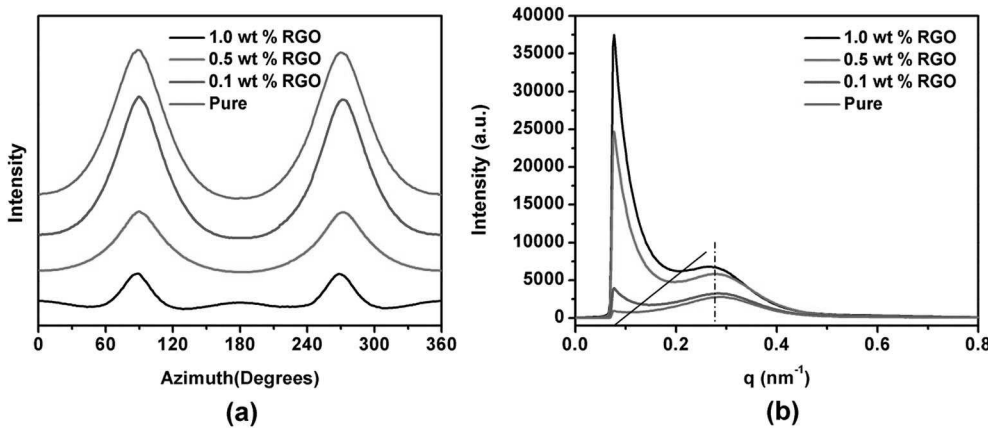


Fig. 9 Azimuthally integrated (a) and radially integrated, (b) profiles of pure HDPE and its nanocomposites with different RGO contents.

HDPE chains can be absorbed on the RGO surface and grow into crystals at the cooling process because of epitaxial crystallization. It is worth mentioning that the *c* axis is not completely paralleling to the flow direction on the basis of WAXD results above because the periodic structure of RGO is along three

directions with the intersection angle of  $60^\circ$ . It should be noted that there seems more epitaxial crystallized crystals in HDPE/RGO nanocomposites compared to PCL/RGO nanocomposites from the SAXS result mentioned above. It is known that the epitaxial crystallization is due to the lattice matching between

RGO and polymer lamellae. Therefore the quantities of epitaxial crystallization on the surface of RGO during the injection process are generally determined by the lattice matching. The lattice mismatch  $R$  between an epitaxial crystal and a substrate crystal can be calculated as follows

$$R [\%] = \frac{d_E - d_S}{d_S} \times 100 \quad (3)$$

were  $d_E$  and  $d_S$  are spacings of 2D lattices at the interface of the epitaxial crystal and the substrate crystal, respectively. The  $a$ -axis of RGO was measured to be 0.246 nm.<sup>52</sup> Previous literature showed that the mismatch rate between polyethylene and graphene was  $-5.0\%$ .<sup>53</sup> According to the crystal cell of PCL,<sup>54</sup> the mismatch rate between PCL and graphene was calculated to be  $(1.726 - 0.246 \times 7)/(0.246 \times 7) = 0.2\%$ . The epitaxial crystallization of HDPE on RGO is weaker than that of PCL only considering the mismatch rate. But it cannot be ignored that the calculation of mismatch rate between PCL and RGO above is based on seven periods and ester group in PCL chain seriously destroys the match between C-C and RGO. That more epitaxial crystallized crystals are obtained in HDPE/RGO nanocomposites may be attributed to the combination of the two above reasons. It is worth noting that the increase of mechanical properties of PCL/RGO nanocomposites is slightly higher than that of HDPE/RGO with same weight ratio RGO. It is may be due to that the affection of epitaxial crystallization on RGO on the mechanical properties of PCL is slightly higher because the mechanical properties are measured at room temperature which is near to the melting point of PCL compared to HDPE. According to the above analysis, the improvement in mechanical properties can be summed up in two aspects: one aspect is the natural excellent strength of graphene,<sup>55</sup> another one is speculated be attributed to epitaxial interaction between RGO and HDPE as the results exhibited above.

## 4. Conclusions

The effects of RGO on the crystallization and orientation of HDPE matrix in HDPE/RGO nanocomposites have been investigated by DSC, SAXS and WAXD measurements. The crystalline peak moves to the high temperature with the increase of RGO contents, indicating that RGO can significantly enhance the melt crystallization of HDPE. Though low orientation level of the matrix crystalline phase is observed in all nanocomposites but the WAXD results indicate that RGO can enhance the crystalline orientation of HDPE in the injection-molded bars. SAXS results suggest HDPE chains can be absorbed on the RGO surface and grow into crystals at the cooling process, which induces HDPE periodic structure increasing. This research is expected to be helpful for understanding the enhancement mechanism of layered nanofiller on the structures and corresponding mechanical properties of semi-crystalline polymer film or slice. To best understand the enhancement mechanism of polymer/layered nanofiller nanocomposites, especially for the nanofiller with space lattice matching to polymer, *in situ* structural evolution investigation during the stretching process

of PCL/RGO and HDPE/RGO nanocomposites injection bars by online SAXS/WAXD measurements is ongoing.

## Acknowledgements

This work was supported by the National Science Foundation of China (U1532114), Natural Science Foundation of Ningbo Municipal (2015A610021), and K. C. Wong Magna Fund in Ningbo University. Financially supported by the Opening Project of State Key Laboratory of Polymer Materials Engineering (Sichuan University) (Grant No. sklpme2016-4-26). We thank Shanghai Synchrotron Radiation Facility (SSRF) for supporting the SAXS and WAXD test.

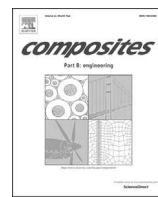
## References

- P. B. Willis and C. H. Hsieh, *Kobunshi*, 2000, **49**, 52.
- M. T. Demeuse, *Biaxial Stretching of Film: Principles and Applications*, Woodhead Publishing: Oxford, 2011.
- J. S. Kang, T. H. Han, Y. J. Kang and H. Y. Chai, *Composites, Part B*, 2009, **40**, 404–412.
- G. Choudalakis and A. D. Gotsis, *Eur. Polym. J.*, 2009, **45**, 967–984.
- A. U. Chaudhry and V. Mittal, *Polym. Eng. Sci.*, 2013, **53**, 78–88.
- Y. F. Chen, Y. Y. Qi, Z. X. Tai, X. B. Yan, F. L. Zhu and Q. J. Xue, *Eur. Polym. J.*, 2012, **48**, 1026–1033.
- Z. Q. Hu and G. M. Chen, *Adv. Mater.*, 2014, **26**, 5950–5956.
- L. R. Liang, C. Y. Gao, G. M. Chen and C. Y. Guo, *J. Mater. Chem. C*, 2016, **4**, 526–532.
- M. Rahmat and P. Hubert, *Compos. Sci. Technol.*, 2011, **72**, 72–84.
- B. Na, Q. Zhang, Q. Fu, G. Zhang and K. Z. Shen, *Polymer*, 2002, **43**, 7367–7376.
- T. X. Liu, K. P. Lim, W. C. Tjiu, K. P. Pramoda and Z. K. Chen, *Polymer*, 2003, **44**, 3529–3535.
- W. Cao, K. Wang, Q. Zhang, R. N. Du and Q. Fu, *Polymer*, 2006, **47**, 6857–6867.
- P. Zhao, K. Wang, H. Yang, Q. Zhang, R. N. Du and Q. Fu, *Polymer*, 2007, **48**, 5688–5695.
- K. Kalaitzidou, H. Fukushima and L. T. Drzal, *Composites, Part A*, 2007, **38**, 1675–1682.
- K. Kalaitzidou, H. Fukushima and L. T. Drzal, *Carbon*, 2007, **45**, 1446–1452.
- S. Kanagaraj, F. R. Varanda, T. V. Zhil'tsova, M. S. A. Oliveira and J. A. O. Simoes, *Compos. Sci. Technol.*, 2007, **67**, 3071–3077.
- W. D. Zhang, L. Shen, I. Y. Phang and T. X. Liu, *Macromolecules*, 2004, **37**, 256–259.
- I. Neitzel, V. Mochalin, I. Knoke, G. R. Palmese and Y. Gogotsi, *Compos. Sci. Technol.*, 2011, **71**, 710–716.
- J. N. Coleman, U. Khan, W. J. Blau and Y. K. Gun'ko, *Carbon*, 2006, **44**, 1624–1652.
- C. Peng, W. B. Hu, Y. T. Zhao, C. H. Fan and Q. Huang, *Small*, 2010, **6**, 1686–1692.
- J. J. Ma, Y. Li, X. D. Yin, Y. Xu, J. Yue, J. J. Bao and T. Zhou, *RSC Adv.*, 2016, **6**, 49448–49458.



- 22 Z. J. Wang, F. Cheng, T. Winsor and Y. M. Liu, *Nanotechnology*, 2016, **27**, 412001.
- 23 K. L. Xu, G. M. Chen and D. Qiu, *J. Mater. Chem. A*, 2013, **1**, 12395–12399.
- 24 C. Y. Gao and G. M. Chen, *Compos. Sci. Technol.*, 2016, **124**, 52–70.
- 25 K. S. Novoselov, A. K. Geim, S. V. Morozov, D. Jiang, Y. Zhang, S. V. Dubonos, I. V. Grigorieva and A. A. Firsov, *Science*, 2004, **306**, 666–669.
- 26 C. Lee, X. Wei, J. W. Kysar and J. Hone, *Science*, 2008, **321**, 385–388.
- 27 H. Kim, A. A. Abdala and C. Macosko, *Macromolecules*, 2010, **43**, 6515–6530.
- 28 T. Kuilla, S. Bhadra, D. Yao, N. Kim, S. Bose and J. Lee, *Prog. Polym. Sci.*, 2010, **35**, 1350–1375.
- 29 R. Verdejo, M. M. Bernal, L. J. Romasanta and M. A. Lopez-Manchado, *J. Mater. Chem.*, 2011, **21**, 3301–3310.
- 30 E. Belyarova, M. E. Itkis, P. Ramesh, C. Berger, M. Sprinkle, W. A. Herr and R. C. Haddon, *J. Am. Chem. Soc.*, 2009, **131**, 1336–1337.
- 31 Y. Li, *Polymer*, 2011, **52**, 2310–2318.
- 32 C. Shan, H. Yang, D. Han, Q. Zhang, A. Ivaska and L. Niu, *Langmuir*, 2009, **25**, 12030–12033.
- 33 J. T. Paci, T. Belytschko and G. C. Schatz, *Phys. Rev. B: Condens. Matter*, 2006, **74**, 184112.
- 34 J. Petermann, G. Broza, U. Rieck and A. Kawaguchi, *J. Mater. Sci.*, 1987, **22**, 1477–1481.
- 35 J. Petermann and Y. Xu, *Colloid Polym. Sci.*, 1991, **269**, 455–459.
- 36 B. Gross and J. Petermann, *J. Mater. Sci.*, 1984, **19**, 105–112.
- 37 T. Fukumaru, T. Fujigaya and N. Nakashima, *Macromolecules*, 2013, **46**, 4034–4253.
- 38 B. J. Wang, Y. J. Zhang, J. Y. Zhang, H. Y. Li, P. Chen, Z. B. Wang and Q. Gu, *Ind. Eng. Chem. Res.*, 2013, **52**, 15824–15828.
- 39 B. J. Wang, Y. G. Li, G. S. Weng, Z. Q. Jiang, P. Chen, Z. B. Wang and Q. Gu, *Compos. Sci. Technol.*, 2014, **96**, 63–70.
- 40 S. K. Yan, D. C. Yang and J. Petermann, *Polymer*, 1998, **39**, 4569–4578.
- 41 S. K. Yan, J. Petermann and D. C. Yang, *Polymer*, 1996, **37**, 2681–2685.
- 42 Y. J. Sun, H. H. Li, Y. Huang, E. Chen, L. Zhao, Z. H. Gan and S. K. Yan, *Polymer*, 2006, **47**, 2455–2459.
- 43 J. C. Wittmann and B. Lotz, *Prog. Polym. Sci.*, 1990, **15**, 909–948.
- 44 Y. Takenaka, H. Miyaji, A. Hoshino, A. Tracz, J. K. Jeszka and I. Kucinska, *Macromolecules*, 2004, **37**, 9667–9669.
- 45 Y. Wang, Z. H. Li, D. H. Hu, C. T. Lin, J. H. Li and Y. H. Lin, *J. Am. Chem. Soc.*, 2010, **132**, 9274–9276.
- 46 B. J. Wang, H. Y. Li, L. Z. Li, P. Chen, Z. B. Wang and Q. Gu, *Compos. Sci. Technol.*, 2013, **89**, 180–185.
- 47 A. P. Hammersley, S. O. Svensson and A. Thompson, *Nucl. Instrum. Methods Phys. Res.*, 1994, **346**, 312–321.
- 48 A. Prasad, R. Shrof, S. Rane and G. Beaucage, *Polymer*, 2001, **42**, 3103–3113.
- 49 C. P. Yuan, J. H. Zhang, G. M. Chen and J. P. Yang, *Chem. Commun.*, 2011, **47**, 899–901.
- 50 C. P. Yuan, J. J. Wang, G. M. Chen, J. H. Zhang and J. P. Yang, *Soft Matter*, 2011, **7**, 4039–4044.
- 51 W. B. Hu, A. Buzin, J. S. Lin and B. Wunderlich, *J. Polym. Sci., Part B: Polym. Phys.*, 2003, **41**, 403–417.
- 52 F. Tuinstra and E. Baer, *J. Polym. Sci., Part B: Polym. Phys.*, 1970, **8**, 861–865.
- 53 Y. Takenaka, H. Miyaji, A. Hoshino, A. Tracz, J. K. Jeszka and I. Kucinska, *Macromolecules*, 2004, **37**, 9667–9669.
- 54 H. L. Hu and D. L. Dorset, *Macromolecules*, 1990, **23**, 4604–4607.
- 55 C. G. Lee, X. D. Wei, J. W. Kysar and J. Hone, *Science*, 2008, **321**, 385–388.





# Ultra high molecular weight polyethylene/graphene oxide nanocomposites: Thermal, mechanical and wettability characterisation

S. Suñer <sup>a,\*</sup>, R. Joffe <sup>a</sup>, J.L. Tipper <sup>b</sup>, N. Emami <sup>a</sup>

<sup>a</sup> Division of Machine Elements, Luleå University of Technology, Luleå SE-971 87, Sweden

<sup>b</sup> Institute of Medical and Biological Engineering, Leeds, UK

## ARTICLE INFO

### Article history:

Received 24 January 2015

Received in revised form

21 March 2015

Accepted 24 March 2015

Available online 1 April 2015

### Keywords:

A. Polymer-matrix composites (PMCs)

A. Nano-structures

D. Mechanical testing

D. Thermal analysis

Total joint replacements

## ABSTRACT

Numerous carbon nanostructures have been investigated in the last years due to their excellent mechanical properties. In this work, the effect of the addition of graphene oxide (GO) nanoparticles to UHMWPE and the optimal %wt GO addition were investigated. UHMWPE/GO nanocomposites with different GO wt% contents were prepared and their mechanical, thermal, structural and wettability properties were investigated and compared with virgin UHMWPE. The results showed that the thermal stability, oxidative resistance, mechanical properties and wettability properties of UHMWPE were enhanced due to the addition of GO. UHMWPE/GO materials prepared with up to 0.5 wt% GO exhibited improved characteristics compared to virgin UHMWPE and nanocomposites prepared with higher GO contents.

© 2015 Elsevier Ltd. All rights reserved.

## 1. Introduction

Over the last century, joint replacements have enabled thousands of people with joints damaged by disease or trauma to enjoy a more active lifestyle. Advances in manufacturing techniques, materials and implant designs, as well as operative techniques, have resulted in implants able to last for more than 20 years [1]. Ultra high molecular weight polyethylene (UHMWPE) is the material most commonly used among hard-on-soft bearings in artificial joints. UHMWPE implants have exhibited excellent clinical performance during the last two decades [2]. However, wear and oxidation of this material are two major problems directly related to the eventual failure of joint implants [3].

To date, crosslinking of the polyethylene molecular chains through gamma irradiation has been the method used to improve the wear performance of UHMWPE. Previous studies have demonstrated that, after exposure to 10 MRad irradiation, the wear resistance of UHMWPE is improved by up to 90% [4]. Although irradiation leads to enhanced wear characteristics, the mechanical properties of UHMWPE are compromised after crosslinking [5]. In

addition, free radicals generated during the irradiation process lead to a higher susceptibility to oxidation. Different post-irradiation processing methods have been developed to minimise the negative impacts of irradiation on the final properties of polyethylene [6]. Nevertheless, a compromise between mechanical strength, oxidative resistance and wear resistance remains.

In order to address these issues, the development of novel materials with improved wear and oxidative resistance, able to extend the life of the implant, has generated great interest. In particular, the addition of carbon nanostructures to improve the final performance of materials has been a topic of interest over the last few years not only in the orthopaedic field but also in other industries, such as the automotive and aerospace industries [7]. Multi-walled carbon nanotubes have been investigated as a reinforcement material to improve the final mechanical properties of neat polyethylene [8,9]. These materials have demonstrated the ability to improve the wear characteristics and oxidative resistance of UHMWPE without compromising its biocompatibility [10–12] and research concerning material processing and manufacturing to achieve homogeneous nanocomposites are currently ongoing [13].

Graphene oxide has also been suggested as an interesting filler for polymers due to its superior mechanical properties, such as excellent in-plane strength and high surface area [14,15], but little

\* Corresponding author. Tel.: +46 (0)920 49 2832.

E-mail address: [silvia.suner@ltu.se](mailto:silvia.suner@ltu.se) (S. Suñer).

attention has been paid to the possibilities of using graphene oxide as a reinforcement material for UHMWPE matrices [16,17].

The main objectives of this work were to investigate the effect of the addition of GO nanoparticles to UHMWPE and to determine the optimal %wt GO addition to achieve an enhanced nanocomposite performance. In this work, UHMWPE/GO nanocomposites with different GO wt% contents were prepared and their mechanical, thermal, structural and wettability properties were investigated and compared with virgin UHMWPE.

## 2. Materials and methods

### 2.1. Materials

UHMWPE/GO nanocomposites were manufactured with UHMWPE GUR 1020 powder supplied by Ticona (Germany) and GO monolayer powder obtained from Nanoinnova Technologies (Spain). UHMWPE GUR 1020 had an average molecular weight of  $3.5 \times 10^6$  g/mol, density of 0.93 g/cm<sup>3</sup> and the average size of particles was 140 µm. GO sheets had an average particle length of 3–5 µm and a thickness of 0.7–1.2 nm.

### 2.2. Nanocomposite preparation

A ball milling technique was utilised under optimised conditions [17] to prepare UHMWPE/GO nanocomposite powders with different GO wt% content (0.1, 0.3, 0.5, 0.7, 1 and 2 wt%). Briefly, the following steps were followed to prepare the UHMWPE/GO mixtures; first, the required GO wt% content was dispersed in 30 ml of ethanol and blended with the UHMWPE powder. The slurry was then sealed in a zirconium oxide grinding jar containing zirconium oxide balls with a diameter of 5 mm. A planetary ball mill (Retsch PM 100, Germany) was used at a mixing speed of 400 rpm during 2 h to prepare the UHMWPE/GO mixtures. These parameters have been previously identified as optimal conditions for preparing UHMWPE/GO nanocomposites [17]. After ball milling, ethanol was removed at 60 °C in an oil bath under stirring and the powder was kept at 60 °C in an oven during 24 h until it was fully dried. Nanocomposite and UHMWPE GUR 1020 powders were moulded into 65 × 25 × 2 mm<sup>3</sup> and 115 × 17 × 2 mm<sup>3</sup> sheets using a hot press at 185 °C under 15 MPa pressure.

### 2.3. Characterisation techniques

#### 2.3.1. Thermal characterisation

Differential scanning calorimetry (DSC, Mettler Toledo, Germany) measurements were performed to study the melting temperature, crystallisation temperature and crystallinity of virgin UHMWPE GUR 1020 and the different UHMWPE/GO nanocomposites. Experiments were performed under nitrogen atmosphere at a rate of 80 ml/min and samples weighed between 6 and 7 mg. Samples were subjected to a heating-cooling-heating scan to eliminate thermal histories between 30 °C and 200 °C at 10 °C/min. The crystallinity of the samples was calculated according to Eq. (1).

$$X_c(\%) = \frac{\Delta H}{\Delta H_{100}} \cdot 100 \quad (1)$$

where ΔH is the total heat energy per unit mass and ΔH<sub>100</sub> is the enthalpy of fusion of a 100% crystalline sample, fixed to be 289 J/g [18]. The range of integration used was 50–160 °C. The reported values were the average of three measurements.

Thermal stability of the samples was evaluated by thermogravimetry analysis (TGA). Tests were performed under air atmosphere on a TG Q500 (TA Instruments, New Jersey USA) between

room temperature and 700 °C at a heating rate of 10 °C/min and samples weighed between 6 and 7 mg, according to the method of Martinez-Morlanes et al. [19]. The reported values were the average of three measurements.

#### 2.3.2. Mechanical characterisation

Tensile tests were performed on a tensile machine (Instron 3366). Young's modulus, yield stress, fracture stress and fracture strain were determined from the stress-strain curves. Tests were performed at a crosshead speed of 10 mm/min with a gauge length of 60 mm. Fracture toughness tests were performed in selected samples (virgin UHMWPE GUR 1020, UHMWPE/GO 0.3 wt% and UHMWPE/GO 2 wt%). Tests were performed using a dynamic test machine (Instron Electropuls 10000) in nitrogen atmosphere at –100 °C. Single edged notched bend specimens were tested in three point bending and K<sub>IC</sub> was calculated according to [20]. The reported values were the average of three measurements. Microhardness measurements were carried out with a load of 10 g in all the UHMWPE/GO nanocomposites and virgin UHMWPE GUR 1020. The reported values were the average of ten measurements.

#### 2.3.3. Contact angle measurements

The wettability of the UHMWPE/GO nanocomposites and virgin UHMWPE GUR 1020 was determined by contact angle measurements. A 4 µl drop of distilled water was deposited on the sample surface and measurements were taken after one second. The sessile drop method was used to determine the water contact angles. The reported values were the average of ten measurements.

#### 2.3.4. High resolution scanning electron microscopy (HR-SEM)

HR-SEM was employed to investigate the fracture surface of samples. Prior to observation, samples were frozen in liquid nitrogen and fractured.

#### 2.3.5. Gamma irradiation and ageing effects

In order to determine the effect of gamma irradiation and ageing on the UHMWPE/GO nanocomposites, selected samples (virgin UHMWPE GUR 1020, UHMWPE/GO 0.5 wt% and UHMWPE/GO 2 wt%) were prepared and subjected to gamma irradiation and posterior ageing. Gamma irradiation of the samples was performed in air at room temperature with a dose of 75 KGy (Synergy Health, Netherlands). Ageing was performed in air at 80 °C for 3 weeks according to [21]. Tensile tests on irradiated samples and irradiated-aged samples were performed under same conditions described for non-irradiated samples. The reported values were the average of three measurements.

## 3. Results

### 3.1. Thermal characterisation

Differential scanning calorimetry (DSC) and thermogravimetric analysis were used to evaluate the effect of the addition of GO at different %wt on the thermal stability of UHMWPE. Melting temperature (T<sub>m</sub>), crystallisation temperature (T<sub>c</sub>) and degree of crystallinity (X<sub>c</sub>) of virgin UHMWPE GUR 1020 and the UHMWPE/GO nanocomposites are shown in Table 1. Melting and crystallisation temperatures remained constant at all of the GO concentrations and similar values were observed to virgin UHMWPE. Little change in the degree of crystallinity was observed due to the addition of GO.

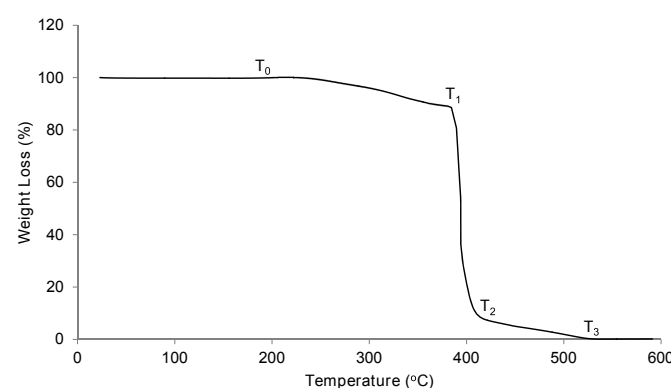
An example of the TGA decomposition curves obtained for UHMWPE showing demarcated temperatures, T<sub>0</sub>, T<sub>1</sub>, T<sub>2</sub>, and T<sub>3</sub>, is shown in Fig. 1. Demarcated temperatures for virgin UHMWPE and UHMWPE/GO nanocomposites are reported in Fig. 2. The addition

**Table 1**

Crystallisation parameters of UHMWPE/GO nanocomposites and UHMWPE.

Material	$T_m$ (°C) ± SD	$T_c$ (°C) ± SD	$X_c$ (%) ± SD
Virgin UHMWPE	134.9 ± 0.5	115.0 ± 0.7	51.2 ± 0.6
UHMWPE/GO 0.1 wt%	135.4 ± 0.5	114.5 ± 0.6	49.2 ± 1.4
UHMWPE/GO 0.3 wt%	134.5 ± 0.6	115.8 ± 0.6	50.4 ± 1.1
UHMWPE/GO 0.5 wt%	135.1 ± 0.2	114.9 ± 0.3	50.4 ± 0.7
UHMWPE/GO 0.7 wt%	136.7 ± 0.7	113.7 ± 0.4	50.0 ± 0.1
UHMWPE/GO 1.0 wt%	135.5 ± 0.3	115.0 ± 0.3	50.5 ± 1.5
UHMWPE/GO 2.0 wt%	135.3 ± 0.4	114.9 ± 0.5	50.4 ± 0.8

SD: Standard deviation.

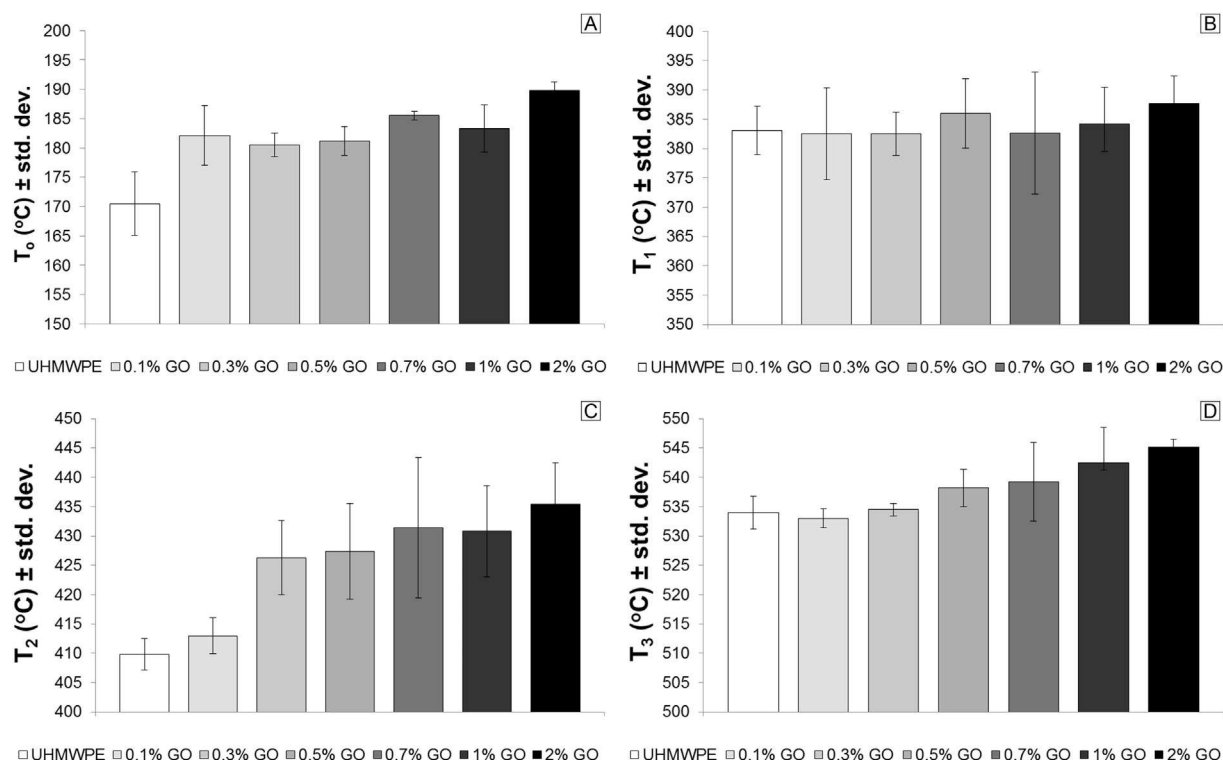
**Fig. 1.** Thermogravimetry analysis. Typical decomposition curve for virgin UHMWPE.

of GO had a notable influence on the thermal behaviour of UHMWPE. The oxidation temperatures,  $T_o$  (Fig. 2a), measured for the UHMWPE/GO nanocomposites increased with increasing concentration of GO, being significantly higher than that of virgin

UHMWPE at all the concentrations. The linear weight loss stage,  $T_1$  (Fig. 2b), experienced a slight increase due to the addition of GO. An increase at the end of the linear weight loss,  $T_2$  (Fig. 2c), compared with virgin UHMWPE was found for the UHMWPE/GO nanocomposites for all the concentrations, being more noticeable with increasing amounts of GO. A similar trend was found for the temperature of complete volatilisation,  $T_3$  (Fig. 2d), which experienced an increase compared to that of virgin UHMWPE due to the addition of GO.

### 3.2. Mechanical characterisation

The influence of GO on the Young's modulus, yield stress, fracture stress, fracture strain and fracture toughness of UHMWPE is shown in Fig. 3. UHMWPE/GO nanocomposites showed enhanced mechanical properties compared to virgin UHMWPE. The Young's modulus (Fig. 3a) and yield stress (Fig. 3b) increased by approximately 15% due to the addition of GO. The fracture stress (Fig. 3c) of the nanocomposites increased up to approximately 25% compared to virgin UHMWPE. Slight changes were measured in the fracture strain (Fig. 3d) of the samples, except for the UHMWPE/GO 2 wt%, which exhibited a significant decrease compared to virgin UHMWPE. In general, the mechanical properties of the nanocomposites improved for samples prepared with a small wt % GO content, reaching an optimum up to 0.5 wt% and then started to decrease with the addition of higher concentrations of GO. This trend can be clearly seen in the reported fracture stress and fracture strain values, where optimum values were obtained for samples prepared with up to 0.5 wt% and significantly lower values compared to virgin UHMWPE were found for nanocomposites prepared with 2 wt % GO content. A similar trend was observed for the fracture toughness (Fig. 3e) experiments performed on UHMWPE, UHMWPE/GO 0.3 wt % and UHMWPE 2 wt%. Virgin UHMWPE and UHMWPE/GO 0.3 wt% samples exhibited similar

**Fig. 2.** Thermal stability parameters,  $T_o$  (A),  $T_1$  (B),  $T_2$  (C) and  $T_3$  (D), of UHMWPE and UHMWPE/GO nanocomposites.

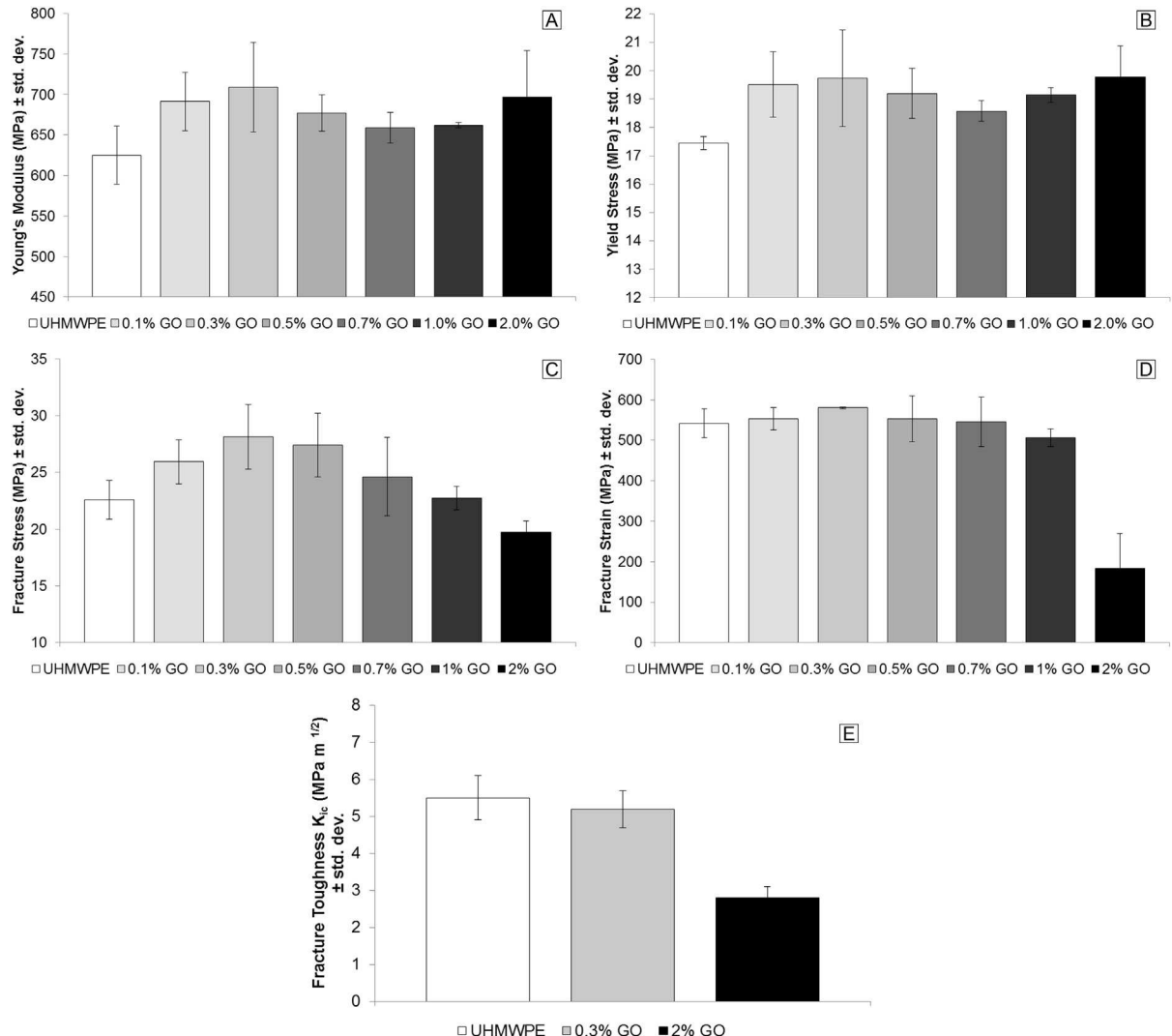


**Fig. 3.** Mechanical properties, Young's modulus (A), yield stress (B), fracture stress (C), fracture strain (D) and fracture toughness (E), of UHMWPE and UHMWPE/GO nanocomposites.

fracture toughness values,  $K_{Ic}$ , while UHMWPE/GO 2 wt% exhibited a significantly lower  $K_{Ic}$ . Microhardness measurements are detailed in Fig. 4. UHMWPE/GO nanocomposites showed higher hardness compared to virgin UHMWPE, exhibiting an increase with increasing amount of wt% GO content.

### 3.3. Contact angle measurements

The contact angles measured for the UHMWPE/GO nanocomposites and virgin UHMWPE are reported in Fig. 5. Nanocomposites prepared with 0.1, 0.3 and 0.5 wt% exhibited

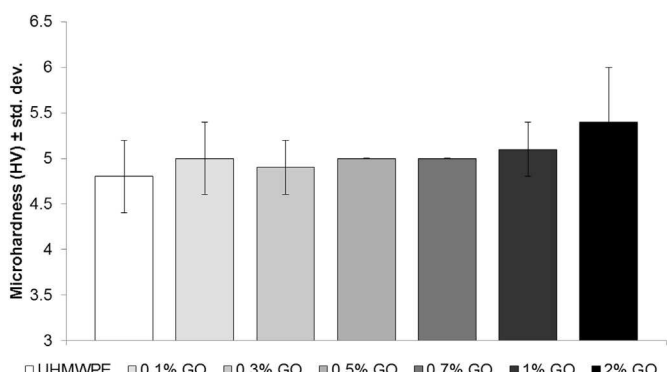


**Fig. 4.** Microhardness values of UHMWPE and UHMWPE/GO nanocomposites.

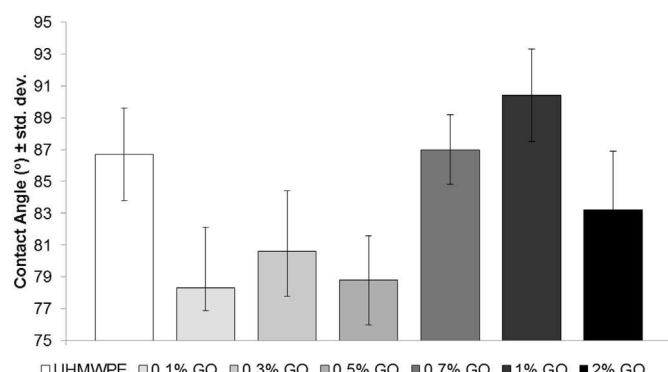


**Fig. 5.** Contact angle measurements of UHMWPE and UHMWPE/GO nanocomposites.

significantly lower contact angles and, consequently, significantly enhanced wettability compared to virgin UHMWPE. Nano-composites prepared with higher % wt GO content (0.7, 1 and 2 wt %) exhibited a similar contact angle and, consequently, similar wettability to that reported for virgin UHMWPE.

#### 3.4. Gamma irradiation and ageing effects

The influence of gamma irradiation and ageing on the mechanical properties of virgin UHMWPE and UHMWPE/GO 0.5 wt% and 2 wt% is reported in Fig. 6. The Young's modulus (Fig. 6a) increased for all the samples exposed to the gamma irradiation treatment and further increased due the ageing treatment, however the Young's Modulus of UHMWPE/GO samples (0.5 and 2 wt%)

were affected to a lesser extent by the ageing treatment than virgin UHMWPE (~28% increase versus ~5% and 7% increase, respectively). The yield stress (Fig. 6b) of virgin UHMWPE and UHMWPE/GO samples increased after gamma irradiation and ageing, again UHMWPE/GO nanocomposites were affected to a lesser extent than the virgin UHMWPE. The fracture stress (Fig. 6c) for virgin UHMWPE followed a different trend compared to the GO nano-composites. While the fracture stress of virgin UHMWPE increased after gamma irradiation, the fracture stress of the UHMWPE/GO nanocomposites decreased after treatment. After ageing, the fracture stress of virgin UHMWPE significantly decreased (~32%) however, the UHMWPE/GO nanocomposites were much less affected (~18% decrease for 0.5 wt% and ~3% decrease for 2 wt%).

#### 3.5. Fracture surfaces

The fracture surfaces of virgin UHMWPE and the UHMWPE/GO nanocomposites are shown in Fig. 7. Samples prepared with 0.1, 0.3 and 0.5 wt% GO content exhibited an even fracture surface, similar to that of virgin UHMWPE. No aggregates of GO were observed for any of the UHMWPE/GO samples. However, samples prepared with higher concentration of GO exhibited a different fracture surface compared to that of virgin UHMWPE, showing a more uneven surface for the sample with the highest wt% GO amount (UHMWPE/GO 2 wt%).

#### 4. Discussion

Through the present study, the effect of the addition of GO as a UHMWPE reinforcement has been investigated, and differences between nanocomposites prepared with different GO wt% content have been analysed. Although the thermal behaviour of UHMWPE was enhanced with increasing concentrations of GO, the mechanical and wettability properties, as well as the SEM investigation, showed a different trend for nanocomposites prepared with up to 0.5 wt% GO content compared to nanocomposites prepared with higher GO concentrations (0.7–2 wt%). For example, nanocomposites prepared with 2 wt% GO content exhibited a ~30% reduction in fracture stress compared to nanocomposites prepared with 0.3 wt% GO content. In general, UHMWPE/GO materials prepared with concentrations of GO up to 0.5 wt% exhibited optimal mechanical and wettability properties compared to virgin UHMWPE and nanocomposites with higher GO content. These differences might be attributed to the formation of GO clusters when high concentration is added to the polymer, leading to inhomogeneous samples and, consequently, failure to achieve optimal properties. It could also be hypothesised that the polyethylene matrix might be saturated when high concentrations of GO are added, leading to a decrease in the mechanical performance of the material. This hypothesis is supported by results from a study by Tai et al. [16], who found that the wear resistance of UHMWPE/GO composites decreased as the GO content increased, up to values of 0.7 wt %, but after that the wear rate showed little change. Ionita et al. [22] also reported similar results on the effect of graphene oxide on polysulfone; composites with low content of GO, up to 1 wt%, showed enhanced tensile strength in comparison to neat polysulfone, but further addition of GO induced mechanical properties detraction due to poor dispersion.

In order to maximise the potential of GO as a reinforcement material for polyethylene matrices, it is not only the wt% of GO that is important, but also the method of preparation of the materials. In a study performed by Chen et al. [23] UHMWPE/GO nanocomposites were prepared by ultrasonication. However, the reported tensile test values showed little or no enhancement compared to virgin UHMWPE. In our investigation, UHMWPE/GO

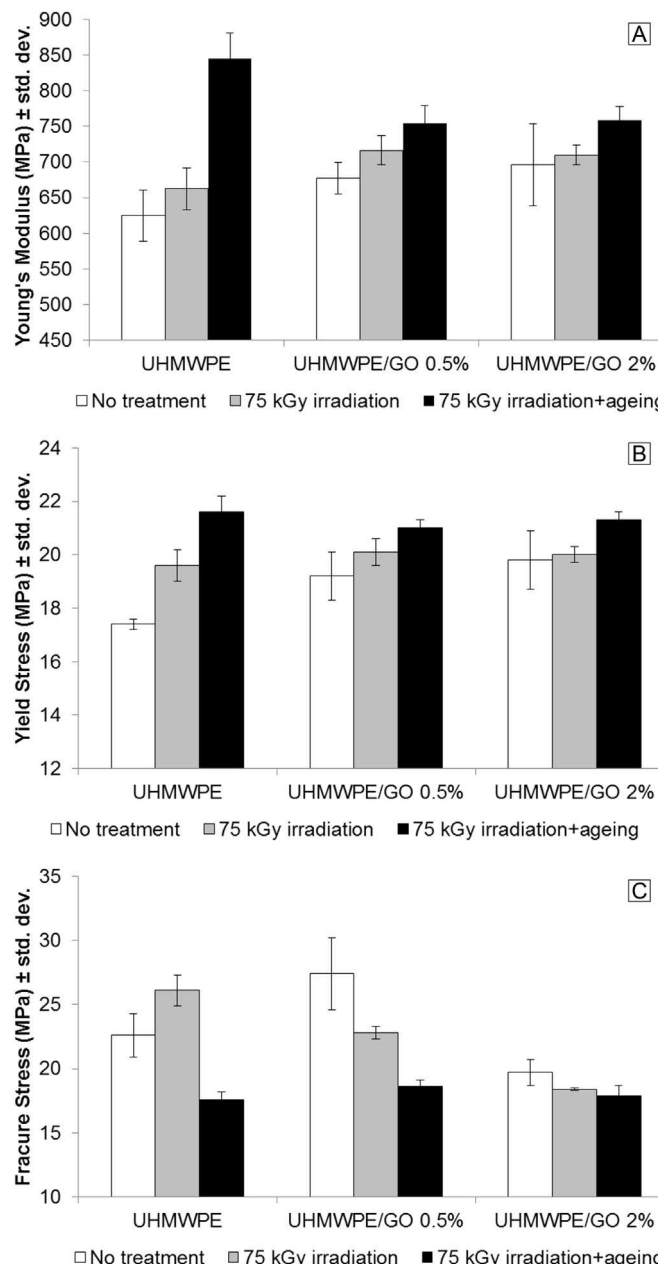


**Fig. 6.** Mechanical properties, Young's modulus (A), yield stress (B) and fracture stress (C) of non-treated, irradiated and irradiated plus aged UHMWPE and UHMWPE/GO nanocomposites.

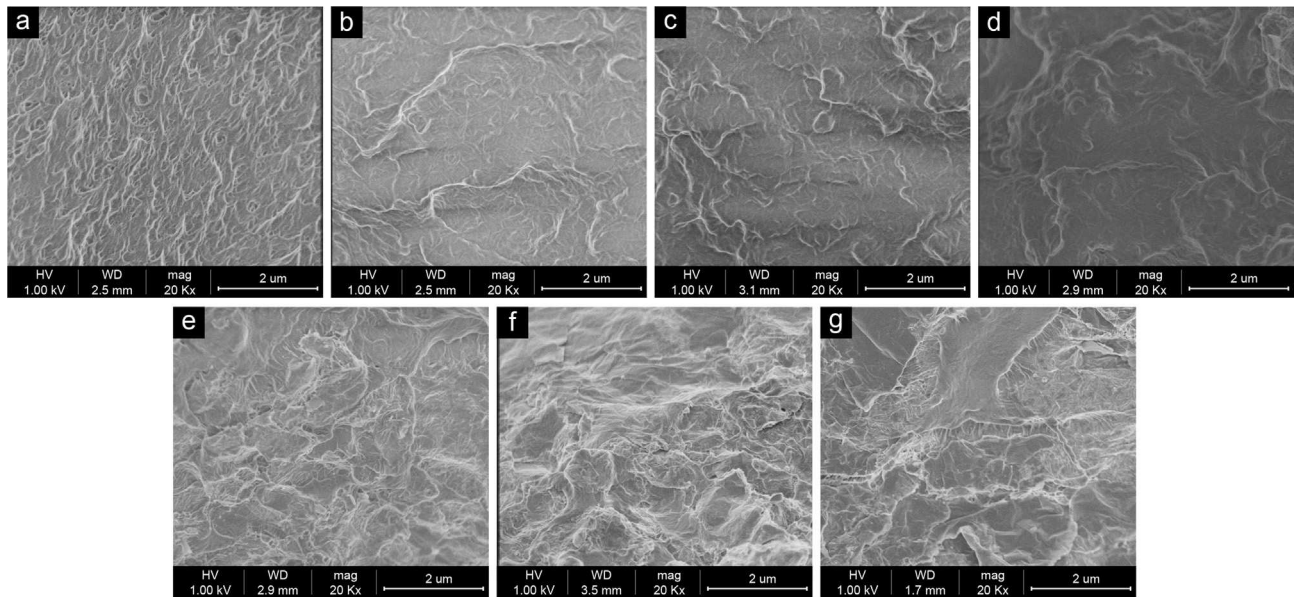


**Fig. 7.** SEM images of fracture surfaces of virgin UHMWPE (a) and UHMWPE/GO nanocomposites with 0.1 (b), 0.3 (c), 0.5 (d), 0.7 (e), 1 (f) and 2 wt% (g).

nanocomposites were prepared using an optimised ball mill technique [17], and significant improvements in the mechanical properties of the materials were found, indicating the potential of ball milling as a processing method for synthesising nanocomposites.

UHMWPE/GO nanocomposites (up to 0.5 wt%) showed little change in the degree of crystallinity due to the addition of GO. A more notable effect on the degree of crystallinity of nanocomposites has been previously reported. A study performed by Todd et al. [24], reported up to a 9% decrease in crystallinity for a thermally reduced graphite oxide reinforced polyethylene composite compared to virgin polyethylene. Martinez-Morlanes et al. [25] also reported a lower crystallinity for multi-walled carbon nanotube reinforced UHMWPE. On the other hand, a higher degree of crystallinity due to the addition of graphene has been reported [23]. These differences may be attributed to the quality of the nanoparticles and their ability to create bonding with the polyethylene matrix.

Thermogravimetric analysis demonstrated enhanced thermal stability of UHMWPE due to the addition of GO. This effect was also reflected in the mechanical behaviour of irradiated samples subjected to accelerated ageing. Aged UHMWPE samples exhibited a reduction of more than 30% in fracture stress, which was associated to the oxidative degradation of the polyethylene. However, when GO was added, the reduction was only ~18% and 3% for UHMWPE/GO 0.5 wt% and 2 wt%, respectively. Similar effects have been reported previously when adding carbon nanoreinforcements to UHMWPE. Sreekanth et al. [12] reported limited degradation of the mechanical properties of UHMWPE when multi-walled carbon nanotubes were added and Martinez-Morlanes et al. [11] demonstrated the positive contribution of MWCNTs in increasing the oxidative stability of virgin UHMWPE. Prior to implantation, UHMWPE implants are subjected to irradiation, post-irradiation processing and storage, undergoing natural aging and resulting in oxidative degradation of the material [26]. It has been postulated that graphene oxide has the ability to quench the effect of free radicals generated during the thermal decomposition of UHMWPE [15]. Chemical reactions between the oxygen molecules present in the polyethylene and free radicals generated due to irradiation causes scission in the polymer chains, leading to a reduction in the properties of UHMWPE [27], and causing a reduction in wear

resistance [28]. The addition of graphene oxide to UHMWPE matrix might be an interesting alternative to moderate the negative effects of irradiation and oxidation on the long term performance of UHMWPE implants.

In addition, GO was shown to have beneficial effects on the wettability of UHMWPE. The hydrophobic nature of virgin UHMWPE has generated some concerns in joint bearing applications. Since increased friction between the bearings can lead to modifications in the lubrication of the joint [29], previous investigations have focused on modifying the surface of UHMWPE or adding particles to improve its hydrophilicity [30,31]. By adding GO, enhanced wettability was achieved, which may lead to enhanced lubrication and improved friction in the bearing [32], improving the tribological performance of the artificial joints.

The results of this study have shown the ability of GO to improve the performance of conventional UHMWPE and further research concerning the tribological performance and biocompatibility of UHMWPE/GO nanocomposites is currently under investigation.

## 5. Conclusions

This work has focused on the influence of graphene oxide nanoparticles on the performance of UHMWPE. UHMWPE/GO nanocomposites with different concentrations of GO wt% were successfully prepared by means of an optimised ball milling technique and their thermal, mechanical and wettability properties were evaluated. The following conclusions can be drawn:

1. Graphene oxide nanoparticles have the ability to improve the thermal, mechanical and wettability properties of virgin UHMWPE.
2. The final properties of UHMWPE/GO nanocomposites can vary depending on the wt% concentration of GO nanoparticles added. The selection of the optimal %wt GO concentration is fundamental to maximise the benefits of the GO nanoparticles on the final performance of UHMWPE.
3. UHMWPE/GO materials prepared with up to 0.5 wt% GO exhibited improved characteristics compared to virgin UHMWPE and nanocomposites prepared with higher GO contents.

4. The incorporation of GO has been shown to have the potential to counteract the negative effects of gamma irradiation and the subsequent oxidation process of UHMWPE.
5. Further studies concerning the tribological performance and biocompatibility of UHMWPE/GO nanocomposites are required in order to fully assess the suitability of these materials for use in total joint replacements.

## Acknowledgements

The authors would like to thank Kempe Stiftelsen (grant no. SMK-2932) for funding this project.

## References

- [1] Katz JN. Total joint replacement in osteoarthritis. *Best Pract Res Clin Rheumatol* 2006;20(1):145–53.
- [2] Gomez Barrena E, Puertolas JA, Munuera L, Konttinen YT. Update on UHMWPE research. From the bench to the bedside. *Acta Orthop* 2008;79(6):832–40.
- [3] Katta J, Jin Z, Ingham E, Fisher J. Biotribology of articular cartilage – a review of the recent advances. *Med Eng Phys* 2008;30(10):1349–63.
- [4] Tipper JL, Galvin AL, Ingham E, Fisher J. Estimation of the osteolytic potential of noncrosslinked polyethylenes and ceramic-on-ceramic total hip prostheses. *J ASTM Int* 2006;6(3):1–16.
- [5] Plumlee K, Schwartz CJ. Improved wear resistance of orthopaedic UHMWPE by reinforcement with zirconium particles. *Wear* 2009;267(5):710–7.
- [6] Brach del Prever EM, Bistolfi A, Bracco P, Costa L. UHMWPE for arthroplasty: past or future? *J Orthop Traumatol* 2009;10(1):1–8.
- [7] Moghadam AD, Omrani E, Menezes PL, Rohatgi PK. Mechanical and tribological properties of self-lubricating metal matrix nanocomposites reinforced by carbon nanotubes (CNTs) and graphene- a review. *Compos Part B Eng* 2015;77:402–20. <http://dx.doi.org/10.1016/j.compositesb.2015.03.014>.
- [8] Breuer O, Sundararaj U. Big returns from small fibers: a review of polymer/carbon nanotube composites. *Polym Compos* 2004;25(6):630–45.
- [9] Chukov DI, Stepashkin AA, Maksimkin AV, Tcherdynsev VV, Kaloshkin SD, Kuskov KV, et al. Investigation of structure, mechanical and tribological properties of short carbon fiber reinforced UHMWPE-matrix composites. *Compos Part B Eng* 2015;76:79–88.
- [10] Suñer S, Bladen CL, Gowland N, Tipper JL, Emami N. Investigation of wear and wear particles from a UHMWPE/multi-walled carbon nanotube nanocomposite for total joint replacements. *Wear* 2014;317(1):163–9.
- [11] Martinez-Morlanes MJ, Castell P, Alonso PJ, Martinez MT, Puertolas JA. Multi-Walled carbon nanotubes acting as free radical scavengers in gamma-irradiated ultrahigh molecular weight polyethylene composites. *Carbon* 2012;50(7):2442–52.
- [12] Rama Sreekanth PS, Naresh Kumar N, Kanagaraj S. Improving post irradiation stability of high density polyethylene by multi walled carbon nanotubes. *Compos Sci Technol* 2012;72(3):390–6.
- [13] Du JH, Jinbo B, Cheng HM. The present status and key problems of carbon nanotube based polymer composites. *Express Polym Lett* 2007;1(5):253–73.
- [14] Lahiri D, Dua R, Zhang C, Socarras-Novoa I, Bhat A, Ramaswamy S, et al. Graphene nanoplatelet-induced strengthening of UHMWPE and biocompatibility in vitro. *ACS Appl Mater Interfaces* 2012;4(4):2234–41.
- [15] Marques P, Gonçalves G, Singh MK, Gracio J. Graphene oxide and hydroxyapatite as fillers of polylactic acid nanocomposites: preparation and characterization. *J Nanosci Nanotechnol* 2012;12(8):6686–92.
- [16] Tai Z, Chen Y, An Y, Yan X, Xue Q. Tribological behaviour of UHMWPE reinforced with graphene oxide nanosheets. *Tribol Lett* 2012;46(1):55–63.
- [17] Suñer S, Emami N. Investigation of graphene oxide as reinforcement for orthopaedic applications. *Tribol Mater Surf Interf* 2014;8(1):1–6.
- [18] Kurtz SM. A primer on UHMWPE. In: Kurtz SM, editor. *UHMWPE Handbook*. Elsevier; 2009. p. 1–9.
- [19] Martinez-Morlanes MJ, Medel FJ, Mariscal MD, Puertolas JA. On the assessment of oxidative stability of post-irradiation stabilized highly crosslinked UHMWPEs by thermogravimetry. *Polym Test* 2010;29(4):425–32.
- [20] ASTM D5045. Standard test methods for plane-strain fracture toughness and strain energy release rate of plastic materials.
- [21] ASTM F2003. Standard practice for accelerated aging of ultra-high molecular weight polyethylene after gamma irradiation in air.
- [22] Ionita M, Pandele AM, Crica L, Pilan L. Improving the thermal and mechanical properties of polysulfone by incorporation of graphene oxide. *Compos Part B Eng* 2014;59:133–9.
- [23] Chen Y, Qi Y, Tai Z, Yam X, Zhu F, Xue Q. Preparation, mechanical properties and biocompatibility of graphene oxide/ultrahigh molecular weight polyethylene composites. *Eur Polym J* 2012;48(6):1026–33.
- [24] Todd AD, Bielawski CW. Thermally reduced graphite oxide reinforced polyethylene composites: a mild synthetic approach. *Polymer* 2013;54(17):4427–30.
- [25] Martinez-Morlanes MJ, Castell P, Martinez-Nogues V, Martinez MT, Alonso PJ, Puertolas JA. Effects of gamma-irradiation on UHMWPE/MWCNT nanocomposites. *Compos Sci Technol* 2011;71(3):282–8.
- [26] Costa L, Bracco P, Brach del Prever EM, Kurtz SM, Gallinaro P. Oxidation and oxidation potential in contemporary packaging for polyethylene total joint replacement components. *J Biomed Mater Res B Appl Biomater* 2006;78(1):20–6.
- [27] Shen FW, McKellop HA. Interaction of oxidation and crosslinking in gamma-irradiated ultrahigh molecular-weight polyethylene. *J Biomed Mater Res* 2002;61(3):430–9.
- [28] McKellop H, Shen FW, Lu B, Campbell P, Salovey R. Effect of sterilization method and other modifications on the wear resistance of acetabular cups made of ultrahigh molecular weight polyethylene. A hip-simulator study. *J Bone Jt Surg Am* 2000;82A(12):1708–25.
- [29] Heisel C, Silva M, Schmalzried TP. Bearing surface options for total hip replacement in young patients. *J Bone Jt Surg Am* 2003;85A(7):1366–79.
- [30] Xiong D, Yuan N. Biotribological properties of UHMWPE reinforced by nano-ZrO<sub>2</sub> nanoparticle. *Key Eng Mat* 2007;330:1211–4.
- [31] Liu H, Pei Y, Xie D, Deng X, Leng YX, Jin Y, et al. Surface modification of ultrahigh molecular weight polyethylene (UHMWPE) by argon plasma. *Appl Surf Sci* 2010;256(12):3941–5.
- [32] Kanaga Karuppiah KS, Sundararajan S, Xu ZH, Li X. The effect of protein adsorption on the friction behaviour of ultra-high molecular weight polyethylene. *Tribol Lett* 2006;22(2):181–8.